Dissecting the roles of JNK/AP-1 signalling in the regulation of redox homeostasis within neurons

Nathan Garnham

Doctor of Philosophy

University of York

Biology

September 2016

Abstract

Ageing is characterised by pathological increases in reactive oxygen species (ROS) termed oxidative stress, a known contributor to the pathology underlying many neurodegenerative diseases. Using *Drosophila*, we investigated the role of Fos and Jun, transcription factors of the redox-sensitive JNK/AP-1 signalling pathway, in the neuronal response to oxidative stress.

Feeding larvae with Diethyl Maleate (DEM) depletes glutathione levels and induces mitochondrial oxidative stress. Synaptic overgrowth is observed following treatment with DEM that was shown to require the permissive action of Fos, Jun and the JNKKK, ASK1. Tandem Affinity Purification (TAP)-tagging and subsequent purification of neuronally expressed Fos and Jun led to the identification of the associated protein Punch. *Punch* is the *Drosophila* orthologue of *GTP cyclohydrolase 1* (*GTPCH1*), haploinsufficient mutations of which are found in DOPA-responsive dystonia and Parkinson's disease patients. Punch is the rate-limiting enzyme in the biosynthesis of tetrahydrobiopterin (BH_4), an essential cofactor in the synthesis of dopamine and serotonin as well as a potent ROS scavenger. Treatment with DEM appeared to cause dissociation of Punch from AP-1 upon increased oxidative stress. It was found that Punch, Fos and Jun are localised to the motor neuron cell nuclei. Analysis of larval neuromuscular junctions revealed JNK/AP-1-mediated synaptic overgrowth in *Punch* heterozygote mutants. This is rescued when the oxidative stress or dopamine deficit is relieved. Punch overexpression also rescues synaptic overgrowth associated with elevated JNK/AP-1 signalling in the absence of oxidative stress, suggesting Punch constrains AP-1 action. Punch expression is able to reduce oxidative stress-synaptic overgrowth potentially via synthesis of BH_4 and increased ROS scavenging, suggesting a link between standing and transcriptional defences against oxidative stress.

Punch may serve as a neuroprotective agent with implications for patients suffering from oxidative stress-induced neurodegenerative diseases.

Table of Contents

Table of Figures

Table of Tables

Acknowledgments

First, I would like to thank my supervisor Sean, for providing continuous support, ideas and a wealth of knowledge, as well as being a mentor and friend. Next I would like to thank my co-supervisor David for all his encouragement and expertise throughout this project. My thanks also extend to all members of the Sweeney and Elliott labs, including Chris Elliott, Amy Cording, Rebecca Furmston, Stavroula Petridi, Stuart Forrest and Ryan West for help on day-to-day activities. I would also like to express thanks to my TAP members, Gareth and Will for their fantastic ideas and help over the years.

I would like to thank my whole family for their lifelong support, encouragement and love, especially my mum who I owe everything to.

Finally I would like to thank Rebecca for her undying love and support, she has transitioned from friend, to best friend, to fiancée all within this PhD. I cannot thank her enough, not only for pushing me to be a better scientist, but a better man.

Declaration

I hereby declare that all work presented in this thesis is original work and I am the sole author, except where stated in the figures or text. Upon submission date, this work has not been presented for an award at this, or any other, University.

1. Introduction

1.1 Ageing

Ageing is the persistent decline in age-specific fitness or function due to internal physiological degeneration (Rose, (1991)). The decline of function is in part due to degeneration of the cell as it progresses through the ageing cycle, of growth, decline and death. This is also described as the process of biological ageing or senescence, explained as a programmed change in gene expression or a culmination of damage occurring through living. Ageing can be facilitated by reactive oxygen species (ROS). As a cell enters senescence, it remains metabolically active while accumulating damaged or dysfunctional macromolecules toward the end of the lifespan. Organelles are degraded via the lysosome, which with ageing becomes relatively inefficient and some dysfunctional molecules remain, often within the endolysosomal system. As these aggregate they are able to form a non-degradable waste material named lipofuscin, also known as the age pigment (Katz and Robison, 2002). Lipofuscin accumulates over time and acts as an exponentially increasing source of ROS, characteristic of ageing. Most senescent cells will undergo apoptosis when pathological levels of ROS induce mass cellular damage; however, terminally differentiated neurons are not readily replaced and normally act to avoid apoptosis (Oppenheim, 1991). This, coupled with a high metabolic demand and relatively low antioxidant defence system mean neurons are particularly susceptible to oxidative stress (Wang and Michaelis, 2010). Pathological levels of ROS in neurons have therefore been implicated in a number of neurodegenerative disorders.

1.2 Reactive oxygen species

1.2.1 Overview of reactive oxygen species

The term reactive oxygen species collectively describes molecules and free radicals (short-lived, highly reactive molecules with unpaired valence electrons) derived from molecular oxygen. In its ground state, molecular oxygen is a bi-radical and contains two unpaired electrons occupying two degenerate molecular orbitals,

which is also known as a triplet state (Turrens, 2003, Apel and Hirt, 2004). These two unpaired electrons make oxygen quite unreactive as oxidation of molecules require partners that can provide a pair of electrons with parallel spins that fit into its free electron orbitals. However, most organic molecules typically have pairs of electrons with opposite spins, which prevent molecular oxygen directly reacting with them (Cadenas, 1989). Ground state triplet oxygen can however undergo electron transfer reactions in which superoxide radical anions ($O_2^{\bullet -}$) are generated through oxygen reduction. Superoxide anions can act as both an oxidant and reductant, and whilst not the most potent ROS, they can give rise to other extremely reactive free radicals and ROS, most notably hydrogen peroxide (H_2O_2), hydroxyl radicals ($^{\bullet}OH$) and hydroxyl anions (OH^-). Hydrogen peroxide is formed after the rapid dismutation of the highly unstable superoxide anion, catalysed by superoxide dismutase (SOD), which allows the reaction to occur 10,000 times faster (McCord and Fridovich, 1969a, McCord and Fridovich, 1969b). SOD binds two superoxide anions and transfers the extra electron from one superoxide anion to the other, effectively generating one ground state triplet oxygen molecule and one oxygen molecule with two extra electrons, which rapidly react with two hydrogen ions forming hydrogen peroxide (Fridovich, 1989). The reaction follows:

$$O_2^{\bullet -} + O_2^{\bullet -} + 2H^+ \rightarrow H_2O_2 + O_2$$

Hydrogen peroxide, though not a radical is still very reactive and contributes greatly to oxidative stress when in the presence of superoxide anions via the Haber-Weiss/ Fenton reactions (Lipinski, 2011).

The initial step is the reduction of ferric into the ferrous ion by superoxide anions, usually within the lysosome which is a major site of iron storage and recycling (Radisky and Kaplan, 1998) :

$$Fe^{3+} + O_2^{\bullet -} \rightarrow Fe^{2+} + O_2$$

The second step is the Fenton reaction wherein the ferrous ion reacts with hydrogen peroxide generating hydroxyl radicals and hydroxyl anions:

$$Fe^{2+} + H_2O_2 \rightarrow Fe^{3+} + OH^- + {}^{\bullet}OH$$

The hydroxyl radical generated here is the most biologically active free radical formed under hypoxic conditions (Michiels, 2004). The hydroxyl radical causes the majority of oxidative damage via oxidising DNA bases, DNA strand breaks, generating abasic sites and DNA-DNA intra-strand adducts (Randerath et al., 1996, Lloyd et al., 1997, Cadet et al., 1999). Proteins can also undergo direct oxidation at the polypeptide backbone, leading to truncated peptides. Various oxidative modifications may also form carbonyl groups, affecting catalytic and structural function (Baraibar et al., 2012).

1.2.2 Generation of ROS

ROS are produced as natural by-products of normal respiratory metabolism, with the major source being the mitochondria. Other cellular sources of ROS production include the endoplasmic reticulum (Gross et al., 2006), peroxisomes (Boveris et al., 1972), the cytosol (Kukreja et al., 1986), plasma membrane (O'Donnell and Azzi, 1996) and extracellular space (McNally et al., 2003).

1.2.2.1 Mitochondrial generation of ROS

Mitochondria are the cellular energetic powerhouse, producing the majority of energy required in the lifetime of the cell. They are dynamic organelles, that undergo fission and fusion which alters their length and shape (van der Bliek et al., 2013). They have a double-membrane; consisting of an outer membrane surrounding an inner membrane and including an intermembrane space (Palade, 1953). The permeability of the membranes differs. The outer membrane features many protein-based pores to allow the passage of small proteins and ions, whereas the inner membrane is much less permeable. This is to accommodate the mitochondrial matrix, the site of the citric acid cycle, which ultimately produces the adenosine triphosphate (ATP) required by the cell. Mitochondrial respiration involves the movement of electrons through various electron donors, including nicotinamide adenine nucleotide (NADH) and reduced flavin adenine dinucleotide ($FADH_2$), which transfer electrons down the electron transport chain (ETC) between complexes I – IV; electron carriers located in the inner membrane. The electrons are finally transferred to O_2, the most electronegative electron acceptor in

the chain. As electrons pass along the ETC, free energy is released in small increments from NADH and $FADH_2$; these exergenic processes are coupled to proton transport into the intermembrane space, which generates a proton concentration gradient. The outer membrane of the mitochondria is more permeable to protons, which makes the overall pH higher than that of the intermembrane space. Positively charged protons are also pumped out from the matrix making it more negative compared to the intermembrane space, resulting in an electrical potential across the inner membrane. Both the proton concentration gradient and the electrical potential store the free energy released during the oxidation of NADH and $FADH_2$, this is known as the proton-motive force. The consequent flow of protons back into the matrix across the inner membrane is driven by the proton-motive force and by using the stored free energy, ATP is formed from adenosine diphosphate (ADP) and free phosphate (P_i) facilitated by ATP synthase, or complex V. This process is named oxidative phosphorylation and is the major source of ATP in aerobic non-photosynthetic cells. Whilst a relatively efficient process, it is possible for electrons to leak from the electron transport chain where they can reduce molecular oxygen. It only requires a single leaked electron to reduce oxygen to a superoxide anion, the precursor of most ROS produced in the cell (Boveris and Chance, 1973). The estimated steady state concentration of superoxide anions in the mitochondrial matrix is 10^{-10} M, every anion having the potential to induce hydroxyl formation if not rapidly dealt with by the antioxidant system (Cadenas and Davies, 2000).

Ordinarily, the first process in the series of electron transfers is the donation of electrons by NADH to complex I, also named NADH dehydrogenase, or NADH-coenzyme Q oxidoreductase. This protein transfers a pair of electrons from NADH to Coenzyme Q (CoQ), or ubiquinone, which is a lipophilic electron shuttling molecule. This process involves the oxidation of NADH and reduction of CoQ, as shown in the equation below:

$$NADH + 2H^+ + CoQ \rightarrow NAD^+ + H^+ + CoQH_2$$

This reaction releases energy, most of which is used to transport H^+ into the intermembrane space, however, a separate reaction exists wherein CoQ receives

electrons from complex II but is not coupled to the movement of H^+ and no proton-motive force is generated. Complex II, or succinate dehydrogenase, is an enzyme that oxidises succinate to fumarate during the citric acid cycle. The conversion of succinate to fumarate releases two electrons that are initially transferred to redox cofactor, oxidised flavin adenine dinucleotide (FAD) and then to an iron-sulphur carrier before finally reducing CoQ to $CoQH_2$. CoQ can freely diffuse within the membrane and shuttles two electrons to complex III, or $CoQH_2$–cytochrome *c* reductase, regenerating the oxidised CoQ in the process.

Cytochrome *c* reductase is a complex made up of an iron-sulphur protein, two *b*-type cytochromes and cytochrome *c1* of which the electrons transferred from CoQ are shuttled across and finally transferred to oxidised cytochrome *c.* Each pair of electrons transferred here facilitates the translocation of four protons across the inner membrane from the matrix.

Reduced cytochrome *c* now transports electrons to complex IV, or cytochrome c oxidase, the final protein complex in the ETC. The electrons are moved through a pair of copper ions, a cytochrome *a* and then a second complex consisting of another copper ion and cytochrome a_3 before finally O_2 where H_2O is produced. This is also coupled to a movement of protons into the intermembrane space, totalling an estimated 10 protons that are transported from the mitochondrial matrix across the inner membrane for every pair of electrons transferred from NADH to O_2. The proton-motive force is the source of energy required for ATP synthesis, utilised by the F_oF_1 complex, or ATP synthase. F_o is a membrane protein consisting of a transmembrane proton channel, through which protons move from the intermembrane space to the mitochondrial matrix downhill toward F_1. This movement releases energy, which activates a conformational change in F_1, catalysing the synthesis of ATP from ADP and P_i, and completing oxidative phosphorylation. As well as powering ATP synthase, the proton-motive force also provides the energy for the uptake of ADP and P_i from the cytosol into the mitochondria in exchange for the release of ATP and OH^- into the cytosol.

The formation of ROS from the mitochondria is thought to take place primarily at complex I and complex III, the dominant source being organ dependent. At each

complex where electron transfer occurs there is a small chance of a single electron 'leaking' and reducing cellular oxygen, forming superoxide anions. An estimated 0.15% of cellular oxygen is converted into superoxide and some complexes involved in oxidative phosphorylation are more prone to allow ROS formation (St-Pierre et al., 2002). The mitochondria of the heart and lungs exhibit increased ROS formation from complex III, whereas in the mitochondria of the brain this occurs more commonly from complex I in both normal and ageing brains (Turrens and Boveris, 1980, Turrens et al., 1982, Barja and Herrero, 1998, Barja, 1999). The rate of superoxide formation by the ETC is largely controlled by mass action, increasing when the concentration of oxygen rises or when the flow of electrons slows (Turrens et al., 1982). As previously mentioned, the proton gradient powers the production of ATP, however this requires ADP, which when depleted, stops the proton flow through ATP synthase. Consequently, the proton gradient concentration increases, slowing the electron flow, making the respiratory chain more reduced resulting in increased formation of superoxide anions (Boveris et al., 1972).

1.2.2.2 Non-mitochondrial sources of ROS

Whilst most consider the mitochondria the largest source of ROS many other cellular sources of ROS exist including the cytosol (Roy et al., 1994), the endoplasmic reticulum (Gross et al., 2006), peroxisomes (Boveris et al., 1972), the plasma membrane (O'Donnell and Azzi, 1996) and the extracellular space (McNally et al., 2003).

Cytosolic sources of oxidative stress often involve cytosolic enzymes that act to generate ROS as a by-product of their main function. One such enzyme that produces ROS is xanthine oxidase (XO), which generates hydrogen peroxide when it catalyses the conversion of hypoxanthine to xanthine and ultimately to uric acid (Ardan et al., 2004). It is also possible for XO to generate nitric oxide (NO) from the decomposition of reactive nitrogen species (RNS) S-nitrosothiols (RSNO) (Trujillo et al., 1998). NO is a cytosolic ROS which is endogenously synthesised by various nitric oxide synthases (NOS) in a reaction involving reduced nicotinamide adenine dinucleotide phosphate (NADPH), oxygen and L-arginine. Highly reactive but short

lived, NO is an important biological messenger and modulator of neurotransmitter release, but upon neuronal injury its concentration rises at least 10-fold, causing mass damage. NO can react with hydrogen peroxide and form the highly reactive hydroxyl radical (Bondy and Naderi, 1994). It can also outcompete SOD for superoxide, in a reaction that generates peroxynitrite, a powerful toxin and oxidant that contributes to the severity of RSNO and NO (Beckman and Koppenol, 1996).

The endoplasmic reticulum also contributes to the ROS levels in the cell through the action of several enzymes, including endoplasmic reticulum oxidoreductin 1 (ERO1) and protein disulphide isomerase (PDI). ERO1 is a thiol oxidase enzyme that catalyses the formation of disulphide bonds along with PDI within the endoplasmic reticulum. Both proteins contribute to the production of ROS when incomplete reduction of oxygen occurs during the electron exchange process required for disulphide bond formation, producing hydrogen peroxide and superoxide anions (Bhandary et al., 2013).

Another important site of ROS production is the peroxisome; a single membrane bound organelle filled with oxidative enzymes involved in metabolism and the breakdown of various fatty acids. They bud from the endoplasmic reticulum and through beta-oxidation they break down long chain fatty acids to medium chain fatty acids, which are transported to the mitochondria for further breakdown and synthesis of ATP. The oxidative enzymes use oxygen to produce hydrogen peroxide when removing hydrogen atoms from organic substrates, RH_2, in the following equation:

$$RH_2 + O_2 \rightarrow R + H_2O_2$$

The hydrogen peroxide is utilised by catalase to oxidise other cellular substrates like alcohols and phenols in the peroxidation reaction:

$$H_2O_2 + R'H_2 \rightarrow R' + 2H_2O$$

While the peroxisome does produce hydrogen peroxide, the prerequisite to several ROS, it is crucial in the detoxification of toxic molecules in the cell through the peroxidation reaction. Excess hydrogen peroxide can occur in the peroxisome, but is

usually dealt with by catalase, converting it to water and oxygen (Alfonso-Prieto et al., 2009).

Similar to peroxisomes, lysosomes are another single membrane bound organelle, synthesised by the Golgi apparatus instead of the ER. They contain hydrolytic enzymes such as proteases, lipases, peptidases and nucleases used to digest macromolecules of the cell (Bainton, 1981). The lysosome is important for endocytosis and autophagy but is also a potent site of ROS production. Incomplete digestion of macromolecules leads to the formation of age-pigment, lipofuscin. This non-degradable pigment remains in the lysosome, sequestering the hydrolytic enzymes and reducing the efficiency of the lysosomal system over time (Jolly et al., 1995). As this builds up so does lysosomal iron, which accumulates in the lysosome after it is transported via autophagocytosed macromolecules during autophagy. This accumulation is particularly evident in long-lived post mitotic cells such as neurons, and through the Fenton reaction can generate ROS and the extremely reactive hydroxyl radical when reacting with hydrogen peroxide. Hydrogen peroxide generated in the mitochondria that escapes degradation via catalase (cat) and glutathione peroxidase (GPx), is able to diffuse into the lysosome where these antioxidants do not occur (Figure 1.1). It is then free to react with labile iron forming hydroxyl radicals and ferryl compounds, significantly contributing to the level of ROS in the cell and overall oxidative stress (Kurz et al., 2008).

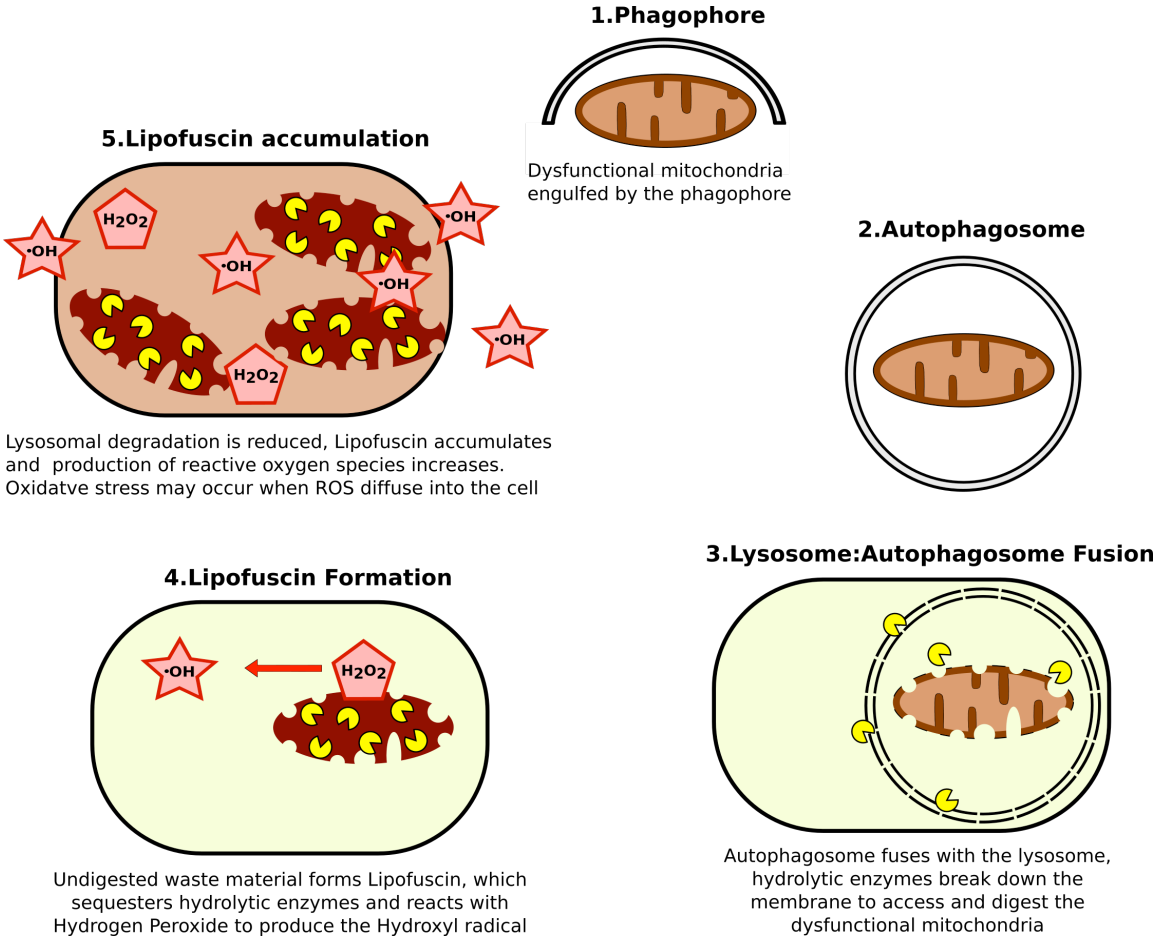

Figure 1.1 Lysosomal dysfunction and oxidative stress

Lysosomal function is decreased upon the accumulation of lipofuscin, a non-degradable waste material that arises from the incomplete degradation of cellular waste. It remains in the lysosome indefinitely and contributes to the generation of ROS and onset of cellular oxidative stress.

1.3 Cellular responses to oxidative stress

1.3.1 Oxidative stress

As previously described, ROS are produced as natural by-products of numerous cellular processes, mitochondrial respiration being the most prevalent (Turrens, 2003). A battery of antioxidants actively removes ROS ensuring a healthy cellular environment where low levels of ROS remain. Maintaining ROS at low physiological levels are the cellular antioxidants, which act to scavenge ROS and retain the tightly regulated redox balance within the cell. Oxidative stress occurs when the native antioxidant system is overwhelmed by ROS, either from a pathological increase of ROS or inadequate detoxification. Oxidative stress causes random damage to the macromolecules of the cell whilst also activating cell-signalling pathways involved in the cellular stress response. Such oxidative damage includes DNA lesions, lipid peroxidation, and oxidisation/fragmentation of peptides often as a result of mass chain reactions initiated by ROS. Consequently, oxidative stress has been implicated in a number of neurodegenerative disorders, including Parkinson's Disease (PD) (Spina and Cohen, 1989) and Alzheimer's disease (AD) (Martins et al., 1986). The cellular stress response involves a number of signalling pathways including several mitogen-activated protein kinase (MAPK) pathways, namely the Jun N-terminal kinase (JNK)/extracellular signal-regulated kinase (ERK)/p38 pathways or the stress-activated protein kinases (SAPK). Also activated are PI3-kinase/AKT, p53 signalling, Nrf2/Keap1 signalling and nuclear-factor κB (NF-κB) signalling pathways. These pathways culminate in the activation of proliferation, growth arrest, autophagy and cellular death (Martindale and Holbrook, 2002). In summary, there are standing constitutive defences against oxidative stress, in the form of enzymatic antioxidants, non-enzymatic antioxidants as well as adaptive transcriptional responses, all of which serve to protect the cell from oxidative damage.

1.3.2 Oxidative damage

Oxidative damage occurs when ROS randomly damage macromolecules of the cell through chain reactions, which result in the exponential formation of more ROS, if

not properly neutralised. Cellular DNA can be damaged by the highly reactive hydroxyl radical through its addition to the double bonds of DNA bases where a hydrogen atom is abstracted from the methyl group of thymine and from the carbon-hydrogen bonds of 2'-deoxyribose (Sonntag, 1987, Cooke et al., 2003). Damage to DNA may also arise in the form of strand breaks when the hydroxyl radical reacts with the sugar moiety of DNA removing the hydrogen atom. ROS cause base and nucleotide modifications, microsatellite instability as well as changes in DNA conformation, which result in inaccurate or blocked replications (Cooke et al., 2003). The methylation status of cytosines in DNA can also be altered by free radicals, changing the expression level of the affected region (Weitzman et al., 1994). Similar to DNA, proteins can be damaged/oxidised by ROS though the hydroxyl-dependant abstraction of hydrogen from amino acids making up the polypeptide backbone (Berlett and Stadtman, 1997). Oxidisation of the protein backbone can also trigger a chain reaction by which alkyl, alkoxyl and alkylperoxyl radicals form, inducing fragmentation of the protein. Peptide cleavage can also occur when ROS attack protein side chains (glutamyl, aspartyl and prolyl), again through hydroxyl-dependant abstraction of hydrogen. Protein function is altered by oxidation of amino acids, cysteine and methionine being especially susceptible where disulphide cross-links form upon oxidation (Berlett and Stadtman, 1997). Fatty acids are also susceptible to damage by ROS. Phospholipid membrane fatty acids, or polyunsaturated fatty acids (PUFA) are oxidised at their double bonds and degraded forming lipid peroxidation products (LPO) including lipid peroxyl radicals. Lipid peroxyl radicals are highly reactive, oxidising adjacent PUFA and attacking membrane proteins. Lipid peroxidation is a self-propagating autocatalytic process capable of exponentially producing more ROS until quenched by antioxidants. When the LPO are broken down the resulting products are able to interact with DNA, causing adducts that are mutagenic, carcinogenic and debilitating to signal transduction pathways (Marnett and Plastaras, 2001, Hulbert et al., 2007).

The exponential production of ROS can occur from chain reactions initiated by single ROS molecules. This makes it difficult to pinpoint the exact cause of oxidative stress. ROS impact upon mitochondrial and lysosomal function increasing ROS

production further (see Figure 1.1). Oxidative stress and ROS increase as we age, overwhelming the native antioxidant defences, causing mass damage to macromolecules and incurring pathology. This is the hallmark of ageing and is implicated in the onset and progression of a number of neurodegenerative diseases. Combatting oxidative stress is a battery of antioxidants that act to convert ROS to less damaging molecules such as oxygen and water. All antioxidants have specific functions and all are important in staving oxidative stress and pathology.

1.3.3 Cellular antioxidant systems

ROS are kept at low physiological levels by the standing cellular antioxidant defence systems. An antioxidant is defined as "any substance that, when present at low concentrations compared with that of an oxidisable substrate, significantly delays or inhibits oxidation of that substrate" (Halliwell B, 1989). Antioxidants are classified into 3 categories:

- Primary antioxidants – prevent formation of oxidants
- Secondary antioxidants – ROS scavengers
- Tertiary antioxidants – repair oxidised molecules through dietary or consecutive antioxidants.

Antioxidants may be enzymatic or non-enzymatic. Enzymatic antioxidants can directly, or indirectly contribute to the defence against ROS. They include superoxide dismutase (SOD), catalase (Cat), glutathione peroxidase (GPx), glutathione reductase (GR) and thioredoxin reductase (Trx). Non-enzymatic antioxidants are ROS scavengers and include glutathione, vitamin E, tetrahydrobiopterin (BH_4), uric acid, albumin, and bilirubin, amongst others (Halliwell, 1996, Birben et al., 2012, Pathak et al., 2015). Primary antioxidants act to break the ensuing chain reactions that lead to exponential ROS production and convert them to less reactive molecules. Secondary antioxidants act to scavenge ROS, becoming oxidised in the process and often through the action of primary antioxidants are reduced to reform the original scavenger whilst removing ROS (Noori, 2012).

SOD is an enzyme that converts the highly unstable superoxide anions into the more stable hydrogen peroxide, which is longer lived and able to diffuse from the mitochondria (McCord and Fridovich, 1969a, McCord and Fridovich, 1969b). Several types of SOD exist that differ in the metal cofactor used in the dismutation of the superoxide anion. In *Drosophila,* there are 2 isoforms; SOD1, which has copper-zinc cofactors (Cu-Zn-SOD) and functions as a homodimer predominantly located in the cytosol (Richardson et al., 1975, Missirlis et al., 2003). SOD2 has a manganese cofactor and functions as a homotetramer predominantly in the mitochondrial matrix (Duttaroy et al., 1997). Extracellular SOD3 (EcSOD) also exists in human but is tissue specific rather than ubiquitous like SOD1 and SOD2 (Fattman et al., 2003).

Hydrogen peroxide is produced upon superoxide dismutation by SOD, and is converted to oxygen and water by the enzymatic function of catalase (May, 1901). Catalase is a tetrameric enzyme containing a heme group (Fe^{3+}) and NADPH in the active centre of each of its four subunits. Catalase has two distinct biological functions depending on the concentration of hydrogen peroxide. At high levels catalase acts to remove hydrogen peroxide by catalytically converting it to oxygen and water. The mechanism involves one molecule of hydrogen peroxide binding catalase, splitting to release water while oxygen binds the Fe^{3+} group facilitating the binding of a second hydrogen peroxide molecule forming water and O_2. (Alfonso-Prieto et al., 2009). At low levels, catalase utilises hydrogen peroxide to detoxify phenols and alcohols via peroxidation. Hydrogen peroxide can also be removed by the thiol-reducing systems of ROS scavengers, thioredoxin and glutathione. Thiol groups contain carbon-bonded sulphydryl groups, reducing agents that can be reversibly oxidised and reduced (Sies, 1997). During the degradation of hydrogen peroxide, thioredoxin is oxidised and then reduced by thioredoxin reductase using electrons donated from NADPH (Holmgren and Lu, 2010). Glutathione also degrades hydrogen peroxide through the catalytic action of glutathione peroxidase, generating water and oxidised glutathione disulphide. Oxidised glutathione is reduced through the action of glutathione reductase using electrons donated from NADPH, regenerating reduced glutathione (Bhabak and Mugesh, 2010). During the course of this investigation, we utilise diethyl maleate (DEM), which generates oxidative stress by depleting glutathione from the cell via conjugation (Weber et al.,

1990) (see Figure 1.2). This increases the level of mitochondrially-produced hydrogen peroxide in the cell as one of the major standing antioxidant defences against this is debilitated, thereby generating oxidative stress (Harlan et al., 1984). Treating flies with DEM gives us a model of oxidative stress, but we also alleviate oxidative stress during this investigation by treating with Trolox. Trolox is a water-soluble non-enzymatic analogue of vitamin E, which is thought to protect against ROS-induced lipid peroxidation and increase intracellular ROS scavenging (Hamad et al., 2010). During several experiments, we manipulate the levels of Punch, an enzyme required in the first rate-limiting step of BH_4 biosynthesis (Hatakeyama et al., 1991). BH_4 also acts to scavenge ROS, being a powerful reducing agent and acting as a preferable oxidisable target in the cell. It is recovered from its oxidised state (BH_2) via the actions of dihydrofolate reductase (DHFR), converting back to the reducing form, BH_4 (Crabtree and Channon, 2011). Following oxidisation and a decrease in BH_4, the levels of BH_2 rise, which block the coupling of BH_4 to endothelial nitric oxide synthase (eNOS), preventing adequate redox reactions by NOS and increasing the production of ROS (Wever et al., 1997, Vasquez-Vivar et al., 2002).

This highlights the importance of regulating antioxidant levels and maintaining low, healthy levels of ROS. The antioxidant defence system is highly complex, it is not sufficient to just remove all ROS, as they are crucial molecules in a number of cell signalling pathways. A balance is required to protect against oxidative damage yet retain proper cellular signalling and function. Consequently, antioxidants are tightly regulated and the cell signalling pathways activated by ROS upregulate antioxidant expression when ROS levels increase, this is described as an adaptive response (Crawford and Davies, 1994). This rapid response increases cellular protection but can also initiate further cellular responses like apoptosis, autophagy, growth arrest or proliferation.

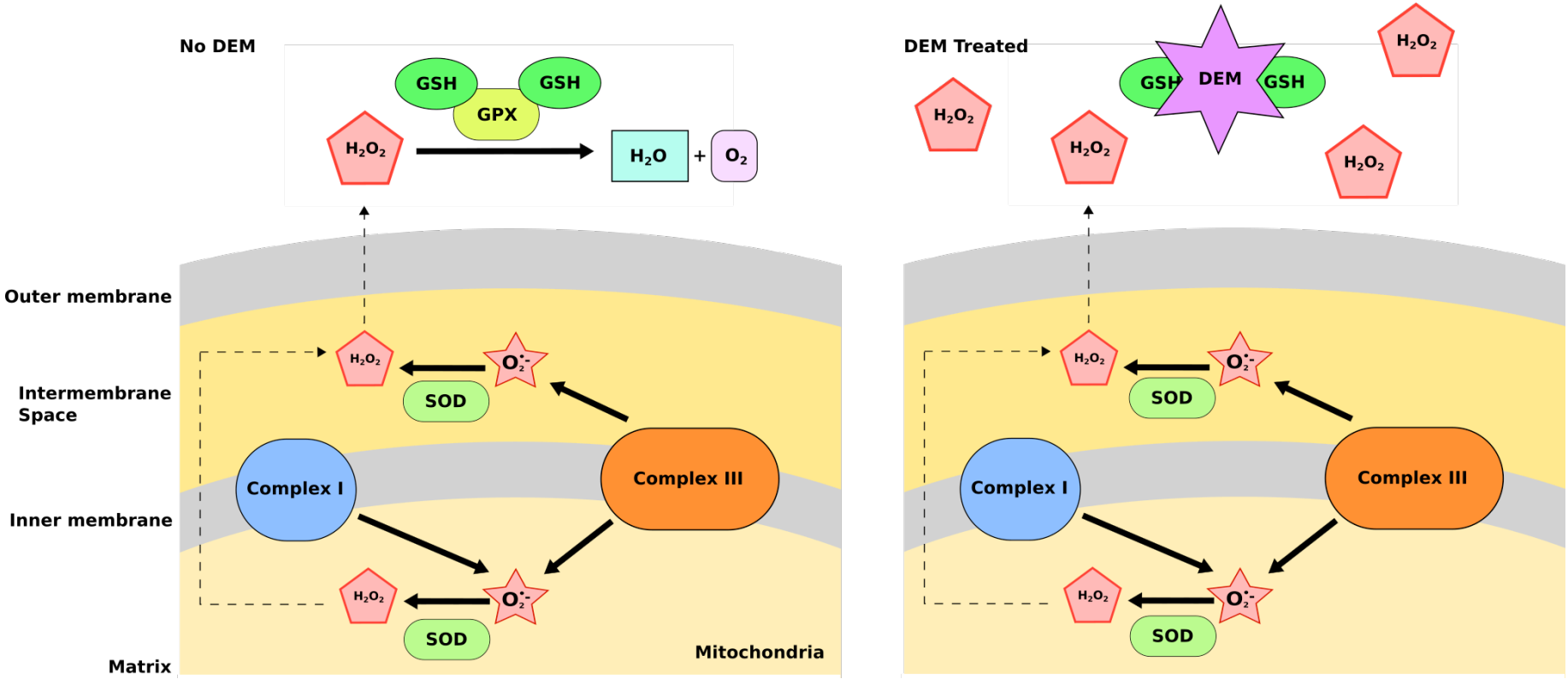

Figure 1.2 Diethyl maleate conjugates glutathione reducing antioxidant defences

Superoxide anions ($O_2^{\bullet-}$) are produced from Complex I and Complex III of the mitochondria and rapidly converted to hydrogen peroxide (H_2O_2) by superoxide dismutase (SOD). Hydrogen peroxide diffuses through the mitochondrial membranes and is normally neutralised by glutathione peroxidase (GPX) and 2 molecules of glutathione (GSH) into water and oxygen. Diethyl maleate (DEM) acts to conjugate GSH, reducing the ability of GPX to neutralise hydrogen peroxide, causing oxidative stress.

1.3.4 Cell signalling responses to oxidative stress

In response to increasing ROS, several important adaptive stress-response pathways are activated, mainly the MAPK signalling pathways JNK/ERK/P38, with JNK signalling being the major redox sensitive signalling pathway. Also playing a major role in the redox response is the nuclear factor erythroid 2 [NF-E2]-related factor 2(Nrf2)/ Kelch-like erythroid cell-derived protein with CNC homology [ECH]-associated protein 1 (Keap1) signalling pathway. These are the adaptive defence systems in combating oxidative stress.

Second to the JNK signalling pathway, the Nrf2/Keap1 signalling pathway is important in cell defence and survival, and crucial in the oxidative stress response. It is responsible for increasing expression of cytoprotective genes after noxious insult (Itoh et al., 1999). Nrf2 is a transcription factor belonging to the Cap'n'Collar (CNC) family and acts to regulate phase II detoxifying and oxidative stress enzyme genes (Itoh et al., 1997). Such genes include *glutathione S-transferase* (*GST*), which encodes a major detoxification enzyme (Chasseaud, 1979), *peroxiredoxin*, which encodes an enzyme that reduces hydrogen peroxide (Rhee et al., 2001), and *heme-oxygenase-1*, which encodes an essential enzyme in heme catabolism wherein neuroprotective carbon monoxide (CO) is produced (Ishii et al., 2000, Hettiarachchi et al., 2014). Keap1, a cytoplasmic actin binding protein binds Nrf2, promoting its proteasomal degradation and regulating its activity. ROS bind to redox sensitive cysteine residues on Keap1, changing its conformation to dissociate from Nrf2. Nrf2 is then primed to translocate to the nucleus and bind the antioxidant response element (ARE) to promote transcription of cytoprotective enzymes (Taguchi et al., 2011). The ARE sequence exhibits high homology to the JNK/AP-1 binding consensus suggesting a level of cross-talk between the two pathways, unsurprising as they are the two major redox sensitive signalling pathways and the cellular response to stress is vastly complex. It has recently been shown that Nrf2 signalling is epigenetically repressed in the developing neuron in order to allow functional maturation. By repressing Nrf2 at its promoter during development it determines a specific redox level within the neuron that allows for increased Wnt and JNK signalling, important for correct neuronal development. Ectopic expression of Nrf2 during development buffers the redox potential of the neuron, keeping the ROS

level low enough to avoid redox-based activation of JNK, leading to developmental deficits (Bell et al., 2015).

JNK, or Jun N-terminal Kinase signalling is activated in response to a number of intracellular and extracellular cues. It is a crucial node in the cellular stress response and will be the main focus of this investigation. JNK is a stress-activated kinase and a central part of the JNK signalling cascade (Hibi et al., 1993). It becomes activated in response to ROS wherein duel phosphorylation occurs at the threonine and tyrosine of its Thr-Pro-Tyr motif (Ip and Davis, 1998). As JNK is the central kinase in the JNK signalling cascade its activation by phosphorylation is regulated by upstream kinase activity from JNK kinases (JNKK) and JNK kinase kinases (JNKKK) (see Table 1.1). MKK7 is a JNKK shown to exhibit oxidative stress responses in mammals and *Drosophila* (Hemipterous (hep)) and has crucial roles in mediating TNF–α signalling and AP-1 dependent transcription (Moriguchi et al., 1997). I focus on *Drosophila* here as it is the best-understood metazoan and members of the JNK signalling pathway are conserved and have limited redundancy. We also use *Drosophila* as our main experimental tool in this investigation. Activated also by environmental stresses such as heat and UV irradiation, MKK7 activates and phosphorylates JNK mainly at the threonine of the Thr-Pro-Tyr motif, with a second JNKK, MKK4 phosphorylating at the tyrosine (Lin et al., 1995, Asaoka and Nishina, 2010). Both MKK4 and MKK7 are involved in the activation of apoptosis contributing to the detrimental effects of AD, and a loss of function confers protective effects against this (Mazzitelli et al., 2011). However, in non-diseased cells mutations in MKK7 have been shown to increase sensitivity to oxidative insults, owing to the protective role of JNK signalling identified by overexpression studies (Wang et al., 2003). Upstream of JNKK are the JNKK kinases, or JNKKK. At least 6 JNKKKs exist in mammals and *Drosophila*, including ASK1 (Pk92B), MLK (slipper) and DLK (wallenda). Apoptosis signal regulating kinase (ASK) 1 is activated in response to oxidative stress and initiates apoptosis (Ichijo et al., 1997). The *Drosophila* orthologue is named Pk92B. ASK1 is inhibited by reduced thioredoxin (Trx) which binds at low ROS levels and inhibits kinase activity as well as ASK1-dependant apoptosis. When ROS levels increase, redox sensitive cysteine residues within the active centre of thioredoxin are oxidised, allowing dissociation

of thioredoxin from ASK1 and the subsequent activation of ASK1 and JNK signalling (Saitoh et al., 1998). Mixed lineage kinase or MLK, also known as slipper (Slpr) in *Drosophila* is implicated in neuronal cell death and directly phosphorylates MKK4 and MKK7, activating JNK as well as P38 and ERK signalling (Sathyanarayana et al., 2003). *Drosophila* Wallenda (Wnd) is homologous to vertebrate dual leucine-zipper-bearing kinase (DLK) and human leucine-zipper-bearing kinase (LZK). Wallenda was originally identified as being required for *Highwire (hiw)*-dependant synaptic overgrowth, and through overexpression was shown to play a role in synaptic growth via JNK activation (Collins et al., 2006). Axonal transport and regeneration following injury are also both regulated by Wallenda (Xiong et al., 2010). The JNKKK, TGF-β activated kinase 1 (TAK1) has also been shown to regulate synaptic growth and is essential for *Rab8*-induced synaptic overgrowth. TAK1 may also represent a bridge between TGF-β and JNK signalling in the regulation of synaptic growth (West et al., 2015). Upstream of these JNKKKs is JNKKK kinase misshapen, which is required for embryonic dorsal closure in *Drosophila* (Su et al., 1998). Importantly, JNK signalling is context dependant, implicated in innate immunity, wound healing, autophagy and even cancer. Depending on the context and stimuli, different JNKKK and JNKKKK's are activated and lead to JNK pathway activity. Our focus is JNK signalling within the neuronal system, its role in oxidative stress protection and its role in synaptic plasticity.

Table 1.1 Members of the JNK signalling pathway

Activity	Mammalian Orthologue	*Drosophila* Gene
JNKKKK	*MINK, TNIK, NIK/HGK*	***Misshapen (msn)***
JNKKK	*ASK*	***Pk92B***
	TAK	***TAK1***
	TAK	***TAK12***
	MLK	***slipper (Slpr)***
	DLK, ZPK	***wallenda (Wnd)***
	MEKK1-4	***Mekk1***
JNKK	*MKK7*	***hemipterous (hep)***
	MKK4	***mkk4***
JNK	*JNK*	***Basket (Bsk)***
Transcription Factor	*Jun*	***Jra***
	Fos	***kayak (kay)***

The JNK signalling pathway has many upstream regulators that tightly control the activation and activity of JNK in a phosphorylation-dependent manner. The extensive number of targets in which JNK phosphorylates and exerts its effects only exacerbates its complexity further. The main transcriptional target is activator protein-1 (AP-1), a dileucine zipper transcription factor consisting of dimers of Fos and Jun, known as kayak (kay) and Jun-related antigen (Jra) in *Drosophila*. AP-1 activity is upregulated upon phosphorylation, wherein it translocates to the nucleus and increases transcriptional output from the 12-O-tetradecanoylphorbol-13-acetate (TPA) DNA responsive element (TRE). A range of stimuli, including stress signals, infection, growth factors and cytokines regulate AP-1 activity, and the transcriptional output mediates such processes as proliferation, differentiation, apoptosis and autophagy (Hess et al., 2004). Fos and Jun are leucine zipper transcription factors with a basic DNA-binding domain. These transcription factors are able to dimerise via their leucine zippers, which also confers their specificity

and stability. In mammals, c-jun and c-fos are known to form heterodimers, c-jun can homodimerise but c-fos cannot (Halazonetis et al., 1988). In *Drosophila* Fos can homodimerise as well as form heterodimers with Jun, which increases its DNA binding efficiency 25-fold (Perkins et al., 1990). AP-1 activity via JNK phosphorylation is essential for the cellular stress response (Yang et al., 1997), in particular the oxidative stress response where ROS directly activate JNK signalling, which has important implications in the onset and progression of neurodegenerative diseases (Chi et al., 2007). However, AP-1 is readily oxidised when ROS levels increase, decreasing its DNA binding efficiency. Thus certain mechanisms exist to keep AP-1 in its reduced state, preserving its ability to bind the TRE. Multiprotein bridging factor-1 (MBF1) prevents oxidation of redox sensitive cysteines upon Jun; and the redox protein apurinic/apyramidic endonuclease/redox factor 1 (APE-1/Ref-1) acts to reduce any oxidised AP-1 as well as facilitate other reducing molecules like glutathione and thioredoxin to maintain AP-1 activity (Jindra et al., 2004, Ando et al., 2008).

Similar to ASK1, JNK is inhibited when the cellular ROS level is low, through the binding of monomeric glutathione S-transferase pi (GSTp), blocking its activity. Upon an oxidative stress burden, GSTp is displaced, forming dimers/oligomers and uninhibiting JNK to become phosphorylated and activated (Adler et al., 1999a). Following activation, the initial output of JNK signalling is the transcription of negative feedback inhibitor, puckered (puc) via AP-1 (Martín-Blanco et al., 1998). Puc rapidly inhibits JNK by acting as a JNK phosphatase and reducing JNK signalling. Puckered expression is JNK-dependent, meaning that JNK signalling regulates expression of its own inhibitor. This is important with regards to its neuronal function, where increased JNK activity leads to a pathological increase in synaptic growth and a disruption of neurotransmitter release (Etter et al., 2005).

1.4 The neuron and oxidative stress

An important consideration about the neuron, in terms of our study into oxidative stress and ageing is its extremely high-energy demand. The neuron is very long and highly polarised, in that a single cell body must differentiate into multiple dendrites and an axon (Amato and Man, 2012). This requires a great level of cellular

biosynthesis in regards to protein and membrane synthesis as well as the shuttling of cellular material to the growing axon tip, all of which require a large amount of energy. The mitochondria provide ATP to fuel these processes; the by-product of this is the generation of ROS (Mattson and Liu, 2002). An established neuron also requires a huge amount of energy, not only to traffic proteins the length of the neuron but also in generating action potentials (Berndt and Holzhutter, 2013). Relatively speaking, the neuron has an extremely high-energy demand and the consequence of this is a higher oxidative stress burden, which is only exacerbated with age (Mattson and Liu, 2002). ROS burdened neurons are also non-autonomous, meaning that their detriment is experienced by surrounding cells, specifically glia, which normally act to maintain neuronal function (Christopherson et al., 2005).

1.5 Mitochondrial dysfunction, oxidative stress and disease

Aged neurons are at increasing risk of dysfunction and disease due to an accumulation of cellular damage and significant rise in oxidative stress. The mitochondria is often the focal point of disease onset in neurons and has been implicated in a number of neurodegenerative diseases such as PD (Mortiboys et al., 2010), AD (Ronnback et al., 2015) and amyotrophic lateral sclerosis (ALS) (Kong and Xu, 1998). Damage to the mitochondrial DNA, unbalanced fission/fusion, reduced membrane potential and aberrant mitophagy can all lead to dysfunction and increased ROS production, owing to the demise of neuronal function (Johri and Beal, 2012).

AD is the most common neurodegenerative disorder and is characterised by cognitive impairments following the accumulation of extracellular β-amyloid peptide (Aβ) plaques and intracellular neurofibrillary tangles consisting of hyperphosphorylated tau proteins (Swerdlow et al., 2010). In sporadic cases it is thought that the accumulation of Aβ plaques follows mitochondrial dysfunction. Several mitochondrial enzymes are thought to contribute to this dysfunction, including a reduction in pyruvate dehydrogenase complex activity (Sorbi et al., 1983) and defective cytochrome oxidase activity which coincides with increased ROS production, reduced membrane potential, increased Aβ plaque production and activation of both apoptotic and stress signalling pathways (Swerdlow, 2007).

PD is the second most common neurodegenerative disorder. It is characterised by a loss of dopaminergic neurons in the *substantia nigra* and the accumulation of Lewy bodies, cytoplasmic inclusions composed of aggregated alpha-synuclein. *Parkin* and *phosphatase and tensin homolog-induced putative kinase 1* (*PINK1*) are known PD risk genes, which are expressed in the mitochondria and have roles in mitophagy. Mutations in *PINK1-parkin* perturb the autophagic removal of dysfunctional mitochondria, failing to remove those producing excessive ROS and generating an oxidative stress within the neuron (Kim et al., 2007a, Deas et al., 2011). The *leucine-rich repeat kinase 2*; *LRRK2* (*G2019S*) mutation has been identified as one of the most common causes of PD and impairs mitochondrial function by an as yet unknown mechanism. A decrease in mitochondrial membrane potential and intracellular ATP levels are observed in the *G2019S* mutation of *LRRK2* (Mortiboys et al., 2010) as well as an imbalance in calcium homeostasis that manifests as excessive mitophagy and dendrite shortening (Cherra et al., 2013).

ALS is a progressive neurodegenerative disorder characterised by the selective death of motor neurons and the onset of muscle weakness, atrophy and ultimately, respiratory failure and death (Hayashi et al., 2015). Though not fully understood, there appears to be a link between ALS and *SOD1* mutations resulting in mitochondrial damage and dysfunction. This appears in 20% of familial cases of ALS, which account for 10% of total cases (Andersen, 2006). Mutations in *SOD1* largely affect the dynamics of motor neuron mitochondria, which display impaired fusion and axonal transport, a reduction in size and density and abnormal localisation within the synapse (Magrane et al., 2012).

Mutations in mitochondrial DNA are thought to contribute to the onset and /or progression of many neurodegenerative diseases. The mitochondrial genome is made up of a multi-copy circular double-stranded DNA molecule, approximately 16.6kb long in humans. This encodes 13 of the 92 polypeptides required for oxidative phosphorylation as well as the necessary RNA machinery required for translation; the nuclear DNA encodes the remaining (Taylor and Turnbull, 2005). Mutations present as either homoplasmic, where each copy of the mitochondrial genome contains the mutation or heteroplasmic where only some copies are mutated. Pathology arises when the number of heteroplasmic mutations crosses a

threshold level. Common diseases involving variants of mitochondrial DNA or mutations include the aforementioned AD and PD (Wallace, 1992), but also diabetes (Lowell and Shulman, 2005) and Leigh syndrome (de Vries et al., 1993). It is thought the pathological levels of ROS can cause somatic mutations in the mitochondrial DNA, and that accumulation of these mutations contributes to the decline of mitochondrial function (Harman, 1992). Certain mutations are known to directly increase the production of ROS from the mitochondria, namely *8993T>G* which affects ATPase 6 and increases superoxide production beyond the capabilities of the cellular antioxidant system, triggering cell death (Geromel et al., 2001).

The neurodegenerative diseases outlined are well studied, often with the use model systems. Common model organisms in the study of mitochondrial defects and ageing are mice, however they have their limitations in the study of PD, as they do not present with the hallmark symptoms including tremors, unsteady gait and rigidity. Mice models also cannot replicate the loss of dopaminergic neurons seen in PD patients. Certain AD mice do not present with the amyloid plaques or neurofibrillary tangles that define the disease, and when they do present with these characteristics they no longer have problems with memory. Whilst no single model is perfect in the study of neurodegenerative diseases, *Drosophila melanogaster* are used very successfully and specific fly lines exist that display characteristic symptoms that are not seen in mouse models.

1.6 Using *Drosophila* to model oxidative stress

1.6.1 *Drosophila* as a model organism

Drosophila melanogaster, also known as the common fruit fly, was first established as a tool for genetic research by Thomas Hunt Morgan and has long since become a widely used model organism. The development of advanced genetic and molecular tools using *Drosophila* has accelerated our understanding of genetics and molecular biology allowing discoveries of developmental processes and disease mechanics. *Drosophila* are easily maintained at high numbers due to their small size and simple diet, making them ideal for raising and storing in the laboratory. A short life cycle

and high fecundity make *Drosophila* ideal for large-scale high-throughput experiments, with a generation time of 10-12 days at 25°C. The lifespan of *Drosophila* can range between 40-120 days depending on their environment and the presence of detrimental factors such as stress or poor diet, meaning that they can be successfully kept as live stocks as long as ample food and space is supplied. They are widely kept in small vials containing yeast/cornmeal-based food at 18°C and are transferred to a new vial every 4-5 weeks. The strong molecular-genetic toolset coupled with a high fecundity and short life cycle make *Drosophila* a cost effective model without compromising the integrity and impact of the research. Humans and *Drosophila* share a large number of developmental processes and structurally/functionally similar proteins. Following the genomic sequencing of *Drosophila* in 2000, it is thought that 77% of genes causing human disease have a functional homolog in *Drosophila,* and that many disease pathways are highly conserved (Adams et al., 2000, Reiter et al., 2001). The *Drosophila* genome consists of approximately 13,600 genes across 4 chromosomes including the sex chromosomes (X/Y) i.e. the first chromosome, and the autosomes or chromosomes 2, 3 and 4. A large array of human diseases and disorders are caused by mutations in genes orthologous to that of *Drosophila,* including neurological, metabolic, developmental and cardiovascular disorders as well as cancer (Bier, 2005). It is well within reason to say that the use of *Drosophila* in the study of genetics and human disease has contributed vastly to their understanding, proving *Drosophila* to be a robust and reliable model animal used with high efficiency as the focal point of many critical studies whilst still being cost effective.

1.6.2 The genetic toolbox of *Drosophila*

Drosophila are incredibly useful in genetic research due to the high number of well-established tools that have been generated. The existence of balancer chromosomes in *Drosophila* also strengthens their role as important model organisms. Balancer chromosomes bear inversions that allow the stable maintenance of lethal mutations as heterozygotes without the need for any selection process (Muller, 1918).They suppress autosomal recombination in females as well as carry markers that allow mutations or insertions to be tracked in stocks (Thompson, 1977, Rubin and Lewis,

2000). This is still not possible in mice giving *Drosophila* an edge as the ideal genetic model.

Another useful property of *Drosophila* is the availability of the UAS/GAL4 system, which allows for targeted gene expression. The system relies on two independent components, GAL4 and an upstream activating sequence (UAS). The GAL4 protein is encoded by 881 amino acids and was identified as a gene regulator in *Saccharomyces cerevisiae*, specific to the UAS (Laughon and Gesteland, 1984). It was established by Brand and Perrimon in 1993 and became a powerful asset in *Drosophila* research, revolutionising how we address gene function *in vivo* (Duffy, 2002). It is a bipartite approach in which the two components, the driver (GAL4) and responder (UAS) are maintained in separate fly stocks and can provide targeted gene expression in both a temporal and spatial fashion (Brand and Perrimon, 1993). Using the enhancer-trap GAL4 construct, *GAL4* was inserted into the genome where its expression is driven by the native genomic enhancers, many GAL4 lines have now been established, expressing GAL4 in a nearly every cell and tissue type, including motor neurons, muscles and glia. A gene containing the GAL4 binding sites in its promoter site is then introduced into the fly, becoming the UAS line; this gene could be your protein of interest or non-coding interfering RNA (RNAi). Crossing the UAS parent line to the GAL4 parent line completes the bipartite system where GAL4 will endogenously bind the UAS in the cell or tissue type allowing ectopic expression of the gene product. One very useful advantage of using the UAS lines is that it is transcriptionally silent until GAL4 is present, allowing controlled expression of gene products that may be toxic, lethal or cause reduced viability, obviating the maintaining of a healthy stock containing both elements together.

As mentioned previously, non-coding RNAs can be expressed in *Drosophila* that knock down expression of individually targeted genes. Since the discovery of double stranded RNA (dsRNA) the use of RNAi has become one of the most powerful reverse genetic approaches to manipulate the expression of genes *in vivo* (Fire et al., 1998, Perrimon et al., 2010). Since the *Drosophila* genome was sequenced several genome-wide RNAi resources have been constructed, allowing those in *Drosophila* research to acquire a vast number of fly lines, each specifically targeting individual

genes and collectively cover most of the genome, upwards of 91% of the total protein-coding genes.

The powerful genetic tool-set in *Drosophila* sets it apart from other animal models in genetic research. With many human-disease gene orthologues present in in the *Drosophila* genome and the ability to specifically target these in a variety of ways *in vivo* we can advance our understanding of disease genes. *Drosophila* are widely used in neuroscience, often through studying the neurons themselves, made possible by the easily accessible neuromuscular junction (NMJ) in the larvae.

1.6.3 The *Drosophila* 3rd instar neuromuscular junction synapse

The 3rd instar *Drosophila* larvae can be dissected to reveal the musculature that lies just within the cuticle (see Figure 1.3). The muscles are arranged in overlapping, striated fibres attached to the body wall, in a pattern that is repeated for each hemisegment. The muscles have been fully annotated and mapped for ease of identification. Each muscle is a single multinucleated cell formed by the fusion of myoblasts and forms part of a set of 30 muscles that make up each abdominal hemisegment from A2 to A7 (Keshishian et al., 1996). Differing slightly in its pattern is hemisegment A1, the most anterior hemisegment. Each hemisegment muscle receives innervation from 2 motor neurons, either the anterior intersegmental nerve (ISN), which innervates the dorsal muscle, or the posterior segmental nerve (SN), which innervates the ventral muscle (Johansen et al., 1989a, Johansen et al., 1989b).

We focus on muscle 6/7 of hemisegment A3, a very well characterised muscle widely used for its large accessible neuromuscular junction (NMJ) synapse. For this synapse, a measure of its growth can be calculated by counting the total number of boutons. Boutons are the pre-synaptic swellings along the synaptic arbour where neurotransmitter release is facilitated. This NMJ is part of the type I class of NMJs as it features only type I boutons and functions to innervate the body wall muscles. Type I NMJs have large boutons and short terminal branches, they are predominantly glutamatergic and two types of boutons are present, type Ib (big) and type Is (small) (Menon et al., 2013). Type II NMJs are neuromodulatory,

determining the excitation state and transmit octopamine and glutamate (Monastirioti et al., 1995). Following glutamate release from the pre-synaptic terminal, it binds to glutamate receptors (GluR) in the post-synaptic membrane of the muscle, leading to innervation. GluRs are receptor-gated ion pores and during *Drosophila* synaptogenesis they are expressed and eventually clustered at NMJ sites upon the muscle opposite the presynaptic processes. The clustering of GluRs requires muscle innervation, and without neural induction, the GluRs fail to localise correctly (Broadie and Bate, 1993).

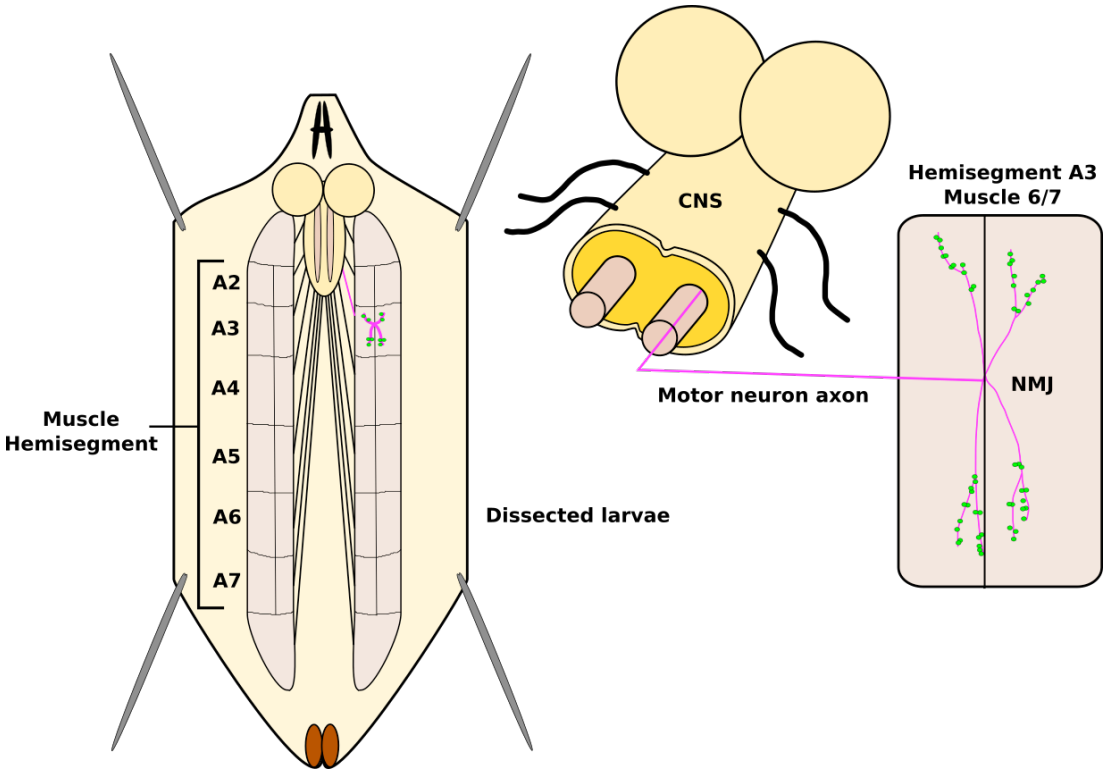

Figure 1.3 The larval neuromuscular junction (NMJ)

A representative diagram of a dissected larva showing the larval brain and its axonal projection that connects to the NMJ, allowing muscle innervation. The synapse (magenta) and synaptic boutons (green) are shown. Adapted with permission from Landgraf et al. (2003)

1.7 NMJ development

The NMJ is a chemical synapse; a specialised junction between cells that facilitates the transmission of neurotransmitters or smalls molecules allowing the traversal of information between the cells. *Drosophila* larval NMJ's have a degree of synaptic plasticity, allowing both structural and functional changes to occur during development and maturation. Synaptic plasticity is thought to be the foundation of learning and memory (Shen and Cowan, 2010, Menon et al., 2013).

The NMJ begins to develop approximately 9-10 hours after egg laying; it begins when the axonal growth cone reaches its target muscle, which is determined genetically. At the site of contact between the growth cone and muscle, small clusters of postsynaptic GluRs and Disks large (Dlg) form. The growth cone then differentiates into a presynaptic terminal, or synaptic bouton. Dlg is the *Drosophila* orthologue of the mammalian postsynaptic scaffolding protein PSD-95, and is critical for the postsynaptic assembly at glutamatergic synapses, specifically controlling glutamate receptor subunit composition (Chen and Featherstone, 2005). The bouton is the site of neurotransmitter storage and release; it houses many small, membrane-bound synaptic vesicles, which contain the neurotransmitter and dock at the active zones of the plasma membrane. Each bouton has multiple actives zones, each of which are apposed to the GluR clusters. Subsynaptic reticulum (SSR) forms around the larval presynaptic boutons, which become submerged deeper within the muscle. The SSR contains the neurotransmitter receptors and postsynaptic signalling complexes as well as scaffolding proteins required for the functionality of both (Rheuben et al., 1999, Ataman et al., 2006). The presynaptic bouton features small sections where synaptic vesicle exocytosis is restricted to which is termed the active zone. These areas house electron-dense projections and in *Drosophila* are referred to as the T bar (Zhai and Bellen, 2004, Südhof, 2012). In *Drosophila*, the active zones/T bars are home to the coiled-coil domain protein, Bruchpilot (BRP) which is required for the formation of the T-bar, calcium channel clustering, proper vesicle fusion and patterned synaptic plasticity (Kittel et al., 2006, Wichmann and Sigrist, 2010).

The formation of neurotransmitter receptor fields, specifically the GluR clusters, depends on the release of glutamate from the presynaptic terminal and is critical in forming the NMJ (Broadie and Bate, 1993). The NMJ is fully formed approximately 16 hours after the larval embryo is laid.

The full development of the post-embryonic larval NMJ in *Drosophila* requires several signalling pathways; some morphogenic pathways direct the overall development of the NMJ like transforming growth factor beta (TGF-β) signalling and Wingless (Wg) creating a basal synapse. Other pathways, MAPK signalling for example, control the size and strength of the synapse during development and augment growth. Autophagy and even environmental or cellular stresses including oxidative stress also play a role in controlling synaptic development.

1.7.1 Morphogenic signalling in NMJ development

The TGF-β family of ligands is a very large superfamily of proteins/ligands and plays a critical role in NMJ development in *Drosophila,* as well as having roles in cell growth, differentiation and apoptosis. The TGF-β family includes TGF-β proteins, bone morphogenetic proteins (BMPs), growth and differentiation factors (GDFs), nodal and activins. These stimulate type I and type II serine/threonine-kinase receptors, which regulates Smad-dependant transcription (Derynck and Zhang, 2003, Wu et al., 2010). Genetic studies of TGF-β signalling, specifically mutations in receptors and ligands of the family, have revealed synaptic defects (Sweeney and Davis, 2002, McCabe et al., 2003, Rawson et al., 2003, Koh et al., 2004). The BMP orthologue *glass bottom boat* (*Gbb*) was found to encode a protein that plays a role in the regulation of synapse growth in *Drosophila*. *Gbb* mutants exhibit reduced NMJ synapse size and neurotransmitter release as well as dysfunctional presynaptic ultrastructure (McCabe et al., 2003). This was also shown to be a retrograde signal, as Gbb expression in the muscle rescued key aspects of the mutant phenotype, owing to the thought that the muscle has an important role in coordinating retrograde signalling for correct NMJ development. Presynaptic roles for TGF-β signalling in NMJ development have also been shown, the E3 ubiquitin ligase Highwire (Hiw) was found to negatively regulate synaptic growth at the NMJ. Mutants of *hiw* have severely overgrown synapses, displaying a larger overall

synapse as well as increased bouton number (Wan et al., 2000, McCabe et al., 2004). Hiw binds to the Smad protein, Medea (Med), which binds to Smad transcription factor Mothers against dpp (Mad) and is part of a presynaptic BMP signalling cascade consisting of 3 receptor subunits, Wishful thinking (Wit), Thickveins (tkv) and Saxophone (Sax). Transcription factor Mad and the type I receptors, Sax and tkv have been shown to have roles in structural and functional development of the *Drosophila* NMJ, and mutations in *wit*, which encodes the type II receptor displayed smaller synapses, fewer instances of spontaneous vesicle release and defective evoked junctional potentials (Marques et al., 2002, Rawson et al., 2003). However, postsynaptic markers such as Dlg and GluRs were normal in *wit* mutants, and the mutant phenotype was rescued by presynaptic expression of Wit in motor neurons only, not the muscle (Aberle et al., 2002).

The TGF-β superfamily as a whole plays a major role in NMJ development; this is highlighted by the presence of both positive (tkv, Wit, sax, Mad, med) and negative regulation (Daughters against dpp (Dad), Nervous wreck (Nwk)) (Sweeney and Davis, 2002, O'Connor-Giles et al., 2008) as well as both pre- and postsynaptic signalling, striking a balance in the regulatory signals that control NMJ growth and development.

Wnt/Wingless (Wg) play a pivotal role at the NMJ, regulating the formation of pre- and postsynaptic structure (Packard et al., 2002). This occurs through a heparin sulphate proteoglycan (HSPG) called perlecan/trol. Mutations in *trol* cause postsynaptic defects such as a reduction in the SSR as well as increased synaptic boutons at the *Drosophila* NMJ. Postsynaptic expression of the Frizzled (receptor for Wg) nuclear import Wg pathway rescued the postsynaptic defects, in contrast however presynaptic down-regulation of the canonical Wg pathway suppressed the overproduction of synaptic boutons. This suggests Trol bidirectionally regulates the pre- and postsynaptic activities of Wg, by distributing Wg at the NMJ (Kamimura et al., 2013).

1.7.2 MAPK signalling in NMJ development

A role for MAPK signalling in NMJ development has also been shown. Specifically, AP-1 of the JNK signalling pathway has been shown to regulate synapse number and strength during development, as well as long-term plasticity (Sanyal et al., 2002, Sanyal et al., 2003). As outlined above, AP-1 is a transcription factor consisting of either homo or heterodimers of basic leucine zipper proteins Fos and Jun, and is abundantly expressed in the larval motor neuron (Sanyal et al., 2003). AP-1 is activated by JNK, and as part of the JNK signalling pathway is under the control of a negative feedback loop where puc is a direct transcriptional output of JNK activation and acts to rapidly inhibit JNK signalling. To date, the major MAPK pathway shown to function during NMJ development is the Wnd/DLK-JNK pathway. Wnd encodes a JNKKK capable of activating downstream AP-1 (Collins et al., 2006). Aberrant activation of the Wnd/DLK-JNK pathway causes defective synaptic growth and axonal guidance, and loss-of-function mutations in the pathway can impede axonal regeneration after injury (Collins et al., 2006). Though I previously described a role for Highwire in TGF-β signalling, it also plays a major role in the negative regulation of this MAPK pathway. Hiw targets Wnd/DLK for degradation, which suppresses downstream MAPK/JNK signalling via binding to DFsn to restrain synaptic growth. However, *hiw* mutants display synaptic overgrowth, which was found to be a consequence of an inability to degrade Wnd. (Collins et al., 2006, Wu et al., 2007). In complex with Hiw, *SkpA* has also been shown to cause synaptic overgrowth when mutated, this coincides with elevated levels of Wnd, a MAPKKK, which in turn leads to an over activation of JNK signalling and consequently the synaptic overgrowth (Collins et al., 2006, Brace et al., 2014). Removing Wnd/JNK/Fos can attenuate the *hiw/SkpA/DFsn*-induced synaptic overgrowth, showing that JNK signalling is responsible for the increased synaptic growth in the *hiw* mutant and that Hiw normally acts to restrain Wnd/JNK signalling, and regulate this response (Collins et al., 2006).

The JNK signalling pathway also mediates autophagy, and changes in the regulation of autophagy can lead to changes in the NMJ growth.

1.7.3 Autophagy and NMJ growth

Autophagy is a lysosome-dependant degradation mechanism by which autophagosomes are formed. These encapsulate cytoplasmic waste material and transport it to the lysosome. The waste material is transferred into the lysosome through fusion of the loaded autophagosome and the lysosome. Lysosomal enzymes then digest the waste and recycle the resultant lipids, amino acids and sugars (Levine and Klionsky, 2004). Several autophagy (*ATG*) genes exist which are conserved in *Drosophila*, many of which have been mutated or transgenically manipulated in *Drosophila* stocks. Increasing the levels of atg1, an initiator of autophagy induction, has been shown to increase bouton count twofold, primarily though elevated levels of autophagy (Scott et al., 2007, Levine and Kroemer, 2008, Shen and Ganetzky, 2009). Mutations in *atg18* were shown to suppress the NMJ overgrowth in *atg1* overexpression tests, and removing both copies of either *atg1* or *atg18* reveals significant NMJ undergrowth, further suggesting that autophagy plays a large role in NMJ growth (Shen and Ganetzky, 2009). The role of autophagy in NMJ overgrowth involves Hiw, specifically elevated levels of autophagy are thought to reduce levels of Hiw which in turn causes the NMJ overgrowth via a reduction in the inhibition of Hiw upon JNK signalling. Conversely, mutations in *atg* genes lead to an accumulation of Hiw, which increases the level of inhibition on JNK signalling thereby reducing NMJ growth (Shen and Ganetzky, 2009). Following this, oxidative-stress induced synaptic overgrowth is blocked when *atg* mutants are introduced, and JNK and autophagy are contributing to this synaptic overgrowth via the nerve and the muscle. Hiw and Wnd are both found presynaptically, not post-synaptically in muscle which suggests a role for both autophagy and oxidative stress in the regulation of synapse growth that may be independent of Hiw (Milton et al., 2011).

As it emerges, JNK signalling and autophagy are closely regulated in their role in NMJ growth in *Drosophila*, and both are regulated by oxidative stress, which unsurprisingly has a role in the regulation and development of the NMJ.

1.7.4 ROS and neuronal development

As outlined above, ROS are known to activate JNK signalling, and in doing so confers cellular resistance to oxidative damage (Wang et al., 2003). The activation of JNK/AP-1 leads to an array of protective genes being expressed, increasing the tolerance to oxidative stress. Overexpression of the *Drosophila* JNK protein Basket (Bsk) increased resistance to the ROS-generating compound, paraquat, reducing the number of flies that died during a survival test (Arking et al., 1991). Similarly, resistance to paraquat is observed in *puc* mutant heterozygotes, which exhibit increased JNK activity (Wang et al., 2003). However, flies heterozygous for the hypomorphic bsk^{2} allele that exhibit decreased JNK signalling are more sensitive to paraquat treatment, and a greater number died during the survival test (Wang et al., 2003). The role of JNK signalling within neurons is critical, as activation offers increased tolerance to ROS. This is vital in neurons, which are rich with mitochondria and energetically demanding, generating relatively high amounts of ROS. This renders neurons particularly susceptible to oxidative stress due to a relatively low antioxidant defence system. However, ROS are also important signalling molecules in the development of neurons. A low antioxidant level is required for correct development of maturing neurons, and Nrf2 signalling, the second major antioxidant pathway after JNK signalling, is actively repressed in the developing forebrain neurons of mice to ensure correct development (Bell et al., 2015). Ectopic expression of Nrf2 inhibits neurite outgrowth and synaptogenesis, lowering the activity of ROS-dependent JNK and Wnt signalling. It is proposed that the epigenetic repression of Nrf2 helps to create an environment that increases the activation of JNK and Wnt signalling allowing neurons to develop properly, at the cost of low antioxidant defences (Bell et al., 2015). Activation of JNK signalling via ROS is therefore critical to the development of the synapse; not only is AP-1 beneficial for synaptic number and strength, it also protects the cell by lowering the ROS level after the synapse has developed (Sanyal et al., 2003).

However, ROS are highly damaging and without the tight regulation from various signalling pathways can lead to dysfunction and disease with age. The low antioxidant defence that allows the neuron to initially develop correctly eventually

may fail to combat the inevitable rise in ROS, leading to the onset of oxidative stress and disease.

1.8 *Drosophila* as a model for oxidative stress and age-related neurodegenerative diseases

The use of *Drosophila* in the study of age-related neurodegeneration is extensive. Due to their short lifespan, longevity and ageing are easily studied in *Drosophila* and, most human neurodegenerative disease genes have homologs in the fly and can often produce a disease phenotype. The large genetic toolbox allows these disease genes to be characterised and large-scale genetic screens can be performed to identify enhancers or suppressors of genes that exacerbate or alleviate the disease symptoms. Screens of compounds can also be performed to identify potential drugs that could improve disease phenotypes, and this is easily tested using *Drosophila* as the drug can be fed to both the larvae and adult fly by mixing it with specifically designed instant food (Hirth, 2010). Neurodegenerative diseases that have been successfully studied using *Drosophila* include PD, AD and tauopathies, each of which has at some stage implicated JNK/AP-1 signalling in the onset or progression of the disease. Much is known about the role of JNK signalling in ageing and oxidative stress-related neurodegenerative disease. The downstream transcription factors, Fos and Jun have also been extensively studied, but much is left to learn about their specific role in the oxidative stress response and particularly within neurons. AP-1 has been shown to become differentially activated in response to ROS, depending on the source of ROS from within the cell (Milton et al., 2011). ROS generated from the cytosol activates the Fos/Fos homodimer of AP-1, and mitochondrial ROS activates the Fos/Jun heterodimer. This finding indicates that Fos and Jun may have more complex roles in the oxidative stress response than previously thought, and elucidation of this role could reveal cellular mechanisms of ageing and diseases that have not previously been appreciated.

1.9 Aims

This project will aim to investigate the role of Fos and Jun (AP-1) when subject to oxidative stress in the nervous system and will try to elaborate upon the already well-characterised JNK signalling pathway by identifying downstream binding partners during oxidative stress responses in neurons. The chapter specific aims are outlined below:

1. Determine the role of AP-1/JNK signalling in a *Drosophila* model of oxidative stress in neurons.

2. Identify neuronal binding partners of Fos and Jun and determine how they might change during conditions of oxidative stress to generate response specificity.

3. Elucidate the relationship between our novel interacting protein Punch and AP-1 in the oxidative stress response in neurons.

2. Materials and Methods

2.1 *Drosophila* husbandry and techniques

2.1.1 *Drosophila* stocks

During this investigation, *Drosophila* stocks were obtained from Bloomington Stock Centre (Indiana University), as a donation from other labs or generated via microinjection either by Cambridge or by our lab. Some stocks already within the labs repertoire were recombined to generate new stocks. A full list of utilised stocks is shown (see Table 2.1).

2.1.2 *Drosophila* husbandry

Stocks were maintained in 25cm^3 plastic vials (Narrow Polystyrene vials; Flystuff) containing approximately 7ml of Enriched fly food composed of 10g/l Agar (Agar, Pure powder; Acros Organics), 39.12g/l maize flour (Gluten-free organic maize flour), 37g/l Yeast (Pure Yeast, Lesaffre Human care; Lynside), 93.75g/l Sucrose (Sucrose, analytical; Fischer Scientific) and 6.75ml/l Propionic Acid (Acros Organics).

Experimental stocks were raised on instant food (Formula 4.24; Carolina Biological Supplies) containing 10% Ethanol-Yeast paste (inactivated) plus pharmacological agents as required. Instant food was prepared in plastic vials using 3g of instant food and 10ml of ddH_2O and allowed to saturate fully. Inactivated yeast was prepared by mixing 20g of dried yeast (Dried active baking yeast; Allinson) with 100ml ddH_2O, forming a thin yeast paste. This was repeatedly boiled to inactivate the yeast and mixed to reduce the volume to 50ml creating a thick yeast paste, which is stored at 4°C. Approximately 1ml of inactive yeast paste is heated until dry, allowed to cool and mixed with 10% ethanol (Fischer Scientific) to rehydrate before adding to the instant food. Pharmacological agents were made up in 10% ethanol and mixed into the dried yeast paste when required. Vials were plugged with cotton wool (cotton balls for 25mm vials; Flystuff) to prevent flies escaping and to allow the passage of air.

Some experiments required the flies to be starved overnight before treatment, this was performed using fly cages and 2% agar plates which keep the flies hydrated. Agar plates were made up using 20g/l agar (Agar Technical, Agar No.3; Oxoid microbiology products; Thermo scientific) in ddH_2O, heated until clear and allowed to cool to 50°C before pouring 20ml into an empty plastic petri dish (90mm petri dish, single vent; Sterilin, Thermo scientific).

Egg collection in preparation for microinjection requires large numbers of flies to be kept in cages on plates with nutritional value. Apple agar plates were used, made up using ddH_2O and composed of 50g/l sucrose (Fischer Scientific), 20g/l agar (Agar Technical, Agar No.3; Oxoid microbiology products, Thermo scientific) and 100ml/l apple juice which is added after the solution is boiled and cooled to 50°C.

Stocks were maintained at 18°C and are transferred to new food every 4-5 weeks. Experimental crosses were all performed at 25°C and transferred to new food every 3-4 days for as long as required. Fly selection and observation was performed whilst the flies were anaesthetised, achieved via transferring flies to a porous pad connected to a compressed CO_2 gas cylinder (Dutscher Scientific, UK). Dissection microscopes (Stemi 2000 dissection microscope; Zeiss) were use to view the flies.

Table 2.1 A list of *Drosophila* stocks used throughout this investigation

Stock	Chromosome	Description	Source
WILD-TYPES			
Canton-S (*CS*)	n/a	Wild-type, red eyes	Sweeney Lab Stock
w^{1118}	n/a	Wild-type, white eyes	Sweeney Lab Stock
BALANCER STOCKS			
CyO/Sco	Second	Second Chromosome Balancer	Sweeney Lab Stock
CyO-GFP/*Sco*	Second	Second Chromosome Balancer	Kornberg Lab (UCSF,USA). Lab Stock

TM3/TM6b	Third	Third Chromosome Balancer	Sweeney Lab Stock
CyO/If; TM6b/MKRS	Second and Third	Second and Third Chromosome Balancer	Sweeney Lab Stock
CyO-GFP/If; TM6b/MKRS	Second and Third	Second and Third Chromosome Balancer	Kornberg Lab (UCSF,USA). Lab Stock
GAL4 STOCKS			
elavGAL4/*TM6b*	Third	Embryonic lethal abnormal vision promoter :Pan neuronal driver	Goodman Lab (UCSF, USA) (Donation). Lab Stock
SpinGAL4/*TM6b*	Third	Spinster Promoter: Pre- and Post-synaptic driver	(Nakano et al., 2001). Lab Stock
MHCGAL4/*TM6b*	Third	Myosin heavy chain promoter: Muscle driver	Goodman Lab (UCSF, USA) (Donation). Lab Stock
nSybGAL4/*CyO*-GFP	Second	Neuronal synaptobrevin promoter: Pan neuronal driver	Goodwin Lab (Oxford, UK). Lab Stock
OK6GAL4/*CyO*-GFP	Second	Motor neuronal driver	O'Kane Lab (Cambridge, UK). Lab Stock
actin^{5C}GAL4	Second	Actin driver	(Ito et al., 1997). Lab Stock
UAS STOCKS			
UAS-*NTAP-Fos*/*CyO*	Second	N-terminally TAP-tagged Fos isoform B	Generated during this project
UAS-*NTAP-Jun*/*CyO*	Second	N-terminally TAP-tagged Jun isoform A	Generated during this project
UAS-*NTAP-empty*	Second	Empty vector, Tap-tag	Sparrow Lab

vector/CyO		only	(Donation)
UAS-*fos*^{DN}	Third	Impaired transcription activity	(Eresh et al., 1997). Lab Stock
UAS-j*un*^{DN}	Second	Impaired transcription activity	(Eresh et al., 1997). Lab Stock
UAS-*ask1*^{DN}	Second	ASK without kinase activity	(Kuranaga et al., 2002). Lab Stock
UAS-*mCD8*-GFP	Second	Mmus/cd8a fused with GFP; labels cell membrane with GFP	(Lee and Luo, 1999). Lab Stock
UAS-*Punch*	Third	Wild-type Punch isoform A	Generated during this project
UAS-*Punch-RNAi P[TRIP.HMS02399]*	Second	RNAi to reduce Punch activity	Bloomington Stock Centre
UAS-*PunchA-WT*	Third	Wild-type Punch isoform A	O'Donnell Lab (donation)
UAS-*PunchA-S37E*	Third	Altered Punch isoform A sequence at Serine 37 to Glutamic acid	O'Donnell Lab (donation)
MUTANTS			
SOD1^{n1}*/TM6b*	Third	EMS point mutation; Loss of *SOD1*	(Parkes et al., 1998) Lab stock
SOD1^{n64}*/TM6b*	Third	EMS point mutation; Loss of *SOD1*	(Parkes et al., 1998) Lab stock
puc^{E69}*/TM6b*	Third	puckered LACZ reporter(P-element)	(Ring and Martinez Arias, 1993) Lab stock
dad^{J1E4}*/TM6b* (referred to as *dad*^{lacz} in text)	Third	dad LACZ reporter (P-element)	(Tsuneizumi et al., 1997) Lab stock
Punch^{EY02616A}*/CyO*-GFP	Second	Transgenic insertion (P[EPgy2]) disrupting Punch expression	Bloomington Stock Centre
Punch^{r1}*/CyO*-GFP	Second	In(2R)Pur1, spontaneous	(Mackay et al., 1985).

		chromosomal inversion at 57C3-57C4;57D13-57E2; disruption of Punch expression	Bloomington Stock Centre
Df(2R)Exel6072/CyO-GFP	Second	Chromosomal deletion at 57B16--57D4, *Punch* deficient	Bloomington Stock Centre
Df(2R)ED3791/CyO-GFP	Second	Chromosomal deletion at 57B1--57D4, *Punch* deficient	Bloomington Stock Centre
Ddc^{DE1}/*CyO*-GFP	Second	EMS mutation affecting *dopa decarboxylase*	(Bishop and Wright, 1987). Lab Stock
jra^{lA109}/*CyO*-GFP	Second	EMS point mutation within *Jra*	(Hou et al., 1997). Lab Stock
$jra^{76\text{-}19}$/*CyO*-GFP	Second	700bp deletion within *Jra* gene	(Hou et al., 1997). Lab Stock
kay¹/TM6b	Third	Point mutation/deletion of Exon 1 within *kay* gene	(Nüsslein-Volhard et al., 1984)
kay²/TM6b	Third	Hypomorphic mutation within the *kay* gene	(Nüsslein-Volhard et al., 1984). Lab Stock
hiw^{ND9}/Y	First	Highwire null mutation	(Wan et al., 2000). Lab Stock
OTHER TRANSGENES			
Jra-GFP.FLAG	Third	C-terminally GFP.FLAG tagged Jun isoform A, B and C	Bloomington Stock Centre
kay-GFP.FLAG	Second	C-terminally GFP.FLAG tagged kay isoform A, B, D and F	Bloomington Stock Centre

2.1.3 Crossing schemes

2.1.3.1 Crosses

Crosses were performed using virgin females and males of the required genotype. Virgin females were selected either by observation of the meconium (first faecal matter observed as black spot in the abdomen of freshly emerged flies), if the wings were unexpanded or if the fly was known to be less than 8 hours old. Virgin females were kept separate from males for at least 3 days, laid eggs were checked for hatching to ensure no mating has occurred.

2.1.3.2 Balancer chromosomes

Balancer chromosomes were used in *Drosophila* to track mutant alleles or insertions/transgenes. These carry dominant phenotypic markers that are easily and reliably followed in the stocks. Recombination is prevented by the presence of large chromosomal inversions, permanently keeping the stock in a heterozygous state and preventing the loss of your genotype of interest (see Figure 2.1). The balancers used to maintain stocks on the 2nd chromosome were *CyO* and *CyO-GFP*, which display curly wings as adults. The presence of GFP allows the selection of appropriate larvae, as GFP can be detected at this stage using a fluorescence microscope (MZFL III fluorescence scope; Leica). *CyO* is often kept in stock with *Sco* on the opposing chromosome (*CyO/Sco*); *Sco* is a phenotypic marker on the 2nd chromosome, which lacks bristles on the scutellum. The 3rd chromosome is maintained using the balancer *TM6b* that carries *humoral* as its dominant marker in adults, showing increased 'shoulder' bristles. *TM6b* also carries *tubby*, causing shorter and fatter adults and larvae. *TM3* is another 3rd chromosome balancer, which carries *stubble*, which is identified as shortened bristles on the adult thorax. Combined, *TM3/TM6b* exhibit the *ebony* phenotype, which darkens the cuticle of the fly. Often, 2 mutations or transgenes are desired in one stock, which can be achieved using double balancers. In these flies, *If* (*irregular facets*) and *MKRS* are used as markers. *Irregular facets* is a dominant mutation on the 2nd chromosome and results in smaller eyes with fused ommatidia. *MKRS* is a partial balancer marker on the 3rd chromosome carrying the *stubble* mutation.

2.1.3.3 Recombination

It is often necessary to generate stocks carrying 2 separate genetic features that are unfortunately on the same chromosome in their original stocks. Recombination of the genetic features allows us to generate stocks carrying both upon a single chromosome, allowing the stock to be balanced also. In *Drosophila*, only females undergo meiotic recombination. Recombination occurs by crossing the 2 stocks together and selecting the females that carry both genetic features. The females were then crossed to a balancer stock and recombinants selected based on whether they carry attributes from both of the original stocks on one chromosome. This can be checked using eye colour, through complementation or by polymerase chain reaction (PCR).

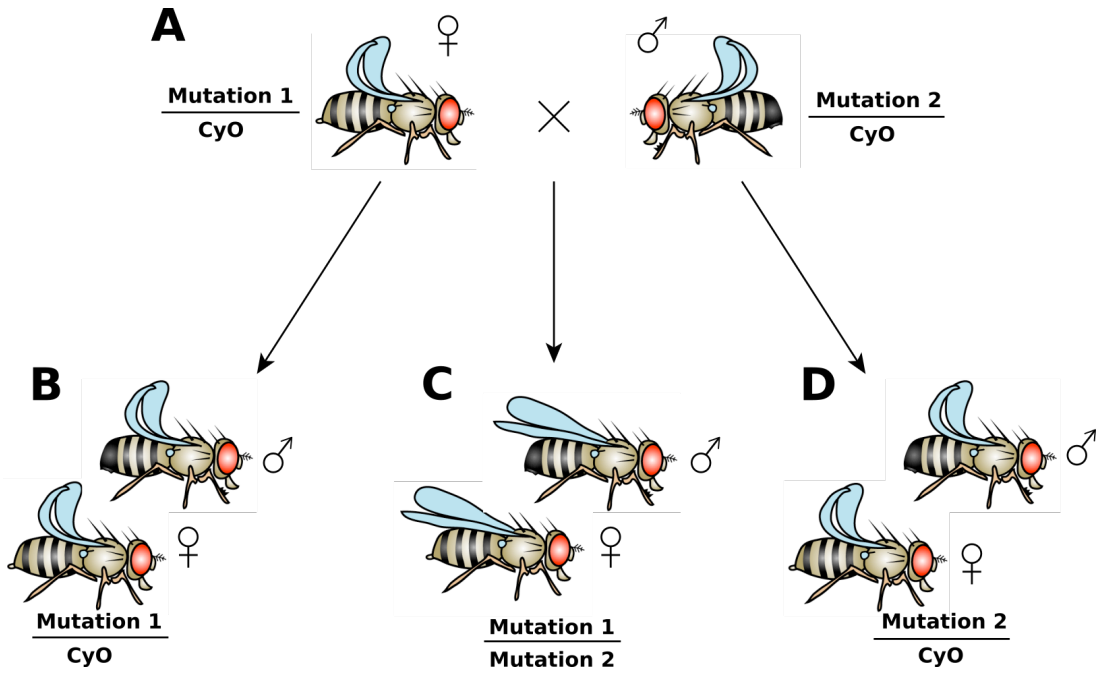

Figure 2.1 Using balancer chromosomes to maintain stocks and track mutations through chromosomal segregation

Balancer chromosomes are used during crossing schemes to track mutations and select the desired genotype of offspring. They also maintain mutations/transgenes within a stock. These 'balancers' are recessive lethal mutations, which prevent the loss of the mutations or transgene and are phenotypically distinct due to the presence of a dominant visible mutation. One example of this is the second chromosome balancer, *CyO* which display curly wings. Crossing 2 stocks that are heterozygous for *CyO* and the desired mutation (A) results in 3 different outcomes; a heterozygous offspring of either mutation 1 (B) or 2 (D) over *CyO*, which have curly wings and a stock expressing both mutations 1 and 2, which display straight wings as *CyO* is not present. Using the phenotypic marker, we can follow crosses and select the desired outcome. Fly images designed using the Genotype Builder from Roote and Prokop (2013).

2.2 Immunohistochemistry and imaging

2.2.1 Third instar larval dissections, fixation and antibody staining

Wandering 3rd instar larvae were selected and dissected in PBS (Phosphate Buffered Saline; Gibco® Invitrogen) and fixed in 3.7% formaldehyde (37% formaldehyde solution; Sigma-Aldrich) in PBS for 7 minutes. Wandering larvae were defined by their exit from the food and movement up the side of the vial; the correct genotype was selected when necessary. The dissection took place in a drop of PBS upon a Sylgard dish (Silicone elastromer kit; Dow Corning). Larvae were dissected by pinning down the anterior and posterior ends of the larvae (Austerlitz Insect Pins 0.1mm; Fine Science Tools) and cutting laterally up the dorsal side using scissors (Vannas Spring Scissors - 3mm Blades; Fine Science Tools). The innards were removed using forceps, leaving the brain intact if necessary. The muscle wall was pinned out in four places forming a rectangle. The PBS was removed and several drops of 3.7% formaldehyde/PBS were added atop the dissected larvae. This was left for at least 7 minutes before unpinning.

Larval dissections were transferred to 1.5ml Eppendorf tubes and were washed in 5 x 3 minutes of 1ml PBS-T (PBS + 0.1% Triton™ X-100; Sigma) before adding primary antibodies staining overnight at 4°C upon a nutator. Dissections were washed again, 5 x 3 minutes of 1ml PBS-T before secondary staining for 2 hours at room temperature upon a nutator. Dissections were washed again, 5 x 3 minutes of 1ml PBS-T before suspending in 70% glycerol/30% PBS (Fischer Chemicals) at 4°C overnight. Dissections were mounted upon microscope slides in mounting media (VECTASHEILD® H-1000; Vector Labs). Coverslips were placed on the preparations and sealed with nail varnish.

Table 2.2 A list of primary antibodies used for larval stains throughout this investigation

Primary Antibody	Stains	Conc^{n}	Host	Source	Comments
Anti-Horseradish-peroxidase-Cy3 (HRP-Cy3)	Neuronal tissue	1:200	Goat	Jackson Laboratories (#111-035-144)	Polyclonal affinity purified, whole protein
Anti-synaptotagmin (Anti-SYT91)	Synaptic boutons	1:2000	Rabbit	Sweeney Lab	Polyclonal serum, whole protein
Anti-Fos88	Fos/kayak	1:1000	Rabbit	Sweeney Lab	Polyclonal serum, whole protein
Anti-Fos89	Fos/kayak	1:1000	Rabbit	Sweeney Lab	Polyclonal serum, whole protein
Anti-Jun59	Jun/Jra	1:1000	Guinea Pig	Sweeney Lab	Polyclonal serum, whole protein
Anti-Jun60	Jun/Jra	1:1000	Guinea Pig	Sweeney Lab	Polyclonal serum, whole protein
Anti-Punch182	GTP cyclohydrolase 1/Punch	1:1000	Rat	Sweeney Lab	Polyclonal serum
Anti-Punch183	GTP cyclohydrolase 1/Punch	1:1000	Rat	Sweeney Lab	Polyclonal serum, whole protein
Anti-Punch	GTP cyclohydrolase 1/Punch	1:1000	Rabbit	O'Donnell Lab	NA

Table 2.3 A list of secondary antibodies used for larval stains throughout this investigation

Secondary Antibodies	Concentration	Source	Comments
Goat Anti-Rabbit-FITC	1:200	Jackson Laboratories (#111-095-003)	Affinity purified, Polyclonal whole IgG
Goat Anti-Rabbit-Alexa fluor® 405	1:200	Jackson Laboratories (#111-475-003)	Affinity purified, Polyclonal whole IgG
Goat Anti-Guinea Pig-Cy3	1:200	Jackson Laboratories (#106-165-003)	Affinity purified, Polyclonal whole IgG
Goat Anti-Rat-FITC	1:200	Jackson Laboratories (#112-095-003)	Affinity purified, Polyclonal whole IgG
Goat Anti-Rat-Cy3	1:200	Jackson Laboratories (#112-165-003)	Affinity purified, Polyclonal whole IgG

2.2.2 Imaging and analysis of *Drosophila* neuromuscular junctions

The quantification and analysis of the *Drosophila* NMJ began with antibody staining, using anti-horseradish-peroxidase-Cy3 (HRP-Cy3) and anti-synaptotagmin (Anti-SYT91)/goat-anti-rabbit-FITC (see Table 2.2 and Table 2.3).

2.2.2.1 Synaptic bouton number analysis and NMJ imaging

Using a fluorescence microscope (Axiovert 200 invert fluorescence microscope; Zeiss), muscles 6/7 at muscle wall segment A3 were identified, and the NMJ lies between muscles 6/7. Each NMJ had its boutons counted using the 40x objective and an image of the muscle was taken using the 10x objective in order to normalise the bouton number according to muscle size. The mean muscle surface area (MSA) of wild-type larvae, which are a cross of w^{1118} and *Canton-S* (w^{1118}*/CS)* and will hereby be referred to as WT, in control food was calculated using ImageJ to measure the length and width of the muscle in pixels, which is converted to μm by ImageJ. The MSA was used to normalise the bouton count from each NMJ (divided by its MSA and multiplied by the mean MSA) in order to adjust for muscle size changes in the larvae. Normalised bouton counts from each test were averaged and the standard error of the mean (SEM) calculated.

One NMJ from each test was imaged using a confocal microscope (LSM 880 on a motorised invert microscope; Zeiss) using a 63x objective (oil immersion). A Z-stack was taken covering the whole NMJ and visualising both the HRP-Cy3 channel and SYT91-FITC channel generating a set of images, which are compiled using Z Project on Image J. A scale bar was generated using Image J and Inkscape was used to build the final image, used to represent the anatomy of NMJs from that experiment.

2.2.2.2 Branch number and NMJ length quantification

Using a confocal microscope (LSM 880) on a 20x objective, 1 NMJ per larvae was imaged by taking a Z-stack on the Cy3 channel only. This generated an image of the whole NMJ when compiled in ImageJ; it was saved as a .tif file. This file was loaded using NeuronJ, an extension for ImageJ that allows the quantification of branch number and NMJ length. The NMJ was manually traced over its entirety. A branch was defined here as any protrusions from the main stem of the motor neuron that consists of more than 2 boutons. Once measured, the data was recorded and normalised using the same process previously mentioned.

2.3 Treating *Drosophila* with pharmacological agents

Each treatment uses 10% ethanol to ensure consistency between tests; controls are also raised in food containing 10% ethanol in yeast paste. Pharmacological agents were made up in 10% ethanol and mixed into yeast paste before applying to saturated instant food (see section 2.1.2).

Various pharmacological agents were used (see Table 2.4). Oxidative stress was induced in *Drosophila* by feeding them diethyl maleate (DEM) (Diethyl Maleate 97%; Sigma-Aldrich). Various concentrations of DEM were used. Oxidative stress was relieved using the antioxidant, Trolox (Trolox®, 97%; Acros Organics). We also treated *Drosophila* with Levodopa (L-DOPA) (3, 4-dihydroxy-L-phenylalanine ≤ 98%; Sigma-Aldrich).

Table 2.4 Pharmacological agents and their concentrations used throughout this investigation

Chemical	Conc^{n}	MW	Vehicle and volume	Amount used
DEM	30mM	172.18	10% Ethanol/ 100ml	517µl
DEM	10mM	172.18	10% Ethanol/ 100ml	172µl
DEM	3mM	172.18	10% Ethanol/ 100ml	51.7µl
DEM	1mM	172.18	10% Ethanol/ 100ml	17.2µl
Trolox	10mM	250.29	10% Ethanol/ 10ml	25.029mg
L-DOPA	1mg/ml^{-1}	197.19	10% Ethanol/ 10ml	10mg

2.4 Molecular biology

2.4.1 Polymerase chain reaction (PCR)

PCR reactions were performed using PCR master mix, consisting of 25 units/ml *Taq* DNA polymerase, *Taq* reaction buffer pH 8.5, 200µM of each dNTP and 1.5mM $MgCl_2$ (PCR Master Mix, 2x; Promega), 1µM of each primer and approximately 1-2ng of plasmid DNA, all of which were combined into PCR reaction tubes (0.2ml PCR tube, Flat cap; STARLAB) kept on ice. Nuclease-free water was used to top up the reaction volume to 20µl. Reactions were run for 30 cycles in a PCR machine (TC-512 PCR Thermal cycler 0.2 x 96; Techne). PCR cycles are detailed below (see Table 2.5). Primers were designed by myself and synthesised by Eurogentec UK. A full list of primers used in this project is shown below (see Table 2.6).

Table 2.5 PCR reaction cycles

Number of cycles	Temperature (°C)	Time (Mins)	Stage
1	95	5	Denaturation
30	95	0.5	Denaturation
	5°C lower than lowest primer melting temperature	1	Annealing
	68	1 per kb	Extension
1	72	10	Final extension
1	4	NA	Hold

Table 2.6 Primers used in PCR throughout this investigation

Primer Name	Sequence
5' NTAP Fos	GCA CTG AAT TCG ATG ACG CTG GAC AGC TAC AAC
3' NTAP Fos	CCT CGA GGC TTA TAA GCT GAC CAG CGG GGA
5' NTAP Jun	CTG CAG AAT TCA ATG AAA ACC CCC GTT TCC GCT
3' NTAP Jun	CCT CGA GGC TTA TTG GTC TGT CGA GTT CGG
5' Punch	ACC AGA AGA TCT ATG AGC TTT ACC CGC CAA
3' Punch	CCT GCG TCT AGA TTA TTT GCT ATT GAC TAA GTT CAG
3' Punch + HA tag	CCTGCGTCTAGATTAAGCGTAATCTGGAACATCGTATGGGT ATTTGCTATTGACTAAGTTCAG
5' pUAST	CTG CAA CTA CTG AAA TCT GC
3' pUAST	ATC TCT GTA GGT AGT TTG TCC A

2.4.2 DNA gel electrophoresis

Agarose gel electrophoresis was performed to analyse PCR products and DNA recovered from restriction digests. Agarose gels (100ml) are made at 0.7% in TAE buffer, which consists of 40mM Tris acetate and 1mM EDTA at pH 8.3. 10µl of SYBR® safe (SYBR® Safe DNA gel stain; Invitrogen) was added to allow visualisation of DNA when exposed to blue light. The gel was submerged in TAE buffer in the electrophoresis tank. DNA was prepared for loading into the gel by mixing with loading dye, consisting of 0.25% w/v bromophenol blue and 30% glycerol v/v in dH_2O. The volume of loaded DNA depends on the purpose of the gel, if run for gel extraction approximately 20µl, if running to check product, 7µl. Depending on the size of expected results, either a 1kb or 100bp DNA ladder (NEB) was run beside DNA samples. Electrophoresis is performed at 100v.

2.4.3 Gel extraction for DNA purification

DNA fragments were cut from the agarose gel using a blade and placed into individual 1.5ml Eppendorf tubes. Gel extraction was performed using a kit (QIAquick® Gel Extraction Kit; Qiagen) and following the provided instructions. A NanoDrop (ND-1000 spectrophotometer; Thermo Scientific) was used to determine the concentration of extracted DNA.

2.4.4 Restriction digest

DNA fragments were prepared for plasmid insertion by generating sticky ends through restriction endonuclease digestion. This allows for the insertion of DNA into plasmids, which are digested using complimentary restriction enzymes. This technique can also be used to cut DNA from plasmids; either for transferring into a different plasmid or to check the cloning has worked correctly. Appropriate restriction enzymes and buffers were incubated with the DNA sample requiring digestion, usually at a concentration that will provide at least 20ng of the smallest possible fragment, in order to visualise post gel electrophoresis. The incubation period was at least 2 hours at 37°C. The restriction enzymes were deactivated by

incubation at 80°C for 15 minutes. Cleaved fragments were analysed by gel electrophoresis.

2.4.5 DNA ligation

Cleaved DNA fragments were ligated into cleaved plasmids via a ligation reaction using 0.2µl of DNA ligase, 2µl of T4 ligase buffer (T4 DNA Ligase and buffer; Fermentas UK) and an appropriate concentration of DNA and plasmid made up to 20µl total volume. This was calculated using a ligation ratio, 3:1 insert:vector (ng) which equates to the following:

Insert mass (ng) = 3 x (insert length in base pairs/vector length in base pairs) x vector mas (ng).

Ligation reactions were performed overnight at 16°C followed by inactivation of the enzyme via 10 minutes at 65°C.

2.4.6 Transformation and amplification of plasmid DNA

We generated plasmids containing our DNA of choice for the eventual generation of new transgenic *Drosophila* lines, this requires the amplification of such plasmid and was achieved by transforming into *E.coli* cells (XL-1 Blue supercompetent *E.coli* cells; Stratagene USA). We transformed our plasmids following the provided instructions, however several changes are made. Instead of 100µl of cells, we used 50µl and scale all subsequent volumes accordingly. We also replaced the use of SOC media with Luria broth (LB) which consisted of 10g/l tryptone, 10g/l NaCl and 5g/l yeast extract. Plasmid transformation required 1µl of the ligation reaction. Transformed cells were plated on LB agar plates, which was standard LB plus 20g/l agar as well as 200µg/ml ampicillin (AMP) for antibiotic selection, and incubated overnight at 37°C.

Individual colonies were picked and transferred into culture tubes (14ml polypropylene round-bottom tubes; Falcon) containing 5ml LB plus AMP. Cultures were incubated for no more than 16 hours, usually 12-16 hours at 37°C with

vigorous shaking at 220 rpm. Glycerol stocks were generated from each culture in a 50:50 mix of glycerol:culture and stored at -80°C.

2.4.7 Plasmid purification

2.4.7.1 MiniPrep purification

Each transformed cell culture was checked for the presence of the plasmid + insert by purifying a sample of the culture via miniprep. 1.5ml of the overnight culture derived from the plated transformants was pelleted at 13000*g* for 2 minutes on a bench top centrifuge (Eppendorf Centrifuge 5417C; Eppendorf). The supernatant was removed and the pellet frozen at -20°C to improve miniprep efficiency. Minipreps were generated using the Qiaprep® Spin MiniPrep Kit (Qiagen, UK) and by following the instructions provided. A NanoDrop (ND-1000; Thermo Scientific) was used to determine the concentration before performing a restriction digest (see section 2.4.4) upon each sample followed by gel electrophoresis to check for the correctly sized insert. PCR was also performed (see section 2.4.1) using appropriate primers to amplify the sequence believed to be present in the amplified plasmid.

2.4.7.2 MidiPrep purification

Following the confirmation of plasmid + insert in the overnight culture (see section 2.4.6) a larger inoculation was set up. 100µl of the overnight culture was added to 100ml LB containing AMP and incubated at 37°C for up to 16 hours (12-16 hours). Cultures were transferred to 2x50ml conical bottom tubes (CELLSTAR® tubes; Greiner bio-one) and centrifuged at 6000rpm for 15 minutes at 4°C. The supernatant was discarded and the pellet frozen at -20°C to improve midiprep efficiency. Midipreps were generated using a kit (HiSpeed® Plasmid midi kit; Qiagen, UK) following the instructions provided.

2.5 Generating transgenic *Drosophila* lines and antibodies

During the course of this investigation, several fly lines were required that were unavailable. In light of this, we generated several *Drosophila* lines to accommodate our research. Several antibodies were also created.

2.5.1 Generation of UAS-NTAP-Fos and UAS-NTAP-Jun constructs

Transgenic *Drosophila* lines were created to express either Fos or Jun, along with an N-terminal tag, which allows its extraction following Tandem Affinity Purification (TAP). Plasmids containing the cDNA of Fos or Jun were miniprepped (see section 2.4.7.1) using overnight cultures of *E.coli* expressing either pOT-CG2275 LD25202 (Jun cDNA sequence) or pOT2-CG33956 SD04477 (Fos cDNA sequence) (see section 2.4.6). Restriction digests upon the purified plasmids excised the required cDNA sequences, this was performed using restriction enzymes EcoR1 and Xho1 and appropriate buffer (Fermentas) (see section 2.4.4). Primers were designed for both 5' and 3' ends of both the Fos and Jun sequences, used in PCR (see section 2.4.1) to amplify the Open Reading Frame (ORF) of Fos and Jun and also add EcoR1 and Xho1 sites flanking the protein coding sequence. Restriction digest using EcoR1 and Xho1 was performed upon the newly PCR-generated Fos and Jun cDNA and the pUAST-NTAP (GS) vector (see Figure 2.2) generating complimentary sticky ends to allow the insertion of Fos and Jun into the NTAP-vector (Veraksa et al., 2005). Gel extraction was performed (see section 2.4.3) to purify the correct sized Fos and Jun cDNA sequences as well as purify the NTAP-vector away from its cleaved sequence. Purified Fos and Jun cDNA sequences were ligated into the purified linear NTAP-vector (see section 2.4.5).

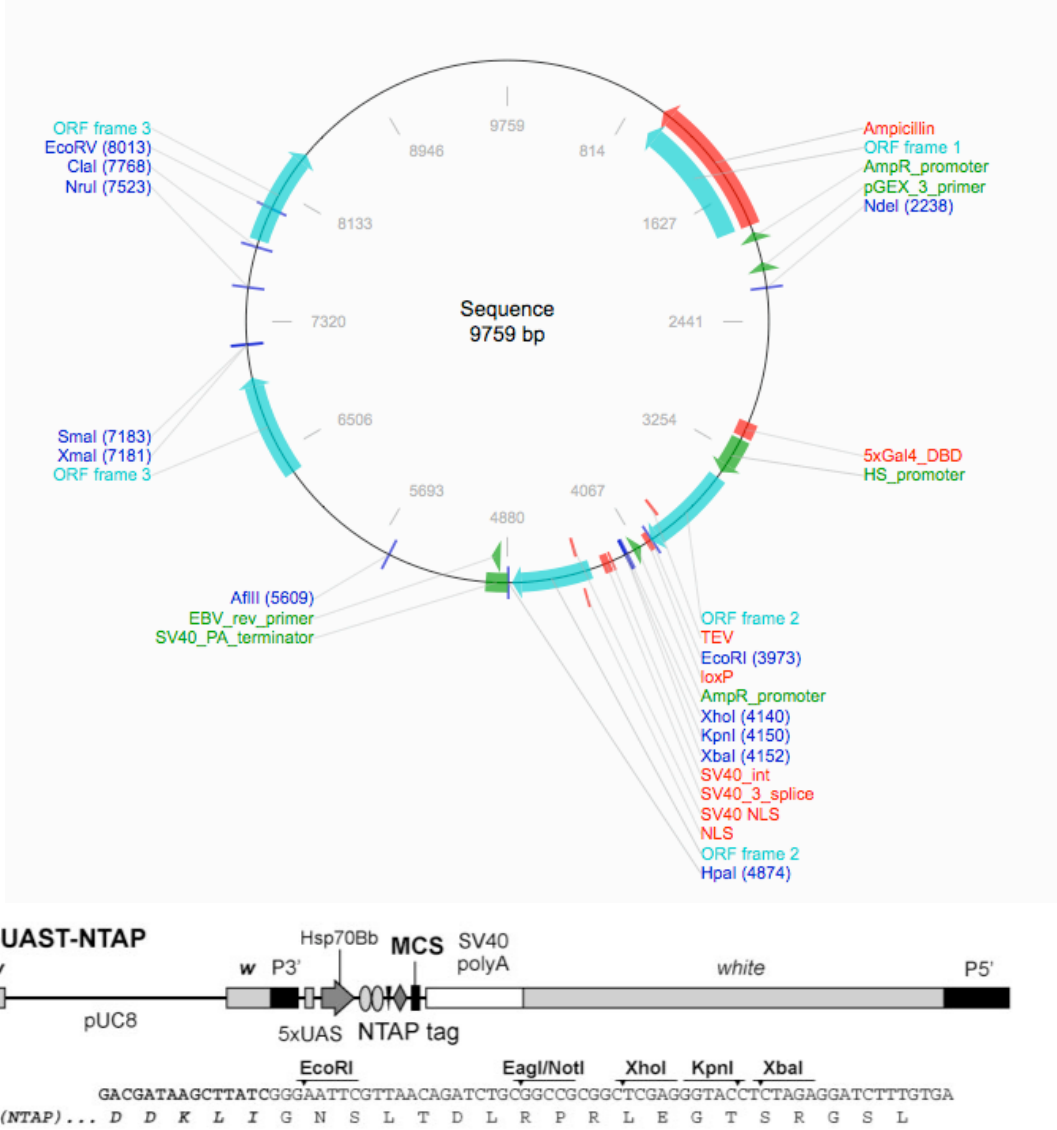

Figure 2.2 The pUAST-NTAP (GS) plasmid vector

The NTAP vector used during this investigation. The cDNA for Fos and Jun was inserted into the multiple cloning site (MCS) in the correct frame for expression with the addition of an N-terminal TAP-tag. The vector image was generated using the Addgene sequence analysis tool. The linear sequence is adapted with permission from Veraksa et al. (2005).

The UAS-NTAP-Fos, and UAS-NTAP-Jun vectors were separately transformed into super-competent *E.coli* cells (see section 2.4.6) Successful transformations were miniprepped (see section 2.4.7.1) checked and sequenced (University of York, Technology Facility, Genomics Lab) to ensure the sequence was correct. 100ml overnight cultures were set up using the successfully transformed cultures before purification via midiprepping (see section 2.4.7.2). The concentrations were determined using a NanoDrop (ND-1000; Thermo Scientific).

20µg (40µl) of purified UAS-NTAP-Fos and Jun vectors were mixed with 5µg (10µl) of transposing P-element (pπhsδ2-3). The DNA is precipitated by adding 5µl of 3M sodium acetate and 120µl of 100% ethanol then incubated overnight at -20˚C. Samples were centrifuged for 30 minutes at 13000 rpm, washed with 70% ethanol, air dried then resuspended in 20µl of Spradling Buffer (5mM KCl, 0.1mM PO_4, pH7.8).

Following the Sweeney lab protocol for microinjection, large numbers of w^{1118} embryos less than 1 hour old were collected and dechorinated using adhesive tape. Dechorinated embryos were lined up on adhesive tape upon a cover slip and allowed to dry for 10 minutes before covering in voltaleff oil. The coverslip is mounted on a microscope slide and microinjected with either NTAP-Fos or Jun. Surviving larvae are raised to adulthood and crossed to w^{1118} flies of the opposite sex. Those that successfully incorporated the NTAP-Fos or Jun vector expressed w^{+}, present because of the insertion, and displayed red/yellow eyes as adults. Stocks were generated from the successful survivors and balanced accordingly. The NTAP tag itself consisted of two IgG binding domains of Protein A (*Staphylococcus aureus*) and a streptavidin binding peptide separated by a Tobacco Etch Virus (TEV) protease cleavage site. This allows us to purify out our tagged proteins by incubating with IgG covered beads, the tag binds the beads and was then cleaved using TEV protease. Adding the cleaved proteins to streptavidin beads gives a second purification step. The still intact streptavidin binding peptide binds the beads, which were then purified and washed to remove any remaining contaminants. Our bound tagged-Fos and Jun were eluted along with any binding partners by boiling in Sodium Dodecyl Sulphate (SDS). The proteins were then identified via mass spectrometry (see section 2.6.4). Following successful

generation of the NTAP-fly stocks, we tested whether the tagged protein was still functional and able to compensate for loss of their respective endogenous protein. We expressed NTAP- tagged-Fos in a Fos null background (*kay*^{1}*/kay*^{2}) using actin^{5C}GAL4 (referred to as actinGAL4 onwards) and searched the progeny for those carrying the compound heterozygote combination (see Figure 2.3). This was repeated for NTAP-tagged Jun, expressing the construct in the Jun null background (*jra*^{IA109}*/jra*$^{76\text{-}19}$) via SpinGAL4 (see Figure 2.4).

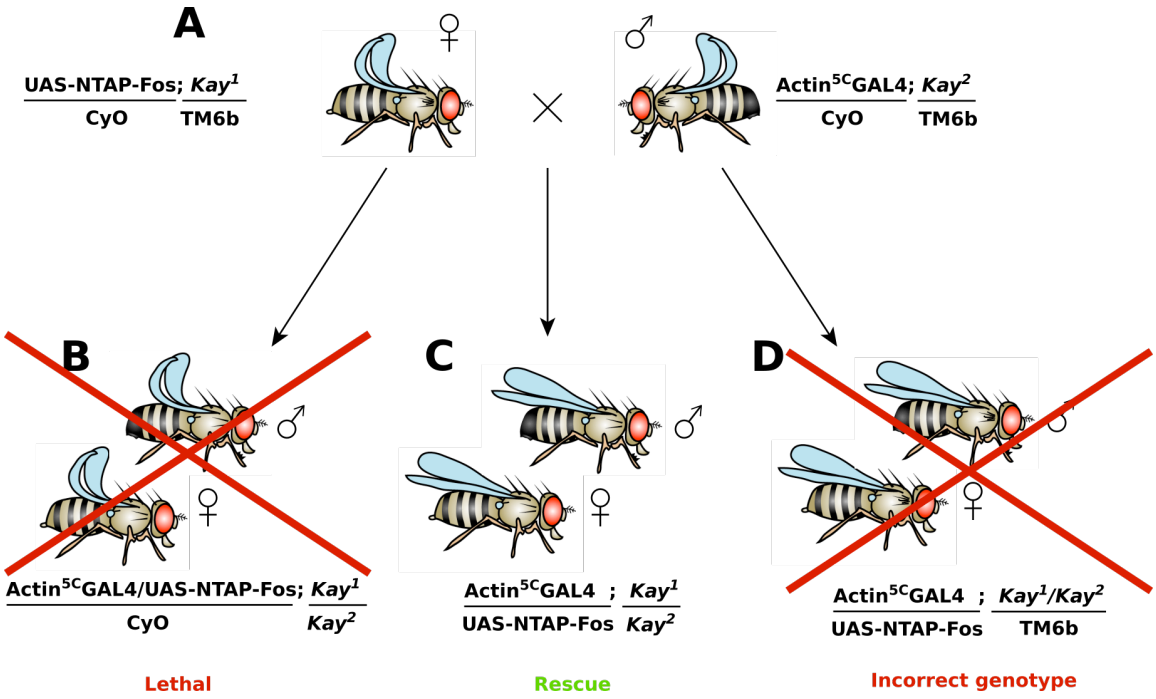

Figure 2.3 Rescuing *kay* mutant lethality using UAS-NTAP-Fos

A: UAS-NTAP-Fos and *kay*^{1} are doubled balanced into the same fly stock are crossed to double balanced Actin^{5C}GAL4 and *kay*^{2} flies. **B**: Progeny from the aforementioned cross displaying curly wings (*CyO*) only carry either Actin^{5C}GAL4 or UAS-NTAP-Fos so tagged Fos is not expressed and the combination of both *kay* mutant alleles is lethal. **C**: This progeny display neither balancer (*CyO/TM6b*) and are expressing tagged Fos in the *kay* null background, allowing rescue of this otherwise lethal combination. **D**: These flies display increased humeral bristles (*TM6b*) and are heterozygous for kay, therefore not a complete Fos null and are discarded. Fly images designed using the Genotype Builder from Roote and Prokop (2013).

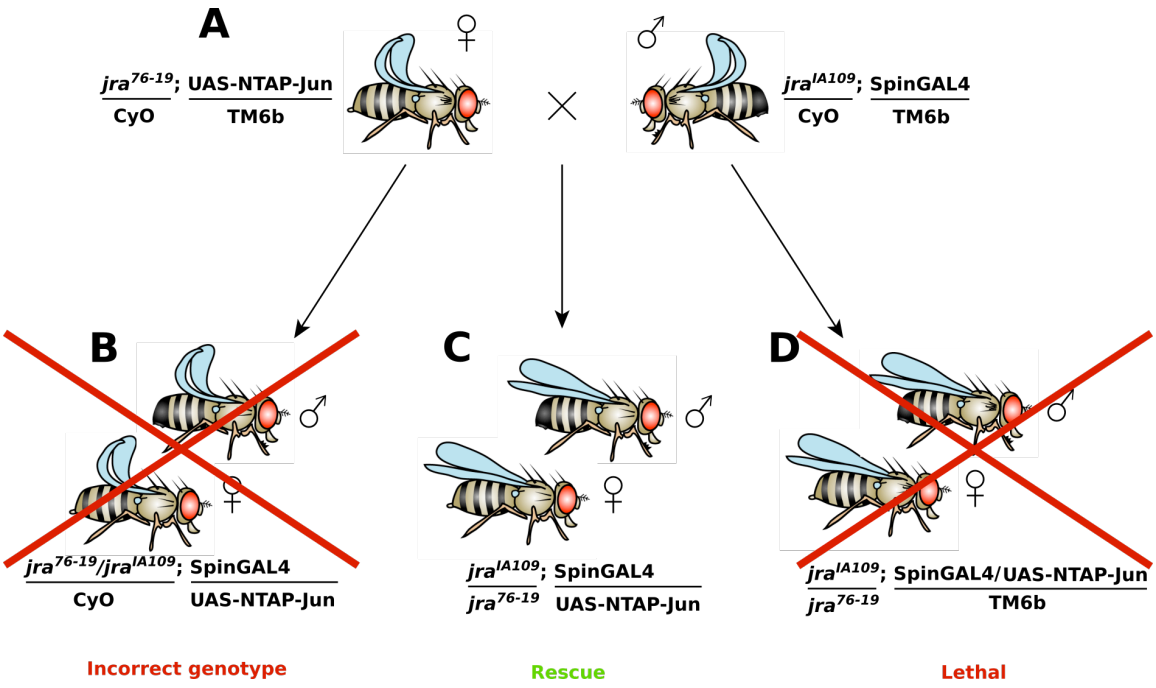

Figure 2.4 Rescuing *jra* mutant lethality using UAS-NTAP-Jun

A: UAS-NTAP-Jun and $jra^{76\text{-}19}$, which are doubled balanced into the same fly stock, were crossed to double balanced SpinGAL4 and jra^{lA109} flies. **B**: Progeny from the aforementioned cross displaying curly wings (*CyO*) are only expressing either $jra^{76\text{-}19}$ or jra^{lA109} therefore not a *Jun* null mutant and are discarded. **C**: This progeny display neither balancer (*CyO/TM6b*) and are expressing tagged Jun in the *jra* null background, allowing rescue of this otherwise lethal combination. **D**: These flies display increased humeral bristles (*TM6b*) and are only expressing either SpinGAL4 or UAS-NTAP-Jun, therefore tagged Jun is not expressed and the combination of both *jra* mutant alleles renders this cross lethal. Fly images designed using the Genotype Builder from Roote and Prokop (2013).

2.5.2 Generation of UAS-Punch and UAS-Punch-HA lines

Punch cDNA was obtained by streaking a chloramphenicol plate using *E.coli* from the Sweeney lab cDNA library (pOT2-LD37787). Streaked plates were incubated overnight at 37°C and single colonies containing pOT2-Punch were picked and grown in 5ml overnight cultures containing 5µl/ml chloramphenicol (see section 2.4.6). Each overnight culture had a sample miniprepped (see section 2.4.7.1). To remove the Punch cDNA from the pOT2 vector, restriction digest was performed (see section 2.4.4) using restriction enzymes XbaI and BGLII and Buffer D (Promega), incubated for 1 hour at 37°C then 20 minutes at 80°C before freezing. Restriction digest products were run on gel electrophoresis to check we obtain the appropriate sized fragment.

In order to insert the punch cDNA into the pUAST-attB vector, both alone and with an added HA tag (hereby referred to as UAS-Punch and UAS-Punch-HA), primers were designed, which incorporated new restriction sites (a single 5' primer + BGLII restriction site for use in both PCR reactions and 2 separate 3' primers, both adding an XbaI but one also adding a HA tag) that would allow ligation of the cDNA into the vector (see Table 2.6). PCR was performed (see section 2.4.1) upon the successful minipreps, amplifying the Punch cDNA as well as adding both new restriction sites for UAS-Punch, plus the HA tag in UAS-Punch-HA. This PCR was modified and is different to the previously outlined method. We altered the reaction volume to 50µl and adjusted the other volumes accordingly. We also ran this PCR for 45 cycles. Gel extraction (see section 2.4.3) of the correct fragments purified them ready for a restriction digest, which was performed upon both newly PCR-generated cDNA fragments as well as the pUAST-attB vector to generate sticky ends ready for ligation (see section 2.4.4). The fragments were gel extracted again before ligation was performed (see section 2.4.5). Ligated products were transformed into *E.coli* and purified following the same protocol as outlined previously (see section 2.5.1).

Upon acquiring midiprepped samples of UAS-Punch and UAS-Punch-HA, both had their concentrations calculated using a NanoDrop (ND-1000, Thermo Scientific). Neither were concentrated enough for microinjection so ethanol precipitation was performed. 100µl of both constructs were incubated with 10µl of 3M sodium

acetate and 330µl of 100% ice cold ethanol, overnight at -20°C. The DNA was pelleted via centrifugation at 13000*g* for 30 minutes at 4°C. The supernatant is removed and the pellet washed with 1ml 70% ethanol and centrifuged again at 13000*g* for 10 minutes. The supernatant is removed and the pellet is air dried for 10 minutes. The pellet is resuspended in 25µl resulting in concentrations for UAS-Punch of 1327.9ng/µl and UAS-Punch-HA of 1078ng/µl as calculated by the NanoDrop. Each of the constructs were sequenced and confirmed to be correct using the GATC light run service. We outsourced the microinjection of these stocks to The University of Cambridge, Department of Genetics, Fly Facility. The phiC31 integrase system can be used as we have inserted the Punch cDNA into the pUAST-attB vector. This system utilises site-directed recombination to insert our sequence into the genome. The phiC31 integrase is a sequence specific recombinase that mediates the recombination between attachment sites, one of which is present in our vector (attB), the other in the target *Drosophila* line (attP). The integrase facilitates the recombination of these sites, inserting the gene of interest into the *Drosophila* line following microinjection. We wanted stocks of UAS-Punch and UAS-Punch-HA on both the 2nd and 3rd chromosome, we utilised the following phiC31 stocks to achieve this:

(2nd) Stock 12-104 51C – y^1 M[vas-int.Dm]ZH-2A w*; M[3xP3-RFP.attP']ZH-51C

(3rd) Stock 13-106: vas-int; attp-3B VK00033 – *y w* M(eGFP, vas-int, dmRFP)ZH-2A;; PBac[y[+]-attP-3B]VK00033

The integrase is removed and successful lines were balanced before we received them back from Cambridge.

2.5.3 Generating antibodies

Four antibodies were generated as part of this study. The cDNA encoding *Drosophila* Jun, isoform A and *Drosophila* Punch, isoform A were used to generate soluble Jun and Punch proteins by the Technology Facility Protein Production Lab (Biology, University of York). These were used to inoculate 2 guinea pigs (Jun) and 2 rats (Punch) over a three-month immunisation scheme (Eurogentec, Belgium) generating 2 guinea pig anti-Jun and 2 rat anti-Punch antibodies. Each animal

received 4 injections of around 30µg (between 10-50µg) of antigen in a maximum volume of 250µl.

2.6 Identifying protein binding partners

This investigation aims to identify the binding partners of Fos and Jun during conditions of oxidative stress compared to controls. We generated *Drosophila* lines, UAS-NTAP-Fos and UAS-NTAP-Jun in order to express these in fly neuronal tissue and extract Fos and Jun utilising the tag that we added. This was achieved by performing tandem affinity purification (TAP) on a homogenised sample of 4500 heads per sample. The details are outlined below.

2.6.1 Generating UAS-NTAP-Fos and UAS-NTAP-Jun fly samples

Large numbers of homozygous UAS-NTAP-Fos and UAS-NTAP-Jun males were crossed to homozygous elavGAL4 virgin females, generating approximately 9000 flies per genotype. We crossed to elavGAL4 to achieve pan-neuronal expression of NTAP-tagged Fos and Jun, as we aimed to determine the role of Fos and Jun in the neurons only. Half of these were immediately stored at -80°C and formed the control, non-oxidatively stressed sample. The remaining 4500 were starved overnight in a cage containing a 2% agar plate (see section 2.1.2). The following day, a mix of 20mM DEM, 5% sucrose (Sucrose; Fisher Scientific) and blue food dye (Blue Food Colouring; Nestle) was used to saturate thick filter paper (Qualitative filter paper, Grade 6, circles; Whatman®) and this was added to the cage of flies which is kept at 25°C for 5 hours. After 1 hour the cage was checked to ensure the flies are consuming the DEM/sugar mix, this was determined by observing the fly abdomen, which was dyed blue due to the presence of the blue food colouring. As the flies have been starved, the majority if not all of the flies had consumed the DEM within the first hour. After 5 hours the flies were stored at -80°C. This was repeated on an empty vector control, which was the UAS-NTAP vector alone and when males are crossed to elavGAL4 female virgins, the progeny expressed the NTAP-tag only. This line will help us determine which bound proteins are non-specific to Fos or Jun and are purely binding the tag. These proteins were eliminated from the final list of

identified proteins. The details of the 6 samples we performed TAP are shown (see Table 2.7).

Table 2.7 Samples generated for TAP

Name	Treatment	Number of flies
UAS-NTAP-Fos/elavGAL4	Control	~4500
UAS-NTAP-Fos/elavGAL4	DEM	~4500
UAS-NTAP-Jun/elavGAL4	Control	~4500
UAS-NTAP-Jun/elavGAL4	DEM	~4500
UAS-NTAP-Empty/elavGAL4	Control	~4500
UAS-NTAP-Empty/elavGAL4	DEM	~4500

2.6.2 Processing UAS-NTAP-Fos and UAS-NTAP-Jun fly samples

Once all samples had been collected and stored at -80°C we began processing the samples. We are only interested in the heads and see needed to separate the head from the remainder of the body. To do so we used a series of molecular sieves (3310/BS: 410-1:2000/ 710 and 425 Micron mesh; ISO). Two separate sieves were used, one with a mesh size of 710 microns which allowed the heads and limbs to pass through but retains the abdomen and wings. The next sieve had a mesh size of 425 microns, which allowed the limbs to pass through, retaining the heads only. We first froze these sieves at -80°C in order to keep the samples chilled during the separation process. The samples were vortexed quickly, which breaks the heads from the rest of the carcass. The samples were added to the chilled sieves which were kept on dry ice in a 4°C cold room and rapidly and vigorously shaken to ensure all heads had passed through to the second sieve and that no limbs remained in the second sieve. We collected the heads from the second sieve into a falcon tube which was quickly transferred back into the -80°C freezer to ensure they do not defrost. The frozen heads were then transferred to a highly polished agate mortar (VWR), which has been pre-chilled with liquid nitrogen. The head samples were ground into a fine powder in liquid nitrogen and the mortar was kept on dry ice to

keep the sample cold. This fine powder was rehydrated and further homogenised in 3ml Bouwmeester's buffer (50mM Tris-HCl (Sigma), 125mM NaCl (Fischer Scientific), 5% glycerol (Sigma), 0.2% NP40 (Igepal; Fluka), 1.5mM $MgCl_2$(Sigma), 1mM DTT (Melfords), 25mM NaF (Sigma), 1mM Na_3VO_4(Sigma), 1mM EDTA (Sigma), 2mM EGTA (Amresco) and 1 tablet/10ml protease inhibitor cocktail (PIC) (cOmplete EDTA-free, mini tablets; Roche)) (Pepper et al., 2012). The fly homogenate was transferred into 1.5ml Eppendorf tubes and centrifuged at 4°C, 13,200*g* for 15 minutes to clarify the homogenate. The supernatant was removed and centrifuged again to clarify further; TAP was performed on this lysate. Small amounts were retained to perform a western blot (running 5µl of each sample) in order to check that the tagged Fos and Jun are present and uncontaminated (see Figure 4.1).

2.6.3 Tandem affinity purification (TAP)

The first step requires incubating the lysates overnight at 4°C with pre-washed agarose beads (Rabbit-IgG Agarose beads; Sigma). Washing of the agarose beads consisted of 200µl of the beads in a 15ml conical bottom tube (Corning) being nutated for 15 minutes with 500µl of Buffer B (20mM hepes (Sigma), 20% glycerol (Sigma), 0.5% NP40 (Igepal; Fluka), 200mM KCl (Sigma), 0.5mM DTT (Melfords), 1mM EDTA (Sigma), 20mM EGTA (Amresco) and 1 tablet/10ml PIC (cOmplete EDTA-free, mini tablets; Roche)) after each wash the tube was centrifuged at 4°C, 100*g* for 2 minutes, the supernatant was removed and another wash was performed, at least 2 washes were required (Veraksa et al., 2005, Tian et al., 2011, Pepper et al., 2012).

Following the overnight incubation of the beads with the lysate, each sample tube was centrifuged at 4°C, 100*g* for 5 minutes. The supernatant was removed and kept; this fraction did not bind to IgG.

The remaining beads were washed 3 times in 1 ml Buffer B, then centrifuged at 4°C, 100*g* for 2 minutes after each wash. The beads were then washed 4 times in 1 ml Buffer C (20mM Hepes (Sigma), 20% glycerol (Sigma) 0.5% NP40 (Igepal; Fluka), 200mM KCl (Sigma) and 0.5mM DTT (Melfords)) then centrifuged at 4°C, 100*g* for 2

minutes after each wash. The beads were washed again twice in 1ml TEV cleavage buffer (10mM Tris-HCl (Sigma), 150mM NaCl (Fischer Scientific), 0.1% NP-40 (Igepal; Fluka), 1mM DTT (Melfords), 0.5mM EDTA (Sigma)) then centrifuged at 4°C, 100*g* for 2 minutes after each wash. A 10µl sample of the beads were retained for western blot analysis, this is the fraction of proteins bound to IgG beads. 40 units of TEV protease (ProTEVplus protease; Promega) were added to 400µl of TEV cleavage buffer and 1mM DTT (Melfords). This was used to resuspend the IgG beads and transfer them to a 1.5ml Eppendorf, this slurry was incubated with nutation overnight at 4°C.

The slurry was centrifuged at 4°C, 300*g* for 1 minute, the supernatant was removed, a sample was taken for analysis (cleaved off the IgG bead fraction) and mixed with 3 times its volume of Bouwmeester's buffer. Streptavidin beads were prepared by adding 100µl into a 1.5ml Eppendorf tube and washed twice with 500µl of Bouwmeester's buffer, then centrifuged at 4°C, 1500rpm for 2 minutes after each wash. The supernatant/buffer mix was added to the washed Streptavidin beads and incubated overnight at 4°C with nutation. Following incubation the beads were centrifuged at 4°C, 1500rpm for 2 minutes. The supernatant was removed and retained; a sample is taken for analysis, which is the fraction that did not bind the streptavidin beads. The remaining beads were washed 3 times with 500µl Bouwmeester's buffer and centrifuged at 4°C, 1500rpm for 2 minutes after each wash.

The purified Fos and Jun proteins, along with their binding partners were eluted from the streptavidin beads by heating in 25µl of SDS sample buffer, 95°C for 5 minutes. A small amount of this elution (1µl, diluted 1 in 6) is kept for western blot analysis. This protocol was adapted from several other studies (Veraksa et al., 2005, Tian et al., 2011, Pepper et al., 2012). The remaining elution was used in mass spectrometry.

Prior to this larger scale experiment, a pilot run was performed using 500 heads per sample. The methods used in pilot run were adapted for the main run. Several differences between the pilot and main run are detailed below. The pilot run used a lysis buffer consisting of 50mM Tris-HCl pH 7.5, 125mM NaCl, 5% (vol/vol) glycerol,

0.3% (vol/vol) NP40, 1.5mM $MgCl_2$, 25mM NaF, 1mM Na_3VO_4, 0.2mM DTT, 0.05mM MG-115, 1mM PMSF, 25mM beta-glycerophosphate, Complete mini protease inhibitor tablets 1 per 10ml extraction solution, EDTA-free, Roche Applied Science. The heads were homogenised in 1ml of this buffer before clarification, this was performed on ice, not in liquid nitrogen This buffer was used until the TEV cleavage step, which used a TEV buffer consisting of 0.15M NaCl, 10mM TrisCl pH 8.0, 0.5mM EDTA 1mM DTT, 0.1% Triton-X100. The incubation of the IgG beads with the lysate was performed for 2 hours; this was adjusted to overnight in the main run.

2.6.4 In-Gel tryptic digest and liquid chromatography–mass spectrometry/mass spectrometry (LC-MS/MS)

Materials and apparatus were supplied by the Proteomics Lab in the Technology Facility who also performed the following protocol (Biology, University of York).

Each elution was loaded (24µl) into a 10% Bis-tris gel (NuPAGE 10% Bis-Tris Gel 1mm x 10 well; Novex) and sodium dodecyl sulphate polyacrylamide gel electrophoresis (SDS-PAGE) (see section 2.7.3) was performed at 200v. We did not want to separate out the proteins as would normally occur in SDS-PAGE, so the electrophoresis was run very briefly so that the sample was in the gel but still running as a single band. The gel was removed from the plastic cassette, rinsed in ddH_2O and stained with SafeBlue (SafeBlue protein stain; NBS biological) for 1 hour before being destained in ddH_2O for 1 hour. The single band was excised from the gel and cut into 1mm pieces before being transferred to a LoBind Eppendorf® tube. The band pieces were destained by washing twice with 100µl of 25mM ammonium bicarbonate in 50% acetonitrile/50% ddH_2O. The supernatant was removed before washing with 100µl acetonitrile for 5 minutes. The gel pieces were then dried in a Speedvac for 20 minutes on medium setting. The gel pieces are then incubated with 100µl of 10mM dithioerythrietol (DTE) in 100mM ammonium bicarbonate for 1 hour at 56°C. The gel pieces were allowed to return to room temperature and the supernatant removed. They were then incubated with 100µl of 50mM iodoacetamide in 100mM ammonium bicarbonate for 30 minutes in the dark at room temperature. The supernatant was removed and the gel pieces washed in 100µl of 100mM ammonium bicarbonate for 15 minutes. The supernatant was

removed and the gel pieces washed again with 25mM ammonium bicarbonate in 50% acetonitrile/50% ddH_2O for 15 minutes. The supernatant was removed and the gel pieces washed in 100µl of acetonitrile for 5 minutes. Again the supernatant was removed and the gel pieces dried in the Speedvac for 20 minutes on a medium setting. The proteins then underwent trypsin digest by adding 10µl of a 0.025µg/µl in 25mM ammonium bicarbonate solution to the dry gel pieces and allowed to soak up the solution for 10 minutes. The gel pieces were then covered in 25mM ammonium bicarbonate using as small a volume possible. These were incubated overnight at 37°C.

The sample was acidified by adding 1/10th volume of 1% Trifluoroacetic acid (TFA). We utilised ZipTipping for the following protocol. The ZipTip was wetted by drawing up 10µl of 100% acetonitrile and expelling to waste and repeated. The tip was then washed by drawing up 10µl 0.1% TFA in water and expelling to waste and repeated. The sample is then drawn into the tip and expelled back into the tube and repeated at least 10 times. As much of the liquid was expelled from the tip as possible the ZipTip was now binding the protein sample. The tip was washed by drawing in 10µl of 0.1% TFA in water and expelled to waste, then repeated. Finally 3µl of 50% acetonitrile/50% water + 0.1% TFA was drawn up into the tip, passing it in and out at least 5 times before expelling to a new clean storage tube.

Following successful tryptic digest, the samples were loaded onto the nanoAcquity Ultra Performance Liquid Chromatography (UPLC) system (Waters). This separates the sample by forcing it through a column using a liquid (acetonitrile, see Solvent B) at high pressure, which is the mobile phase. The column is packed with silica particles with attached chains of octadecylsilyl (C_{18}), which is the modified organic particle that makes up the stationary phase. This system separates the peptides in the sample based on their hydrophobic character by running the sample across a linear gradient of organic solvent, acetonitrile. The peptides are forced through the stationary phase consisting of C_{18} chains bound to silica particles which captures the peptides based on their hydrophobicity followed by their sequential elution. The UPLC system was equipped with a nanoAcquity Symmetry C_{18}, 5µm trap (180µm x 20mm; Waters) and a nanoAcquity HSS T3 1.8µm C_{18} capillary column (75µm x 250mm; Waters). The wash solvent for the trap was 0.1% (v/v) aqueous formic acid

and was washed for 5 minutes before switching flow to the capillary column. The trapping flow rate was 10µl/min. Separation of the sample used a gradient elution of two solvents (Solvent A: 0.1% (v/v) aqueous formic acid; and Solvent B: acetonitrile containing 0.1% (v/v) aqueous formic acid). The capillary column flow rate was 300nL/min and was kept at 60˚C. The gradient profile was linear 2-30% solvent B over 125 minutes followed by linear 30-50% solvent B over 5 minutes. All runs were then washed for 5 minutes using 95% solvent B for 2.5 minutes. The column was re-equilibrated for 25 minutes in initial conditions before injecting into the ionisation system.

The nanoAcquity UPLC system was interfaced with a maXis HD LC-MS/MS system and CaptiveSpray ionisation source (Bruker Daltonics). Positive electrospray ionisation (ESI)-MS and MS/MS spectra were acquired using AutoMSMS mode. ESI produces ions from your sample using an electrospray, which applies high voltage to the sample liquid producing an aerosol of charged ions, moving samples ions from a liquid to gaseous phase (Ho et al., 2003). The instrument settings were: ion spray voltage: 1,450V, dry gas: 3L/min, dry gas temperature 150°C.

The ions emitted to the gaseous phase are accelerated into the mass analyser via an electric filed. The instrument settings for the mass analyser were as follows: ion acquisition range: *m/z* 150-2,000, MS spectra rate: 5Hz, MS/MS spectra rate: 5Hz at 2,500cts to 20Hz at 250,000cts, cycle time: 1 second, quadrupole low mass: 300 *m/z*, collision RF: 1,400 Vpp, transfer time 120ms. The collision energy and isolation width settings were automatically calculated using the AutoMSMS fragmentation table, absolute threshold 200 counts, preferred charge states: 2–4, singly charged ions were excluded.

The mass analyser separates the ions based on their mass to charge ratio (m/z), which is determined by time-of-flight (TOF). TOF measures the time that the peptide ions take to travel over the flight tube within the mass analyser. Peptides with a high m/z travel slower than peptides with a low m/z. A set of known calibrated m/z standards is used to determine the m/z value of the sample peptide ions based on their flight time. A single MS/MS spectrum was acquired for each precursor and former target ions were excluded for 0.8 min unless the precursor

intensity increased fourfold. The mass spectral were searched against a database using the MASCOT program (Matrix Science Ltd., version 2.5.1), through the Bruker ProteinScape interface (version 2.1).

2.6.5 Bioinformatics

2.6.5.1 MASCOT

MASCOT processing matches peptide spectra to sequences within a database in order to identify proteins based on the number of matches a specific peptide sequence accumulates (Mallick and Kuster, 2010). As a result, a list of proteins with their matching peptides is produced. The following criteria were used to refine the MASCOT search. Our peptide sequences were searched against the UniProt_*Drosophila* (20150401) database with the parameters shown below (see Table 2.8).

Table 2.8 MASCOT database search parameters

Search parameter	Selection
Type of search	MS/MS ion search
Enzyme	Trypsin
Fixed modifications	Carbamidomethyl
Variable modifications	Oxidation
Mass values	Monoisotopic
Protein mass	Unrestricted
Peptide mass tolerance	±10ppm
Fragment mass tolerance	±0.1 Da
Max missed cleavages	1
Instrument type	ESI-QUAD-TOF
Significance Threshold	$p<0.05$
Ions score or expect cut-off	$p<0.05$

Both the significance threshold and ions score or expect cut-off were set to $p<0.05$, excluding less significant identifications and less well-matched peptides respectively. It is important to note here that while we have set a stringency to exclude false positive results, there was still a chance that we included false positives in our results. Following the MASCOT search, a list of proteins, identified by their accession numbers, and their matching peptides were generated per sample (see Appendix 4: LC-MS/MS pilot run data and Appendix 5: LC-MS/MS main run data). Each identified protein was given a MASCOT score, the mass, the number of significant matches and sequences as well as the exponentially modified Protein Abundance Index (emPAI) score. The number of significant sequences is determined by the number of peptide sequences identified that match the identified protein. The number of significant matches is determined by the number of times the peptide sequences match the identified protein sequence. The emPAI score represents the relative abundance of the peptide, where the number of peptides per protein is normalised by the theoretical number of peptides (Ishihama et al., 2005).

Proteins identified in both the empty vector control and DEM-treated samples were removed from our experimental data before further analytical processing was performed using WebGestalt and STRING.

2.6.5.2 WebGestalt

The protein accession numbers were entered into WebGestalt (WEB-based GEne SeT AnaLysis Toolkit), specifically searching against the *Drosophila melanogaster* database and identified as dmelanogaster_uniprot_swissprot_accession (Zhang et al., 2005). Some proteins from the original list required their accession number converting to fit this classification, this was performed manually using the Uniprot Consortium (UniprotConsortium, 2015) The proteins were analysed using the GO slim classification to group the proteins based on biological process, their molecular function and cellular classification.

2.6.5.3 STRING

The protein accession numbers were used to generate interaction networks using STRING (Szklarczyk et al., 2015). Default parameters were used and the interaction networks were limited to include only peptides linked within the sample.

2.7 Western blotting

During this investigation, western blotting was used to determine individual protein levels in a variety of experiments, specifically in following bait proteins through TAP, in the characterisation of antibodies and to assess mutants.

2.7.1 Protein extraction from fly heads

The head of the fly was used to assess protein levels, as we are mainly concerned with neuronal cells. Flies were collected in 15ml falcon tubes and frozen at -80°C before transferring to dry ice. The tubes were placed into 50ml falcon tubes containing dry ice and vortexed vigorously for 10 seconds before placing back on dry ice to ensure they did not thaw. A mortar was placed on dry ice and allowed to cool before the vortexed flies were added, at this point the flies are broken into pieces and the heads have separated off. 30 heads were collected from each genotype and placed into tubes containing 30µl of ice cold Radioimmunoprecipitation assay (RIPA) buffer (150mM NaCl, 1.0 % IGEPAL® CA-630, 0.5 % sodium deoxycholate, 0.1 % SDS, 50mM Tris, pH 8.0; Sigma) which we also added 1 tablet/10ml Protease inhibitor cocktail (PIC) (cOmplete EDTA-free, mini tablets; Roche). The heads were homogenised using sterile pellet pestles (Sigma). The homogenate was centrifuged at *13000g* for 15 minutes at 4°C to clarify the sample, the supernatant was removed and rapidly frozen on dry ice before transferring to -80°C for storage.

2.7.2 Quantification of protein concentration: Bicinchoninic acid assay (BCA)

The BCA assay was used to determine protein concentrations within our samples, allowing for more equal loading during SDS-PAGE and improving potential

comparisons made between samples. This assay was performed using a BCA assay kit (Cohesion Biosciences) and following the provided instructions. Protein samples were diluted 1:20, 1:40 and 1:100 and 10µl of each sample was added to individual wells of a 96-well plate in duplicate. A Bovine serum albumin (BSA) standard was also used, performed using dilutions ranging from 2mg/ml BSA down to 0.03125mg/ml BSA and finally 0mg/ml BSA/RIPA buffer. Each dilution was achieved through the addition of RIPA buffer, as this was the vehicle our protein sample was in. 200µl of the reaction assay was added to every used well and incubated at 37°C for around an hour, or until a range of colour change is observed in the BSA standards. The plate was inserted in a plate reader (Multiskan GO; Thermo Scientific) and the absorbance of each well was measured using the on-board program, the measurements were repeated several times to ensure accurate readings. A BSA standard curve was produced of known protein concentrations. Using the absorbance and standard curve, the protein concentration of the samples is calculated and adjusted with RIPA buffer accordingly to achieve samples of equal protein concentration.

2.7.3 Sodium dodecyl sulphate polyacrylamide gel electrophoresis (SDS-PAGE)

Using samples of known protein concentration, SDS-PAGE was performed to separate the proteins. The sample was mixed in a 3:1 ratio with sample buffer, made up as 100µl of β–mercaptoethanol in 900µl of 4x laemmli buffer (Bio-rad). The sample in Laemmli buffer was heated at 85°C for 5 minutes. The protein samples were loaded into pre-cast gels (10 % Mini-PROTEAN® TGX™ pre-cast gel; Bio-rad), which were situated in a tank (Bio-rad) containing running buffer (25mM Tris, 192mM glycine, 0.1 % SDS). A protein ladder was also loaded (7.5µl of Colour Prestained Protein Standard, Broad Range; NEB). SDS-PAGE was performed at 150v until the dye front reaches the bottom of the gel. The gel is removed from the plastic cassette and the wells cut off, the gel was rinsed briefly in ddH_2O before proceeding to transfer.

2.7.4 Protein transfer

Proteins were transferred from the gel to Polyvinylidene fluoride (PVDF) membrane using a Mini-trans-Blot® Cell (Bio-rad). The cell was assembled whilst submerged in transfer buffer (25mM Tris, 192mM glycine, 20% (v/v) methanol, 0.1 % (w/v) SDS), placing mesh pads on either side of the cassette, then 1-2 pieces of Whatman® gel blot paper were added atop the pads. The gel was rinsed in transfer buffer and placed on the gel blot paper from the black (-ve) side of the cassette. The PVDF (Amersham Hybond 0.45 μm PVDF; GE Healthcare) was cut to size and activated in methanol for 60 seconds before rinsing in transfer buffer and placing on the gel blot paper on the white (+ve) side of the cassette. The cassette was folded together and compressed to expel air bubbles that may have been trapped between the layers. The cassette was sealed and placed into the transfer cell in the tank, which was filled with transfer buffer. The whole unit was placed at 4°C and the transfer proceeds at 100v for 1 hour, or 30v overnight followed by 60v for 30 minutes.

2.7.5 PVDF membrane blocking and antibody probing

The membrane containing the transferred proteins was blocked at room temperature in 3%(w/v) Marvel milk or 5%(w/v) BSA in Tris buffered Saline-Tween (TBS-T) (10mM Tris, pH 7.6, 150mM NaCl and 0.1 % (v/v) Tween™-20), depending on the incubation requirements of the desired antibody. The membrane was blocked for at least 1 hour. The primary antibody was incubated with the membrane overnight in the relevant blocking agent at 4°C on a shaker. Following incubation the membrane is washed in TBS-T 5 times for at least 3 minutes. The secondary antibody, HRP-conjugated and appropriate species, was added to the relevant blocking agent and the membrane is incubated with this for 1 hour at room temperature with shaking before 5 washes for at least 3 minutes in TBS-T. The membrane was incubated in enhanced chemiluminescence (ECL) reagent (GE Healthcare) for 1 minute and the excess was blotted off using Whatman® gel blot paper. The membrane was visualised by placing chemiluminescence film (Amersham Hyperfilm™ ECL; GE Healthcare) on top for varying times depending on the level of light emitted. The film was then developed for 1 minute in developer

(Carestream® autoradiography GBX Developer; Sigma) before rinsing for 30 seconds in water and fixed for 1 minute in fixer (Carestream® autoradiography GBX Fixer; Sigma). The antibodies used for western blotting are shown (see Table 2.9).

Table 2.9 Antibodies used for western blotting

Antibody	Stage	Species	Source	Dilution	Comments
Anti-Fos88	Primary	Rabbit	Sweeney Lab	1:10000	Polyclonal serum
Anti-Fos89	Primary	Rabbit	Sweeney Lab	1:10000	Polyclonal serum
Anti-Jun59	Primary	Guinea Pig	Sweeney Lab	1:10000	Polyclonal serum
Anti-Jun60	Primary	Guinea Pig	Sweeney Lab	1:10000	Polyclonal serum
Anti-Punch182	Primary	Rat	Sweeney Lab	1:10000	Polyclonal serum
Anti-Punch183	Primary	Rat	Sweeney Lab	1:10000	Polyclonal serum
Anti-Actin (beta)	Primary	Mouse	Proteintech (#60008-1-Ig)	1:180000	Purified via Caprylic acid/ammonium sulfate precipitation
Anti-Rabbit IgG HRP-linked	Secondary	Goat	Cell Signaling Technology (#7074)	1:2000	Affinity purified
Anti-Guinea Pig IgG HRP-linked	Secondary	Rabbit	Sigma (#A5545)	1:10000	Affinity purified
Anti-Mouse IgG HRP-linked	Secondary	Horse	Cell Signaling Technology (#7067)	1:2000	Affinity purified
Anti-Rat IgG HRP-linked	Secondary	Goat	Cell Signaling Technology (#7077)	1:5000	Affinity purified

3. The role of Fos and Jun in the motor neuron during oxidative stress

3.1 Introduction

As discussed in Chapter 1, neurons may be subject to excessive ROS during ageing and periods of metabolic demand. At low levels, ROS are critical for proper synaptic development and synaptic plasticity (Bell et al., 2015). One of the major redox sensitive pathways is JNK/AP-1 signalling, which has roles in synaptic plasticity and learning/memory (Sanyal et al., 2003). JNK signalling is activated upon an increase in ROS within the cell. In neurons, elevated activity increases the production of ROS, which are important for growth and strengthening synaptic connections (Sanyal et al., 2002). However, the aged neuron may be at risk of high oxidative stress levels, resulting in a continuous or sustained over-activation of JNK signalling. This has been shown to cause synaptic overgrowth in the *Drosophila* larval neuromuscular junction (NMJ) as a result of increased activation of AP-1, a transcription factor consisting of leucine zipper proteins Fos and Jun, the transcriptional effectors of JNK signalling (Milton et al., 2011). Depending on the source of oxidative stress, it has been suggested that AP-1 will form differentially composed dimers. During apparent cytosolic oxidative stress, AP-1 consists of a Fos:Fos homodimer, where Jun has no role. Sources of mitochondrial oxidative stress were shown to activate a Fos:Jun heterodimer of AP-1, suggesting that the source of oxidative stress may lead to different transcriptional outputs and possible divergent responses (Hwang et al., 2010, Milton et al., 2011). Despite being well studied, the role of Fos and Jun in the oxidative stress response is clearly incomplete, particularly in neurons. This differential role for Fos and Jun could be critical to the understanding of age-related neurodegenerative diseases where oxidative stress has been implicated. The aim of this chapter is to define the role of Fos and Jun in motor neurons during mitochondrial oxidative stress, where we will utilise *Drosophila* and establish a model of oxidative stress where we can study this question.

The compound diethyl maleate, (DEM) is used here to generate mitochondrial oxidative stress. When oxidative stress occurs, reduced glutathione is preferentially

oxidised to protect the macromolecules of the cell from redox damage. DEM alkylates the sulfhydryl group of reduced glutathione and blocks its defensive mechanism via conjugation. This induces oxidative stress in the cell as ROS generated from mitochondria accumulate and can attack the macromolecules of the cell with increased frequency (Hidaka et al., 1990). The effects of DEM upon *Drosophila* larvae are to be characterised and the role of Fos and Jun in this response will be identified.

3.2 Results

3.2.1 Diethyl maleate causes synaptic overgrowth in *Drosophila* larvae

Oxidative stress in *Drosophila* causes the larval NMJ to become overgrown when compared to larvae under non-stressed conditions (Milton et al., 2011). The growth of the NMJ is primarily measured by quantifying the synaptic boutons, in relation to muscle size, but it can also be measured in terms of number of synaptic branches and the cumulative overall length of the synapse and branches (Schuster et al., 1996). Treating *Drosophila* larvae with DEM can generate oxidative stress, through a depletion of reduced glutathione, the primary defence to redox damage. A dose response of DEM was performed to determine the concentration required to cause significant growth of the NMJ at muscle 6/7, hemisegment A3. Dehydrated yeast paste was rehydrated with solutions of 1mM, 3mM, 10mM or 30mM DEM (see Table 2.4 and section 2.1.2) that were made up in 10% ethanol and this was added to hydrated instant food in vials. *Canton-S* (*CS*) virgin females and w^{1118} males are crossed to generate wild-type (WT) progeny that were raised in each experimental DEM condition. This cross was the standard wild-type used throughout this study and herein will be referred to as WT. Furthermore, unless stated otherwise; flies are outcrossed to *CS* to generate heterozygotes. These were compared to a control of instant food and a 10% ethanol yeast paste. Third instar larvae from each condition were dissected, stained with antibodies and the NMJ analysed (see section 2.2). Quantification of the mean synaptic bouton number per NMJ normalised to muscle size revealed that 10mM and 30mM DEM are both significantly overgrown compared to 1mM DEM and 3mM DEM as well as the 10% ethanol only control

(Figure 3.1A; $p<0.001$, ANOVA). Normalisation of synaptic bouton number to muscle size is required as synaptic growth and bouton number are proportional to muscle surface area (MSA) (Schuster et al., 1996). Images of the antibody stained NMJ from each condition are also presented, which highlight the synapse (magenta) and the synaptic boutons (green)(Figure 3.1B). We utilise anti-Synaptotagmin (SYT) and anti-HRP-Cy3, which allow the visualisation of synaptic boutons and neuronal tissue respectively. Treatment with DEM does not significantly alter MSA compared to controls (Figure 3.1C; $p>0.05$, ANOVA). However, treatment with 3mM DEM caused a significant, albeit modest, increase in MSA compared to treatment with 10mM DEM ($p<0.05$; ANOVA). The reason for this is unclear.

Mean normalised branch number and NMJ length were also plotted against the concentration of DEM. Mean normalised branch number per NMJ is significantly increased upon treatment with 10mM and 30mM DEM compared to 10% ethanol only controls (Figure 3.2A; $p<0.001$, ANOVA). No significant difference was found between 1mM and 3mM DEM compared to controls (Figure 3.2A; $p>0.05$, ANOVA). Significant increases in NMJ length were also found when treating with 10mM and 30mM DEM compared to 10% ethanol only controls (Figure 3.2B; $p<0.05$, ANOVA). No significant differences were found in mean normalised NMJ length when treating with 1mM and 3mM DEM compared to controls ($p>0.05$, ANOVA). The percentage increases of each the mean normalised bouton number, branch number and size under each treatment was also calculated. The dose at which significant NMJ overgrowth occurs is 10mM DEM; causing bouton number, branch number and NMJ length to increase by 58.1%, 85.2% and 33% respectively (Figure 3.2C). Both percentage change in bouton and branch number significantly increase at 10mM and 30mM DEM compared to 0mM DEM (Figure 3.2C; $p<0.001$, ANOVA). NMJ length at 10mM and 30mM DEM does not show any significant difference in percentage change compared to 0mM DEM, suggesting overall length is less amenable to change due to oxidative stress than bouton and branch number (Figure 3.2C; $p>0.05$, ANOVA).

Treatment with 10mM DEM does not alter muscle size but significantly increases synapse growth in terms of bouton and branch number, and to a lesser extent NMJ

length. 10mM DEM is used to model oxidative stress and induce synaptic overgrowth in all subsequent experiments.

3.2.2 DEM causes synaptic overgrowth that can be rescued by treating with Trolox

In order to confirm treatment with DEM causes increased ROS levels, we determined whether the effects of DEM could be rescued by also feeding flies with an antioxidant. We use the vitamin E analogue, Trolox, which acts to non-enzymatically scavenge ROS and has previously been shown to alleviate the effects of DEM via a reduction in hydrogen peroxide (Hamad et al., 2010, Vergauwen et al., 2015). We found that Trolox-treatment of WT larvae did not significantly change bouton number compared to WT controls (Figure 3.3; $p>0.05$, ANOVA). Treating WT larvae with both 10mM DEM and Trolox resulted in a bouton count significantly lower than WT treated with DEM alone ($p<0.001$, ANOVA). Larvae treated with DEM and Trolox also show no significant difference to WT controls (NS $p>0.05$, ANOVA). Branch number and length (μm) are also significantly increased in DEM-treated WT compared to WT controls (Figure 3.4; $p<0.05$, ANOVA). Both branch number and length are significantly reduced in WT treated with both DEM and Trolox ($p<0.001$ and $p<0.01$ respectively, ANOVA) compared to WT treated with DEM alone.

We conclude that DEM causes overgrowth via an increase in ROS and that Trolox is an effective ROS scavenger, capable of relieving the oxidative stress that 10mM DEM treatment incurs.

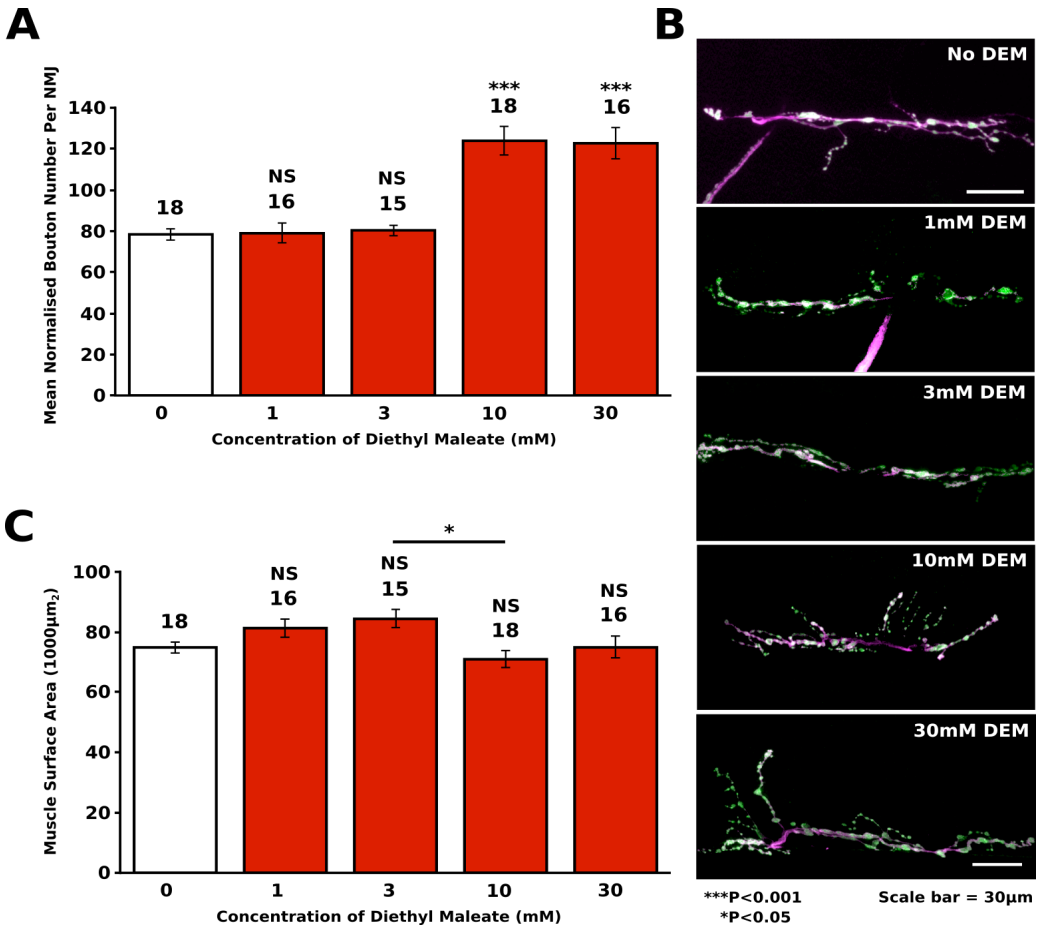

Figure 3.1 DEM increases bouton number without affecting muscle size

A: Analysis of the NMJ at muscle 6/7 segment A3 of 3rd instar WT larvae treated with a yeast paste containing 10mM and 30mM DEM during development show significantly increased mean normalised synaptic bouton numbers (124±6.9, n=18 and 123±7.6, n=16 respectively) compared to controls (78±2.8, n=18) (*WT* + 10% ethanol in yeast paste) (***p<0.001; ANOVA with post hoc Bonferroni correction). Treatments of 1mM (79±4.8, n=16) and 3mM DEM (80±2.6, n=15) show no significant difference compared to controls (NS p>0.05; ANOVA with post hoc Bonferroni correction). Error bars display ±SEM. **B**: Representative image of the NMJ at muscle 6/7 segment A3 imaged from each dose of DEM; increased numbers of boutons (green) and branching of the synapse (magenta) are observed when treating with 10mM and 30mM DEM. Scale bar 30µm. **C:** Analysis of larval muscle surface area (MSA) of muscle 6/7 segment A3 across each dose reveals no significant difference between controls (74892±1956.42µm^2, n=18) and DEM treatments, 1mM (81307±3085.42, n=16), 3mM (84376±3014.2, n=15), 10mM (70958±2744.5, n=18) and 30mM (74900±3597.0, n=16) (NS p>0.05, ANOVA with post hoc Bonferroni correction). Significant difference in MSA was found between 3mM and 10mM DEM treatments (*p<0.05; ANOVA with post hoc Bonferroni correction). Error bars display ±SEM.

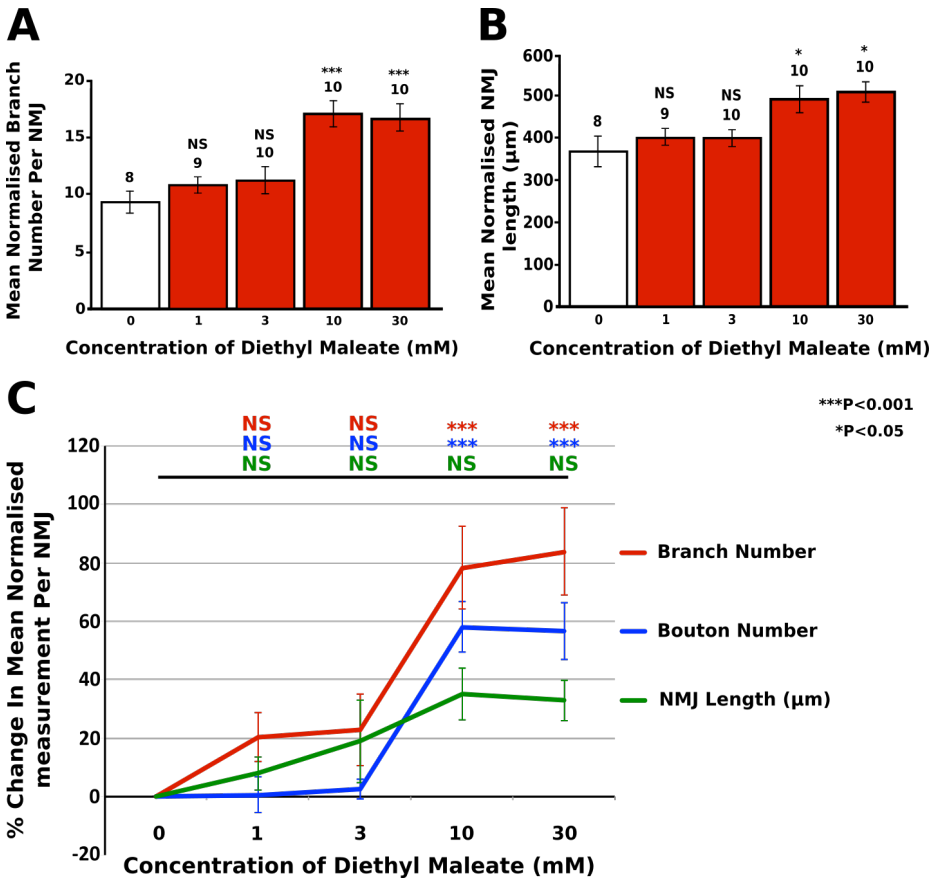

Figure 3.2 DEM increases NMJ branch number and length, causing synaptic overgrowth

A: Analysis of the NMJ at muscle 6/7 segment A3 of 3rd instar WT larvae treated with a yeast paste containing 10mM and 30mM DEM show significantly increased mean normalised NMJ branch number (17.1±1.3, n=10 and 16.9±1.4, n=10 respectively) compared to controls (9.3±1.1, n=8) (*WT* + 10% ethanol in yeast paste) (***p<0.001; ANOVA with post hoc Bonferroni correction). Treatments of 1mM (11±0.78, n=9) and 3mM DEM (11.4±1.1, n=10) do not significantly increase branch number compared to controls (NS p>0.05; ANOVA with post hoc Bonferroni correction). Error bars display ±SEM. **B**: Treatments of 10mM and 30mM DEM display significantly increased mean normalised NMJ length (µm) (496µm±33µm, n=10 and 511µm±26µm, n=10 respectively) compared to controls (373µm±38µm, n=8) (WT + 10% ethanol in yeast paste) (*p<0.05; ANOVA with post hoc Bonferroni correction). Treatments of 1mM (403µm±21.2µm, n=9) and 3mM DEM (403µm±21.5µm, n=10) do not significantly increase NMJ length compared to controls (NS p>0.05; ANOVA with post hoc Bonferroni correction). Error bars display ±SEM. **C:** Dose response data converted to a percentage change from 0mM DEM. Bouton and branch number both significantly increase at 10mM and 30mM DEM treatment (***p<0.001; ANOVA with post hoc Bonferroni correction). However, NMJ length (µm) at 10mM and 30mM DEM show no significant difference in percentage change compared to 0mM DEM. (NS p>0.05; ANOVA with post hoc Bonferroni correction). Error bars display ±SEM.

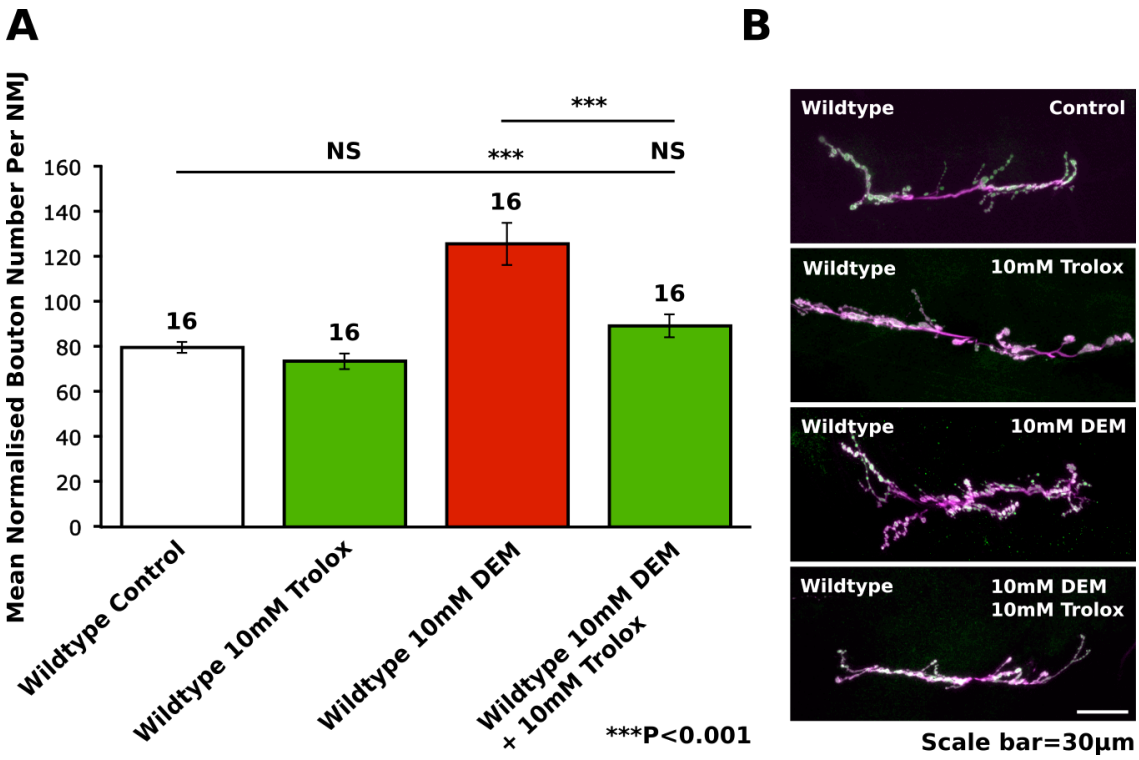

Figure 3.3 Trolox treatment rescues DEM-induced increases in bouton number

A: Analysis of the NMJ at muscle 6/7 segment A3 of WT 3rd instar larvae treated with a yeast paste containing 10mM DEM during development show significantly increased mean normalised synaptic bouton numbers (126±9.5, n=16) compared to controls (80±2.4, n=16) (*WT* + 10% ethanol in yeast paste) (***p<0.001; ANOVA with post hoc Bonferroni correction). Treating with 10mM Trolox shows no significant differences in mean normalised synaptic bouton numbers (74±3.6, n=16) compared to controls (NS p>0.05; ANOVA with post hoc Bonferroni correction). Treating with 10mM DEM and 10mM Trolox significantly reduced mean normalised synaptic bouton number (89±5, n=16) compared to larvae treated with 10mM DEM alone. (***p<0.001; ANOVA with post hoc Bonferroni correction). Error bars display ±SEM. **B**: Representative image of the NMJ at muscle 6/7 segment A3 imaged from each condition of the experiment; increased numbers of boutons (green) and branching of the synapse (magenta) are observed when treating with 10mM DEM, and are reduced upon 10mM Trolox treatment. Scale bar 30µm.

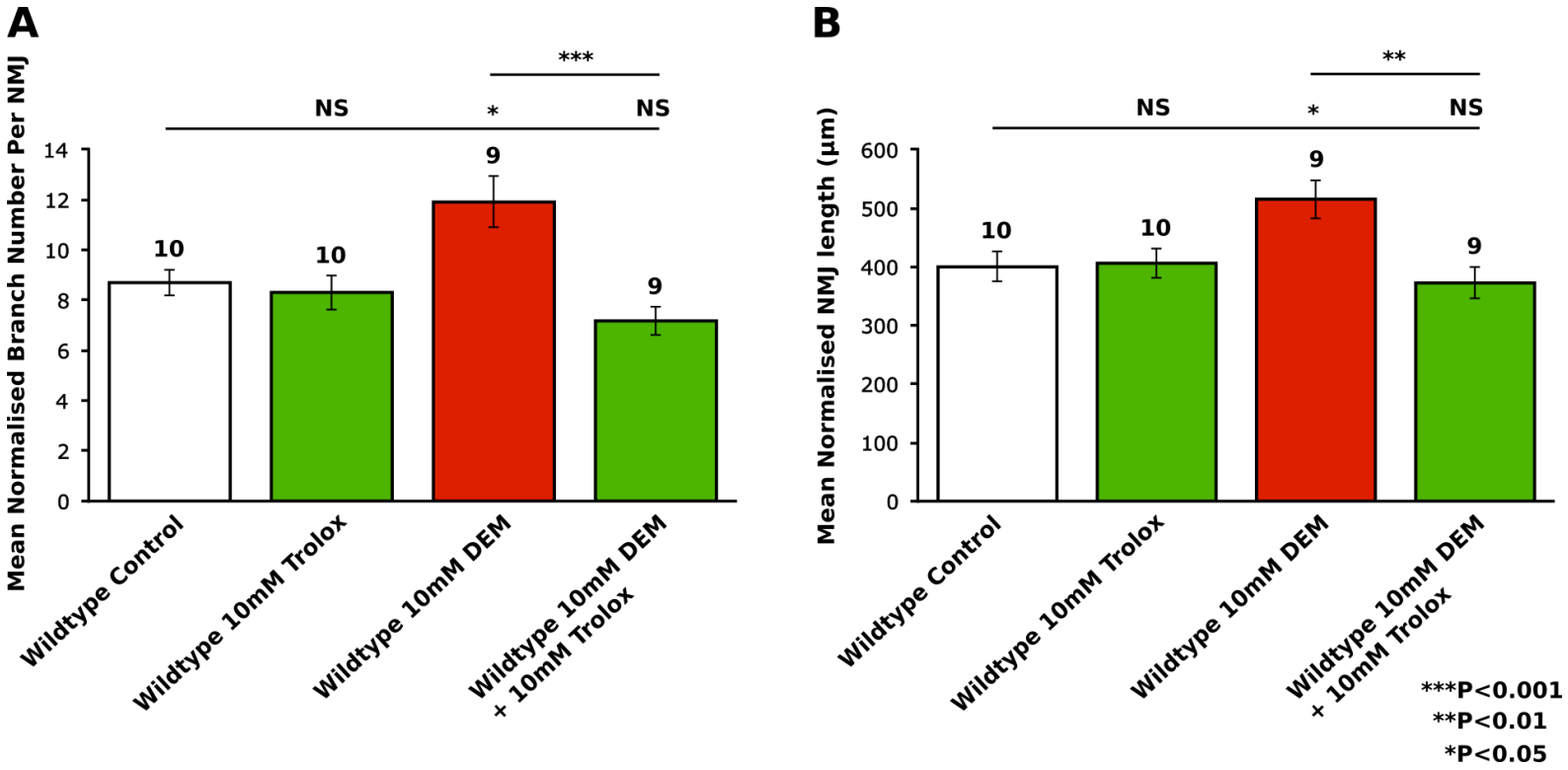

Figure 3.4 Trolox treatment rescues DEM-induced increases in branch number and NMJ length

A: Analysis of the NMJ at muscle 6/7 segment A3 of WT 3rd instar larvae treated with a yeast paste containing 10mM DEM during development show significantly increased mean normalised branch number (11.9±1, n=9) compared to controls (8.7±0.5, n=10) (*WT* + 10% ethanol in yeast paste) (*p<0.05; ANOVA with post hoc Bonferroni correction). Treating with 10mM Trolox shows no significant differences in mean normalised branch number (8.3±0.7, n=10) compared to controls (NS p>0.05; ANOVA with post hoc Bonferroni correction). Treating with 10mM DEM and 10mM Trolox significantly reduced mean normalised branch number (7.2±0.6, n=9) compared to larvae treated with 10mM DEM alone. (***p<0.001; ANOVA with post hoc Bonferroni correction).**B**: Treatment with 10mM DEM showed significantly increased mean normalised NMJ length (µm) (515±32.6, n=9) compared to controls (400±25.5, n=10) (*p<0.05; ANOVA with post hoc Bonferroni correction). Treatment with 10mM Trolox showed no significant difference in NMJ length (µm) (406±24.8, n=10) compared to controls (NS p>0.05; ANOVA with post hoc Bonferroni correction). Treatment with both 10mM DEM and Trolox significantly reduced NMJ length (µm) (373±26.2, n=9) compared to larvae treated with 10mM DEM alone (**p<0.01; ANOVA with post hoc Bonferroni correction). Error bars display ±SEM.

3.2.3 Mutations in *SOD1* cause synaptic overgrowth in *Drosophila* larvae

Synaptic overgrowth can also be modelled by removing both copies of the *SOD1* gene. *SOD1* encodes the enzyme Superoxide Dismutase 1, which acts to metabolise superoxide free radicals within the cytosol and the mitochondrial intermembrane space, acting as a primary defence against ROS generated by the mitochondria (Field et al., 2003, Bernard et al., 2011). Hypomorphic *SOD1* mutants were generated by crossing $SOD1^{n1}$ and $SOD1^{n64}$ flies together. Quantification revealed significantly increased mean normalised bouton number per NMJ in $SOD1^{n1}/SOD1^{n64}$ larvae compared to WT controls (Figure 3.5; $p<0.001$,ANOVA). The overgrowth observed was not significantly different to that achieved via a 10mM DEM treatment ($p>0.05$, ANOVA), which showed significant synaptic overgrowth compared to WT controls ($p<0.001$, ANOVA). Treating *SOD1* mutants with 10mM DEM did not increase the synaptic overgrowth ($p>0.05$, ANOVA), suggesting manipulation of the cellular antioxidant capacity alone has a finite ability to affect the synaptic growth response within the NMJ. We showed that *SOD1* mutant synaptic overgrowth was significantly reduced when treating with Trolox compared to *SOD1* mutant controls (Figure 3.8; $p<0.01$, ANOVA). No significant difference was found between WT controls and *SOD1* mutants treated with Trolox ($p>0.05$, ANOVA). The oxidative stress response was investigated further by manipulating cell-signalling pathways involved in synaptic growth.

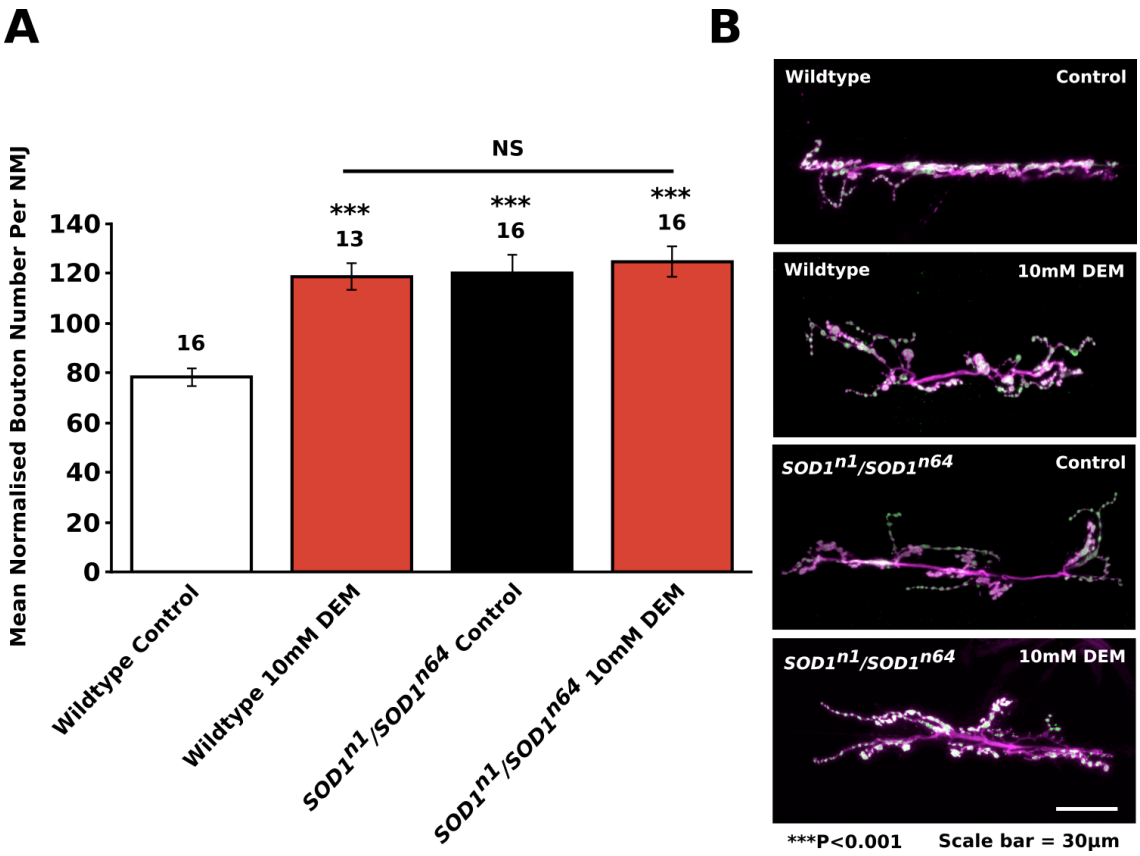

Figure 3.5 *SOD1* mutants exhibit synaptic overgrowth via an increase in oxidative stress

A: Analysis of the NMJ at muscle 6/7 segment A3 of 3rd instar WT larvae treated with a yeast paste containing 10mM DEM during development show significantly increased mean normalised synaptic bouton numbers (119±5.5, n=13) compared to WT controls (78±3.7, n=16) (*WT* + 10% ethanol in yeast paste) (***p<0.001; ANOVA with post hoc Bonferroni correction). Hypomorphic *SOD1* mutants show significant increases in mean normalised synaptic bouton numbers per NMJ (120±7.2, n=16) ($SOD1^{n1}/SOD1^{n64}$ + 10% ethanol in yeast paste) compared to controls (***p<0.001; ANOVA with post hoc Bonferroni correction). Treating *SOD1* mutants with 10mM DEM does not significantly increase mean normalised synaptic bouton number further (125±6, n=16) compared to *SOD1* mutant controls and WT treated with 10mM DEM (NS p>0.05; ANOVA with post hoc Bonferroni correction). Error bars display ±SEM. **B**: Representative image of the NMJ at muscle 6/7 segment A3 imaged from each condition of the experiment; increased numbers of boutons (green) and branching of the synapse (magenta) are observed when treating with 10mM DEM, and when *SOD1* is mutated. Scale bar 30µm.

3.2.4 Relieving inhibition on JNK/AP-1 and TGF-β signalling causes synaptic overgrowth

Two major pathways that regulate synaptic plasticity in *Drosophila* are JNK/AP-1 and TGF-β signalling. Activation of these pathways leads to synaptic growth, which can be manipulated by removing one copy of their feedback inhibitors, *puckered* (*puc*), a JNK-phosphatase and *daughters against Dpp* (*Dad*), a non-phosphorylatable MAD-like protein, respectively (Martín-Blanco et al., 1998, Aberle et al., 2002, Marques et al., 2002, Sanyal et al., 2002, Sweeney and Davis, 2002).

Using heterozygous puc^{E69} flies, a single copy of the *puckered* gene is removed, reducing puc levels and relieving the negative feedback inhibition that puc exerts upon JNK signalling. We showed that *puc* mutants displayed significantly increased mean normalised bouton number per NMJ compared to WT controls (Figure 3.6; $p<0.001$, ANOVA). No significant difference was observed between WT treated with 10mM DEM, heterozygous puc^{E69} mutants, and heterozygous puc^{E69} mutants treated with 10mM DEM ($p>0.05$, ANOVA). This suggests that JNK/AP-1 signalling facilitates the oxidative stress-induced synaptic overgrowth; no further overgrowth occurs when larvae exhibiting reduced JNK inhibition are subject to DEM treatment. It is postulated that DEM-induced oxidative stress activates JNK signalling, increasing its activity causing synaptic overgrowth. We confirmed that increased JNK signalling causes overgrowth and not oxidative stress in the heterozygous puc^{E69} mutants by treating them with 10mM Trolox that did not significantly reduce the bouton number when compared to puc^{E69}/+ controls (Figure 3.8; $p>0.05$, ANOVA).

The puc equivalent within TGF-β signalling is Dad, an inhibitory Smad that is induced by activation of the pathway and acts as a negative feedback regulator. Heterozygous Dad^{lacz} larvae showed significantly increased mean normalised bouton number per NMJ compared to WT controls (Figure 3.7; $p<0.001$, ANOVA). Both Dad^{lacz} control and DEM treated show significantly increased mean normalised bouton number per NMJ compared to WT treated with DEM ($p<0.001$ and $p<0.05$ respectively, ANOVA). No significant differences in synaptic bouton number are found between Dad^{lacz} control and DEM treated ($p>0.05$, ANOVA). These data show

similar results to a previous publication, which shows that TGF-β signalling can mediate synaptic growth and mutations in *Dad* cause synaptic overgrowth (Sweeney and Davis, 2002). It has also been shown that TGF-β promotes the development and maintenance of the nervous system, offering neuroprotection and deficiencies in TGF-β cause neurodegeneration, implying that this signalling pathway has an extremely important role in the neuron (König et al., 2005, Tesseur et al., 2006). Whilst interesting, our investigation encompasses the JNK signalling pathway, which will be the main focus in the forthcoming experiments.

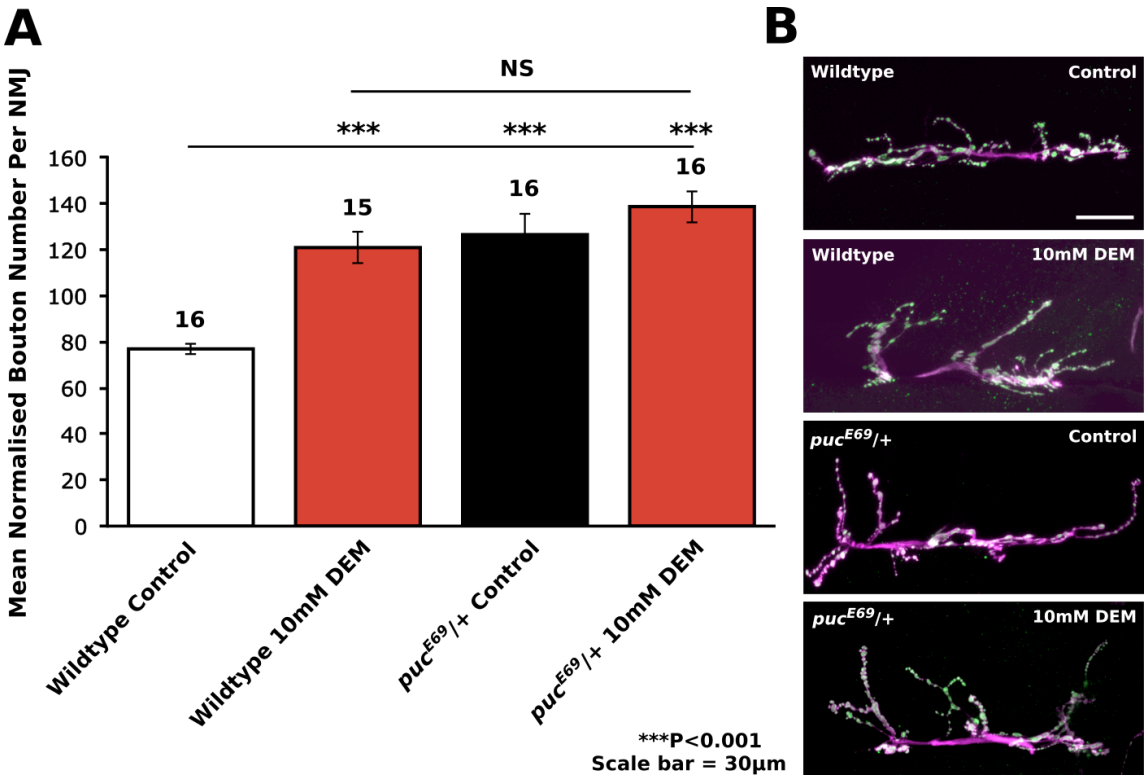

Figure 3.6 Loss of *puckered* causes synaptic overgrowth by relieving JNK inhibition

A: Analysis of the NMJ at muscle 6/7 segment A3 of 3rd instar WT larvae treated with a yeast paste containing 10mM DEM during development show significantly increased mean normalised synaptic bouton numbers (115±4, n=15) compared to WT controls (77±2.5, n=16) (*WT* + 10% ethanol in yeast paste) (***p<0.001; ANOVA with post hoc Bonferroni correction). Heterozygous *puc* mutants show significant increases in mean normalised synaptic bouton numbers per NMJ (120±5.6, n=16) (puc^{E69}/*CS* + 10% ethanol in yeast paste) compared to WT controls (***p<0.001; ANOVA with post hoc Bonferroni correction). Treating *puc* mutants with 10mM DEM does not significantly increase mean normalised synaptic bouton number further (134±7.3, n=16) compared to *puc* mutant controls and wild-types treated with 10mM DEM (NS p>0.05; ANOVA with post hoc Bonferroni correction). Error bars display ±SEM. **B**: Representative image of the NMJ at muscle 6/7 segment A3 imaged from each condition of the experiment; increased numbers of boutons (green) and branching of the synapse (magenta) are observed when treating with 10mM DEM, and when *puc* is mutated. Scale bar 30µm.

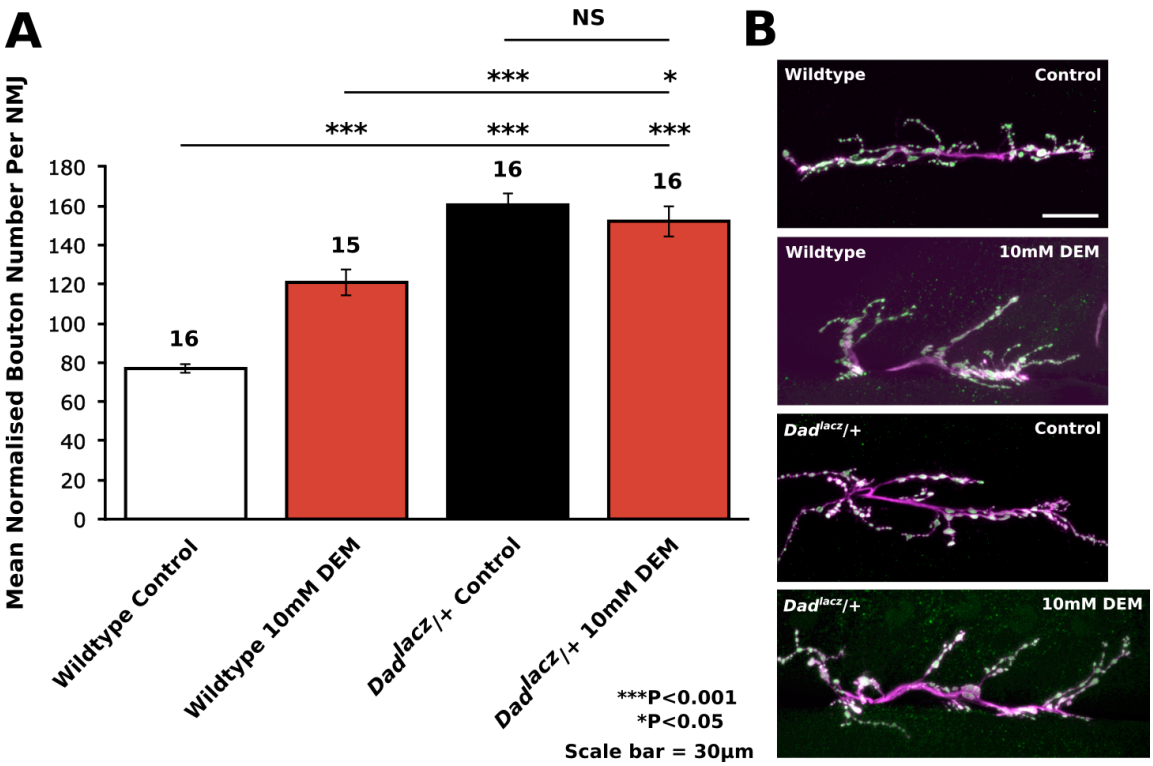

Figure 3.7 Loss of *Dad* causes synaptic overgrowth by relieving TGF-β inhibition

A: Analysis of the neuromuscular junction at muscle 6/7 segment A3 of 3rd instar WT larvae treated with a yeast paste containing 10mM DEM during development show significantly increased mean normalised synaptic bouton numbers (121±6.8, n=15) compared to WT controls (77±2.5, n=16) (*WT*, 10% ethanol in yeast paste) (***p<0.001; ANOVA with post hoc Bonferroni correction). Heterozygous *Dad* mutants show significant increases in mean normalised synaptic bouton numbers per NMJ (161±6.1, n=16) (Dad^{Lacz}/*CS*, 10% ethanol in yeast paste) compared to WT controls (***p<0.001; ANOVA with post hoc Bonferroni correction). Treating *Dad* mutants with 10mM DEM does not significantly change mean normalised synaptic bouton number (152±7.8, n=16) compared to *Dad* mutant controls (NS p>0.05; ANOVA with post hoc Bonferroni correction). Both *Dad* mutant controls and DEM treated show significantly increased mean normalised bouton number per NMJ compared to WT treated with DEM (***p<0.001 and *p<0.05 respectively; ANOVA with post hoc Bonferroni correction). Error bars display ±SEM. **B**: Representative image of the NMJ at muscle 6/7 segment A3 imaged from each condition of the experiment; increased numbers of boutons (green) and branching of the synapse (magenta) are observed when treating with 10mM DEM, and when *Dad* is mutated. Scale bar 30µm.

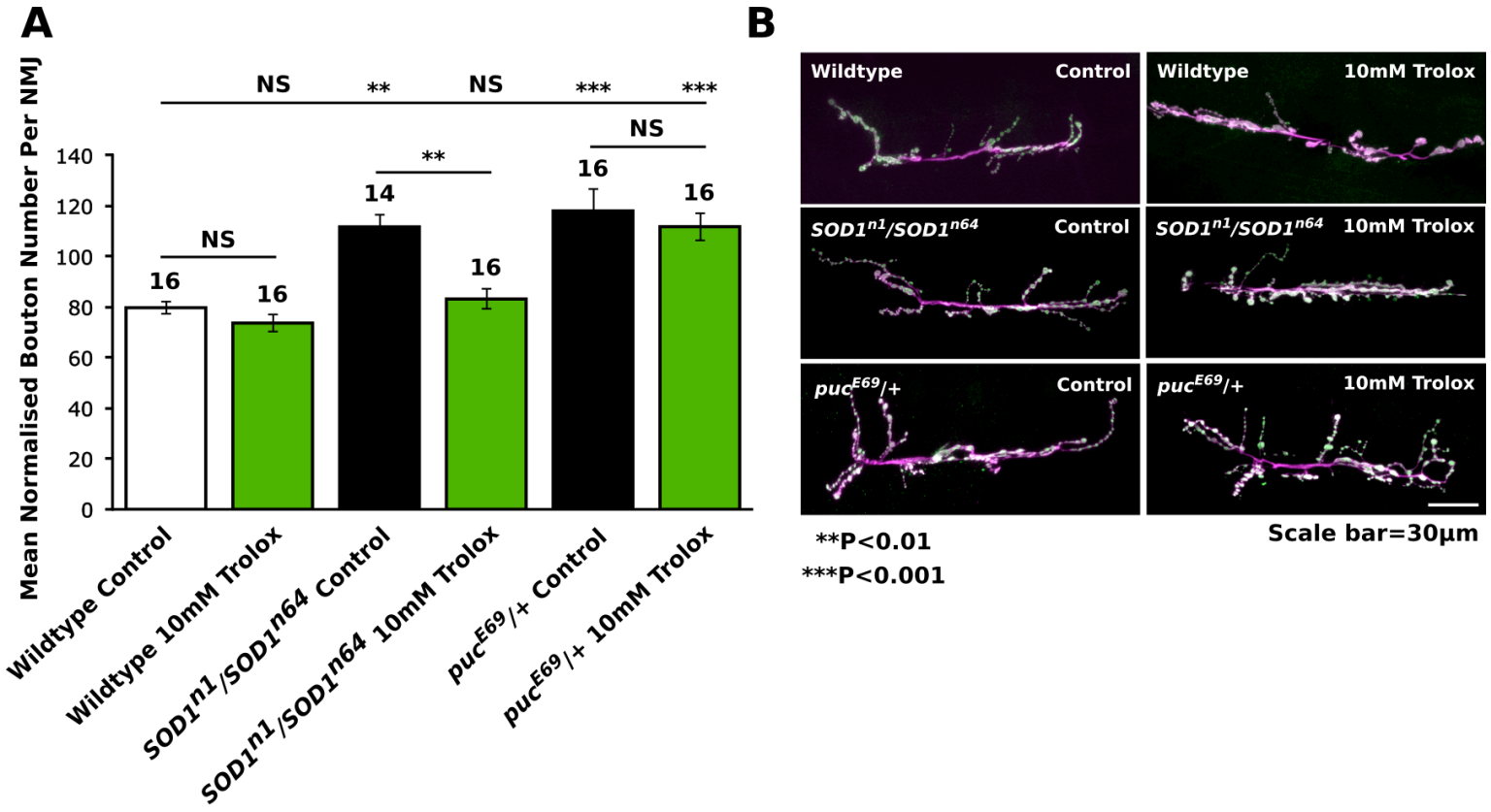

Figure 3.8 Trolox treatment rescues synaptic overgrowth via a reduction in ROS, not by decreasing JNK activity

A: Analysis of the NMJ at muscle 6/7 segment A3 revealed that WT treated with 10mM Trolox (74±3.6, n=16) show no significant difference in mean normalised bouton number per NMJ compared to WT controls(80±2.4, n=16)(NS p>0.05; ANOVA with post hoc Bonferroni correction). Both the hypomorphic $SOD1^{n1}/SOD1^{n64}$ mutants (112±5, n=14) and the heterozyous puc^{E69}/+ mutants (118±9, n=16) show significantly incresed mean normalised bouton numbers per NMJ compared to WT controls (**p<0.01 and ***p<0.001 respectively; ANOVA with post hoc Bonferroni correction). Treating $SOD1^{n1}/SOD1^{n64}$ mutants with 10mM Trolox (83±4, n=16) significantly reduces bouton number compared to their respective control (**p<0.01; ANOVA with post hoc Bonferroni correction) and shows no significant difference to WT controls (NS p>0.05; ANOVA with post hoc Bonferroni correction. Treating puc^{E69}/+ mutants with 10mM Trolox (112±5.4, n=16) shows no significant difference to their repective controls or to WT controls (NS p>0.05; ANOVA). Error bars display ± SEM. **B**: Representitive image of NMJ from each experimental condition. Scale bar=30µm.

3.2.5 JNK signalling facilitates DEM-induced synaptic overgrowth

From my analysis, increased activation of JNK/AP-1 signalling contributes to synaptic overgrowth (Figure 3.6). Given the known prominent role for the JNK/AP-1 signalling pathway in oxidative stress defence in other tissues, mechanism becomes the main focus of our investigation and we aim to elucidate this pathway further by examining the role of Fos and Jun in the DEM-induced oxidative stress response in neurons. The JNK-kinase kinase (JNKKK), ASK1, or apoptosis signal-regulating kinase 1, is activated by oxidative stress, and initiates the phosphorylation cascade that initiates JNK signalling. To investigate their role in synaptic overgrowth we expressed dominant negative (DN) versions of *ask1*, *fos* and *jun* in a pre- and post-synaptic manner via SpinGAL4 and analysed the larval NMJ. Expressing UAS-$ask1^{DN}$, fos^{DN} and jun^{DN} via SpinGAL4 in control conditions showed no significant differences in mean normalised bouton number per NMJ compared to WT controls (Figure 3.9; $p>0.05$, ANOVA). Treating WT with DEM showed significantly increased mean normalised bouton number per NMJ compared to WT controls ($p<0.001$, ANOVA). However, treating the animals expressing dominant negative transgenes with DEM showed no significant increases compared to WT, or their respective non-treated controls ($p>0.05$, ANOVA). Significant reductions in mean normalised bouton number per NMJ were found in fos^{DN} larvae compared to jun^{DN} and $ask1^{DN}$ when treated with DEM ($p<0.001$ and $p<0.05$ respectively, ANOVA). This may indicate a more prominent role for Fos in the synaptic growth response than ASK1 and Jun, though it is possible that due to the potential for Fos to form a homodimer during activation, expressing fos^{DN} may affect both Fos:Fos homodimer and Fos:Jun heterodimer, thus giving a stronger response. Regardless, these data indicate that DEM-induced synaptic overgrowth absolutely requires Fos, Jun and ASK1.

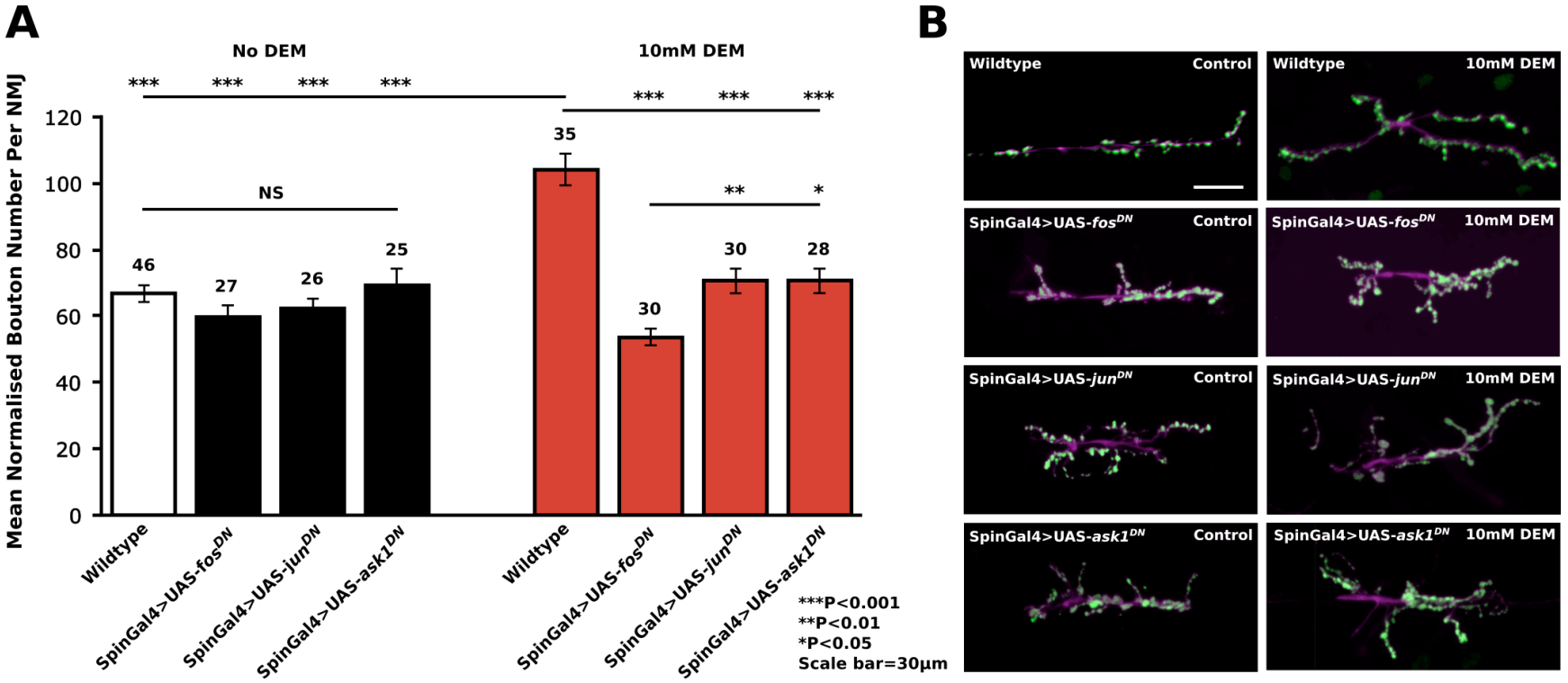

Figure 3.9 Permissive JNK signalling is required for oxidative stress-induced synaptic overgrowth

A: Analysis of the NMJ at muscle 6/7 segment A3 of 3rd instar WT larvae treated with a yeast paste containing 10mM DEM during development show significantly increased mean normalised synaptic bouton numbers (104±4.7, n=35) compared to WT controls (67±2.6, n=46) (*WT* + 10% ethanol in yeast paste) as well as larvae expressing dominant negative versions of members of the JNK signalling pathway, including UAS-fos^{DN} (60±3.4, n=27), UAS-jun^{DN} (62±3.0, n=26) and UAS-$ask1^{DN}$ (69±5.2, n=25), expressed pre- and post-synaptically using SpinGal4 under control conditions (***p<0.001; ANOVA with post hoc Bonferroni correction). Expressing the DN's does not significantly change mean normalised bouton number per NMJ compared to WT controls (NS p>0.05; ANOVA with post hoc Bonferroni correction). WT treated with 10mM DEM show significantly increased mean normalised bouton number compared to fos^{DN} (54±2.4, n=30), jun^{DN} (71±3.8, n=30) and $ask1^{DN}$ (71±3.8, n=28) also treated with 10mM DEM (***p<0.001; ANOVA with post hoc Bonferroni correction). During DEM treatment analysis revealed fos^{DN} to have significantly reduced mean normalised bouton number per NMJ compared to jun^{DN} and $ask1^{DN}$ (**p<0.001 and *p<0.05 respectively, ANOVA). Error bars display ±SEM. **B**: Representative image of the NMJ at muscle 6/7 segment A3 imaged from each condition of the experiment. Scale bar 30µm.

3.2.6 Fos and Jun antibody characterisation

A powerful tool in our investigation into the role of Fos and Jun in the oxidative stress response is the generation of antibodies to detect them. The Sweeney lab previously raised an antibody in rabbits to detect Fos (Rabbit anti-Fos88 and Fos89). To coincide with our investigation we raised an antibody in guinea pigs to detect Jun (Guinea pig anti-Jun59 and Jun60).

3.2.6.1 Investigating the working concentration of Fos and Jun antibodies

Initially, the working concentration for each antiserum was investigated by staining larvae with varying concentrations. We used 1:500 (data not shown), 1:1000 and 1:5000 (data not shown) and both antisera against Fos and Jun were determined to work at 1:1000 most efficiently (Figure 3.10). Anti-Fos 88 and anti-Fos 89 both work effectively at 1:1000 and both labelled nuclei in the ventral nerve cord (VNC) (Figure 3.10A) as well as the muscle (Figure 3.10B). Similarly, anti-Jun 59 and anti-Jun 60 also worked effectively at 1:1000 and labelled the nuclei in the VNC (Figure 3.11A) and muscle (Figure 3.11B)

3.2.6.2 Specificity of Fos and Jun antibodies

The specificity of each antibody was determined initially by using them to stain larvae expressing GFP tagged Jun (Jra-GFP.FLAG) or Fos (kay-GFP.FLAG) (Figure 3.12). The Jra-GFP.FLAG construct was generated via the introduction of a GFP and FLAG-tag epitope cassette, recombined into a copy of the Jra locus and inserted into the 3rd chromosome via a PiggyBac transposon (Spokony and White, 2013). In doing so Jra protein isoforms A, B and C were tagged with GFP and expressed in flies under near-normal endogenous promoter conditions whilst co-staining with anti-Jun59 and Jun60. This allowed us to determine how specific our antibodies were based on expression patterns. We observed colocalisation of both anti-Jun59 (Figure 3.12A(IV)) and Jun60 (Figure 3.12B(IV)) with Jra-GFP.FLAG, which was identified by the presence of white labelled nuclei, resulting from colocalised GFP expression with Cy3 (magenta) fluorescence. Fos and Jun are known to form

heterodimers, which should be detectable as colocalisation when co-staining with both anti-Jun59/Jun60 and anti-Fos88/Fos89. Colocalisation was found, determined by the presence of white-labelled nuclei, when staining with anti-Jun59-Cy3 (magenta) and anti-Fos88-FITC (green) (Figure 3.12A(V)) as well as when stained with Jun60-Cy3 (magenta) and anti-Fos89-FITC (Figure 3.12B(V)) (green). The kay-GFP.FLAG construct was generated in a similar manner to the Jra-GFP.FLAG construct, was used similarly to determine the specificity of the anti-Fos antibodies (Spokony and White, 2013). Staining larvae expressing kay-GFP.FLAG with both anti-Fos88 (Figure 3.12C(III)) and anti-Fos89 (Figure 3.12D(III)) showed colocalisation of our antibodies to GFP tagged Fos.

This data suggests that our antibodies show some specificity to their target proteins, as they are likely to be staining either the endogenous Fos or Jun in the same nuclei or the tagged versions of Fos and Jun themselves. We have not, however, fully characterised these antibodies, therefore caution is advised when using them, as there may exist some non-specific binding to undesired targets.

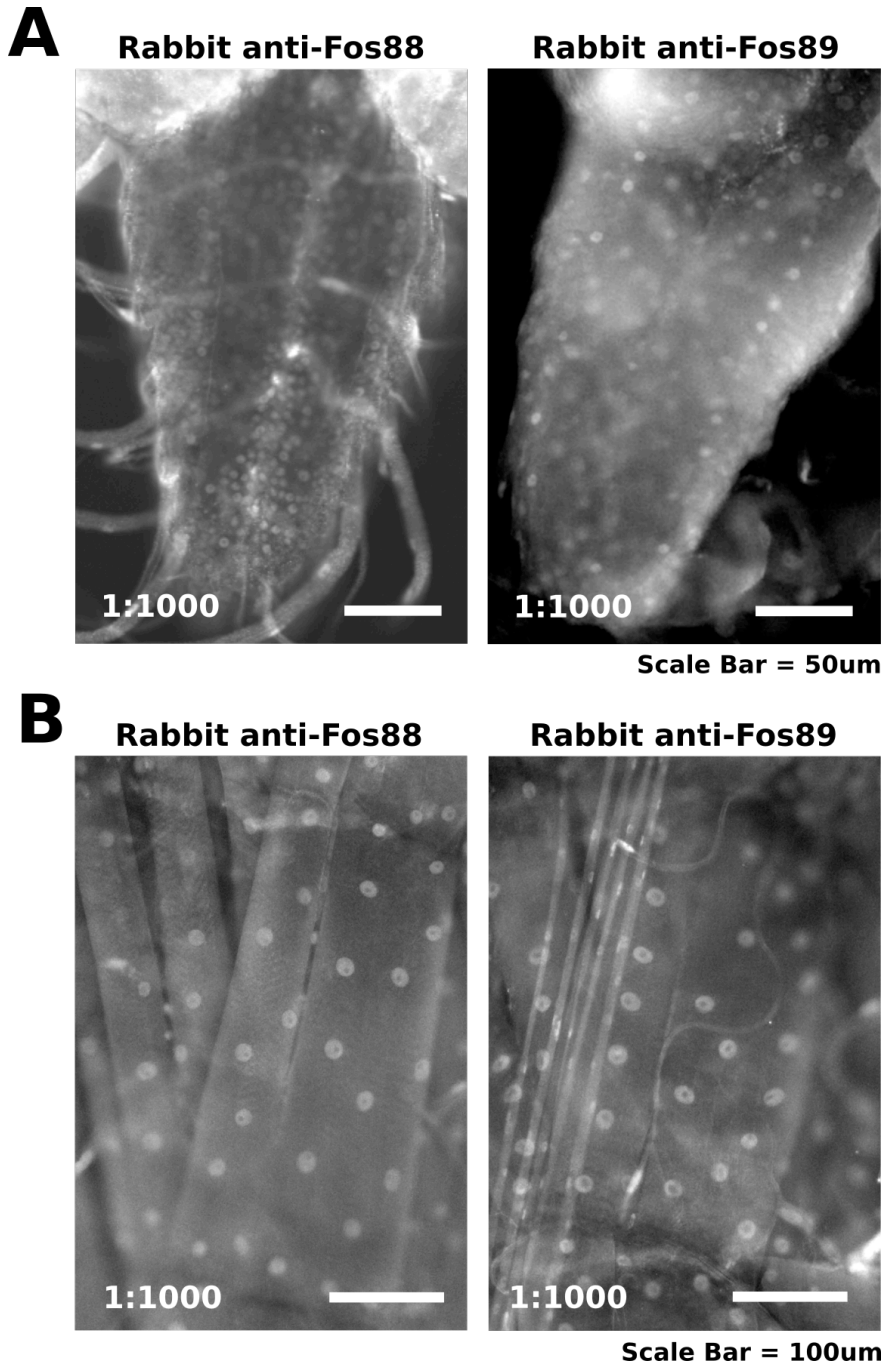

Figure 3.10 Rabbit anti-Fos88 and Fos89 stain in the ventral nerve cord and muscle

Staining WT larval dissections with rabbit anti-Fos88 and Fos89 at a 1:1000 dilution reveals nuclear staining within the ventral nerve cord (**A**) and muscle (**B**).

(**A**): Scale bar = 50µm; (**B**): Scale bar = 100µm

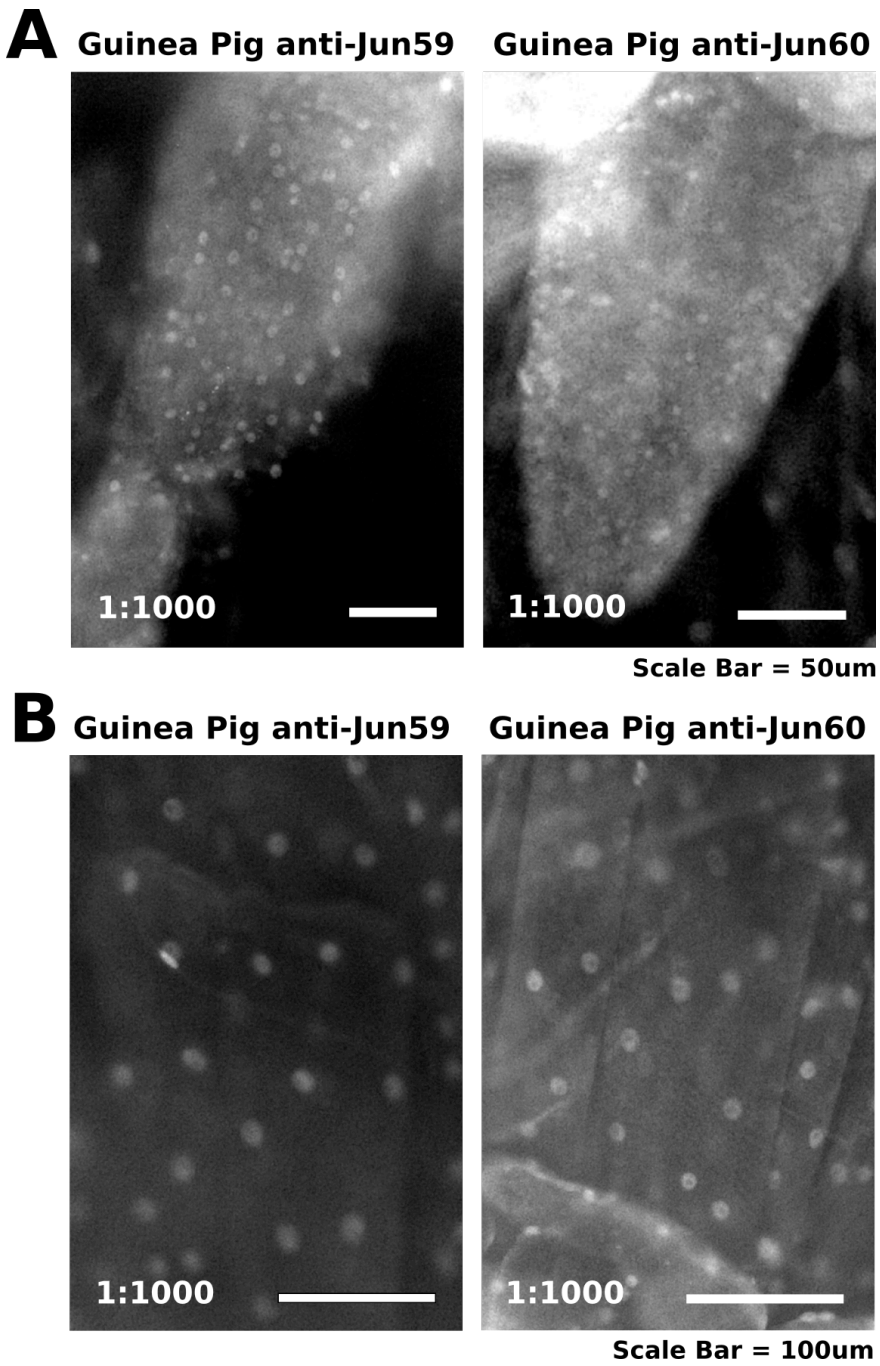

Figure 3.11 Guinea pig anti-Jun59 and Jun60 stain in the ventral nerve cord and muscle

Staining WT larval dissections with guinea pig anti-Jun59 and Jun60 at a 1:1000 dilution reveals nuclear staining within the ventral nerve cord (**A**) and muscle (**B**).

(**A**): Scale bar = 50µm; (**B**): Scale bar = 100µm

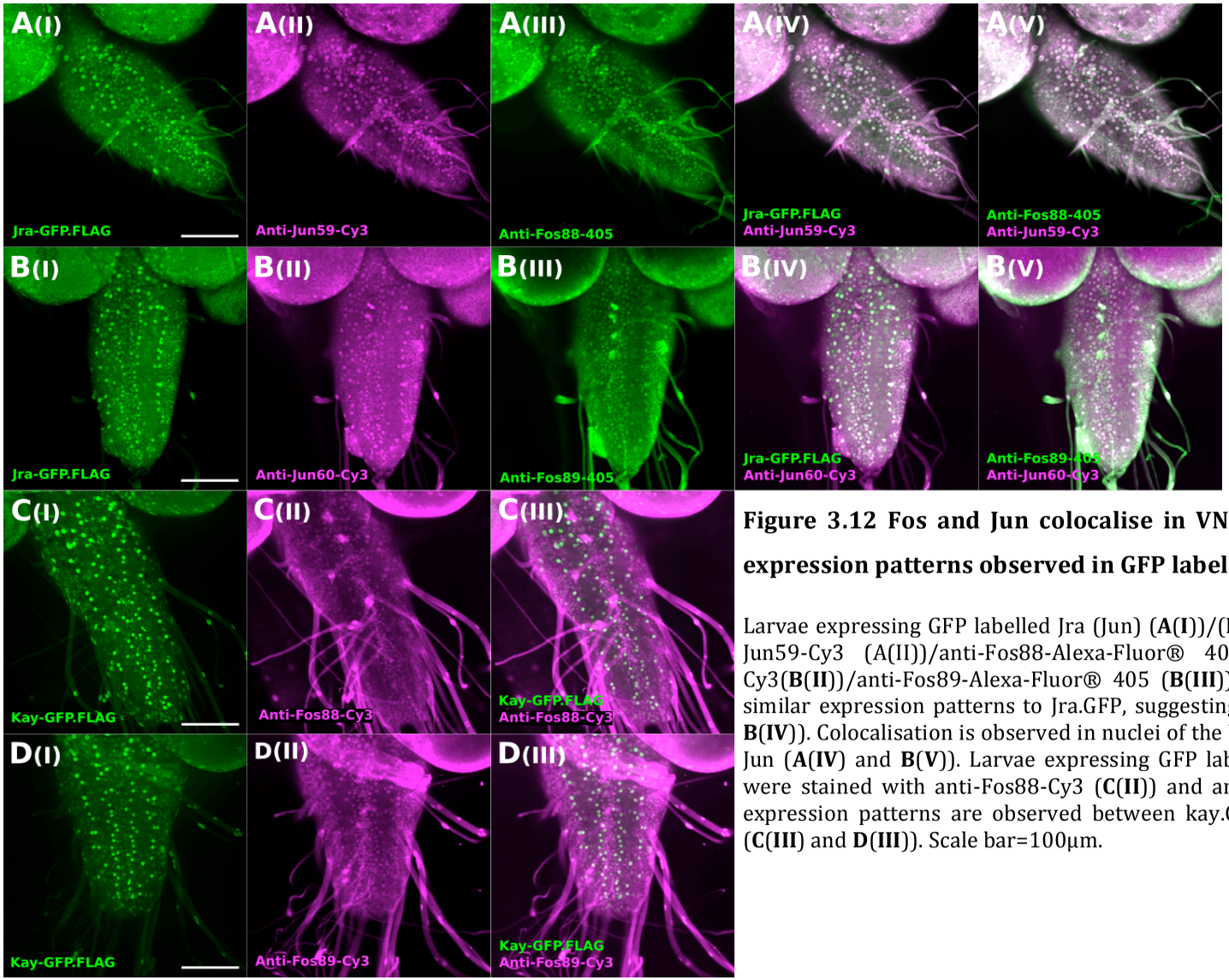

Figure 3.12 Fos and Jun colocalise in VNC nuclei, consistent with expression patterns observed in GFP labelled Fos and Jun

Larvae expressing GFP labelled Jra (Jun) (**A**(**I**))/(**B**(**I**)) were stained using anti-Jun59-Cy3 (A(II))/anti-Fos88-Alexa-Fluor® 405 (**A**(**III**)) and anti-Jun60-Cy3(**B**(**II**))/anti-Fos89-Alexa-Fluor® 405 (**B**(**III**)). The Jun antibodies display similar expression patterns to Jra.GFP, suggesting some specificity (**A**(**IV**) and **B**(**IV**)). Colocalisation is observed in nuclei of the VNC (white) between Fos and Jun (**A**(**IV**) and **B**(**V**)). Larvae expressing GFP labelled kay (Fos) (**C**(**I**))/(**D**(**I**)) were stained with anti-Fos88-Cy3 (**C**(**II**)) and anti-Fos89-Cy3 (**D**(**II**)). Similar expression patterns are observed between kay.GFP and both Fos antibodies (**C**(**III**) and **D**(**III**)). Scale bar=100µm.

3.2.6.3 Fos and Jun colocalise in the motor neuron nuclei

To determine the role of Fos and Jun in the oxidative stress response within the motor neuron, we confirmed their expression there. The OK6-GFP reporter construct was used to identify the motor neurons. OK6GAL4 (GAL4 expression in the motor neurons) was initially recombined with UAS-mCD8-GFP (GFP expression at the cell membrane) (Lee and Luo, 1999, McCabe et al., 2004). Larvae positive for this construct express GFP at the cell membrane of the motor neuron cells, which encompass a large nucleus shown as an absence of staining within the membrane. Co-staining these larvae with anti-Fos88 and anti-Jun59 revealed enrichment and colocalisation of Fos and Jun at the motor neuron nuclei (Figure 3.13).

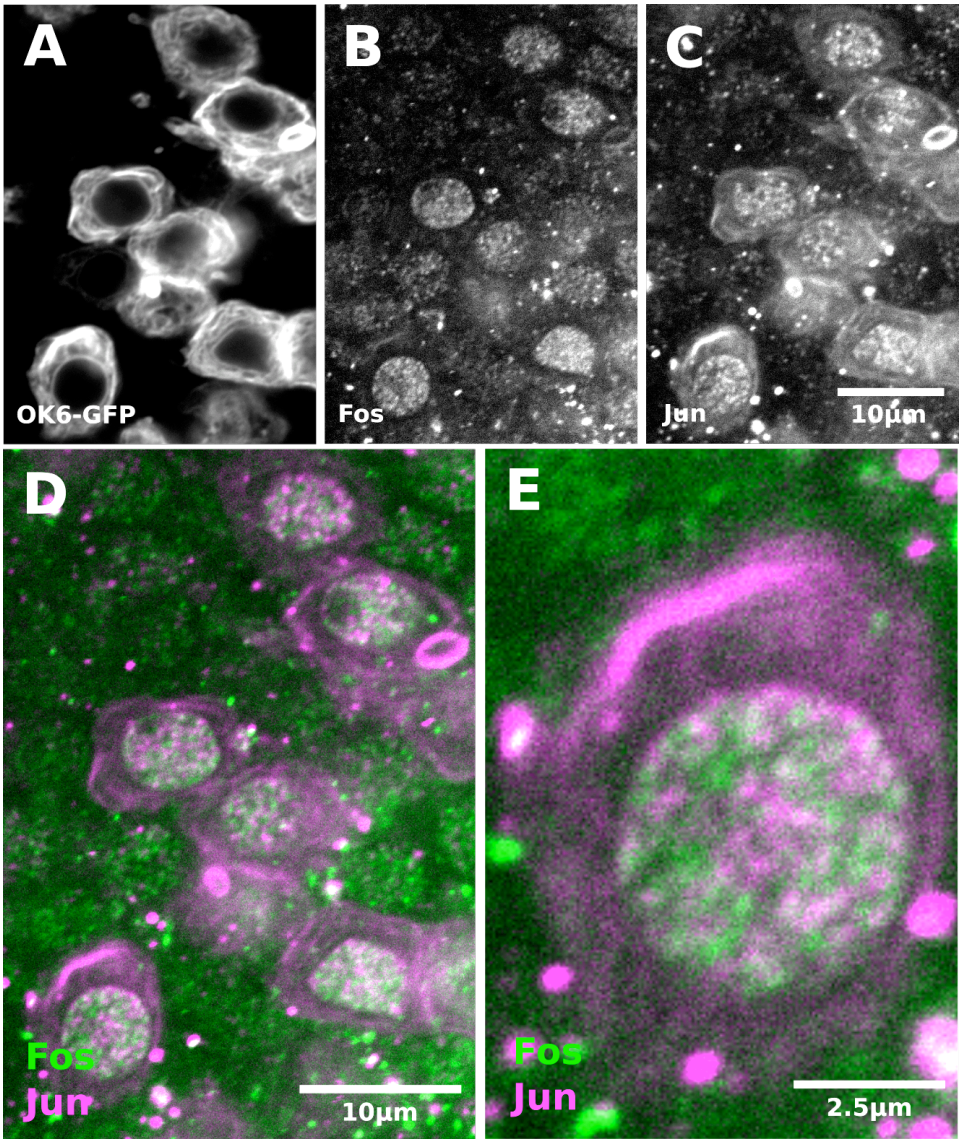

Figure 3.13 Fos and Jun colocalise in the motor neuron nuclei

Larvae expressing the motor neuron denoting OK6-GFP reporter construct which highlights the cell membrane of the motor neuron (**A**) were co-stained with anti-Fos88 (Alexa-Fluor® 405 (green)) (**B**) and anti-Jun59 (Cy3 (magenta)) (**C**) revealing enrichment and colocalisation of Fos and Jun in the motor neuron nuclei (**D-E**).

(**A-C**): Scale bar = 10µm; (**D**): Scale bar = 10µm; (**E**): Scale bar = 2.5µm

3.3 Discussion

Cellular ageing is characterised by an increase in ROS and the onset of oxidative stress. The high metabolic demand of neurons, their aversion to undergo apoptosis and the inability to replace these post-mitotic cells means these cells are longer lived and particularly susceptible to oxidative stress (Benn and Woolf, 2004). A number of neurodegenerative diseases implicate oxidative stress and damage to their onset and progression. In our *Drosophila* model of mitochondrial oxidative stress we find that above a certain threshold, oxidative stress leads to synaptic overgrowth, which is mediated by members of the JNK/AP-1 signalling pathway. Synaptic overgrowth can occur regardless of redox status due to over-activation/decreased inhibition of JNK signalling, as long as Fos and Jun are still functionally active. Fos and Jun dimerise forming AP-1, and are enriched in the motor neuron nuclei of *Drosophila* larval brains.

3.3.1 Oxidative stress causes synaptic overgrowth

In this investigation, we devised a model for mitochondrial oxidative stress in *Drosophila.* Feeding larvae DEM, we were able to cause significant overgrowth of the NMJ, which we know is caused by increases in ROS. In the mitochondria, glutathione is the main line of defence against ROS, maintaining the appropriate redox environment and preventing oxidative damage and mitochondrial dysfunction. Glutathione mainly acts to efficiently remove hydrogen peroxide from the mitochondria, before it reacts with lipid membranes and generates the more potent hydroxyl radical. Its importance lies in its versatility, not only acting to combat ROS but also as a critical cofactor in other antioxidant mechanisms that act to buffer redox changes (Marí et al., 2009). DEM acts to deplete levels of glutathione in the cell via conjugation, lowering the antioxidant defences and allowing much of the ROS produced by the mitochondria to go unchallenged. Raising larvae on 10mM DEM caused significant synaptic overgrowth, which cannot be exacerbated by increasing the concentration of DEM. This suggests that 10mM DEM is depleting enough glutathione within the mitochondria so that standing defences are no longer adequate. Increasing the concentration of DEM has no further effect, as presumably the majority of glutathione is conjugated to DEM. Treating larvae with 1mM and

3mM DEM did not cause significant overgrowth; the abundance of glutathione in these larvae must be high enough to combat the ROS produced by the mitochondria.

One of the major antioxidants in the mitochondrial matrix is SOD1, which acts to convert superoxide anions into hydrogen peroxide (May, 1901). Superoxide anions are produced via the mitochondrial respiratory chain in the mitochondrial matrix. We found that hypomorphic *SOD1* mutants exhibit synaptic overgrowth similar to treatment with 10mM DEM. This overgrowth was likely to be caused by increased levels of superoxide anions generating oxidative stress. Normally, SOD1 converts superoxide anions into hydrogen peroxide, which is then neutralised by several glutathione dependent antioxidant enzymes, such as glutathione peroxidase and peroxiredoxin (Bhabak and Mugesh, 2010). Treating *SOD1* mutant larvae with DEM showed overgrowth similar to that observed in WT treated with DEM; glutathione acting mainly on hydrogen peroxide and its downstream derivatives means that the superoxide anions remain unchallenged and depleting glutathione via DEM has no further effect when hydrogen peroxide is not generated due to mutations in the *SOD1* gene.

In summary, we have developed a mitochondrial model of oxidative stress in *Drosophila*. Using 10mM DEM causes an accumulation of ROS in the mitochondria, causing oxidative stress and synaptic overgrowth of the NMJ.

3.3.2 Synaptic overgrowth requires JNK/AP-1 signalling

A recent publication, described that ROS are major regulators of synaptic overgrowth via activation of the JNK signalling pathway (Milton et al., 2011). The *Drosophila spin* mutants were studied as a starting point. When analysed, the *spin* mutants displayed cytosolic oxidative stress-induced synaptic overgrowth. This study went on to demonstrate that the activation of JNK and Fos are required for *spin* mutant synaptic overgrowth, but not Jun and ASK1, suggesting a context-dependent activation of Jun in the regulation of synapse growth (Milton et al., 2011). It is well documented that Fos can homodimerise during cytoskeletal stress, and along with the *spin* mutant data suggests that ASK1 and Jun are not required in all responses to oxidative stress (Massaro et al., 2009). It was conceived that Jun

and ASK1 may only have a role in mediating synaptic overgrowth when the source of oxidative stress is the mitochondria. Using our model we showed that mitochondrial oxidative stress-induced overgrowth of the NMJ requires the activity of both ASK1 and Jun, as well as Fos. This reinforces the idea that there truly is a context-dependent role of Fos and Jun during oxidative stress and that the Fos/Jun heterodimer mediates this synaptic overgrowth response.

The larger question is "why does oxidative stress cause synaptic overgrowth via JNK signalling?" Following on from this, "Is this increased growth functional and acting to relieve the problem, or is it pathological and contributing to the problem?" Currently the answer remains unclear. It is thought that JNK signalling acts to protect against oxidative stress through autophagy activation. Several autophagy (*ATG*) genes are transcriptionally activated upon JNK activation and the protective effects of JNK signalling are reduced upon a loss of these *ATG* genes (Wu et al., 2009). Suppression of neuronal autophagy in mice causes protein aggregation and neurodegeneration, and with age, the levels of *ATG* gene expression in *Drosophila* neural tissues are reduced. It has been shown that *atg8a* mutations lead to increased sensitivity to oxidative stress, and that overexpression of the same protein, presumably increasing autophagy, leads to increased resistance (Simonsen et al., 2008). Autophagy, which is important for synaptic development has been shown to positively regulate the *Drosophila* NMJ; promoting NMJ growth by reducing Highwire (Hiw) levels (Shen and Ganetzky, 2009). Hiw is an E3 ubiquitin ligase that normally acts to restrain growth of the synapse by down-regulating Wallenda (Wnd), a mitogen activated protein kinase kinase kinase (MAPKKK). Wnd also triggers JNK activation (Ma et al., 2015). Hiw also negatively regulates TGF-β/BMP signalling, which is proposed to occur by targeting Medea for degradation; the associated NMJ overgrowth can also be partially rescued by introducing BMP family mutations (McCabe et al., 2004, Liebl, 2006).

This may help to explain why we observe synaptic overgrowth. DEM-treatment continually activates JNK signalling causing an overexpression of autophagy genes and maintaining low levels of Hiw. Unrestrained Wnd would then increase synaptic growth via further activation of JNK signalling, leading to a vicious cycle of sustained JNK activity. We have shown that ASK1 is required for DEM-induced

overgrowth; therefore Wnd and ASK1 may have similar functions. Synaptic overgrowth results from dysfunctional regulation of the JNK/AP-1 pathway and a failure to negatively regulate TGF-β/BMP signalling. It was shown during this chapter that removing the inhibition on TGF-β leads to severe synaptic overgrowth and this may help to explain how oxidative stress is also causing overgrowth. Normally, a cell exhibiting high levels of oxidative stress and dysfunctional signalling may undergo apoptosis. However, the critical functional importance of the terminally differentiated neuron has generated a mechanism where the default apoptotic pathway is shut down, to avoid loss of neurons that underlie functionality (Benn and Woolf, 2004). Neuronal cells may undergo apoptosis through the TNFα-mediated JNK-dependent cell death pathway under conditions of high oxidative stress (Guadagno et al., 2013). HSP70 and HSP72 however, exist to supress JNK-mediated apoptosis, preserving critical neurons (Gabai et al., 1997, Gabai et al., 1998). Neurons also require low levels of ROS for proper development; a necessary process aided by the fact that Nrf2 signalling, the other major antioxidant pathway, is repressed in young neurons to maintain ROS at a level adequate to induce JNK/AP-1 signalling (Bell et al., 2015). In mature neurons, short bursts of increased ROS following elevated neuronal activity activates JNK signalling, which is rapidly switched off following the transcription of puckered. This mediates synaptic plasticity and increases synaptic strength (Sanyal et al., 2002). This fundamental process persists during ageing due to its importance for cognitive function. However, the accumulation of ROS and onset of oxidative stress with age may lead to more frequent activation of JNK, contributing to neuronal decline and possibly neurodegenerative diseases.

3.3.3 Conclusions

In summary, neurons require ROS for proper development and synaptic plasticity, which may act through JNK/AP-1 signalling, a pathway that has one of its major roles, apoptosis, repressed in order to preserve adult neurons. Apoptotic repression means that ROS-induced over activation of JNK/AP-1 signalling in neurons does not result in cell death, and instead it leads to synaptic overgrowth, possibly through misregulation of TGF-β signalling.

The reasons behind the context-dependent forms of AP-1 are still unclear. We would expect the transcriptional output from AP-1 activated via mitochondrial ROS to be different than cytosolic ROS in order for the pathway to respond to the contextual ROS. The role of both Fos and Jun in the mitochondrial oxidative stress response may indicate this form has more prominent roles in responding to neuronal activity and metabolism, when mediating synaptic plasticity. How binding partners of Fos and Jun change when mitochondrial oxidative stress occurs, may help us clarify the role of AP-1 in this context.

4. Identifying binding partners of neuronal Fos and Jun in the presence and absence of oxidative stress

4.1 Introduction

The major aim of our project was to identify binding partners of neuronal Fos and Jun during normal conditions and under oxidative stress. To achieve this, N-terminally Tandem Affinity Purification-tagged (NTAP) versions of Fos and Jun were created and expressed pan-neuronally in flies. We removed and collected 4500 heads and performed tandem affinity purification before identifying the binding partners via mass spectrometry (see section 2.6). Fos and Jun play crucial roles in the oxidative stress response and mediate synaptic overgrowth in the NMJ when an oxidative burden occurs (see section 3.2.5). Whilst well studied, the role of Fos and Jun in synaptic plasticity is not fully understood, and identifying possible interactors of Fos and Jun may elucidate their role in the oxidative stress response further.

4.2 Results

4.2.1 Confirming the addition of a TAP-tag and functionality

Before we began tandem affinity purification, we ran an initial western blot to confirm the presence of the NTAP-tag in our Fos and Jun constructs when expressed via the UAS-NTAP-Fos and UAS-NTAP-Jun transgenes respectively. Each of the TAP-tagged constructs were expressed using elavGAL4, to generate pan-neuronal expression in flies, before their heads were removed and a protein sample prepared (see section 2.7.1). The empty vector control was used to determine the size of the TAP-tag (see Figure 4.1). The blot was stained with anti-mouse-IgG, which binds to the TAP-tag and not Fos or Jun. The TAP-tag itself appears to be ~27kDa. Fos isoform B cDNA which is ~58kDa was cloned into the NTAP-vector (Veraksa et al., 2005). With the addition of the TAP-tag we would expect a band ~85kDa, which we observe. Jun isoform A, which is ~31kDa was cloned into the NTAP-vector. Along

with the TAP-tag, we would expect a band of ~58kDa, and we observe a band at a little over 55kDa. This confirms that we have successfully added a TAP-tag to Fos and Jun and they are expressed when crossed to elavGAL4.

Whilst expressed, we do not know whether the addition of the TAP-tag affects their functionality. To test this, we expressed the TAP-tagged-Fos or Jun in a null mutant background. Expressing tagged-Fos in a null background (*kay*^{1}*/kay*^{2}) using actinGAL4 rescued the otherwise lethal null mutant, as we observed flies containing both mutations (absence of *TM6b* phenotype) surviving (see Figure 2.3). We also expressed tagged-Jun in the Jun null background (*jra*^{lA109}*/jra*$^{76\text{-}19}$) via SpinGAL4 and observed flies carrying the compound heterozygote combination (absence of *CyO* phenotype), which is not observed in this normally lethal combination, due to the expression of a TAP-tagged-Jun protein (see Figure 2.4). Therefore, both NTAP-tagged Fos and Jun retain their functionality whilst bound to a TAP-tag. With this in mind we proceeded to perform tandem affinity purification (see section 2.6.3) and mass spectrometry (see section 2.6.4) upon heads from animals in our 6 experimental conditions (see Table 2.7).

4.2.2 Identification of proteins bound to Fos and Jun

Following LC-MS/MS (see section 2.6.4), we generated a table of all bound proteins identified from each condition (see section Appendix 5: LC-MS/MS main run data). The LC-MS/MS data was initially processed with Bruker software and then searched using MASCOT using defined search parameters (see section 2.6.4). The identifications were restricted to *Drosophila* proteins in the UniProt database. Unfortunately, we identified relatively few peptides (80 unique across 4 samples); this was largely due to high levels of contamination in the samples. As a consequence, the number of peptide matches per protein was low, many only identified by a single peptide. On this basis we decided not to focus on aspects such as relative abundance of each protein, which can be quantified using the exponentially modified Protein Abundance Index (emPAI) score, or the MASCOT protein score which is generated using the number and quality of peptide matches. Our table of identified proteins focuses purely on what was present in the sample, showing only the number of significant peptide sequences that matched the

identified protein (see Table 4.1). All proteins that were identified in the empty vector control groups were removed, as they are assumed to be binding non-specifically to the tag rather than our bait proteins.

Importantly and reassuringly, we identify the bait proteins, Fos and Jun from each condition. We also identify Jun in the NTAP-Fos control condition, and Fos in the NTAP-Jun control and DEM treated condition. This adds confidence to our data as we pull down the proteins known to dimerise with our bait, as well as the bait itself. We identified 80 unique proteins across the 4 different tests and our main focus was to identify proteins bound to both Fos and Jun in either control or DEM-treated conditions that were not present in the opposing condition (see Table 4.2). We identify 6 proteins that were bound to both Fos and Jun in control conditions only and the protein with the most hits was GTP cyclohydrolase I, also known as Punch in *Drosophila*, which will be our focus later in this chapter. We also found 3 proteins bound to Fos/Jun in DEM-treated conditions only. We also performed a small scale pilot run with only 500 heads per sample, whilst it was concluded more heads were needed, we identified Punch bound to Jun, reinforcing data from the scaled up run (see Appendix 4: LC-MS/MS pilot run data).

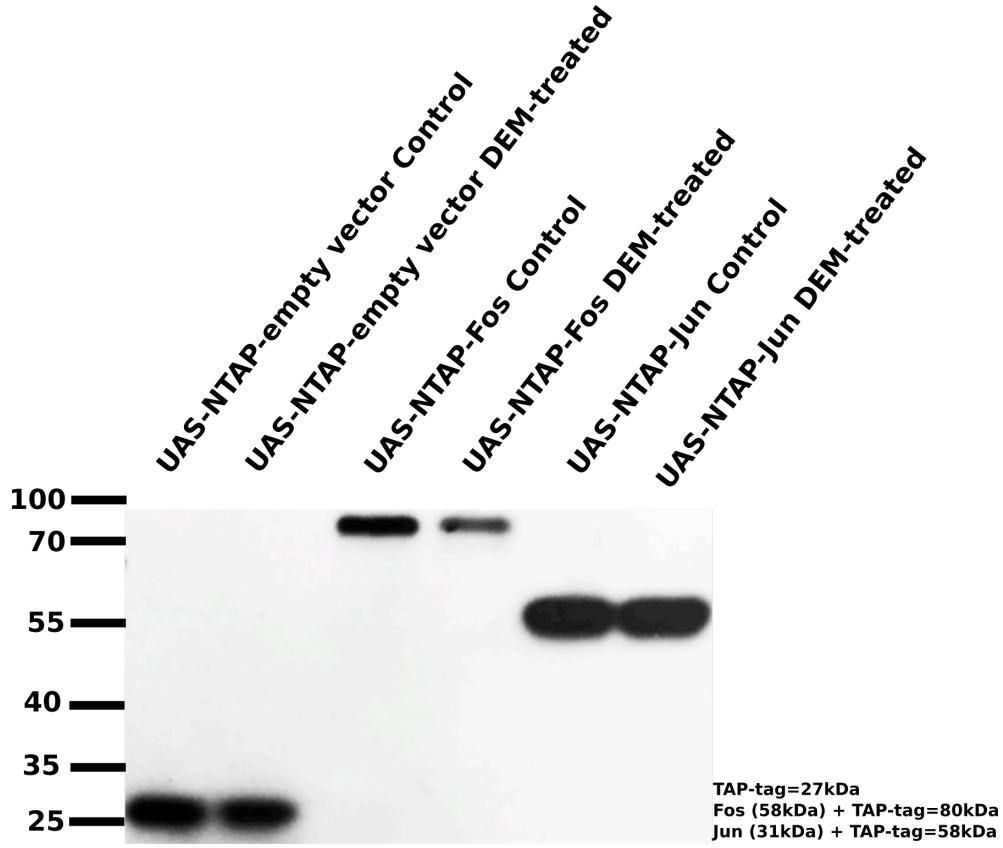

Figure 4.1 Expressing TAP-tagged Fos and Jun

Western blot of fly head samples expressing UAS-NTAP-empty vector/Fos/Jun via elavGAL4 reveals that the TAP-tag itself is 27kDa. The blot was performed using anti-mouse-IgG, which binds the TAP-tag only. Fos is known to be 58kDa, along with the TAP-tag we observe a band of around 85kDa. Jun is 31kDa, and we observe a band of around 55kDa, which would correlate to the addition of the TAP-tag.

Table 4.1 Number of significant sequences identified for each unique protein across the samples

		Number of Significant Sequences			
Identified Protein	**Gene Name**	**NTAP-Fos Control**	**NTAP-Fos DEM**	**NTAP-Jun Control**	**NTAP-Jun DEM**
Kayak	kay	4	3	2	2
Jun-related antigen	Jra	2	0	3	5
GTP cyclohydrolase 1	Pu	2	0	2	0
Heterogeneous nuclear ribonucleoprotein at 27C	Hrb27c	2	0	0	0
Ribosomal protein L17	RpL17	1	1	0	1
Protein-L-isoaspartate (D-aspartate) O-methyltransferase	Pcmt	1	1	1	0
Jonah 74E	Jon74E	1	1	1	0
CG5805	CG5805	1	1	0	0
CG14016-PA	tomb	1	1	0	0
CG11876	CG11876	1	0	1	1
Ionotropic receptor 54a	Ir54a	1	0	1	0
ATP synthase subunit gamma, mitochondrial	ATPsyn-gamma	1	0	1	0
Short Spindle 5	ssp5	1	0	1	0
CG15825-PB	fon	1	0	1	0
Trehalose-6-phosphate synthase 1	Tps1	1	0	1	0
14-3-3zeta	14-3-3zeta	1	0	0	0
CG11180	CG11180	1	0	0	0
Ribosomal protein S15	RpS15	1	0	0	0
CG42619	PRY	1	0	0	0
CG2861	CG2861-RA	1	0	0	0
CG5720	Nab2	1	0	0	0
Cell surface receptor TOLLO	Tollo	1	0	0	0
UpSET	upSET	1	0	0	0
CG9634	goe	1	0	0	0
CG15611	CG15611	0	1	0	1
CG4341	CG4341	0	1	0	1
Spindle D	spn-D	0	1	0	1
CG14692	CG14692	0	1	1	0
Phosphotidylinositol 3 kinase 59F	Pi3K59F	0	1	1	0
Tropomyosin 1	Tm1	0	1	0	0
CG34355	CG34355	0	1	0	0
LDL receptor protein 1	LRP1	0	1	0	0
Dystrophin	Dys	0	1	0	0
Misfire	mfr	0	1	0	0
CG42814	CG42814-RA	0	1	0	0
Four way stop	fws	0	1	0	0

Histone H2B	His2B	0	1	0	0
CG16739	CG16739	0	1	0	0
Ribosomal protein L40	RpL40	0	1	0	0
Transport and golgi organization 5	Tango5	0	1	0	0
Coiled-coil domain-containing protein CG32809	CG32809	0	1	0	0
Alpha-mannosidase	LManII	0	1	0	0
Protein phosphatase 1c interacting protein 1	Ppi1	0	1	0	0
CG12428	CG12428	0	1	0	0
Distracted	dsd	0	1	0	0
Nucleoporin 133kD	Nup133	0	1	0	0
Dipeptidase B	Dip-B	0	1	0	0
CG3940	CG3940	0	1	0	0
CG9272	CG9272	0	1	0	0
CG9170	CG9170	0	1	0	0
Rudhira	rudhira	0	1	0	0
CG32813	CG32813	0	1	0	0
Phosphodiesterase 11	Pde11	0	1	0	0
Translocation protein 1	Trp1	0	1	0	0
Phosphoenolpyruvate carboxykinase [GTP]	Pepck	0	0	1	1
Rootletin	Rootletin	0	0	1	1
Stonewall	stwl	0	0	0	1
Tyrosine-protein kinase hopscotch	hop	0	0	0	1
CG8468	CG8468	0	0	0	1
polyhomeotic distal	ph-d	0	0	0	1
CG4393	CG4393	0	0	0	1
CG10211	CG10211	0	0	0	1
CG8668	CG8668	0	0	0	1
CG11449	CG11449	0	0	0	1
Ubiquinol-cytochrome c reductase core protein 2	UQCR-C2	0	0	0	1
CG9861	CG9861-RA	0	0	0	1
CG3902	CG3902-RA	0	0	3	0
Scribbled	scrib	0	0	1	0
Isocitrate dehydrogenase [NADP]	Idh	0	0	1	0
Phosphodiesterase 8	Pde8	0	0	1	0
V(2)k05816	v(2)k05816	0	0	1	0
Alcohol dehydrogenase	Adh	0	0	1	0
40S ribosomal protein S25	RpS25	0	0	1	0
CG2051	CG2051	0	0	1	0
Hemomucin	Hmu	0	0	1	0
Probable cytochrome P450 313a2	Cyp313a2	0	0	1	0
CG10137	CG10137	0	0	1	0
Contactin	Cont	0	0	1	0

Probable medium-chain specific acyl-CoA dehydrogenase	CG12262	0	0	1	0
Protein O-mannosyltransferase 1	rt	0	0	1	0

Table 4.2 Peptides bound to both Fos and Jun in either control or DEM-conditions only

Control conditions only	DEM-treated conditions only
GTP cyclohydrolase I	CG15611
Ionotropic receptor 54a	CG4341
ATP synthase subunit gamma, mitochondrial	Spindle D
Short Spindle 5	
CG15825-PB	
Trehalose-6-phosphate synthase 1	

4.2.3 WebGestalt

The protein results were input into the WEB-based GEne SeT AnaLysis Toolkit (WebGestalt), in order to group the proteins based on their biological process, their molecular function and their subcellular location. This was performed via GO slim classification, which generated graphs for the biological process, molecular function and cellular component. The protein results were split into the following before WebGestalt/GO slim analysis; NTAP-Fos control and DEM-treated (Figure 4.2), NTAP-Jun control and DEM-treated (Figure 4.3), NTAP-Fos and NTAP Jun control only (Figure 4.4) and finally NTAP-Fos and NTAP-Jun DEM-treated only (Figure 4.5). When analysing proteins bound to Fos in both conditions, we observe that almost half of the proteins have an involvement in metabolic processes, followed closely by roles in cellular component organisation, biological regulation and response to stimuli (Figure 4.2A). We identify the majority of proteins as having molecular functions such as protein binding, hydrolase activity, ion binding and nucleic acid binding (Figure 4.2B). The cellular components that the majority of our

proteins were found in are macromolecular complexes followed by the nucleus, lipid particles, the membrane and in the cytoskeleton (Figure 4.2C).

When analysing the proteins bound to Jun only in control and DEM-treated conditions, similar patterns are observed. We identify the majority of bound proteins to be involved in metabolic processes, but also a large number have roles in biological regulation, cellular component organisation and response to stimuli (Figure 4.3A). Similarly, the Jun-bound proteins are also largely involved in ion binding as well as nucleotide binding and exhibit transferase activity (Figure 4.3B). Like the Fos-bound proteins, the majority of proteins bound to Jun reside in macromolecular complexes, lipid particles and the membrane, however, more than double are located in the mitochondria compared to Fos-bound proteins, suggesting Jun may have a larger role interacting with mitochondrial proteins than Fos (Figure 4.3C).

We then analysed proteins bound to Fos and Jun from control conditions only. We observe that the majority of proteins bound in control conditions are also involved in metabolic processes, followed closely with involvement in cellular component organisation, biological regulation and response to stimuli (Figure 4.4A). The molecular functions that the majority of proteins exhibit are ion binding, protein binding, nucleotide binding and nucleic acid binding (Figure 4.4B). The main cellular localisation of these proteins includes the macromolecular complex, the lipid particle, the nucleus and the mitochondria. Following recent work by the Sweeney lab, it was postulated that Jun plays a role in mitochondrially-sourced oxidative stress, such as DEM, therefore observing that a large number (~20%) of bound proteins are mitochondrial adds weight to this observation (Figure 4.4C).

Finally, we analysed the proteins bound to Fos and Jun in DEM-treated conditions. We again find that the majority of proteins are involved in the process of metabolism, but also biological regulation and response to stimuli (Figure 4.5A). The difference we see here is that upon DEM treatment, a large number (~35% compared to ~23% in control conditions) of the proteins identified are involved in localisation. This may indicate that DEM-treatment is initialising a cellular response, and may be up-regulating proteins involved in the localisation of activated AP-1.

Again, the majority of bound proteins here are involved in ion binding, as well as protein binding, hydrolase activity and nucleic acid binding (Figure 4.5B). The majority of proteins bound to Fos and Jun in DEM-treated conditions are localised to macromolecular complexes, not unlike the previous conditions. Many are also localised in the cytoskeleton, membrane-bound lumen, the membrane, nucleus and mitochondria (Figure 4.5C).

To summarise, it appears we have pulled down proteins largely involved in the metabolic process, cellular organisation and regulation, as well as response to stimuli. Whilst this gives a good overview of what our bound proteins may be involved in, it doesn't indicate any specific roles that may allude to how Fos and Jun control synaptic plasticity. Also due to the nature of our results and the problems we had concerning contamination, we put a very limited weight on any analysis we performed. However, due to the presence of our bait protein in each condition during the main run and that we also identified Punch bound to Jun in control conditions during our pilot run, we are confident in this hit.

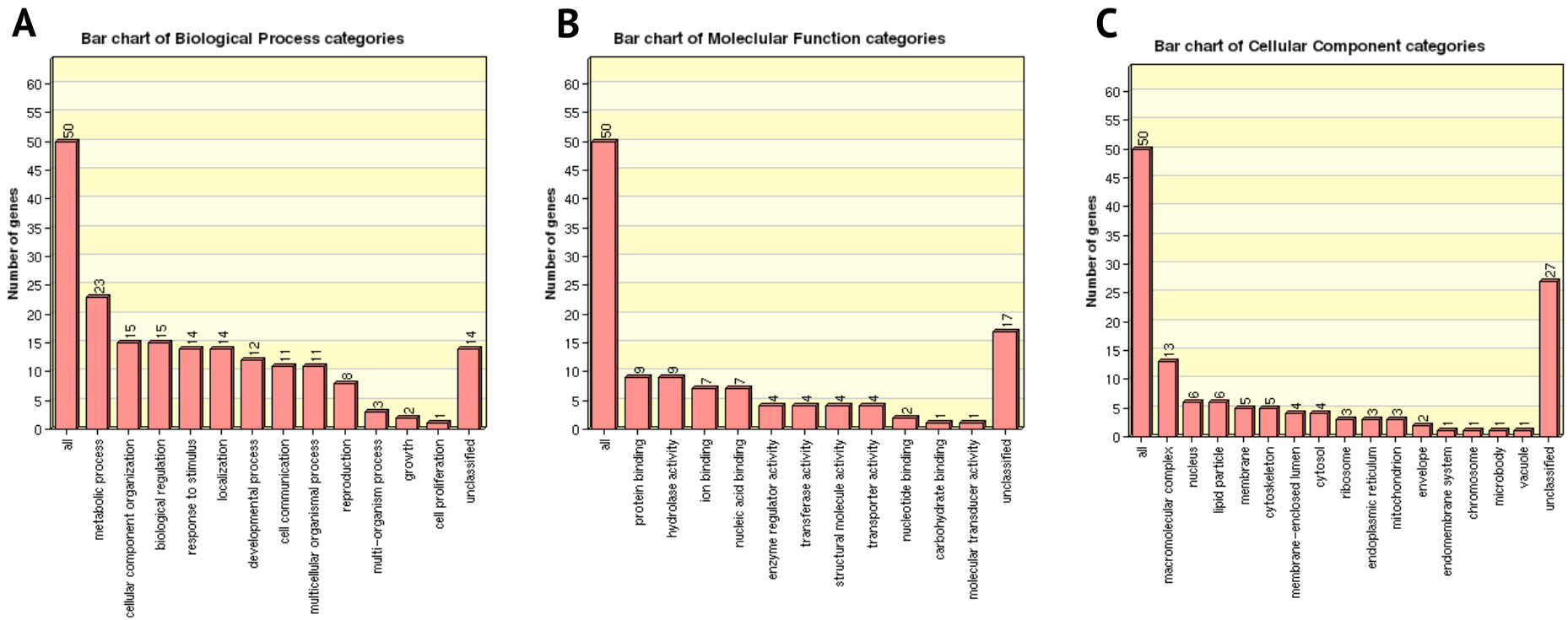

Figure 4.2 WebGestalt/GO slim classification analysis of proteins identified in NTAP-Fos control and DEM-treated conditions

Proteins identified in the NTAP-Fos control and DEM-treated samples were input into WebGestalt and analysed via GO slim classification to group the proteins via their biological processes (A), their molecular function (B) and the cellular component (C) they reside in. Almost half of the proteins identified are involved in a metabolic process. The majority of proteins exhibit either protein binding or hydrolytic activity and reside in macromolecular complexes.

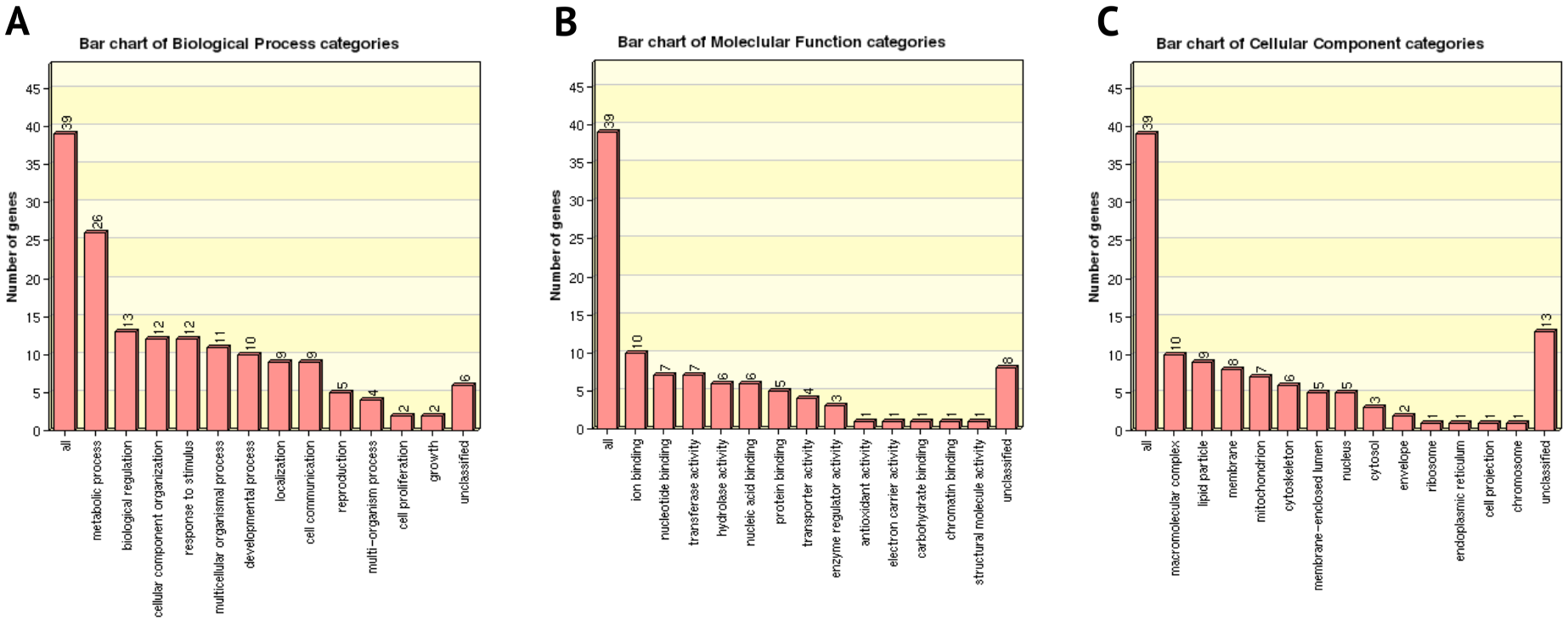

Figure 4.3 WebGestalt/GO slim classification analysis of proteins identified in NTAP-Jun control and DEM-treated conditions

Proteins identified in the NTAP-Jun control and DEM-treated samples were input into WebGestalt and analysed via GO slim classification to group the proteins via their biological processes (A), their molecular function (B) and the cellular component (C) they reside in. Over half of the proteins identified are involved in a metabolic process. The majority of proteins exhibit ion binding activity and reside in macromolecular complexes.

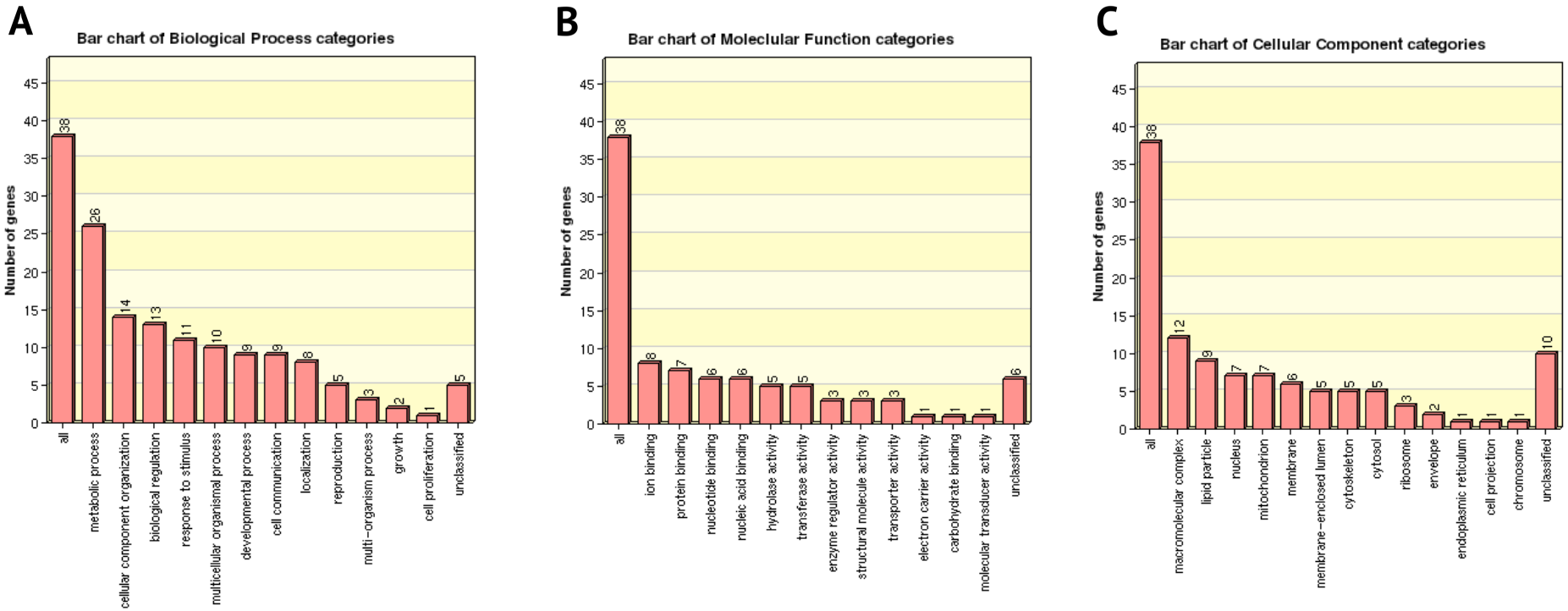

Figure 4.4 WebGestalt/GO slim classification analysis of proteins identified in NTAP-Fos and NTAP-Jun control conditions

Proteins identified in the NTAP-Fos and NTAP-Jun control samples were input into WebGestalt and analysed via GO slim classification to group the proteins via their biological processes (A), their molecular function (B) and the cellular component (C) they reside in. Over half of the proteins identified are involved in a metabolic process. The majority of proteins exhibit ion-binding activity and reside in macromolecular complexes.

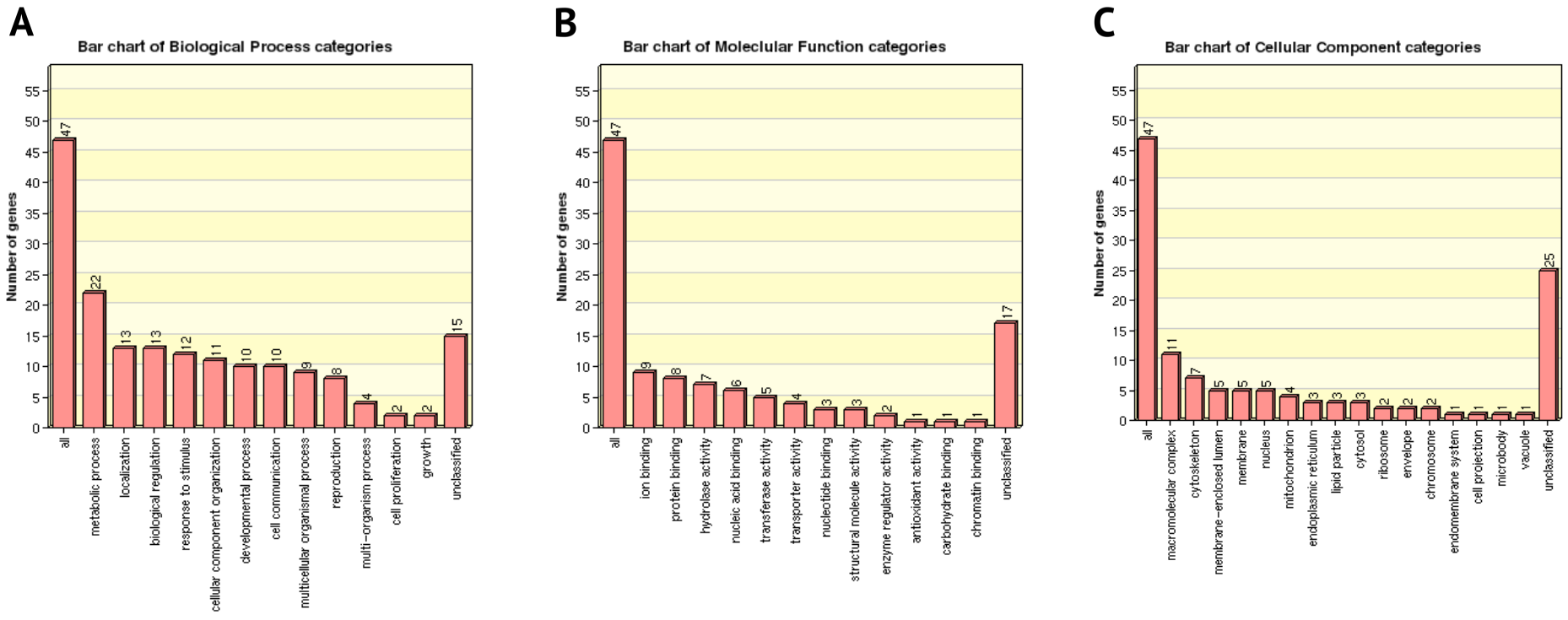

Figure 4.5 WebGestalt/GO slim classification analysis of proteins identified in NTAP-Fos and NTAP-Jun DEM-treated conditions

Proteins identified in the NTAP-Fos and NTAP-Jun DEM-treated samples were input into WebGestalt and analysed via GO slim classification to group the proteins via their biological processes (A), their molecular function (B) and the cellular component (C) they reside in. Almost half of the proteins identified are involved in a metabolic process. The majority of proteins exhibit ion-binding activity and reside in macromolecular complexes.

4.2.4 STRING analysis

The protein results were analysed using STRING, which generated protein-protein interaction networks of our results. STRING is a database of known and predicted protein-protein interactions, including direct and indirect associations. The STRING database derives its basis of interaction from various sources including genomic context predictions, which uses the observations that 2 or more proteins with the same expression pattern or absence in different genomes most likely have a functional link, high-throughput experiments, co-expression data, automated text-mining and from previous knowledge gained from other databases (Szklarczyk et al., 2015). Several runs of analysis were performed using different combinations of our results looking only at the proteins that are networked. The output of STRING analysis is shown below (Figure 4.6-Figure 4.9). The STRING analysis was split to show interaction networks of proteins identified from NTAP-Fos control and DEM-treated (Figure 4.6), NTAP-Jun control and DEM-treated (Figure 4.7), NTAP-Fos and NTAP Jun control only (Figure 4.8) and finally NTAP-Fos and NTAP-Jun DEM-treated only (Figure 4.9). Identified proteins that showed no known interaction with any other protein identified in that group were excluded. The colour of the STRING represents how the interaction was determined. The basis for interactions is shown in the figure key.

4.2.4.1 STRING-generated network using Fos-bound proteins only

Without taking into account the change in oxidative stress status, when analysing results from the NTAP-Fos control and DEM-treated condition we see Fos (kay) linked to Jun (Jra) which was an expected interaction. Both Fos and Jun are in an interaction network including Dystrophin (Dys), Tropomyosin 1 (Tm1) and Transport and golgi organisation 5 (Tango 5) (Figure 4.6). Dys is required for appropriate synaptic retrograde communication and forms part of the Dystrophin Glycoprotein Complex (DGC). The DGC complex acts to maintain the integrity of skeletal and cardiac muscle whilst also acting as a protein scaffold for proteins involved in cell signalling. DGC accumulates at the NMJ as well as other synapses of the peripheral and central nervous system where it is important for the maturation of neurotransmitter receptor complexes and in regulating neurotransmitter release

itself. Mutations in this gene in humans cause Duchenne muscular dystrophy, characterised by muscle wastage and also occasionally mental retardation (Pilgram et al., 2010). Tm1 promotes cytoskeleton remodelling in response to oxidative stress via the ERK signalling pathway. When unrestrained, Tm1 causes axons to grow longer but also results in smaller growth cones (Houle et al., 2003). Tango5 is the *Drosophila* homolog of vacuole membrane protein 1 (VMP1), a protein that interacts with Beclin1 to regulate autophagy induction (Molejon et al., 2013).

4.2.4.2 STRING-generated network using Jun-bound proteins only

Similar to Fos, when analysing the Jun-bound proteins, from both control and DEM-treated conditions, we find several proteins in this interaction network that are known/predicted to interact with Jun/Fos (Figure 4.7). However, these proteins differ from those bound to Fos. Importantly we have identified Fos in these pull downs, known to bind Jun and form AP-1. Other proteins in the more immediate interaction network include Hopscotch (Hop), Scribbled (Scrib) and Phosphoenolpyruvate carboxykinase (PEPCK). The *Hop* gene encodes *Drosophila* Janus Kinase (JAK), which plays an important role in long-term memory formation within the mushroom bodies (Copf et al., 2011). Scrib is required for short-term synaptic plasticity. At the NMJ, Scrib colocalises with Discs-large (Dlg), in complex they are critical for the development of normal synapse structure and function. The phenotypes of *scrib* mutants are observed as increases in synaptic vesicles in synaptic boutons that act as the vesicle reserve pool, reduction in the number of active zones, a loss of facilitation and faster synaptic depression. It is thought that synaptic vesicle dynamics are also impaired in *scrib* mutants, and taken together highlights that Scrib is essential for synaptic plasticity (Roche et al., 2002). PEPCK is essential in glucose homeostasis, as it catalyses the rate controlling step in gluconeogenesis, the process of which glucose is produced. This metabolic protein, which we identify as being bound to Jun and in the STRING network is predicted to bind to Fos, may highlight important roles for AP-1 in metabolism, though currently its role is unclear.

To summarise, the predicted direct interaction network may suggest a role for Jun in memory and synaptic plasticity, which again fits with data presented in Chapter

3, showing that both Fos and Jun are required for oxidative stress-induced synaptic overgrowth and therefore have a clear role in synaptic plasticity. We also find Jun bound to metabolic proteins, as highlighted earlier (Figure 4.2A). An important network identified here shows Punch bound to alcohol dehydrogenase (Adh), in a network of metabolic proteins that connects Punch to Fos and Jun. Adh is the protein responsible for metabolising alcohol, isocitrate dehydrogenase (Idh) is responsible for metabolising isocitrate and CG11876 exhibits pyruvate dehydrogenase activity, leading to PEPCK and Fos/Jun. Currently, there is no published data to suggest that Punch binds either Fos or Jun; however we identified it within our samples of Fos and Jun in control conditions only (Figure 4.8). There is the possibility that Punch was purified because it was bound to another protein that binds Fos or Jun, not directly bound. However, if this is true, we did not identify this protein or it is not currently known to bind Fos or Jun.

4.2.4.3 Comparing STRING-generated networks of Fos and Jun-bound proteins from control to DEM-treated conditions

One aim of this investigation was to determine how Fos and Jun binding partners change when oxidative stress ensues. We generated a STRING interaction network of the binding partners of Fos and Jun in control conditions only, to reveal that no known or predicted interactions occur between any of the identified proteins and Fos and Jun (Figure 4.8). Interestingly, in control conditions we still identify Punch being bound into the metabolic protein network mentioned previously, bound via Adh to Idh, CG11876 etc. This network is not present when treating with DEM (Figure 4.9). Firstly we do not identify Punch, Adh, Idh or CG11876 when treating with DEM, suggesting that Fos and Jun may have a more metabolic role when the cell is not oxidatively stressed. Upon DEM treatment, we identified Dys, Hop and Tango5, which have roles in regulating neurotransmitter release/acting as a signalling scaffold, in long-term memory formation and in regulating autophagy. These represent physiological changes that may occur because oxidative stress ensued, activating AP-1 as an outcome and interacting with the identified proteins.

These observations are purely hypothetical, as the STRING networks include predicted interactions and the unlinked identified proteins are removed from the

figures. We utilise STRING mainly to derive insight into the data and gain some idea of how Fos and Jun are functioning. Unfortunately, we identified relatively few proteins in this experiment, and the proteins we do identify do not appear often. Because of this we focused our attention to proteins in the list that were identified in either control or DEM-treated conditions only (Table 4.2). Exploring the literature we found GTP cyclohydrolase I, or Punch to be of interest, and it is one of the few proteins identified that is only bound in control conditions, yet lost in oxidative stress conditions. As mentioned previously, we also identified Punch in the smaller scaled pilot study, giving confidence to this hit. Because of this, Punch became the focus of the project going forward.

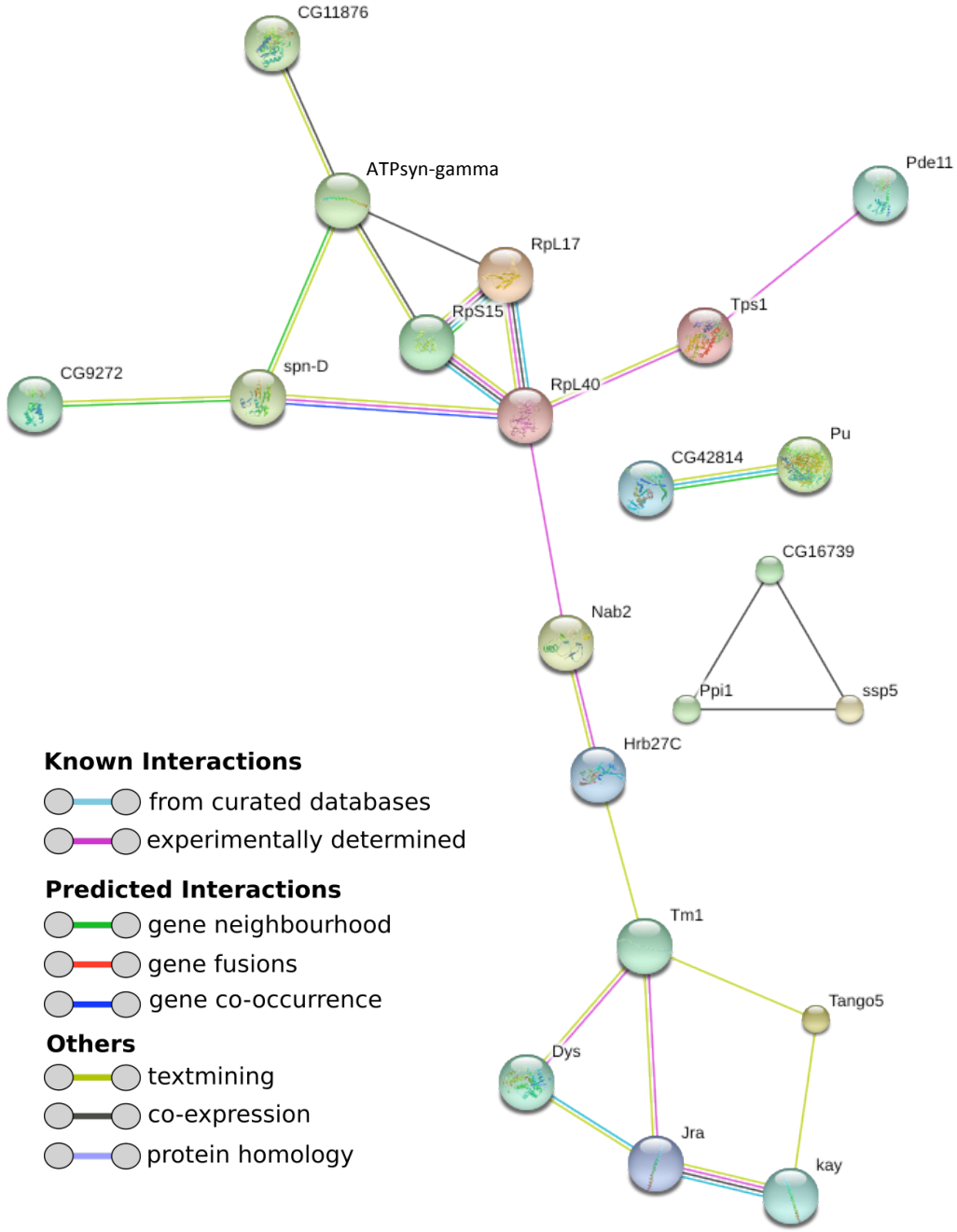

Figure 4.6 Interaction networks of proteins identified from NTAP-Fos control and DEM-treated conditions, derived in STRING

Proteins identified in NTAP-Fos control and DEM-treated conditions were subject to STRING analysis to generate networks of known interactions within our results. Fos (kay) is shown to interact with Jun (Jra) in this network and is linked to Dystrophin (Dys), Tropomyosin 1 (Tm1) and Transport and golgi organisation 5 (Tango 5). See key for the basis of interaction.

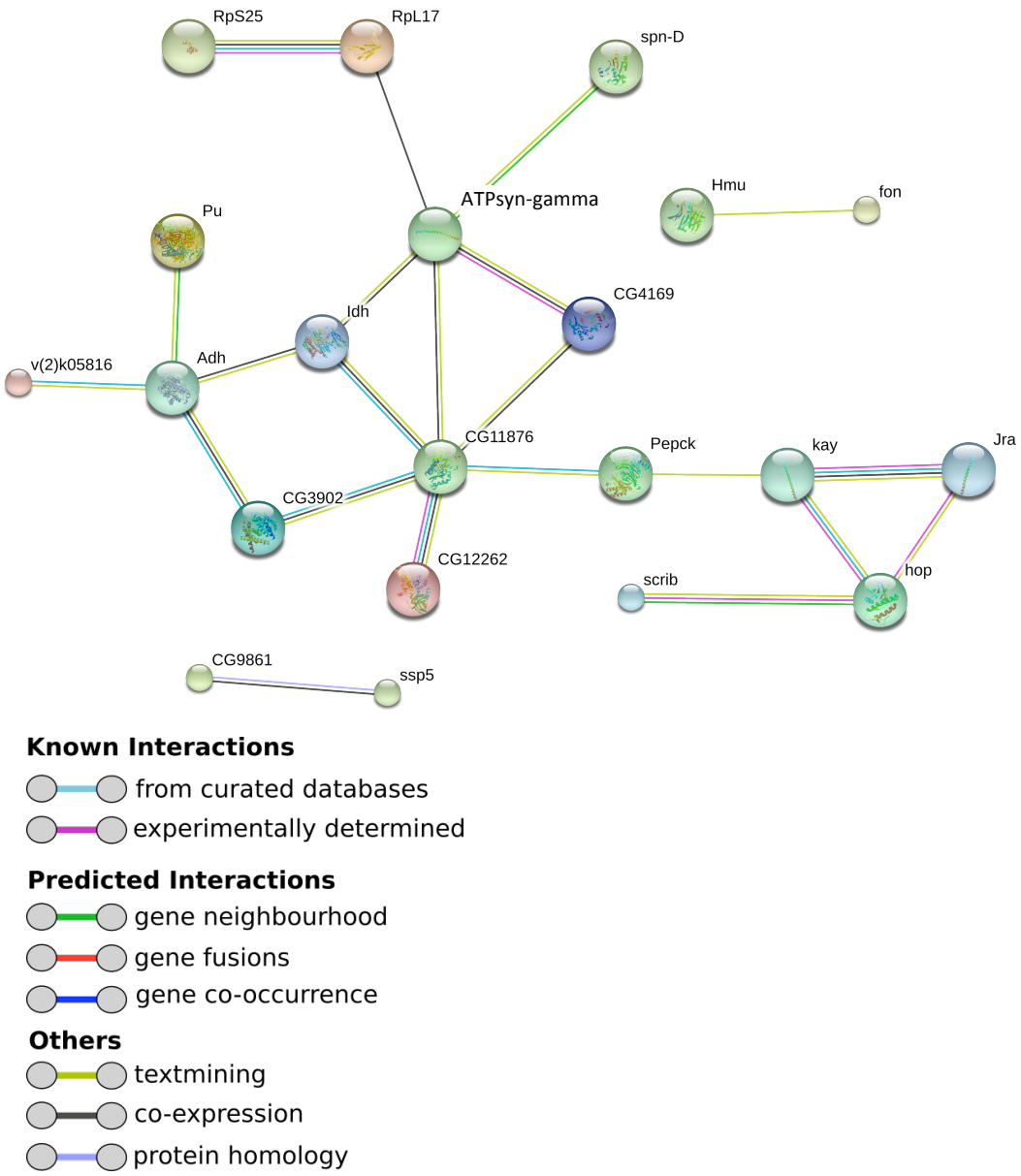

Figure 4.7 Interaction networks of proteins identified from NTAP-Jun control and DEM-treated conditions, derived in STRING

Proteins identified in NTAP-Jun control and DEM-treated conditions were subject to STRING analysis to generate networks of known interactions within our results. Fos (kay) is shown to interact with Jun (Jra) in this network. This network also links GTP cyclohydrolase I (Punch (Pu)) to Fos and Jun via Alcohol Dehydrogenase (Adh), Isocitrate Dehydrogenase (Idh), CG11876 (Pyruvate Dehydrogenase) and Phosphoenolpyruvate carboxykinase (Pepck). See key for the basis of interaction.

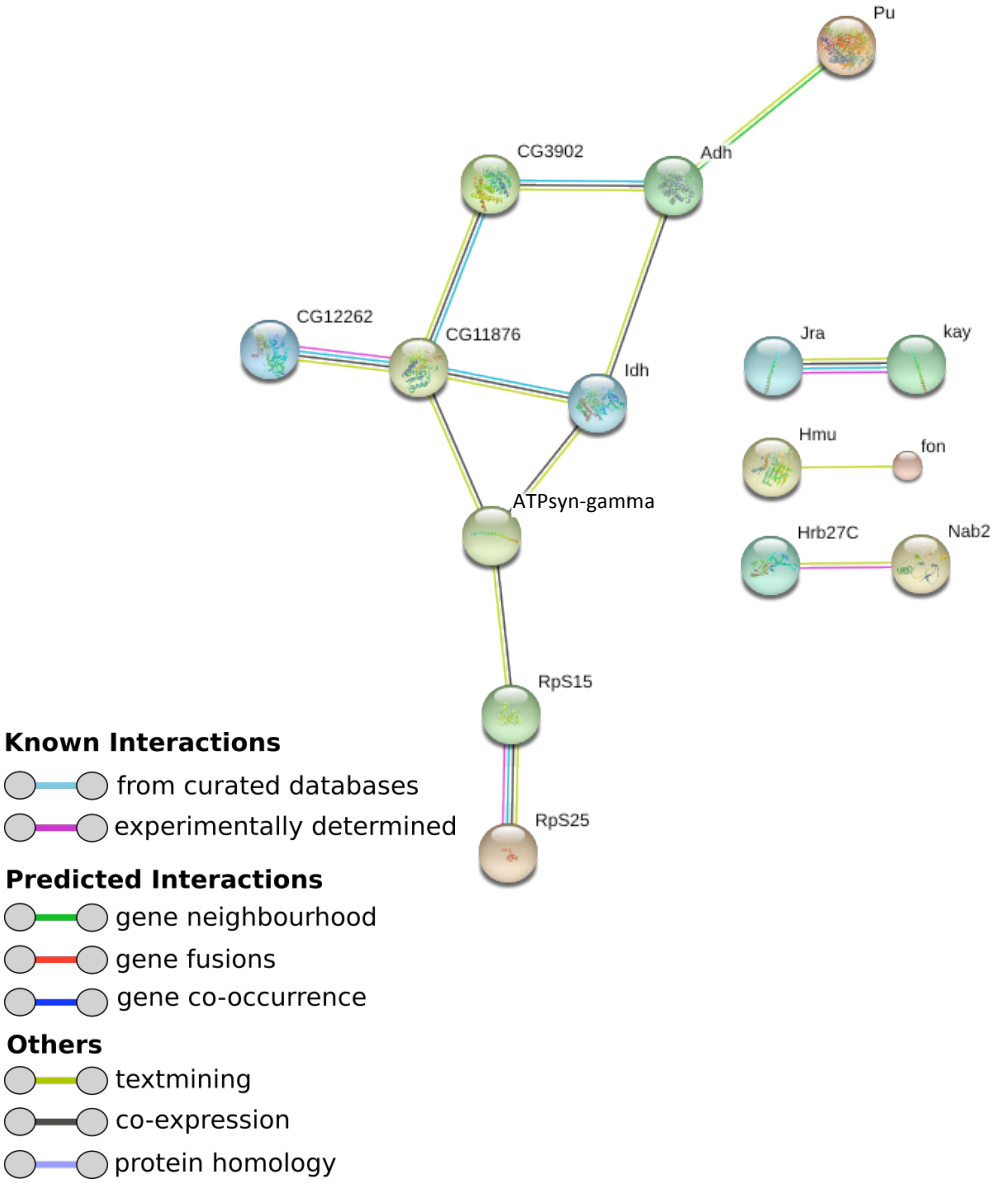

Figure 4.8 Interaction networks of proteins identified from NTAP-Jun and NTAP-Fos control conditions, derived in STRING

Proteins identified in NTAP-Jun and NTAP-Fos control conditions were subject to STRING analysis to generate networks of known interactions within our results. Fos (kay) is shown to interact with Jun (Jra) in this network, but with nothing else. This network also shows GTP cyclohydrolase I (Punch (Pu)) linked to Alcohol Dehydrogenase (Adh) but is not connected in the network to Fos or Jun. See key for the basis of interaction.

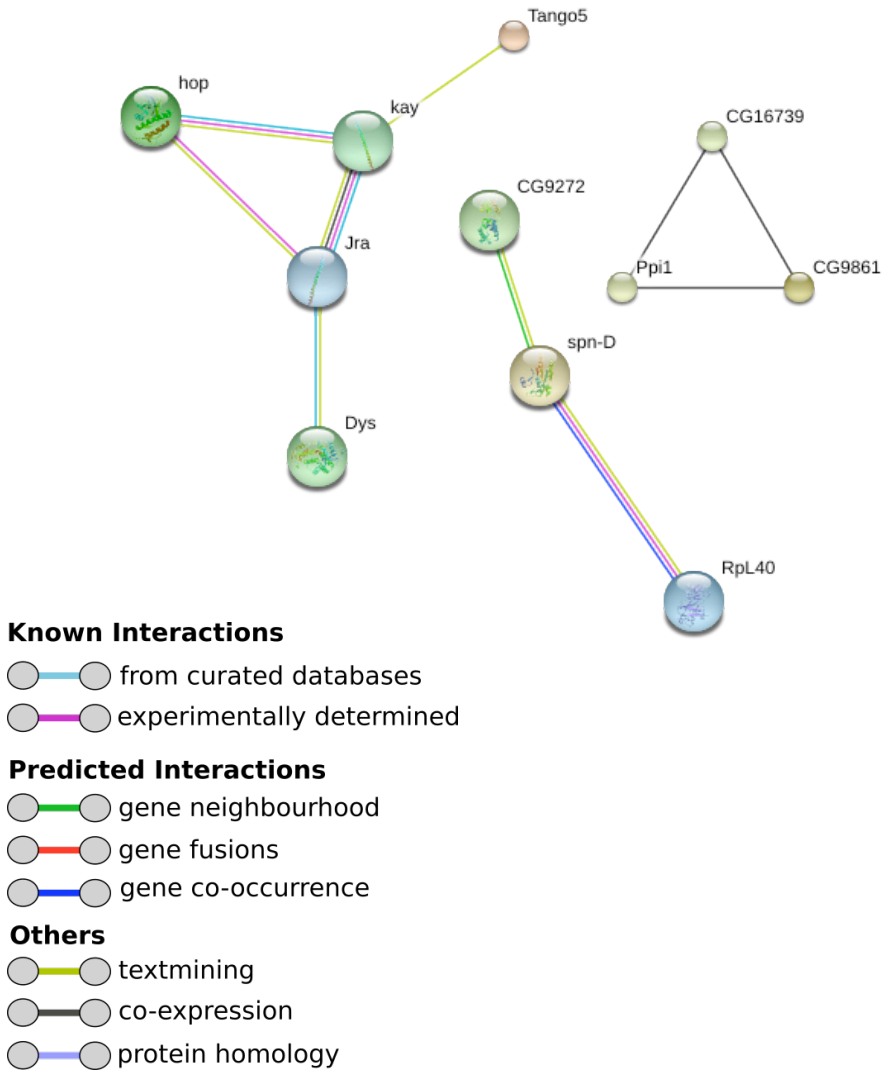

Figure 4.9 Interaction networks of proteins identified from NTAP-Jun and NTAP-Fos DEM-treated conditions, derived in STRING

Proteins identified in NTAP-Jun and NTAP-Fos DEM-treated conditions were subject to STRING analysis to generate networks of known interactions within our results. Fos (kay) is shown to interact with Jun (Jra) in this network; both also interact with hopscotch (hop), Dystrophin (Dys) and Tango5. See key for the basis of interaction.

4.2.5 Identifying the expression patterns of GTP cyclohydrolase 1

GTP cyclohydrolase 1 (GTPCH1), encoded by the *Punch* gene in *Drosophila*, is the rate-limiting enzyme in the biosynthesis of tetrahydrobiopterin (BH_4) (Frank et al., 1998, Tegeder et al., 2006). GTPCH1 is normally inhibited by BH_4, keeping it in an inhibitory state. In humans, GTPCH1 feedback regulatory protein (GFRP) also acts to regulate the active state of GTPCH1, keeping it inhibited by negative feedback and limiting excessive BH_4 production (Yoneyama and Hatakeyama, 2001). Upon the oxidation of BH_4 or its expenditure during its role as an essential cofactor, GTPCH1 is released into its stimulatory state which initiates the first, rate-limiting step in the biosynthesis of BH_4. The rise in BH_4 leads to negative feedback inhibition upon GTPCH1, returning it to its inhibited state (Thony et al., 2000). BH_4 is tightly regulated and rapidly synthesised when required to fulfil its role in a variety of cellular processes.

GTPCH1 is a homodecameric protein complex that consists of two 5-fold symmetric pentameric rings, which dimerise. The resulting decamer has 10 active sites, which form at the interface between 3 subunits. These active sites contain a GTP-binding site (Nar et al., 1995). It is localised in the cytosol, the nucleus and the cell membrane and has important roles in neurotransmitter synthesis, specifically for serotonin and dopamine (DA) (Du et al., 2009). When mutated, levels of DA and serotonin are dramatically reduced, contributing to several human diseases including DOPA-responsive dystonia (DRD) and sepiapterin reductase (SR) (Nagatsu and Ichinose, 1999). Mutations in *GTPCH1* have also been linked to the onset of PD (Lewthwaite et al., 2015). This, combined with its role in the synthesis of the potent ROS scavenger, BH_4, makes its potential interaction with Fos and Jun exciting. It could link the redox-sensitive JNK signalling pathway to GTPCH1/BH_4, which exhibits clear roles in redox defence within the neuron and may have implications in PD. This could be critical to the understanding of ageing, oxidative stress and disease in the neuron. With this in mind we began our investigation into Punch using *Drosophila*, beginning with attempting to determine its interaction with Fos/Jun and defining its localisation within the cell.

4.2.5.1 Characterising the Punch antibodies

We began to confirm the Fos/Jun and Punch interaction by developing 2 new Punch antibodies (see section 2.5.3). Both anti-Punch182 and anti-Punch183 were characterised to confirm the working concentration for larval dissections and western blots and its localisation pattern in larval dissections. Their specificity toward Punch in both larval dissections and western blots was also determined, utilising *Punch* mutants to reduce the overall levels of detectable Punch as a negative control.

4.2.5.2 Characterising the Punch antibodies for larval staining

Both anti-Punch182 and 183 were found to work at a concentration of 1:1000 for larval dissections. Staining WT larvae with both antibodies revealed localisation to nuclei in the ventral nerve cord (VNC) (Figure 4.10A). Staining *Punch* mutant larvae (*Punch*^{r1}*/Df(2R)Exel6072*) with both antibodies revealed a loss of the VNC nuclei staining, suggesting the antibody shows some specificity to Punch, though caution should be taken as there may be undesired interactions with other proteins that we have not identified (Figure 4.10B).

4.2.5.3 Punch is expressed in the larval motor neurons

To determine whether Punch could possibly be interacting with Fos and Jun, we sought to confirm that Punch is expressed in the motor neuron nuclei, as Fos and Jun are found to be. Again, we utilised the OK6-GFP reporter to identify the motor neurons. Larvae expressing OK6-GFP were co-stained with Rabbit anti-Punch (courtesy of the O'Donnell group) (Alexa-Fluor® 405, green) and anti-Jun59 (Cy3, magenta). Not only do we show that Punch is expressed in the motor neuron, we also observe possible colocalisation with Jun (Figure 4.11). Unfortunately, the anti-Punch antibody is raised in rabbit, meaning we cannot co-stain with Rabbit-anti-Fos88 as we would not be able to differentiate between Fos and Punch following secondary antibody stain. We also find that co-staining larval dissections with anti-Punch182 or 183 (raised in rat) and anti-Fos88 or 89 reduces the already defined expression patterns of the antibodies, yielding poor results. To counteract this we

stained larvae that express kay-GFP.FLAG, with anti-Punch182 showing that Punch is localised to cells where Fos is also enriched (Figure 4.12). We find Punch is expressed in the larval VNC and that it is present in the motorneuron nuclei, where Fos and Jun are enriched (Figure 3.13). Importantly, we find possible colocalisation of Punch with Jun, and Punch enriched in VNC nuclei where Fos is present, reinforcing the idea that Punch and AP-1 could be interacting.

4.2.5.4 Characterising Punch antibodies by western blotting

Both anti-Punch182 and 183 work at a concentration of 1:10000 for western blots. Their specificity was determined by comparing blots of protein sample extracted from the heads of WT's, elavGAL4>UAS-Punch, *Punch* mutants (*Punch*^{EY02616A}*/Df(2R)Exel6072*) and elavGAL4>UAS-Punch-RNAi. Both antibodies are specific to Punch, as we see a complete loss of detectable Punch in the *Punch* mutant sample, a substantial loss when expressing Punch-RNAi, yet present in both WT and UAS-Punch samples (Figure 4.13). Blotting with anti-actin shows that all wells have been equally loaded, and the absence of Punch in this blot is not due to a complete absence of sample.

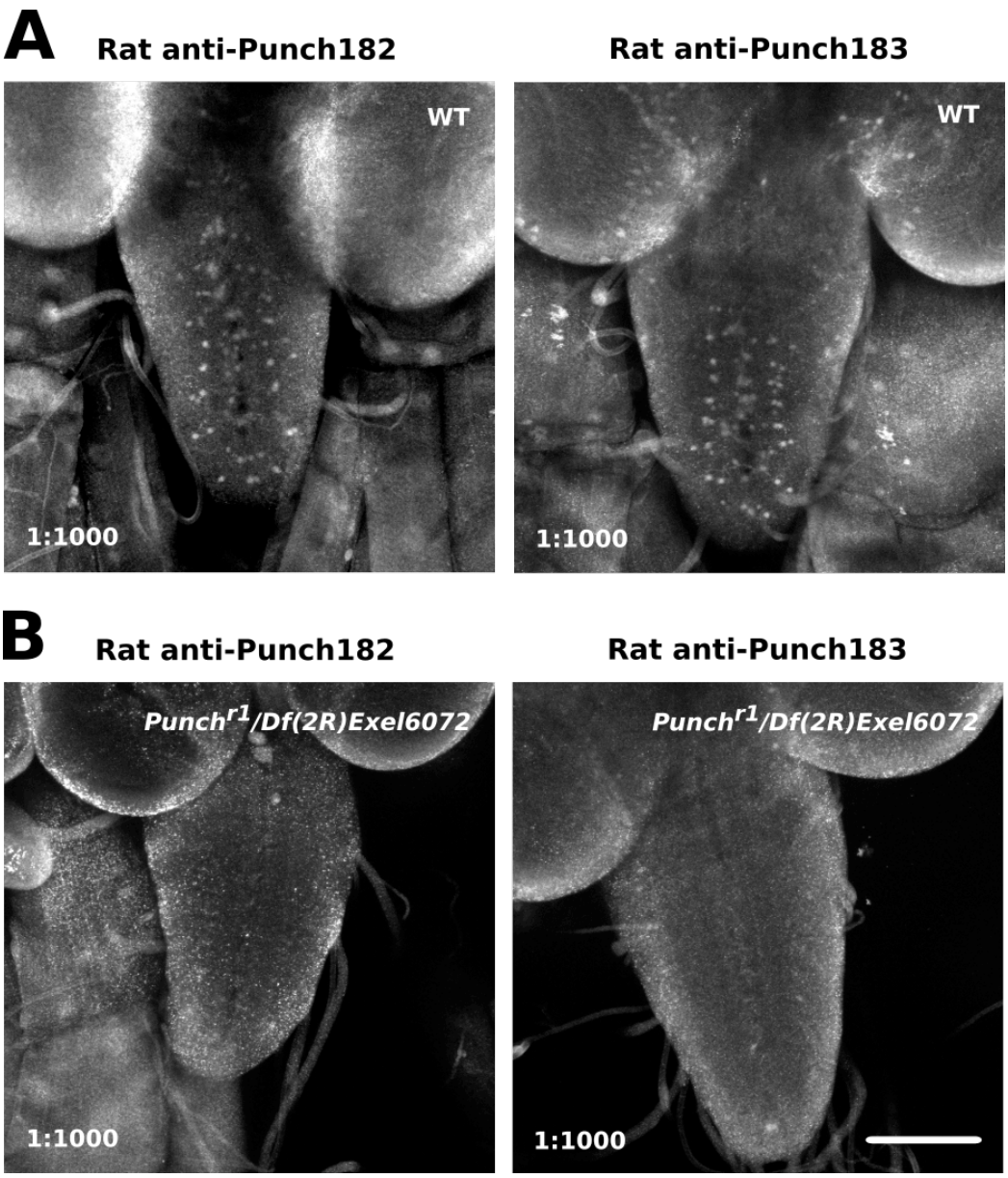

Figure 4.10 Punch antibodies characterised via larval staining

Staining WT larval dissections with rat anti-Punch182 and 183 at a 1:1000 dilution reveals nuclear staining within the ventral nerve cord (**A**) however, this is lost when staining *Punch* mutants (*Punch^{r1}/Df(2R)Exel6072*) (**B**) suggesting our antibodies show some specificity to Punch. Scale bar = 100µm.

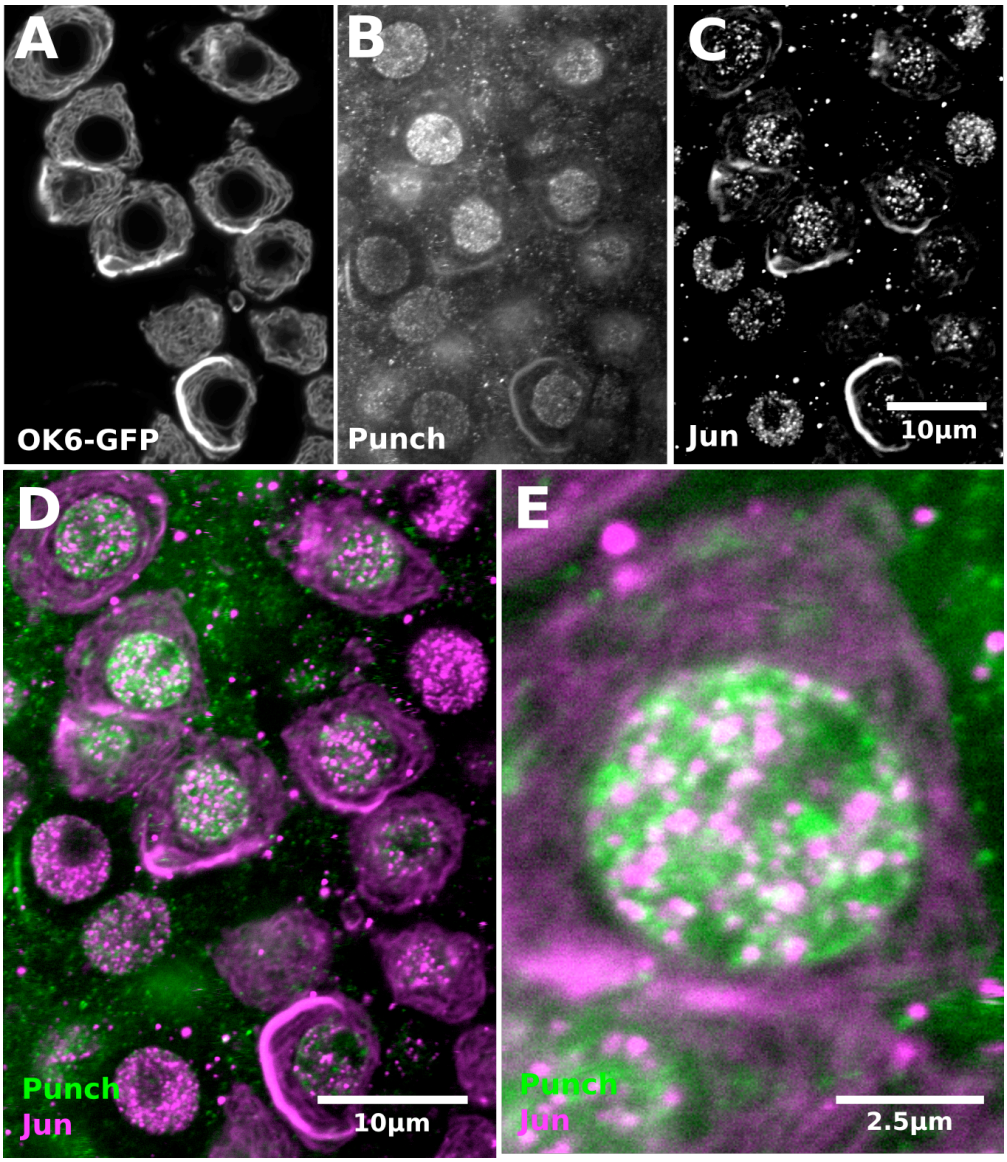

Figure 4.11 Punch and Jun colocalise in the motor neuron nuclei

Larvae expressing the motor neuron denoting OK6-GFP reporter construct (**A**) were co-stained with anti-Punch (Alexa-Fluor® 405 (Green)) (**B**) and anti-Jun59 (Cy3 (magenta)) (**C**), revealing enrichment and possible colocalisation of Punch and Jun in the motor neuron nuclei (**D-E**).

(**A-C**): Scale bar = 10µm; (**D**): Scale bar = 10µm; (**E**): Scale bar = 2.5µm.

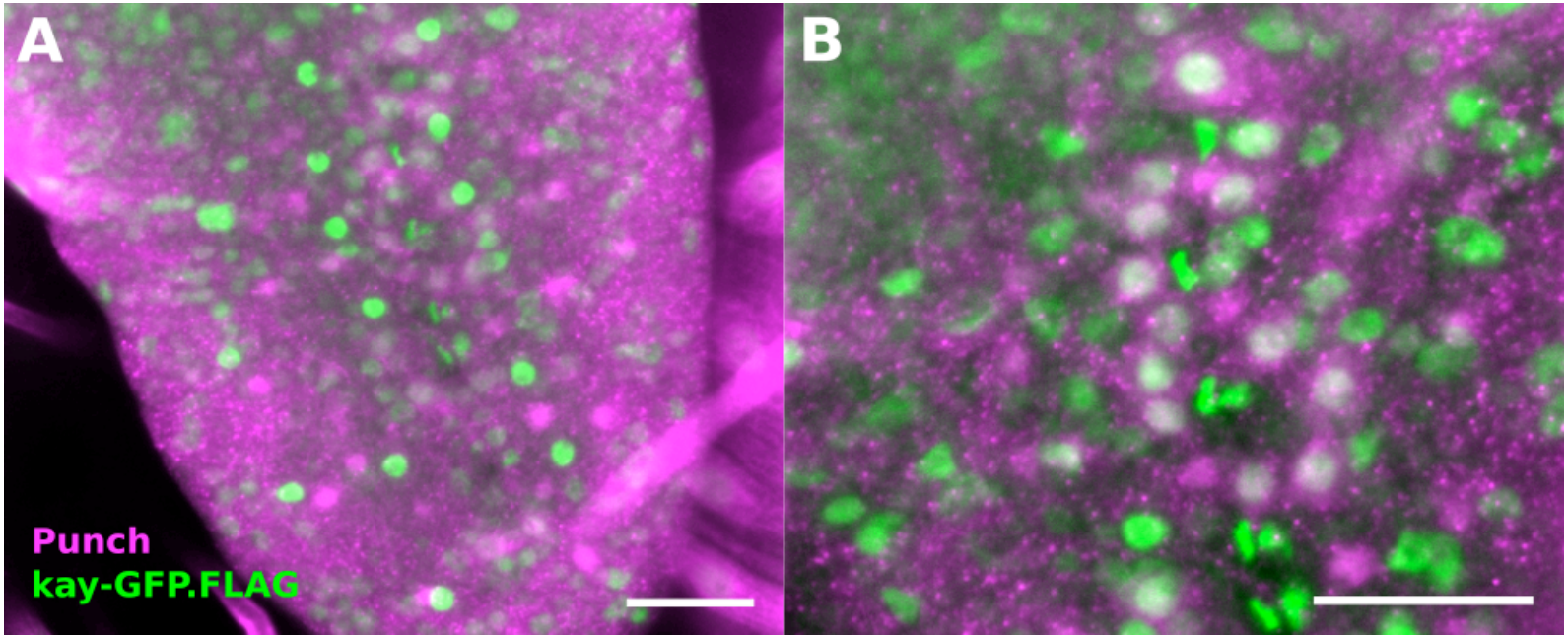

Figure 4.12 Punch expressed in the Fos-enriched VNC nuclei

Staining larvae expressing kay-GFP.FLAG (green) with rat anti-Punch182 (Cy3(magenta)) reveals expression of Punch in a subset of VNC nuclei that are also expressing Fos (**A**). Colocalisation is observed in these nuclei (white). A magnified image is included to emphasise colocalisation. (**A-B**) Scale bar=30μm.

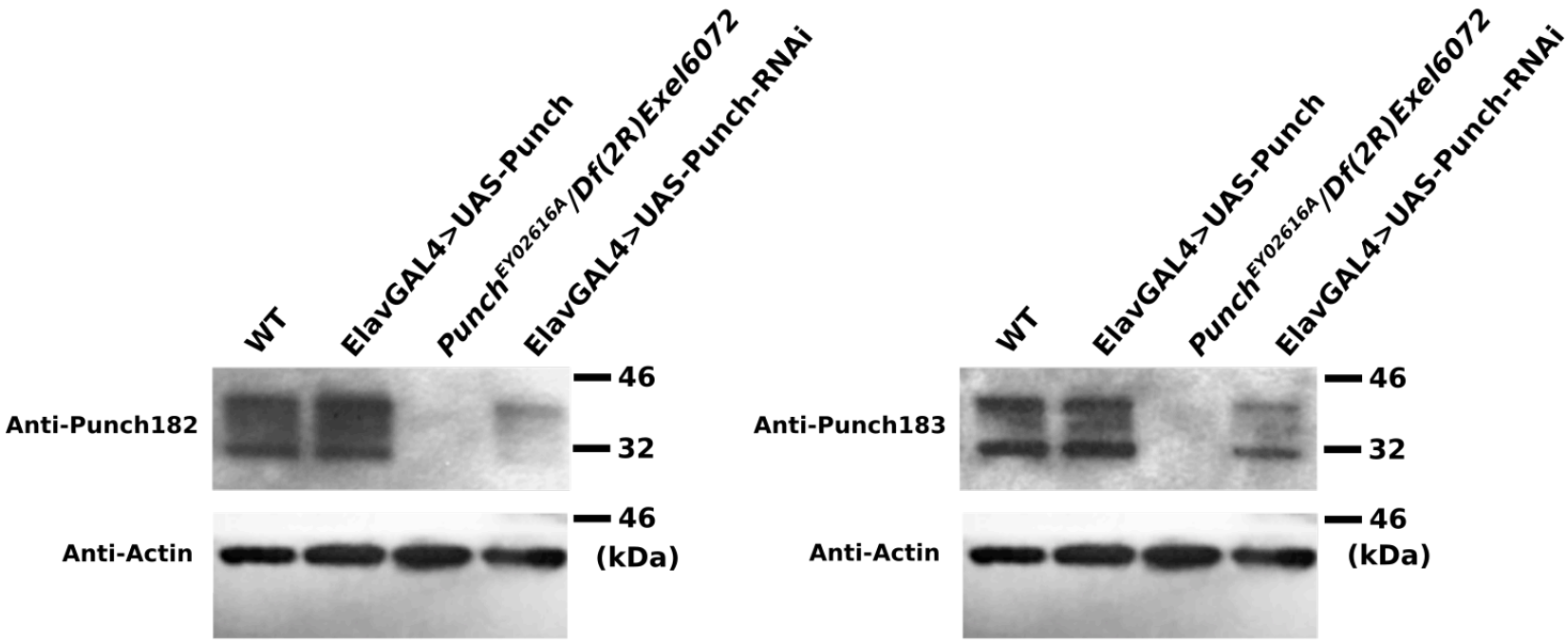

Figure 4.13 Punch antibodies characterised via western blot

Blotting protein samples extracted from the heads of WT flies, elavGAL4>UAS-Punch flies, *Punch* mutant flies (*Punch^{r1}/Df(2R)Exel6072*) and elavGAL4>UAS-Punch-RNAi flies. A loss of detectable Punch in the mutant sample, and a substantial reduction in the Punch-RNAi sample suggests our antibodies are specific to Punch, which is clearly observed in the WT and UAS-Punch sample. Loading control=anti-actin.

4.3 Discussion

In this chapter we identified 80 unique proteins that were bound to Fos and Jun in control and/or oxidative stress conditions. Whilst the results of the mass spectrometry were not ideal due to high levels of contamination, we were able to gain insight into the types of proteins AP-1 putatively binds. Many of the proteins were involved in responding to cellular stimuli and protein regulation; surprisingly a large proportion were also involved in metabolism. We identified more metabolically associated proteins bound to Jun than Fos. Using STRING analysis we found a variety of closely associated proteins with neuronal roles that could indicate how AP-1 controls synaptic plasticity. Importantly, we identify the protein Punch, an important enzyme responsible for the biosynthesis of BH_4, a critical cofactor in the synthesis of neurotransmitters, dopamine and serotonin.

4.3.1 WebGestalt analysis of AP-1 bound proteins

Being part of the JNK signalling pathway, a major pathway involved in the cellular stress response, it is unsurprising that we identify proteins involved in response to stimuli and protein regulation. AP-1 is activated in response to stress (heat, UV, ROS), cytokines and growth factors (Kyriakis, 1999, Rahmani et al., 1999, Zhou et al., 2007, Milton et al., 2011, Zhang et al., 2015). With this in mind it was surprising to see such a large involvement of metabolic proteins. This may indicate that Fos/Jun have a role in metabolism, possibly acting as a form of metabolic defence in response to increased oxidative stress from the mitochondria or as a response to starvation, activating AP-1 and subsequently autophagy to increase recycling of cellular components and maintain protein levels in the cell (Heymann, 2006). The ion binding function of the majority of identified proteins may indicate roles in ROS binding or the electron transport chain. The majority of proteins were found to reside in macromolecular complexes, followed by the nucleus, mitochondria, lipid particle, membrane and cytoskeleton. This is a relatively vague designation but does suggest that AP-1 may directly interact with macromolecular complexes involved in stress responses. AP-1 has a role in a variety of cellular processes and may bind other complexes during these roles. For example, in hepatoma tissue culture cells, AP-1 is shuttled into the nucleus in complex with Importin-β1; and in *Drosophila*,

AP-1 and STAT form a complex during the innate immune response (Forwood et al., 2001, Kim et al., 2007b). Also, the interaction of AP-1 and Smad facilitates AP-1 to induce transcription of TGF-β-related growth genes via a binding of this complex with DNA-binding sites (Liberati et al., 1999).

To summarise, AP-1 may bind a variety of complexes during its response to cellular stresses, and our identification of proteins involved in regulating proteins and response to stimuli represents this. However, it tells us little about how AP-1 controls synaptic plasticity.

4.3.2 STRING analysis of AP-1 bound proteins

Several proteins we identified bound to Fos in control and DEM-treated conditions are known or predicted to bind directly to Fos and have roles in neurotransmitter receptor regulation and release, axonal growth/remodelling in response to oxidative stress, and finally autophagy. This fits with data previously presented in Chapter 3, showing that increased activation of Fos, in response to oxidative stress leads to synaptic overgrowth which may occur via autophagy. We identified Tm1, a protein that may regulate synaptic growth via ERK signalling. It has been shown that increased ERK signalling leads to AP-1 activation (Karin, 1995). ERK signalling has also been show to regulate NMJ growth by modulating levels of FasII (Koh et al., 2002). Reducing FasII levels causes NMJ growth, and ERK signalling is inversely correlated to FasII levels (Schuster et al., 1996). Therefore increasing ERK signalling can cause NMJ growth via a reduction in FasII and coincides with an activation of AP-1. We identify Tm1 bound to Fos during DEM conditions. Jun has also been associated with Tm1 and the interplay between Tm1-ERK and JNK could shed light on how AP-1 controls synaptic plasticity.

Increasing the transcription of autophagy genes leads to NMJ overgrowth, via down regulation of Highwire and an upregulation of JNK signalling (Shen and Ganetzky, 2009). Tango5 is the fly homolog of VMP1, which forms a complex with Beclin 1 to induce autophagy (Molejon et al., 2013). Beclin 1-induced autophagy is also mediated by JNK signalling and using STRING analysis we identify Tango5 bound to Fos during DEM conditions (Li et al., 2009a). Tm1 and Tango5 are also believed to

interact with each other, according to our STRING analysis. This may highlight a role for Fos mediating Tango5/Beclin 1 in autophagy induction and that JNK regulates many aspects of autophagy via different pathways. Finally, we identified Dys bound to Fos during DEM-treated conditions, and STRING analysis reveals a predicted interaction with Jun. Dys is shown to be important for retrograde control of neurotransmitter release at the NMJ. In *dys* mutants, short-term facilitation is decreased, whereas evoked neurotransmitter release is increased, suggesting Dys may have a role in synaptic plasticity (van der Plas et al., 2006).

During STRING analysis of Jun-bound proteins, we identified several that have roles in mediating synaptic plasticity and morphology. Both Hop and Scrib have important neuronal roles, and whilst no current data suggest that Scrib binds Jun, we identified it in Jun control conditions. Hop was identified in DEM-treated conditions, and encodes the *Drosophila* Janus Kinase (JAK) protein. It is an important regulatory protein required for proper patterning of embryonic segments, as well as in the developing eye (Binari and Perrimon, 1994, Luo et al., 1999). Importantly, the JAK/STAT pathway is involved in mammalian synaptic plasticity, specifically for the induction of long-term depression (LTD) in synapses (Nicolas Cé et al., 2012). LTD is an important regulatory process that reduces synaptic strength in synapses. LTD has been linked to AD, where it has been shown that soluble amyloid beta protein facilitates LTD in the hippocampus, and may be responsible for the onset of dementia and synaptic failure (Li et al., 2009b). The association of Hop with Jun during DEM-conditions could indicate an activity dependent mechanism where the neuron responds to ROS by increasing synaptic growth but also dampening down the synaptic strength of certain synapses, possibly in order to induce long-term potentiation (LTP) in preferred synapses for memory formation. Pathological oxidative stress may lead to a greater frequency of LTD induction, possibly explaining the relationship between ageing, oxidative stress and the onset of synaptic failure and neurodegenerative diseases. However, it is worth noting that this theory is in contrast to already published data stating that increases in Fos and Jun activity leads to increases in synaptic strength, not decreases (Sanyal et al., 2002).

Scrib is widely known as a tumour suppressor in *Drosophila*, however, it has been shown to regulate activity dependent synaptic plasticity and is required to maintain synaptic vesicle concentrations within release sites (Roche et al., 2002). The function of scrib in the synapse is critical, as it is required for short-term facilitation, vesicle recycling, post-tetanic potentiation and regulating synaptic depression. This is very similar to the *dunce* mutation, and we identified the dunce protein bound to Fos under oxidative stress conditions.

Bringing all these data together it appears that Fos and Jun may interact with a large array of proteins that regulate synaptic plasticity, and whilst it is still unclear as to their role within these interactions, it potentially highlights their importance.

4.3.3 Identification of Punch bound to AP-1

Possibly the most intriguing protein identified by mass spectrometry was Punch, or GTP cyclohydrolase 1. Punch was identified in Fos and Jun samples under non-stressed conditions. Whilst we only observed two significant sequence hits per Fos and Jun, it was still one of our strongest results. Punch was also identified in a small-scale pilot run of our pull down experiment, where it was bound to Jun in control conditions but not under oxidative stress conditions. Punch also fit our criteria of only binding in one condition, suggesting that a change in redox status alters its function. During STRING analysis, we find Punch interacts with Adh, and is linked to AP-1 via a chain of metabolic proteins. Whilst this sheds no light on the interaction of Punch and AP-1, it was of particular interest because of its role in the biosynthesis of tetrahydrobiopterin, or BH_4. BH_4 is an essential cofactor in the synthesis of dopamine and serotonin, but also acts to scavenge ROS. To begin our investigation we developed Punch antibodies, which we have shown are specific to Punch during larval stains and western blots. Using these antibodies we find Punch is enriched in motor neuron nuclei where both Fos and Jun are also enriched, reinforcing the idea that Punch may bind Fos and Jun.

4.3.4 Conclusions

In conclusion, several identified proteins reveal exciting potential interactions with Fos and Jun that could elucidate their role in controlling synaptic plasticity. Whilst

we haven't looked further into investigating the majority of these proteins, they could potentially be critical future experiments. In the interest of time, we focused purely on Punch, which we have shown is localised to motor neuron nuclei, where Fos and Jun are enriched; strengthening our theory that AP-1 and Punch may be interacting. In the next chapter, we explore the nature of Punch in the oxidative stress response and its role in synaptic plasticity.

5. The role of Punch/BH_4 in the motor neuron during oxidative stress

5.1 Introduction

GTPCH1, or Punch in *Drosophila* is the first, rate-limiting enzyme in the biosynthesis of BH_4, an essential cofactor involved in a variety of cellular processes. One such role involves the hydrolysis of amino acids, where BH_4 is required by hydroxylases for the conversion of phenylalanine, tyrosine and tryptophan into other useful molecules (Thony et al., 2000). These are classified as biopterin-dependent aromatic amino acid hydroxylases. Phenylalanine hydroxylase and cofactor BH_4 act to metabolise excess phenylalanine into tyrosine, an important regulatory process that prevents hyperphenylalaninemia (HPA). Severe HPA causes phenylketonuria (PKU), a disease in humans that causes postnatal brain damage and mental retardation (Kaufman, 1999). Tyrosine hydroxylase (TH) and BH_4 convert tyrosine to the catecholamine, dopamine (DA) (Daubner et al., 2011). DA is an important neurotransmitter for movement control in humans, and also plays a role in memory formation (Yamagata et al., 2015). Communication between neurons of the *Substantia nigra* and the basal ganglia occurs via DA release. Loss of DA causes PD, as well as DOPA-responsive dystonia, and can result from a mutation in *GTPCH1*/reduction in BH_4 (Dauer and Przedborski, 2003, Ichinose et al., 1994). Tryptophan hydroxylase and BH_4 are involved in the initial and rate limiting step in the synthesis in serotonin, as well as melatonin. Serotonin is an important regulatory neurotransmitter for such processes as sleep, mood and pain. BH_4 has been determined to be an intrinsic regulator of pain, where inhibiting BH_4 biosynthesis can reduce sensitivity to pain (Tegeder et al., 2006).

Secondary to its role as an essential cofactor for amino acid hydroxylases, BH_4 has important roles in the nitric oxide synthase (NOS) pathways, acting as an electron donor. NO synthases act to catalyse the formation of nitric oxide (NO) and require BH_4 as a cofactor. NO is an important molecule required for immunity, maintaining blood pressure and long-term memory/synaptic plasticity (Koshland, 1992). NO is produced from L-arginine in the presence of BH_4. However, in the absence of BH_4,

NO is no longer produced and hydrogen peroxide is generated. This ROS can lead to the production of the hydroxyl ion, an extremely reactive free radical (Scott-Burden, 1995). Despite having beneficial roles, NO can cause cytotoxicity. However, neurons that generate NO are also resistant to their cytotoxic effects. BH_4 is proposed to act as a self-protecting factor against NO toxicity, and these NO-producing neurons have been shown to survive degeneration in neurodegenerative diseases (Koshimura et al., 1998). NO is also known to induce transcription of SOD and GST, potent antioxidants. Direct antioxidant activity has also been shown for BH_4, which acts as a potent scavenger of superoxide anions and hydroxyl radicals (Kojima et al., 1995). Normally BH_4 acts to inhibit Punch activity, regulating its own synthesis. When BH_4 is oxidised following interactions with ROS, it is released as BH_2 and Punch is then free to synthesise more BH_4, replenishing the levels in order to combat oxidative stress.

The importance of Punch depends on its role in BH_4 biosynthesis. As previously mentioned, human diseases have implicated a loss of *GTPCH1* as the main contributor to the pathology. DOPA-responsive dystonia results from a single copy loss of *GTPCH1,* and PKU results from both copies of *GTPCH1* being mutated. Mutations in *GTPCH1*, specifically heterozygous single nucleotide polymorphisms (SNP's) that result in nonsense mutations have recently been identified as risk factors in the onset and progression of PD (Nalls et al., 2014).

Our identification of Punch as a potential binding partner of both Fos and Jun may prove critical in the understanding of the oxidative stress response in motor neurons, linking the JNK signalling pathway, known to induce a transcriptional response to ROS, to a neuroprotective constitutive defence pathway known to reduce ROS. The following chapter will attempt to elucidate the role of Punch in *Drosophila* NMJ synapse growth and function, its relationship with Fos and Jun activity and how this relationship contributes to our understanding of ROS regulation and neurodegenerative diseases.

5.2 Results

5.2.1 Reducing Punch activity causes synaptic overgrowth

Heterozygous loss of *GTPCH1* in humans leads to a potent haploinsufficient pathological response. We show here that the same is true for *Drosophila* where heterozygous mutations in *Punch* lead to severe NMJ overgrowth. Two *Punch* mutants were studied, $Punch^{EY02616A}$, an insertional mutant generated by the introduction of a transposable P-element into the genomic sequence of Punch, and $Punch^{r1}$, a spontaneous mutation that causes a loss of enzymatic activity (Mackay et al., 1985, Bellen et al., 2004). Each *Punch* mutant was analysed as a heterozygote by crossing to either *Canton-S* (*CS*) or w^{1118}. Punch is involved in the biosynthesis of drosopterins, a red pigment which gives rise to the red eye phenotype of *Drosophila* (Kim et al., 2013). Mutations in *Punch* cause much of the red pigment to be lost, producing a light orange/yellow eye colour and crossing to either the red-eyed *CS* or white-eyed w^{1118} could affect the activity of certain pathways that involve Punch in the synthesis of pigments. Therefore we test the *Punch* mutants in both red and white-eyed colour backgrounds to ensure this does not affect synaptic growth.

We found mean normalised bouton number was significantly increased in both heterozygous $Punch^{EY02616A}$ and $Punch^{r1}$ when crossed to either *CS* or w^{1118}, compared to WT controls, suggesting that disruptions in the eye colour pigmentation pathway does not affect the severity of the synaptic overgrowth in terms of bouton number (Figure 5.1; $p<0.001$, ANOVA). Combining both *Punch* mutants together did not produce any further increase in bouton number, suggesting each heterozygous mutant is exhibiting a sufficient and debilitating reduction in Punch activity. It is possible that mutations in *Punch* lead to dominant negative effects in the cell, blocking the action of the remaining functional Punch and causing the severe mutational response.

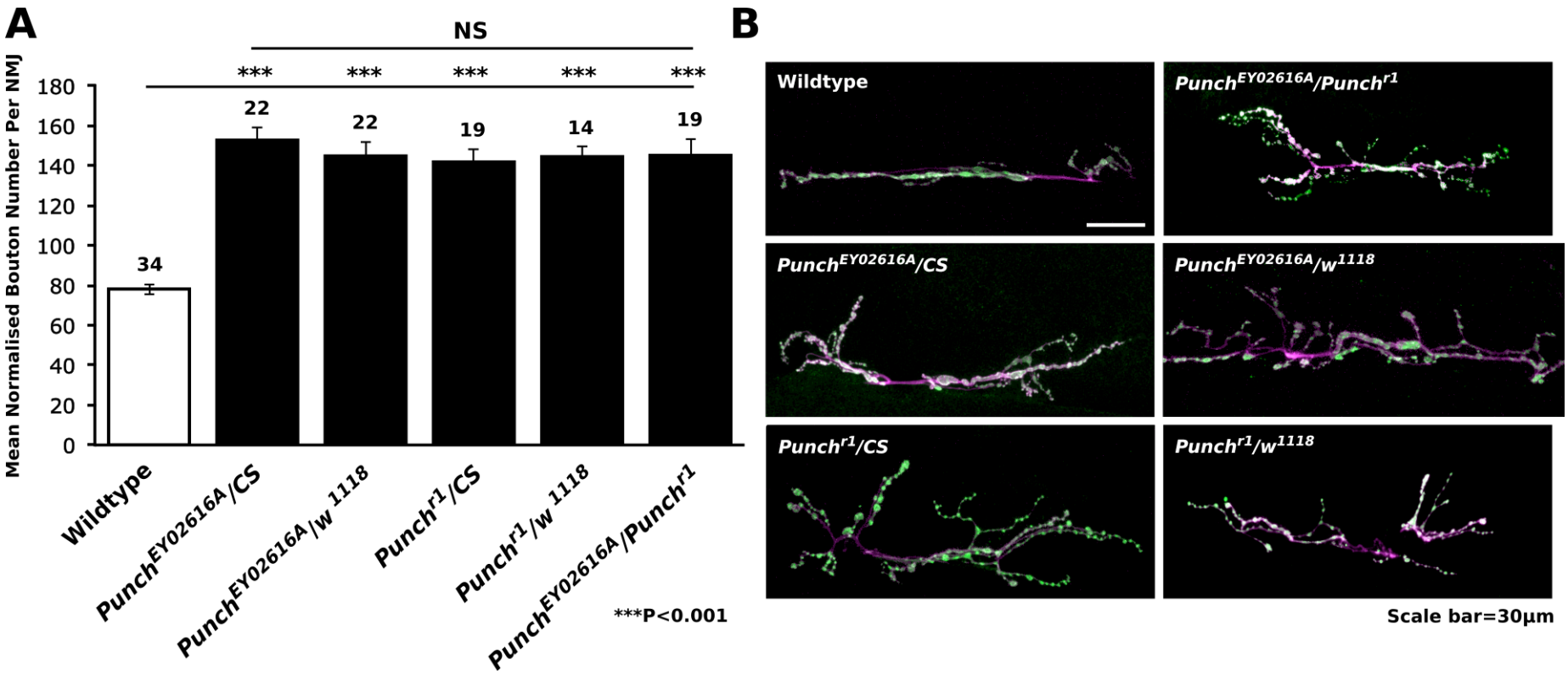

Figure 5.1 Heterozygous *Punch* mutants exhibit synaptic overgrowth

A: Analysis of the NMJ at muscle 6/7 segment A3 of 3rd instar larvae revealed that the heterozygous *Punch* mutant, *Punch*^{EY02616A} displays significantly increased mean normalised bouton number per NMJ when crossed to either *CS* (153±6.5, n=22), *w*^{1118} (145±6.7, n=22) or combined with *Punch*^{r1} (145±7.8, n=19), compared to WT controls (78±2.6, n=34) (***p<0.001; ANOVA with post hoc Bonferroni correction). Heterozygous *Punch*^{r1} mutants crossed to either *CS* (142±6.3, n=19) or *w*^{1118} (145±5.3, n=14) also display significantly increased mean normalised bouton number per NMJ compared to WT controls (***p<0.001; ANOVA with post hoc Bonferroni correction). No significant difference is found when comparing any of the *Punch* mutants with each other (NS p>0.05; ANOVA with post hoc Bonferroni correction). Error bars display ±SEM. **B**: Representative image of the NMJ at muscle 6/7 segment A3 imaged from each heterozygous *Punch* mutant combination, significant synaptic overgrowth is observed. Scale bar 30µm.

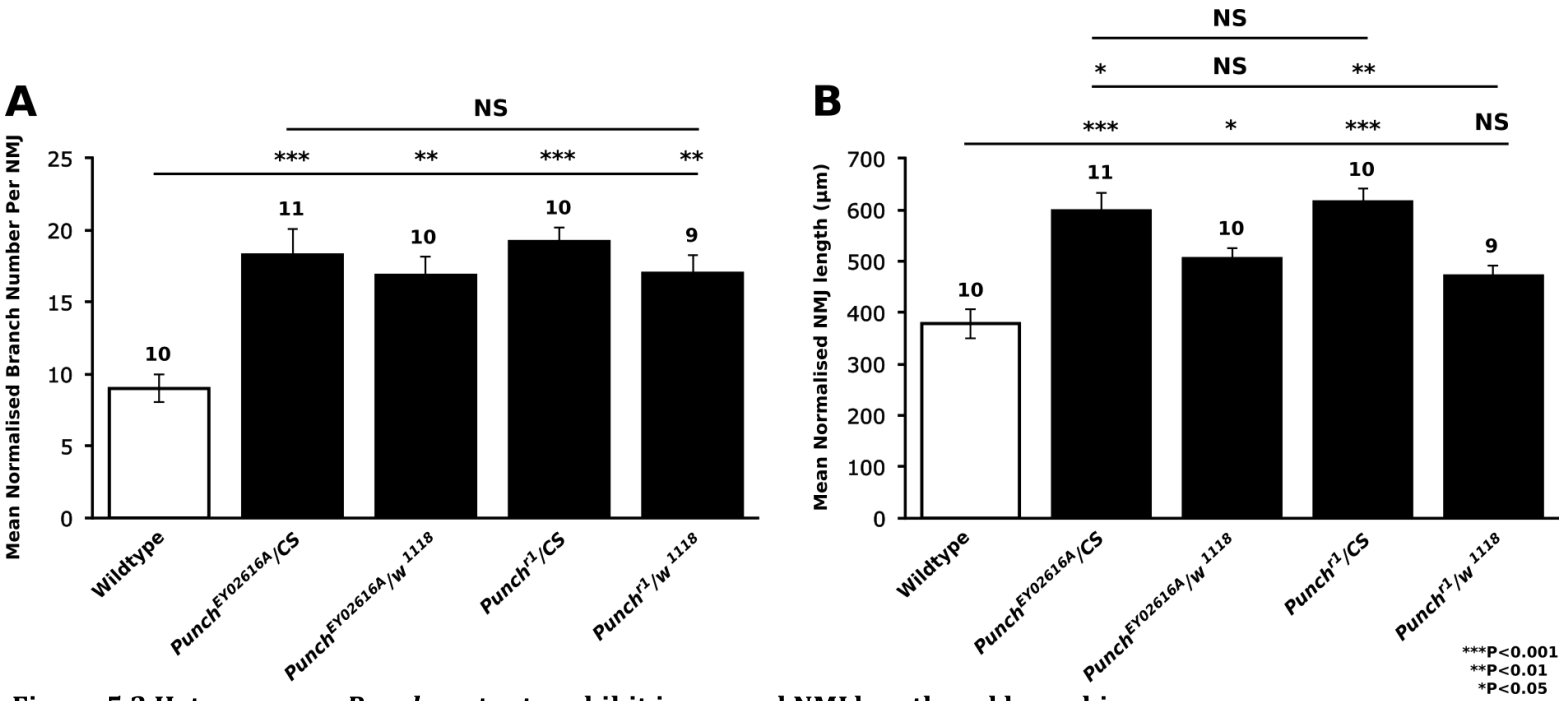

Figure 5.2 Heterozygous *Punch* mutants exhibit increased NMJ length and branching

A: NMJ analysis of heterozygous *Punch* mutant 3rd instar larvae ($Punch^{EY02616A}$ and $Punch^{r1}$) revealed significantly increased mean normalised branch number per NMJ when crossed to either *CS* ($Punch^{EY02616A}/CS$: 18±1.85, n=11) ($Punch^{r1}/CS$: 19±1, n=10) (***p<0.001; ANOVA with post hoc Bonferroni correction), or w^{1118} ($Punch^{EY02616A}/w^{1118}$: 17±1.3, n=10) ($Punch^{r1}/w^{1118}$: 17±1.2, n=9) compared to controls (w^{1118}/CS: 9±1, n=10) (**p<0.01; ANOVA with post hoc Bonferroni correction). No significant difference is found when comparing each *Punch* mutant crossed to either *CS* or w^{1118} together (NS p>0.05; ANOVA with post hoc Bonferroni correction). Error bars display ±SEM. **B**: Mean normalised NMJ length (µm) is significantly increased in heterozygous *Punch* mutants crossed to *CS* ($Punch^{EY02616A}/CS$: 598±33.9, n=11) ($Punch^{r1}/CS$: 616±24.3, n=10) compared to WT controls (w^{1118}/CS: 379±28.8, n=10) (***p<0.001; ANOVA with post hoc Bonferroni correction). $Punch^{EY02616A}$ mutants crossed to w^{1118} display significantly increased mean normalised NMJ length (µm) (505±20.3, n=10) compared to WT controls (*p<0.05; ANOVA with post hoc Bonferroni correction). However $Punch^{r1}$ mutants crossed to w^{1118} showed no significant difference in mean normalised NMJ length (µm) (472±20, n=9) compared to WT controls (NS p>0.05; ANOVA with post hoc Bonferroni correction). Furthermore, NMJ length (µm) of $Punch^{r1}/w^{1118}$ was found to be significantly different to both $Punch^{EY02616A}/CS$ and $Punch^{r1}/CS$ (*p<0.05 and **p<0.01 respectively; ANOVA with post hoc Bonferroni correction). No significant difference is found between $Punch^{EY02616A}/CS$, $Punch^{EY02616A}/w^{1118}$ and $Punch^{r1}/CS$ (NS p>0.05; ANOVA with post hoc Bonferroni correction). Error bars display ±SEM.

Analysis of branch number in these heterozygous *Punch* mutants revealed significant increases when crossed to either *CS* (Figure 5.2A; $p<0.001$, ANOVA) or w^{1118} ($p<0.01$, ANOVA) when compared to WT controls. No significant difference is found between these *Punch* mutants when crossed to *CS* or w^{1118} ($p>0.05$, ANOVA). The NMJ length of *Punch* mutants appears to be more susceptible to the eye colour. Both $Punch^{EY02616A}$ and $Punch^{r1}$ when combined with *CS* show significant increases in NMJ length (μm) compared to WT controls (Figure 5.2B; $p<0.001$, ANOVA). However, only $Punch^{EY02616A}/w^{1118}$ showed significant difference to WT controls ($p<0.05$, ANOVA). $Punch^{r1}/w^{1118}$ showed no significant difference to WT controls ($p>0.05$, ANOVA), yet was found to be significantly different to both $Punch^{EY02616A}/CS$ ($p<0.05$, ANOVA) and $Punch^{r1}/CS$ ($p<0.01$, ANOVA). No significant difference was shown between $Punch^{EY02616A}/w^{1118}$ and $Punch^{EY02616A}/CS$ or $Punch^{r1}/CS$ ($p>0.05$, ANOVA).

NMJ length does not appear to increase as much when *Punch* mutants are in a white-eyed background. Whilst all subsequent heterozygous *Punch* mutant investigations will be outcrossed to *CS*, it is worth noting that NMJ length may not be as susceptible to morphological changes than bouton and branch number, an observation that was made previously in this investigation (see section 3.2.1).

To confirm that a reduction in Punch activity causes NMJ overgrowth we utilised the UAS/GAL4 system to express Punch-RNAi in various tissue and cell types.

UAS-Punch-RNAi (see Table 2.1) was expressed pre-/post-synaptically using SpinGAL4, pan-neuronally using elavGAL4 and in the muscle using MHCGAl4 in order to interfere with Punch expression. In each, a reduction in Punch activity leads to the same severe synaptic overgrowth observed in the *Punch* mutants (Figure 5.3; $p<0.001$, ANOVA). This data supports the idea that NMJ overgrowth is caused by a reduction in Punch activity.

To remove any suspicion that the NMJ overgrowth is caused by second site or background mutations we analysed the NMJ's of flies that are deficient for a large section of their genome, which spans the *Punch* gene. Two *Punch* deficiency fly stocks were used, the first is *Df(2R)Exel6072* which is deficient for chromosomal

region 57B16-57D4. The second is *Df(2R)ED3791*, deficient in the region of 57B1-57D4. Both regions are deficient for the entire *Punch* gene, and used as heterozygotes produce the same severe NMJ overgrowth as the $Punch^{EY02616A}$ and $Punch^{r1}$ mutants. Significant increases in bouton number are observed in *Df(2R)Exel6072*/+ and *Df(2R)ED3791*/+ when compared to WT controls (Figure 5.4; $p<0.001$, ANOVA). No significant difference in bouton number is observed between the 2 Punch-deficient lines and $Punch^{EY02616A}$/+ and $Punch^{r1}$/+ mutants ($p>0.05$, ANOVA). This supports the idea that reducing Punch causes synaptic overgrowth.

We previously observed that combining $Punch^{EY02616A}$ and $Punch^{r1}$ mutants did not further significantly increase bouton number (Figure 5.1). This suggests that both copies of the *Punch* gene must be fully functional to avoid such NMJ overgrowth in *Drosophila,* as such we can describe the *Punch* gene as haploinsufficient, able to generate the full mutant phenotype as heterozygotes. To confirm that the severity of the *Punch* mutant phenotype does not increase upon both copies of *Punch* being mutated, the deficiency lines were combined with the *Punch* mutants.

Both *Punch* deficiencies were combined with $Punch^{EY02616A}$ and $Punch^{r1}$ and the bouton number analysed. No significant differences were found between any of the combinations of *Punch* mutants and deficiencies (Figure 5.5; $p>0.05$, ANOVA). This supports the notion that loss of a single copy of *Punch* is sufficient to produce a potent mutational response and cannot be exacerbated by further reduction in Punch activity.

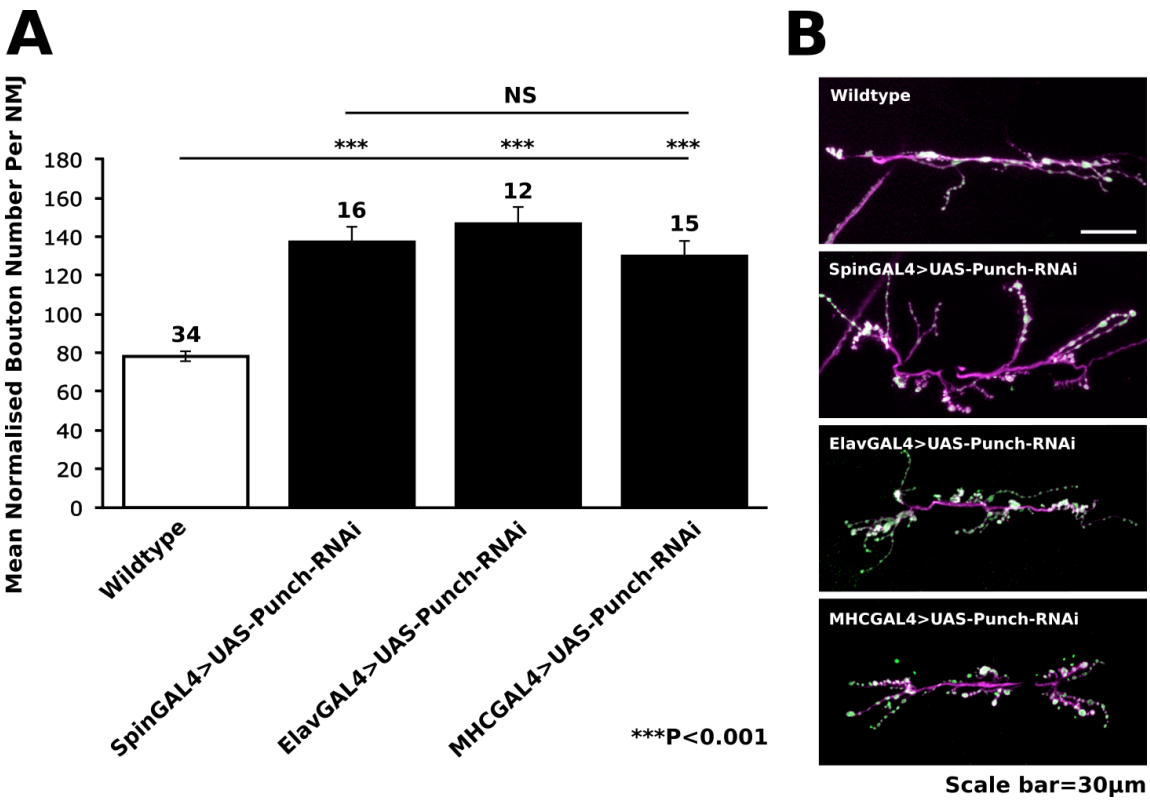

Figure 5.3 Neuronal and muscle expression of Punch-RNAi causes synaptic overgrowth

A: Analysis of NMJ's from larvae expressing Punch-RNAi via SpinGAL4 (137±7.9, n=16), elavGAL4 (147±8.6, n=12) and MHCGAL4 (130±8, n=15) reveal significantly increased mean normalised bouton number per NMJ compared to WT controls (78±2.6, n=34) (***p<0.001; ANOVA with post hoc Bonferroni correction). No significant differences in mean normalised bouton number were observed when comparing larvae expressing Punch-RNAi via SpinGAL4, elavGAL4 and MHCGAL4 (NS p>0.05; ANOVA with post hoc Bonferroni correction). Error bars display ±SEM. **B**: Representative image of the NMJ at muscle 6/7 segment A3 imaged from each condition of the experiment. Scale bar 30µm.

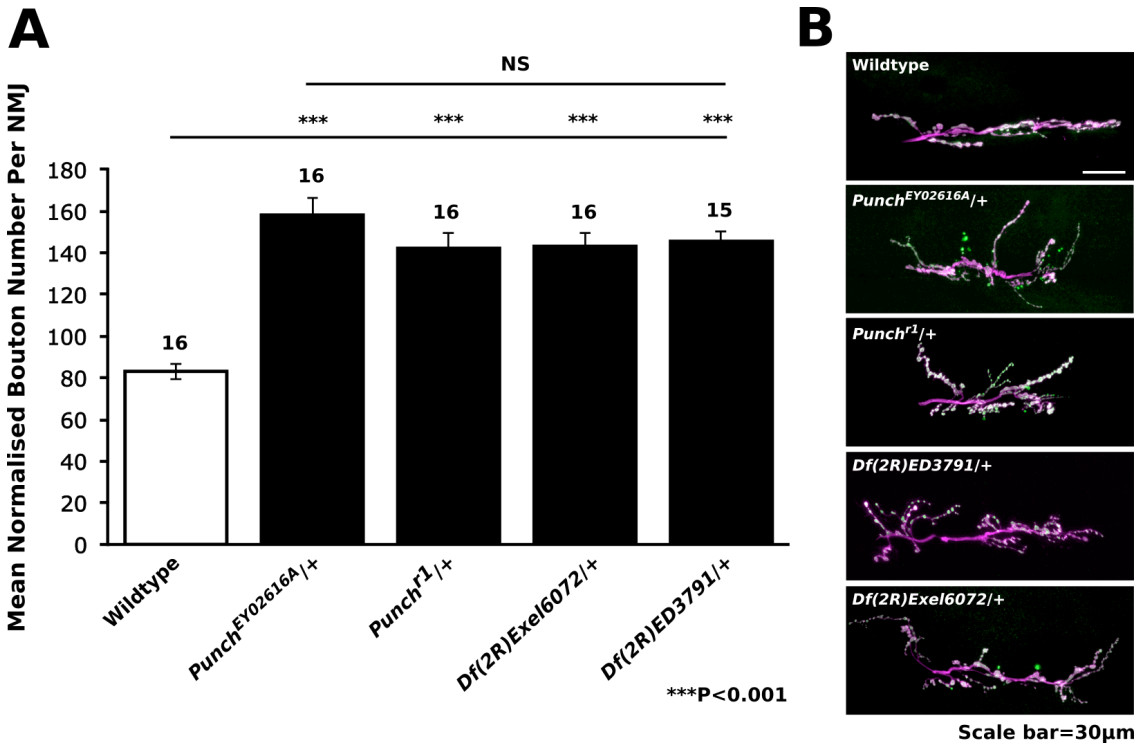

Figure 5.4 Flies deficient in the genomic region encoding the *Punch* gene display synaptic overgrowth

A: NMJ analysis of larvae from 2 fly lines that are deficient in the genomic region encoding *Punch* (Df(2R)Exel6072 and Df(2R)ED3791) crossed to *CS* show significantly increased mean normalised synaptic bouton numbers per NMJ (143±6.2, n=16 and 146±4.6, n=15, respectively) compared to WT controls (83±3.8, n=16) (***p<0.001; ANOVA with post hoc Bonferroni correction). Heterozygous *Punch* mutants, *Punch*^{EY02616A} and *Punch*^{r1} crossed to *CS* show significantly increased mean normalised bouton number per NMJ (158±8.3, n=16 and 142±7.7, n=16, respectively) compared to WT controls (***p<0.001; ANOVA with post hoc Bonferroni correction), but neither show significant differences compared to *Punch* deficient lines, *Df(2R)Exel6072* and *Df(2R)ED3791* (NS p>0.05; ANOVA with post hoc Bonferroni correction). Error bars display ±SEM. **B**: Representative image of the NMJ at muscle 6/7 segment A3 imaged from each heterozygous *Punch* mutant. Scale bar 30µm.

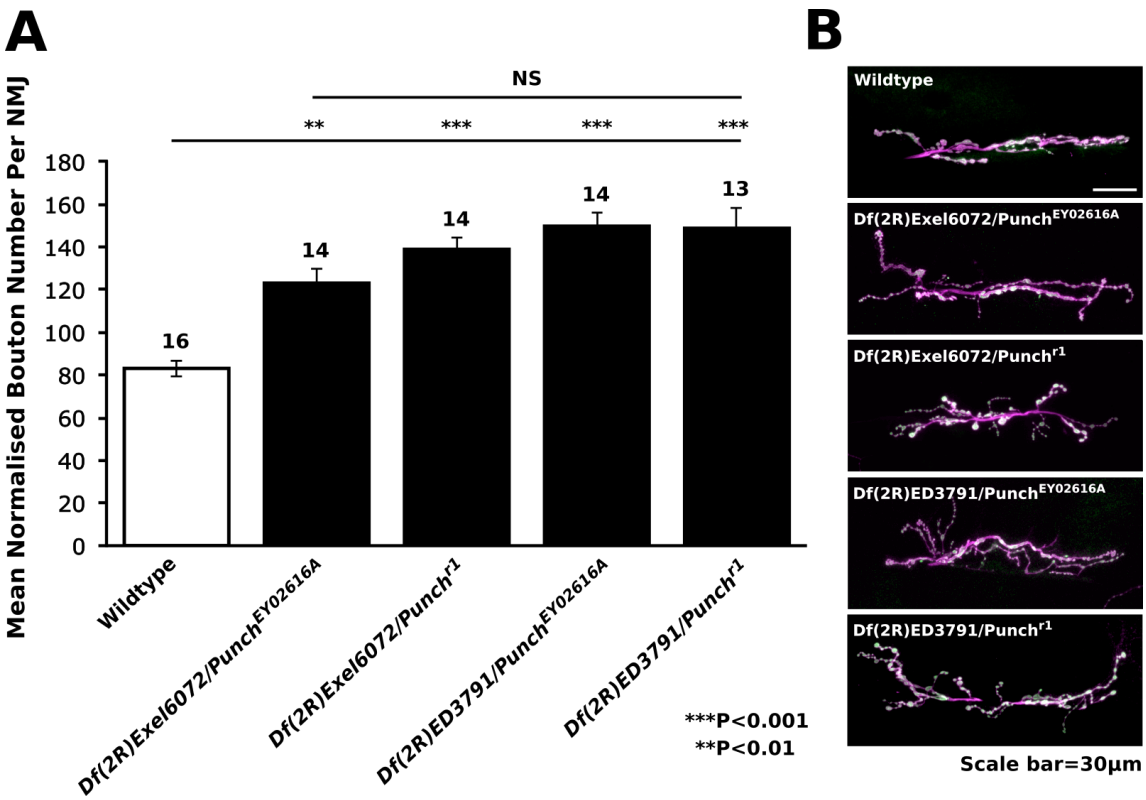

Figure 5.5 *Punch*-deficient flies combined with *Punch* mutants also display synaptic overgrowth but no further severity is observed

A: NMJ analysis of *Punch*-deficient larvae (*Df(2R)Exel6072* and *Df(2R)ED3791*) combined with *Punch*^{EY02616A} show significantly increased mean normalised synaptic bouton numbers per NMJ (123±7, n=14 and 150±6.3, n=14, respectively) compared to WT controls (83±3.8, n=16) (**p<0.01 and ***p<0.001 respectively; ANOVA with post hoc Bonferroni correction). *Punch*-deficient larvae combined with *Punch*^{r1} also show significantly increased mean normalised bouton number per NMJ (139±5.7, n=14 and 149±9.3, n=13, respectively) compared to WT controls (***p<0.001; ANOVA with post hoc Bonferroni correction). No significant difference is observed between any of the *Punch*-deficient/*Punch* mutant combinations (NS p>0.05; ANOVA with post hoc Bonferroni correction). Error bars display ±SEM. **B**: Representative image of the NMJ at muscle 6/7 segment A3 imaged from each *Punch*-deficiency crossed to a *Punch* mutant. Scale bar 30µm.

5.2.2 *Punch* mutants are subject to an oxidative stress burden

It is known that Punch is essential for the biosynthesis of BH_4, which has been identified as a neuroprotective agent and potent ROS scavenger (Thony et al., 2000). In the absence of BH_4, increased hydrogen peroxide production occurs via the NOS synthase pathway (Scott-Burden, 1995). We postulate that *Punch* mutants exhibit reduced levels of BH_4, increasing the ROS production and reducing the ROS scavenging potential in the NMJ. We have shown that increased levels of ROS in *Drosophila* lead to synaptic overgrowth (Figure 3.1) (Milton et al., 2011) and hypothesise that the *Punch* mutants may be reacting similarly. If *Punch* mutants are subject to oxidative stress, this will likely be mediated by the JNK signalling pathway and treating the *Punch* mutants with DEM would not further increase the NMJ overgrowth, as the synaptic growth induced by JNK signalling will already be active. If the *Punch*-mediated overgrowth were not due to oxidative stress, treating these flies with DEM would activate the JNK signalling pathway potentially causing further overgrowth.

We tested this by treating *Punch* mutants and larvae expressing UAS-Punch-RNAi using various GAL4's, with 10mM DEM. No significant difference was observed when treating either, $Punch^{EY02616A}$/+ or $Punch^{r1}$/+ with DEM compared to their non-treated control (Figure 5.6A; NS $p>0.05$, ANOVA). Importantly, $Punch^{EY02616A}$/+ controls ($p<0.001$, ANOVA), as well as $Punch^{EY02616A}$/+ and $Punch^{r1}$/+ treated with DEM ($p<0.001$ and $p<0.01$ respectively, ANOVA) showed significant increases in synaptic bouton number compared to WT treated with DEM. Similarly, treating UAS-Punch-RNAi larvae expressed either pre and post-synaptically (SpinGAL4), pan-neuronally (elavGAL4) and in the muscle (MHCGal4) also showed no significant difference to their non-treated controls (Figure 5.6B; $p>0.05$, ANOVA. No further overgrowth was observed when treating with DEM, suggesting *Punch* mutants are subject to oxidative stress, which is likely to be causing synaptic overgrowth via the JNK signalling pathway.

To confirm this, we treated *Punch* mutants with 10mM Trolox. Previously, we showed that treating flies with Trolox does not increase synaptic bouton number and that it can reduce DEM-induced synaptic overgrowth (see section 3.2.2).

Upon treatment with Trolox, the increased synaptic bouton number observed in both *Punch*^{EY02616A}/+ and *Punch*^{r1}/+ was significantly reduced (Figure 5.7; $p<0.001$, ANOVA). Trolox-treated *Punch*^{EY02616A}/+ and *Punch*^{r1}/+ did not show any significant difference in bouton number compared to WT controls ($p>0.05$, ANOVA). Branch number was also reduced when treating *Punch*^{EY02616A} (Figure 5.8A; $p<0.01$, ANOVA) and *Punch*^{r1} ($p<0.05$, ANOVA) mutants with Trolox compared to their relative controls, which are significantly increased compared to WT controls ($p<0.01$, ANOVA). NMJ length (μm) was only significantly increased when comparing *Punch*^{EY02616A}/+ to WT controls (Figure 5.8B; $p<0.05$, ANOVA). No significant difference was found in NMJ length when treating either *Punch* mutant with Trolox ($p>0.05$, ANOVA).

Whilst NMJ length remains unaffected, both bouton and branch number were significantly rescued in *Punch* mutants when treated with Trolox. This confirms that *Punch* mutants are exhibiting an oxidative stress burden, however it does not explain the severity of this overgrowth compared to DEM-treated larvae which also have an oxidative stress burden yet are significantly less overgrown than DEM-treated *Punch* mutants. This may be indicative of other roles for Punch in the oxidative stress response or that generation of neurotransmitters can affect synaptic growth.

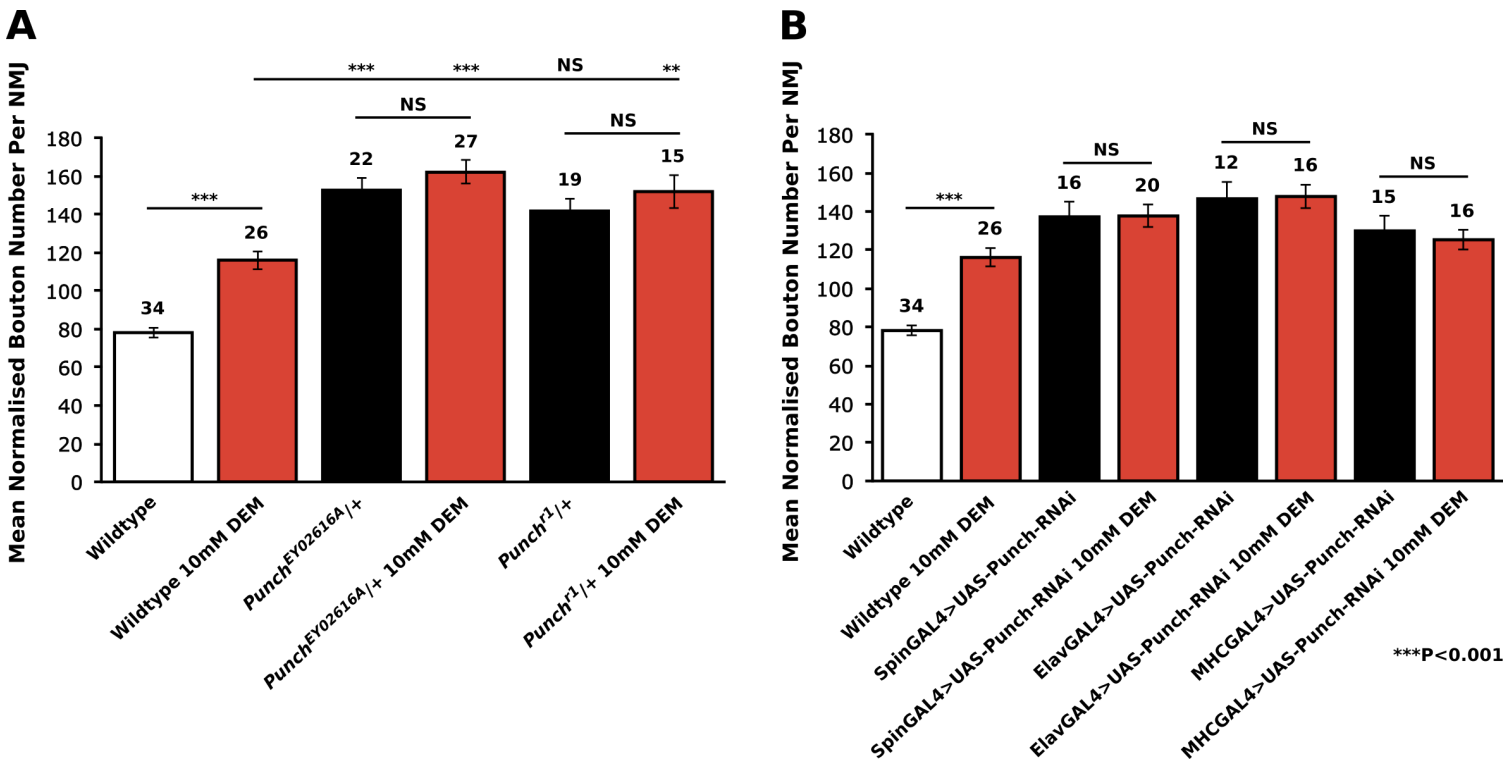

Figure 5.6 Synaptic overgrowth caused by reduced Punch activity is not exacerbated by DEM treatment

A: Analysis of larval WT NMJ's treated with 10mM DEM revealed significantly increased mean normalised bouton number per NMJ (116±4.8, n=26) compared to WT controls (78±2.6, n=34) (***p<0.001; ANOVA with post hoc Bonferroni correction). However, treating heterozygous *Punch* mutants (*Punch*^{EY02161A} and *Punch*^{r1}) with DEM does not significantly increase mean normalised bouton number per NMJ (162±6.1, n=27 and 152±8.6, n=15 respectively) compared to their respective non-treated controls (153±6.5, n=22 and 142±6.3, n=19 respectively) (NS p>0.05; ANOVA with post hoc Bonferroni correction). *Punch*^{EY02161A}/+ control and *Punch*^{EY02161A}/+ and *Punch*^{r1}/+ treated with DEM show significantly increased mean normalised synaptic bouton number per NMJ compared to WT treated with DEM (***p<0.001, ***p<0.001 and **p<0.01 respectively; ANOVA with post hoc Bonferroni correction). *Punch*^{r1}/+ controls do not show any significant difference to WT treated with DEM (NS p>0.05; ANOVA with post hoc Bonferroni correction). Error bars display ±SEM. **B**: Treating larvae expressing Punch-RNAi via SpinGAL4, elavGAL4 and MHCGAL4 with 10mM DEM (138±5.8, n=20; 148±6, n=16 and 125±5.3, n=16 respectively) does not significantly alter mean normalised bouton number per NMJ compared to their respective non-treated controls (137±7.9, n=20; 147±8.6, n=16 and 130±8, n=16 respectively) (NS p>0.05; ANOVA with post hoc Bonferroni correction). Error bars display ±SEM.

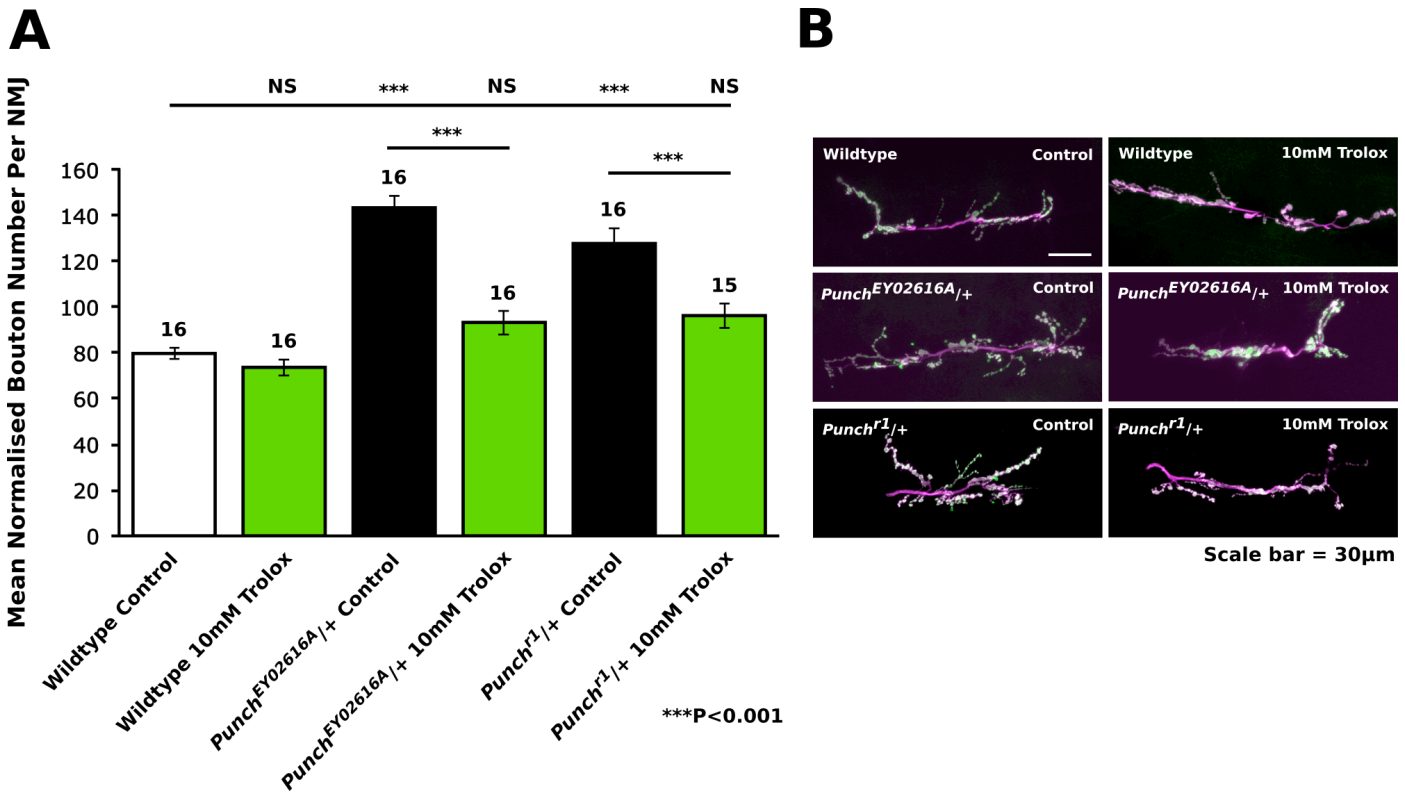

Figure 5.7 Trolox treatment rescues the increased bouton number observed in heterozygous *Punch* mutants

A: Analysis of the NMJ at muscle 6/7 segment A3 of WT 3rd instar larvae treated with a yeast paste containing 10mM Trolox during development show no significant difference in mean normalised synaptic bouton numbers (74±3.6, n=16) compared to WT controls (80±2.4, n=16) (WT + 10% ethanol in yeast paste) (NS p>0.05; ANOVA with post hoc Bonferroni correction). Heterozygous *Punch* mutants ($Punch^{EY02616A}$/*CS* and $Punch^{r1}$/*CS*) display significantly increased mean normalised bouton number per NMJ (143±5.4, n=16 and 128±7, n=16 respectively) compared to WT controls (***p<0.001; ANOVA with post hoc Bonferroni correction). Treating heterozygous *Punch* mutants ($Punch^{EY02616A}$/*CS* and $Punch^{r1}$/*CS*) with 10mM Trolox significantly reduced mean normalised bouton number per NMJ (93±5.3, n=16 and 96±5.4, n=15 respectively) compared to their respective controls (***p<0.001; ANOVA with post hoc Bonferroni correction). No significant differences were found between heterozygous *Punch* mutants treated with 10mM Trolox and WT controls (NS p>0.05; ANOVA with post hoc Bonferroni correction). Error bars display ±SEM. **B**: Representative image of the NMJ at muscle 6/7 segment A3 imaged from each condition of the experiment. Scale bar 30µm.

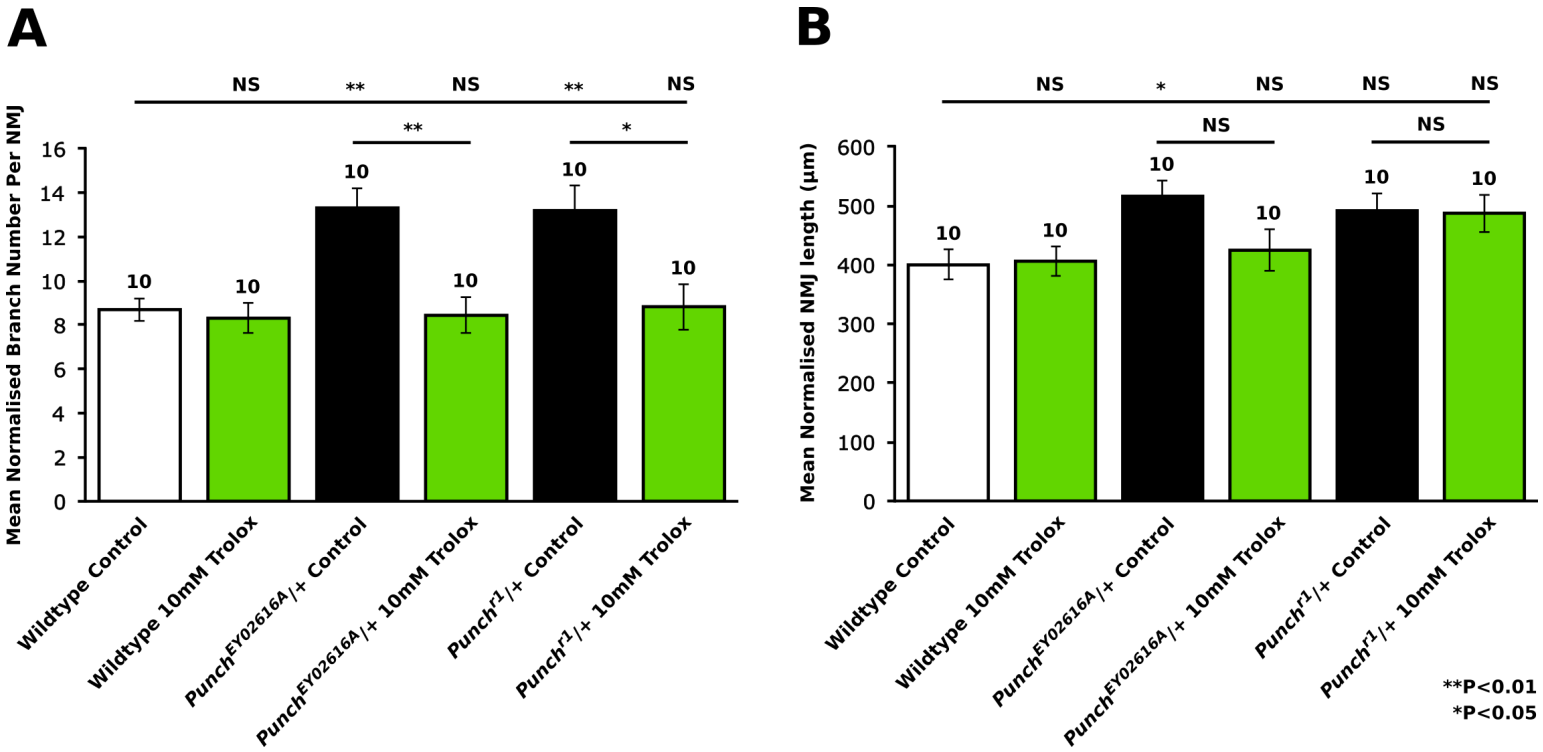

Figure 5.8 Trolox treatment rescues increased branch number observed in heterozygous *Punch* mutants

A: Analysis of the NMJ at muscle 6/7 segment A3 of WT 3rd instar larvae treated with a yeast paste containing 10mM Trolox during development show no significant difference in mean normalised branch number (8.3±0.7, n=10) compared to WT controls (8.7±0.5, n=10) (WT + 10% ethanol in yeast paste) (NS p>0.05; ANOVA with post hoc Bonferroni correction). Heterozygous *Punch* mutants ($Punch^{EY02616A}$/*CS* and $Punch^{r1}$/*CS*) display significantly increased mean normalised branch number per NMJ (13.3±0.9, n=10 and 13.2±1.2, n=10 respectively) compared to WT controls (**p<0.01; ANOVA with post hoc Bonferroni correction). Treating heterozygous *Punch* mutants ($Punch^{EY02616A}$/*CS* and $Punch^{r1}$/*CS*) with 10mM Trolox significantly reduced mean normalised branch number per NMJ (8.4±0.8, n=10 and 8.8±1, n=10 respectively) compared to their respective controls (**p<0.01 and *p<0.05 respectively; ANOVA with post hoc Bonferroni correction). No significant differences were found between heterozygous *Punch* mutants treated with 10mM Trolox and WT controls (NS p>0.05; ANOVA with post hoc Bonferroni correction). Error bars display ±SEM. **B**: NMJ length (µm) is increased significantly when comparing $Punch^{EY02616A}$/+ control (516±26.5, n=10) to WT controls (400±25.5, n=10) (*p<0.05; ANOVA with post hoc Bonferroni correction). No significant difference is found when comparing WT treated with Trolox (406±24.8, n=10), $Punch^{EY02616A}$/+ treated with Trolox (425±36, n=10), $Punch^{r1}$/+ control (492±30.3, n=10) and $Punch^{r1}$/+ treated with Trolox (487.5±32, n=10) to WT controls (NS p>0.05; ANOVA with post hoc Bonferroni correction). Error bars display ±SEM.

5.2.3 A role for dopamine in synaptic plasticity

BH_4 acts as a ROS scavenger, and low levels of BH_4 may incur an oxidative stress burden, but, as mentioned previously in this chapter, another primary role for BH_4 is in the biosynthesis of DA. Reducing Punch activity causes a reduction in DA levels (Nagatsu and Ichinose, 1999). We sought to determine whether treatment with L-3,4-dihydroxyphenylalanine, commonly know as Levodopa (L-DOPA), a precursor of DA would also rescue NMJ overgrowth.

We found the significant synaptic overgrowth observed in both *Punch* mutants (*Punch*^{EY02616A} and *Punch*^{r1}) compared to WT controls (Figure 5.9; $p<0.001$, ANOVA) was significantly reduced when treating with L-DOPA ($p<0.001$, ANOVA). Treating WT with L-DOPA shows no significant difference to WT controls ($p>0.05$, ANOVA). This data suggests that the reduced levels of DA in *Punch* mutants are contributing to the synaptic overgrowth.

To further reinforce these data we tested both *DOPA decarboxylase* (*Ddc*) and *SOD1* mutants to determine if DA reduction causes the overgrowth and whether L-DOPA treatment can rescue oxidative stress-induced synaptic overgrowth. Ddc is responsible for the synthesis of DA and serotonin via decarboxylation of L-DOPA and L-5-hydroxytryptophan (Burkhard et al., 2001). Mutations in *Ddc* result in reduced levels of DA due to a reduced capacity to convert L-DOPA. We tested heterozygous *Ddc* mutants (*Ddc*^{DE1}/*CS*) and found they too exhibit significant synaptic overgrowth compared to WT controls (Figure 5.10; $p<0.001$, ANOVA). This overgrowth was significantly reduced following L-DOPA treatment compared to *Ddc* mutant controls ($p<0.001$, ANOVA), resulting in bouton numbers that were not significantly different to WT controls ($p>0.05$, ANOVA). The significant synaptic overgrowth observed in *SOD1* mutants (*SOD1*^{n1}/*SOD1*^{n64}) compared to WT ($p<0.001$, ANOVA) was not rescued when treating with L-DOPA and showed no significant difference to *SOD1* mutant controls (Figure 5.10; $p>0.05$, ANOVA). Neither WT nor *SOD1* mutants were affected by L-DOPA treatment suggesting that L-DOPA is not reducing bouton number and that it cannot rescue oxidative stress-induced overgrowth. L-DOPA treatment reduced the overgrowth observed in *Ddc*

mutants, likely to be occurring via increased conversion of the added L-DOPA from the remaining functional Ddc, supplying enough DA to reduce the overgrowth.

Currently, why a reduction in DA causes synaptic overgrowth remains unclear, however the link between Punch, DA synthesis and synaptic plasticity is very intriguing. To further investigate the *Punch*-induced synaptic overgrowth we decided to test the role of JNK/AP-1.

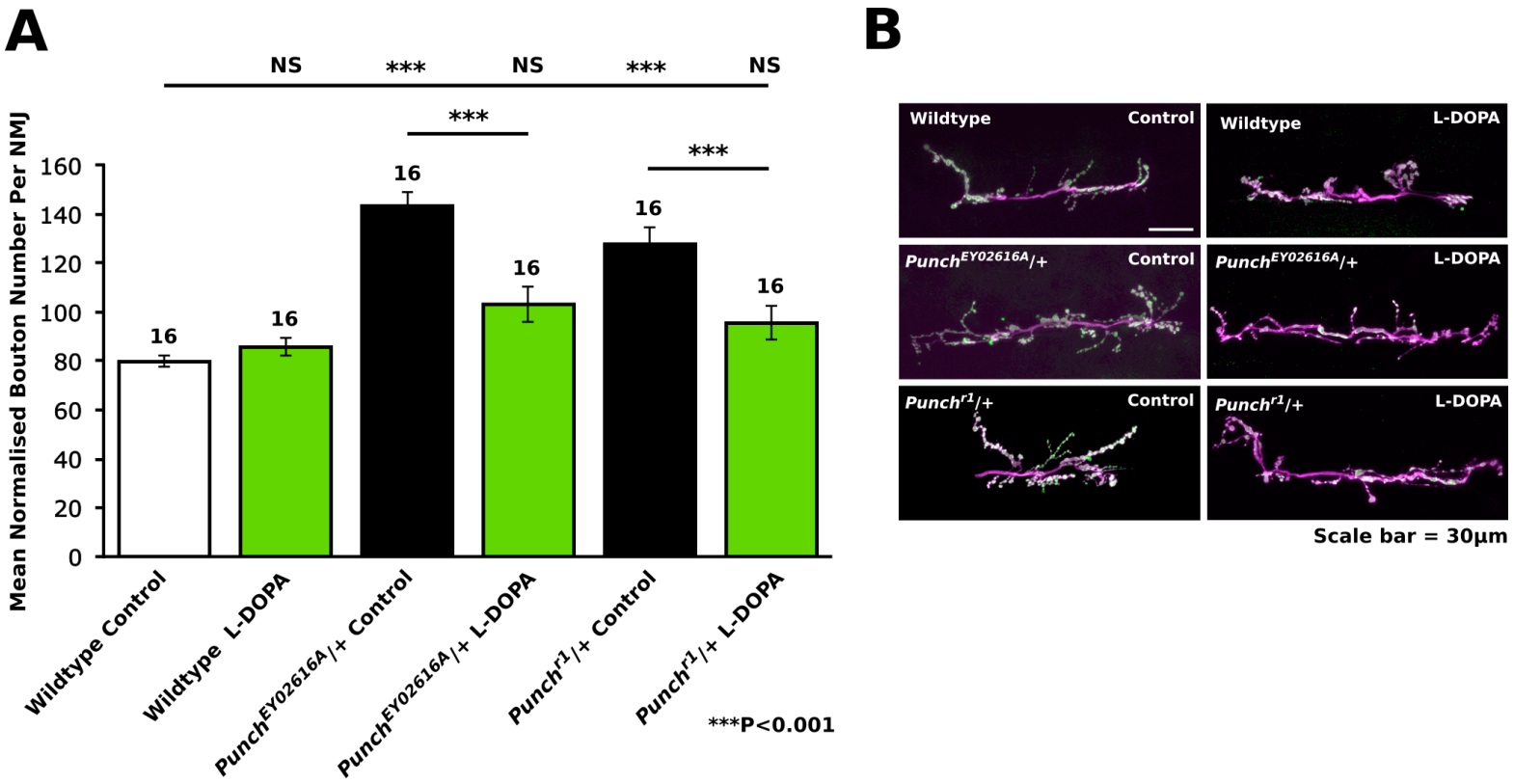

Figure 5.9 L-DOPA treatment rescues the synaptic overgrowth observed in heterozygous *Punch* mutants

A: Analysis of the NMJ at muscle 6/7 segment A3 of WT 3rd instar larvae treated with a yeast paste containing 1mg/ml L-DOPA during development show no significant difference in mean normalised synaptic bouton numbers (86±3.6, n=16) compared to WT controls (80±2.4, n=16) (WT + 10% ethanol in yeast paste) (NS $p>0.05$; ANOVA with post hoc Bonferroni correction). Heterozygous *Punch* mutants ($Punch^{EY02616A}/CS$ and $Punch^{r1}/CS$) display significantly increased mean normalised bouton number per NMJ (143±5.4, n=16 and 128±7, n=16 respectively) compared to WT controls (***$p<0.001$; ANOVA with post hoc Bonferroni correction). Treating heterozygous *Punch* mutants ($Punch^{EY02616A}/CS$ and $Punch^{r1}/CS$) with 1mg/ml L-DOPA significantly reduced mean normalised bouton number per NMJ (103±7.3, n=16 and 96±6.8, n=15 respectively) compared to their respective controls (***$p<0.001$; ANOVA with post hoc Bonferroni correction). No significant differences were found between heterozygous Punch mutants treated with 1mg/ml L-DOPA and WT controls (NS $p>0.05$; ANOVA with post hoc Bonferroni correction). Error bars display ±SEM. **B**: Representative image of the NMJ at muscle 6/7 segment A3 imaged from each condition of the experiment. Scale bar 30µm.

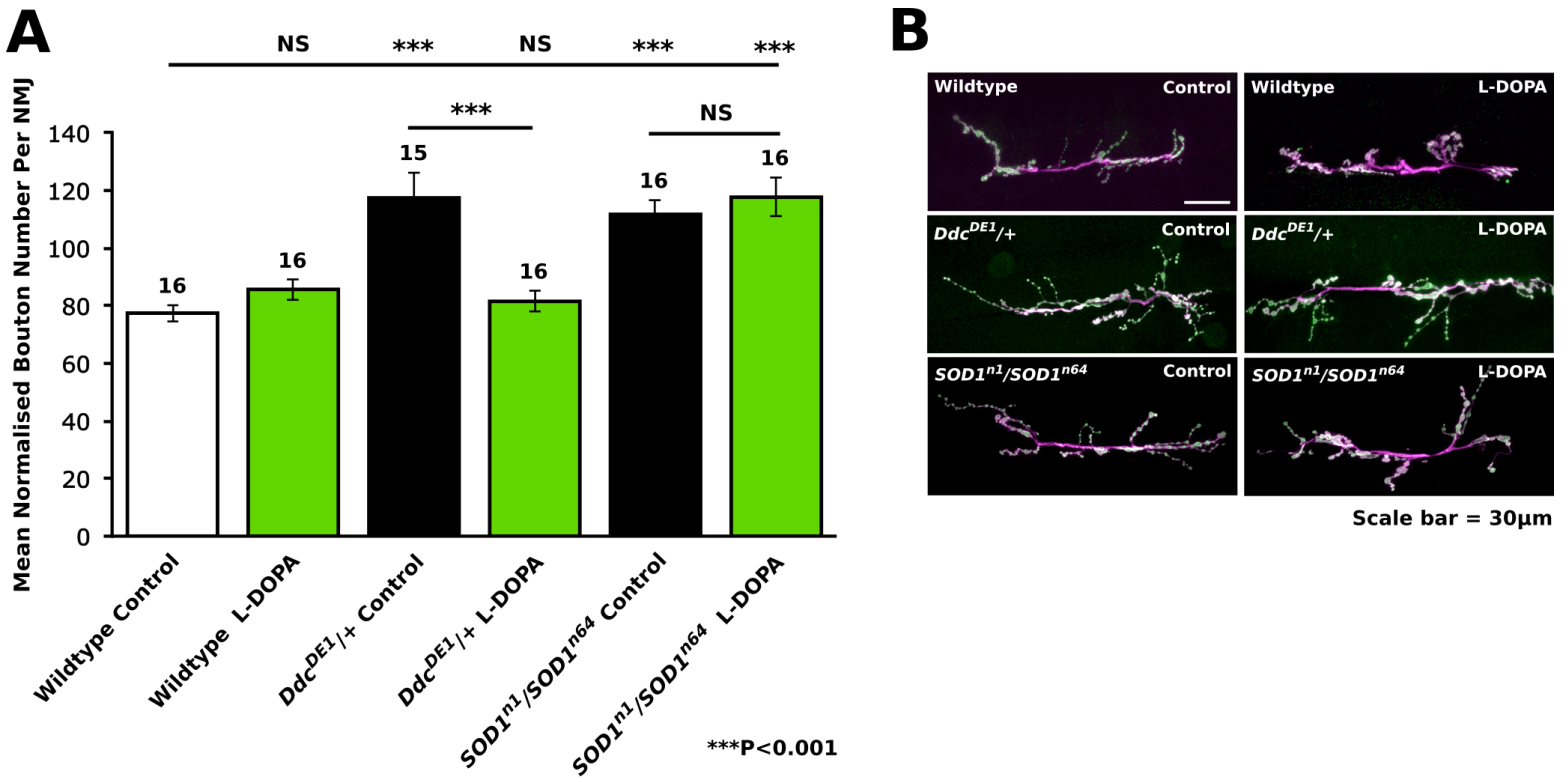

Figure 5.10 L-DOPA treatment rescues the synaptic overgrowth observed in heterozygous *dopa decarboxylase* mutants

A: Analysis of the NMJ at muscle 6/7 segment A3 of WT 3rd instar larvae treated with a yeast paste containing 1mg/ml L-DOPA during development show no significant difference in mean normalised synaptic bouton numbers (86±3.6, n=16) compared to WT controls (80±2.4, n=16) (WT + 10% ethanol in yeast paste) (NS p>0.05; ANOVA with post hoc Bonferroni correction). Heterozygous *dopa decarboxylase (Ddc)* mutants (Ddc^{DE1}/CS) display significantly increased mean normalised bouton number per NMJ (118±8.6, n=15) compared to WT controls (***p<0.001; ANOVA with post hoc Bonferroni correction). Upon treatment with L-DOPA, *Ddc* mutants show significant decreases in synaptic boutons number (82±3.5, n=16) compared to *Ddc* mutant controls (***p<0.001; ANOVA with post hoc Bonferroni correction) and show no significant difference to WT controls (NS p>0.05; ANOVA with post hoc Bonferroni correction). *SOD* mutant controls ($SOD1^{n1}/SOD1^{n64}$) show significantly increased mean normalised synaptic bouton number (112±5, n=16) compared to WT controls (***p<0.001; ANOVA with post hoc Bonferroni correction) but show no significant difference when treating with L-DOPA (118±6.6, n=16) compared to *SOD* mutant controls (NS p>0.05; ANOVA with post hoc Bonferroni correction). Error bars display ±SEM. **B**: Representative image of the NMJ at muscle 6/7 segment A3 imaged from each condition of the experiment. Scale bar 30µm.

5.2.4 *Punch*-mutant induced NMJ overgrowth is mediated by JNK signalling

We have shown that reducing Punch activity causes NMJ overgrowth, and that relieving the oxidative stress burden/reduction in DA levels in these larvae can rescue this overgrowth. Oxidative stress-induced NMJ overgrowth is mediated by JNK signalling. With this in mind it is plausible that the *Punch*-mediated overgrowth may also be mediated by JNK signalling. We investigated this by crossing the *Punch* mutant, $Punch^{EY02616A}$ to the Jun mutant, jra^{IA109} and by examining larvae expressing the dominant negative Jun via SpinGAL4 (SpinGAL4>UAS-jun^{DN}) in a *Punch/+* background. We also repeated this to investigate the role of Fos, by crossing $Punch^{EY02616A}$ to Fos mutant kay^{1}, and into larvae expressing Fos^{DN} (UAS-fos^{DN}) via SpinGAL4 in a *Punch/+* background.

Significantly increased bouton number was observed in heterozygous *Punch* mutants ($Punch^{EY02616A}$/+) (Figure 5.11; $p<0.001$, ANOVA). Reducing Jun activity alone (jra^{IA109}/+) showed no significant difference in bouton number compared to WT controls ($p>0.05$, ANOVA). However, crossing the jra^{IA109} mutant or expressing the dominant negative Jun via SpinGAL4 in the heterozygous *Punch* mutant background significantly rescued this overgrowth ($p<0.001$, ANOVA) resulting in bouton counts not significantly different to WT controls ($p>0.05$, ANOVA).

The same was true when repeated with the Fos mutant, kay^{1} and when reducing Fos activity via dominant negative Fos expression; when introduced into the heterozygous *Punch* mutant background, synaptic overgrowth no longer occurred resulting in significantly reduced bouton numbers compared to $Punch^{EY02616A}$/+ alone (Figure 5.12; $p<0.001$, ANOVA) and no significant difference compared to WT controls ($p>0.05$, ANOVA). No significant difference was found between kay^{1}/+ alone and WT controls ($p>0.05$, ANOVA).

This is further evidence to suggest a reduction in Punch activity causes an oxidative stress burden, as this overgrowth is mediated by and is completely dependent on functionally active JNK signalling, which we have shown controls oxidative stress-induced synaptic overgrowth in flies treated with DEM (see section 3.3.2). We

believe the oxidative stress burden is caused by a reduction in BH_4, which is a potent ROS scavenger acting to protect the neuron from oxidative stress. If so, overexpression or increased activity of Punch should act to protect the cell from oxidative stress.

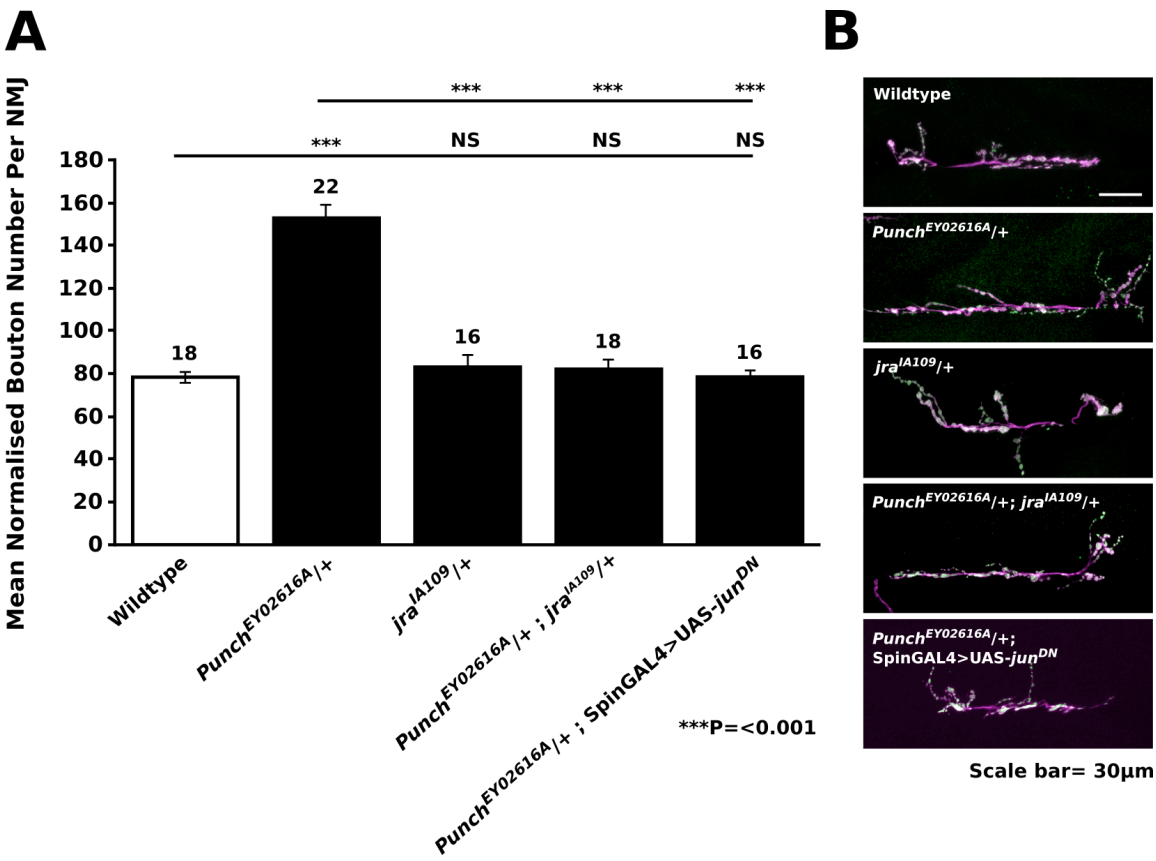

Figure 5.11 Reducing Jun activity rescues the synaptic overgrowth observed in heterozygous *Punch* mutants

A: Analysis of the NMJ at muscle 6/7 segment A3 of $Punch^{EY02616A}$/+ 3rd instar larvae revealed significantly increased mean normalised synaptic bouton number per NMJ (153±6.5, n=22) compared to WT controls (78±2.8, n=18)(***p<0.001; ANOVA with post hoc Bonferroni correction). No significant difference in mean normalised bouton number per NMJ is found when comparing jra^{IA109}/+ (83±5.6, n=16) to WT controls (NS p>0.05; ANOVA with post hoc Bonferroni correction). However, significant reduction in mean normalised bouton number per NMJ is found when comparing larvae heterozygous for both the jra^{IA109} and $Punch^{EY02616A}$ mutations (82±4.2, n=18) to $Punch^{EY02616A}$/+ alone (***p<0.001; ANOVA with post hoc Bonferroni correction). Expressing the dominant negative version of Jun (UAS-jun^{DN}) pre- and post-synaptically (79±3.2, n=16) via SpinGAL4 in the $Punch^{EY02616A}$/+ larvae also significantly reduces mean normalised bouton number per NMJ when compared to $Punch^{EY02616A}$/+ alone (***p<0.001; ANOVA with post hoc Bonferroni correction). Neither $Punch^{EY02616A}/jra^{IA109}$ or $Punch^{EY02616A}$/+; SpinGAL4>UAS-jun^{DN} larvae displayed any significant difference in mean normalised bouton number per NMJ compared to WT controls (NS p>0.05; ANOVA with post hoc Bonferroni correction). Error bars display ±SEM. **B**: Representative image of the NMJ at muscle 6/7 segment A3 imaged from each condition of the experiment. Scale bar 30µm.

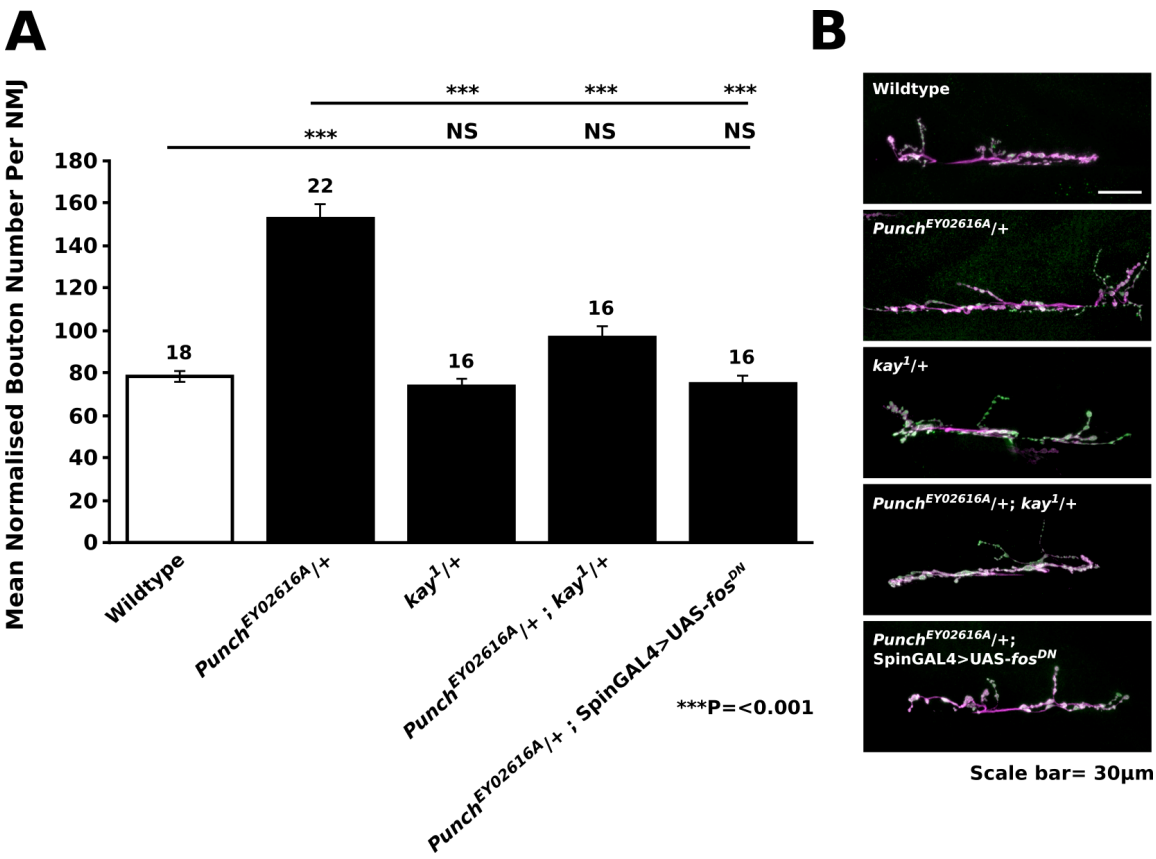

Figure 5.12 Reducing Fos activity rescues the synaptic overgrowth observed in heterozygous *Punch* mutants

A: Analysis of the NMJ at muscle 6/7 segment A3 of $Punch^{EY02616A}$/+ 3rd instar larvae revealed significantly increased mean normalised synaptic bouton number per NMJ (153±6.5, n=22) compared to WT controls (78±2.8, n=18)(***p<0.001; ANOVA with post hoc Bonferroni correction). No significant difference in mean normalised bouton number per NMJ is found when comparing kay^1/+ (74±3.4, n=16) to WT controls (NS p>0.05; ANOVA with post hoc Bonferroni correction). However, significant reduction in mean normalised bouton number per NMJ is found when comparing larvae heterozygous for both the kay^1 and $Punch^{EY02616A}$ mutations (97±5, n=16) to $Punch^{EY02616A}$/+ alone (***p<0.001; ANOVA with post hoc Bonferroni correction). Expressing the dominant negative version of Fos (UAS-fos^{DN}) pre- and post-synaptically (75±4, n=16) via SpinGAL4 in the $Punch^{EY02616A}$/+ mutant background also significantly reduces mean normalised bouton number per NMJ when compared to $Punch^{EY02616A}$/+ alone (***p<0.001; ANOVA with post hoc Bonferroni correction). Neither $Punch^{EY02616A}/kay^1$ or $Punch^{EY02616A}$/+; SpinGAL4>UAS-fos^{DN} larvae displayed any significant difference in mean normalised bouton number per NMJ compared to WT controls (NS p>0.05; ANOVA with post hoc Bonferroni correction). Error bars display ±SEM. **B**: Representative image of the NMJ at muscle 6/7 segment A3 imaged from each condition of the experiment. Scale bar 30µm.

5.2.5 Punch offers neuroprotection against oxidative stress

We aimed to determine whether increased expression of Punch could offer neuroprotection against oxidative stress, presumably through increases in BH_4. We used UAS-Punch fly lines to overexpress Punch pre- and post-synaptically via SpinGAL4. Two UAS-Punch lines were used, the first UAS-PunchA-WT, is purely Punch isoform A; the second is UAS-PunchA-S37E, a variation of Punch isoform A that exhibits increased enzymatic activity due to Serine 37 being modified to glutamic acid (Funderburk et al., 2006). To determine their functionality we expressed both UAS-Punch versions via SpinGAL4 in a heterozygous $Punch^{EY02616A}$ mutant background, both were able to fully rescue the increase in synaptic bouton number seen in $Punch^{EY02616A}$/+ mutants (Figure 5.13; $p<0.001$, ANOVA).

Significantly increased branch number was observed in $Punch^{EY02616A}$/+ mutants compared to WT controls (Figure 5.14A; $p<0.001$, ANOVA). Branch number was significantly lower when expressing UAS-PunchA-WT in the heterozygous *Punch* mutant background ($p<0.01$, ANOVA), however NMJ length was not (Figure 5.14B; $p>0.05$, ANOVA) when comparing to heterozygous *Punch* mutants alone. $Punch^{EY02616A}$/+ mutant larvae in this experiment did not show any significant increases in NMJ length compare to WT controls ($p>0.05$, ANOVA), further suggesting NMJ length is less amenable to change than bouton and branch number. Expression of the high activity UAS-PunchA-S37E, in the heterozygous *Punch* mutant background rescued the increases in branch number ($p<0.001$, ANOVA) and was significantly lower than the NMJ length observed in heterozygous *Punch* mutants alone ($p<0.01$, ANOVA).

This shows that expression of UAS-Punch is restoring the activity levels enough to rescue the NMJ overgrowth of *Punch* mutants, at least in terms of bouton and branch numbers quantified from NMJ analysis, confirming UAS-PunchA-WT and UAS-PunchA-S37E are functioning as expected.

Protection from oxidative stress was tested by treating larvae expressing either UAS-PunchA-WT or UAS-PunchA-S37E via SpinGAL4 with 10mM DEM. Synaptic bouton number was significantly increased in WT larvae treated with DEM (Figure

5.15; p<0.01, ANOVA). However, upon treating both UAS-Punch lines with DEM, no significant difference was found compared to their respective controls, or WT controls (p>0.05, ANOVA).

Branch number was also significantly increased in DEM treated larvae compared to WT controls (Figure 5.16A; p<0.05, ANOVA). Treating either UAS-PunchA-WT or UAS-PunchA-S37E with DEM did not result in any significant increase in branch number compared to their respective controls or when compared to WT controls (p>0.05, ANOVA).

No significant difference in NMJ length (μm) was found when treating WT larvae with DEM compared to WT controls (Figure 5.16B; p>0.05, ANOVA). Comparing DEM treated UAS-PunchA-WT and UAS-PunchA-S37E to their respective controls, and to WT controls revealed no significant difference in NMJ length (p>0.05, ANOVA).

Expression of UAS-Punch acts to protect the NMJ from treatment with DEM, increasing resistance to oxidative stress-induced synaptic overgrowth.

The ability for both UAS-Punch lines to restore Punch activity as well as increase resistance to oxidative stress-induced synaptic overgrowth was also tested. UAS-PunchA-WT and UAS-PunchA-S37E were expressed in larvae via SpinGAL4 in heterozygous *Punch* mutant backgrounds ($Punch^{EY02616A}$) and treated with DEM during development. Both WT and $Punch^{EY02616A}$/+ larvae treated with DEM showed significant increases in synaptic bouton number compared to WT controls (Figure 5.17; p<0.01 and p<0.001 respectively, ANOVA). Expression of either UAS-PunchA-WT or UAS-PunchA-S37E in the heterozygous *Punch* mutant background treated with DEM displayed significantly reduced synaptic bouton number when compared to $Punch^{EY02616A}$/+ treated with DEM alone (p<0.001, ANOVA) and were not significantly different to WT controls (p>0.05, ANOVA). Branch number was also analysed, both WT and $Punch^{EY02616A}$/+ larvae treated with DEM showed significant increases in synaptic branch number compared to WT controls (Figure 5.18A; p<0.05, ANOVA). However, no significant difference between $Punch^{EY02616A}$/+ larvae treated with DEM and either UAS-Punch expressed in the heterozygous *Punch*

mutant background treated with DEM was found ($p>0.05$, ANOVA). WT controls also showed no significant difference to either UAS-Punch expressed in the heterozygous *Punch* mutant background treated with DEM ($p>0.05$, ANOVA).

Neither WT nor $Punch^{EY02616A}$/+ larvae treated with DEM showed any significant difference in NMJ length (μm) when compared to WT controls (Figure 5.18B; $p>0.05$, ANOVA). However, expression of UAS-PunchA-S37E in a heterozygous *Punch* mutant background treated with DEM showed significantly lower NMJ length when compared to $Punch^{EY02616A}$/+ larvae treated with DEM alone ($p<0.05$, ANOVA).

NMJ length and to some degree, branch number are unchanged in the experiments described above. However, the major overgrowth phenotype observed as increases in synaptic bouton number in *Punch* mutants, DEM treated wild-types and even DEM treated *Punch* mutants are rescued by elevated levels of Punch/BH_4, suggesting they have a crucial role in bolstering the cellular resistance to oxidative stress.

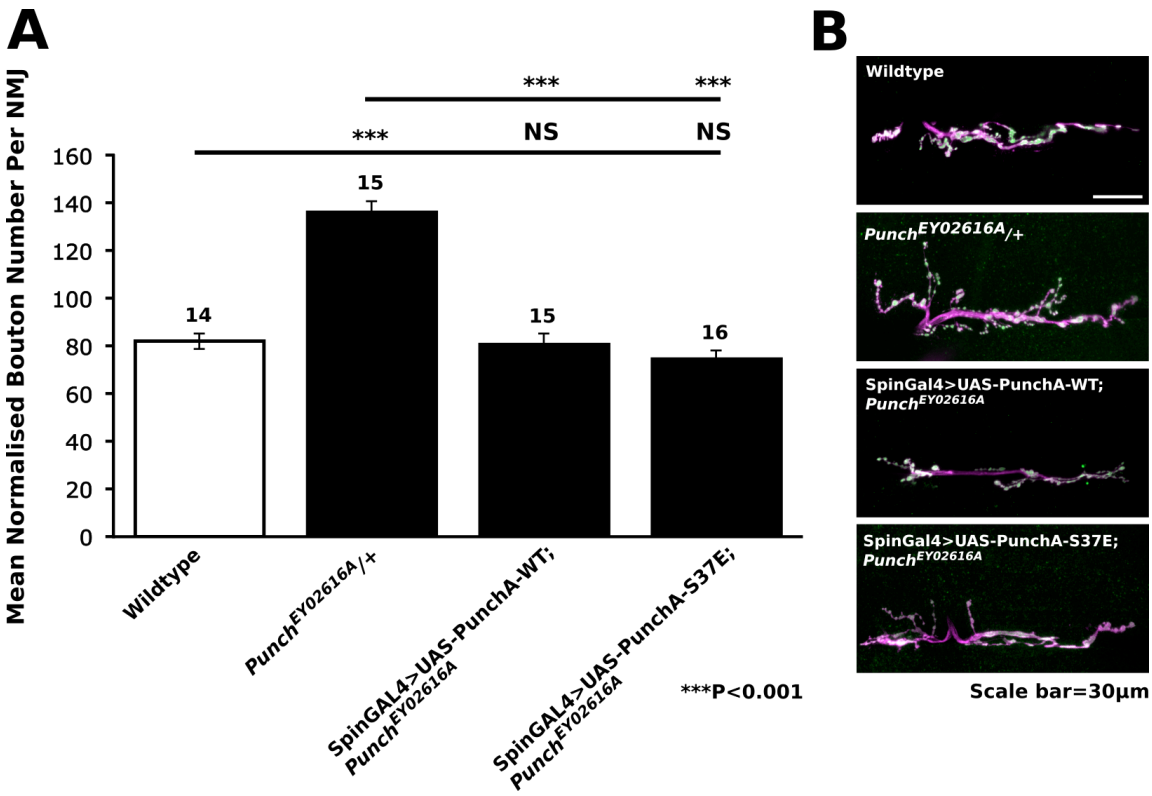

Figure 5.13 Punch overexpression rescues the synaptic overgrowth observed in heterozygous *Punch* mutants

A: Analysis of the NMJ at muscle 6/7 segment A3 of *Punch*^{EY02616A}/+ 3rd instar larvae revealed significantly increased mean normalised synaptic bouton number per NMJ (136±4.8, n=15) compared to WT controls (82±3.3, n=14)(***p<0.001; ANOVA with post hoc Bonferroni correction). SpinGAL4 driven expression of UAS-PunchA-WT and UAS-PunchA-S37E (high enzymatic activity) (81±4.6, n=15 and 75±3.6, n=16, respectively) in a heterozygous *Punch*^{EY02616A} mutant background show no significant difference in mean normalised bouton number per NMJ compared to WT controls (NS p>0.05; ANOVA with post hoc Bonferroni correction). They also show significant reduction in mean normalised bouton number per NMJ compared to *Punch*^{EY02616A}/+ alone (***p<0.001; ANOVA with post hoc Bonferroni correction). Error bars display ±SEM. **B**: Representative image of the NMJ at muscle 6/7 segment A3 imaged from each condition of the experiment. Scale bar 30µm.

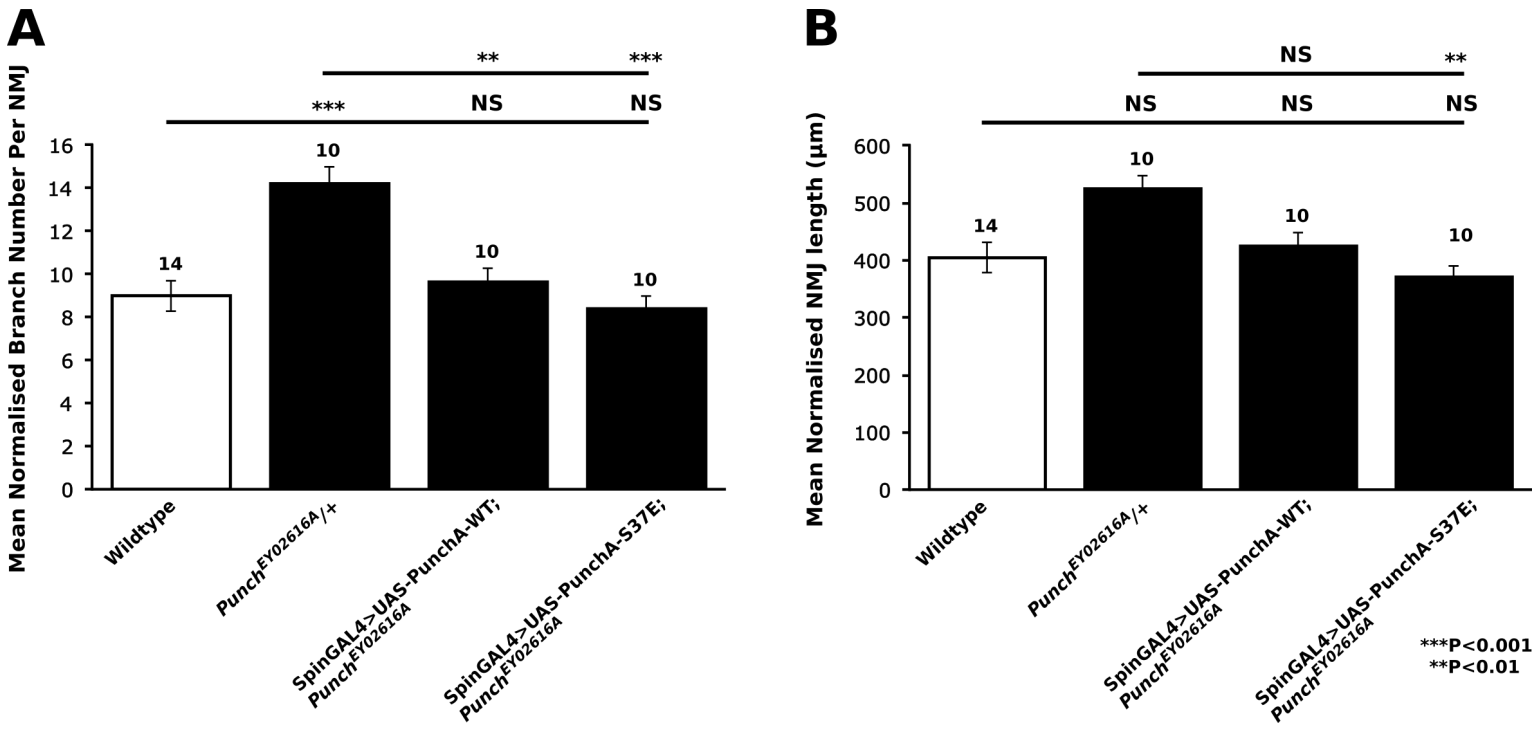

Figure 5.14 Overexpression of PunchA-S37E rescues branch number and length in heterozygous *Punch* mutants

A: Analysis of the NMJ at muscle 6/7 segment A3 of *Punch*^{EY02616A}/+ 3rd instar larvae revealed significantly increased mean normalised synaptic branch number per NMJ (14.2±0.8, n=10) compared to WT controls (9±0.7, n=14)(***p<0.001; ANOVA with post hoc Bonferroni correction). SpinGAL4 driven expression of UAS-PunchA-WT and UAS-PunchA-S37E (high enzymatic activity) (9.6±0.6, n=10 and 8.4±0.6, n=10, respectively) in a heterozygous *Punch*^{EY02616A} mutant background show no significant difference in mean normalised branch number per NMJ compared to WT controls (NS p>0.05; ANOVA with post hoc Bonferroni correction). Significant reduction in mean normalised branch number per NMJ is observed when UAS-PunchA-WT and UAS-PunchA-S37E are compared to *Punch*^{EY02616A}/+ alone (**p<0.01 and ***p<0.001 respectively; ANOVA with post hoc Bonferroni correction). Error bars display ±SEM. **B:** No significant difference in mean normalised NMJ length (µm) is observed when comparing *Punch*^{EY02616A}/+ (525±23, n=10), and SpinGAL4 driven expression of UAS-PunchA-WT (425±23, n=10) and UAS-PunchA-S37E (high activity) (371±19, n=10) in a *Punch*^{EY02616A} mutant background compared to WT controls (404±25, n=10) (NS p>0.05; ANOVA with post hoc Bonferroni correction). SpinGAl4 driven expression of UAS-PunchA-S37E in a Punch^{EY02616A} background shows significantly reduced mean normalised NMJ length (µm) compared to *Punch*^{EY02616A}/+ alone (**p<0.01; ANOVA with post hoc Bonferroni correction). Error bars display ±SEM.

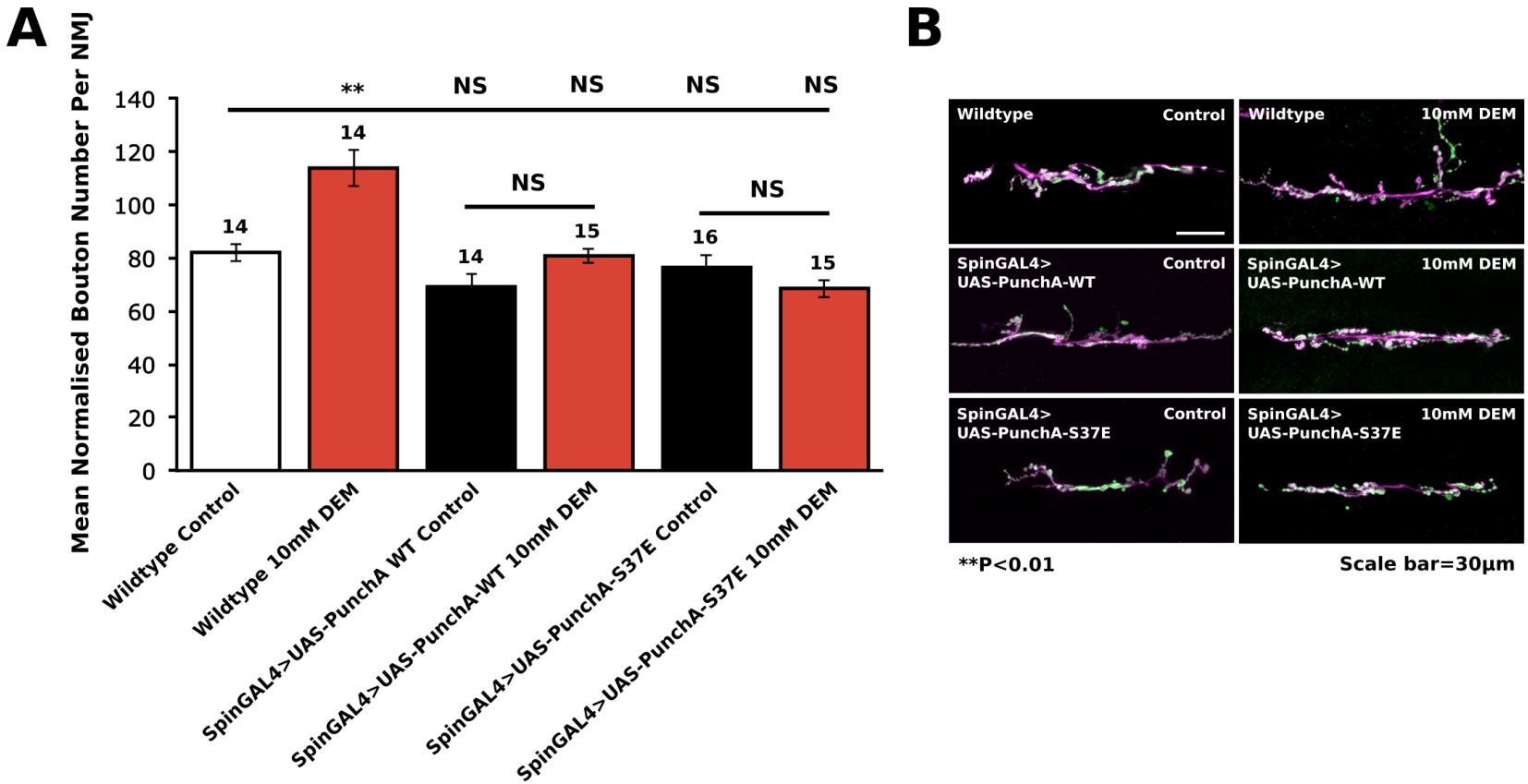

Figure 5.15 Punch overexpression rescues DEM-induced synaptic overgrowth

A: Analysis of the NMJ at muscle 6/7 segment A3 of WT 3rd instar larvae treated with a yeast paste containing 10mM DEM during development show significantly increased mean normalised synaptic bouton number per NMJ (114±7, n=14) compared to WT controls (82±3.3, n=14) (WT + 10% ethanol in yeast paste) (**p<0.01; ANOVA with post hoc Bonferroni correction). SpinGAL4 driven expression of UAS-PunchA-WT and UAS-PunchA-S37E (high enzymatic activity) in control conditions (69±5, n=14 and 77±4.9, n=16, respectively) and when treated with 10mM DEM (81±2.6, n=15 and 67±3.3, n=15, respectively) show no significant difference in mean normalised synaptic bouton number per NMJ compared to WT controls and each other (NS p>0.05; ANOVA with post hoc Bonferroni correction). Error bars display ±SEM. **B**: Representative image of the NMJ at muscle 6/7 segment A3 imaged from each condition of the experiment. Scale bar 30µm.

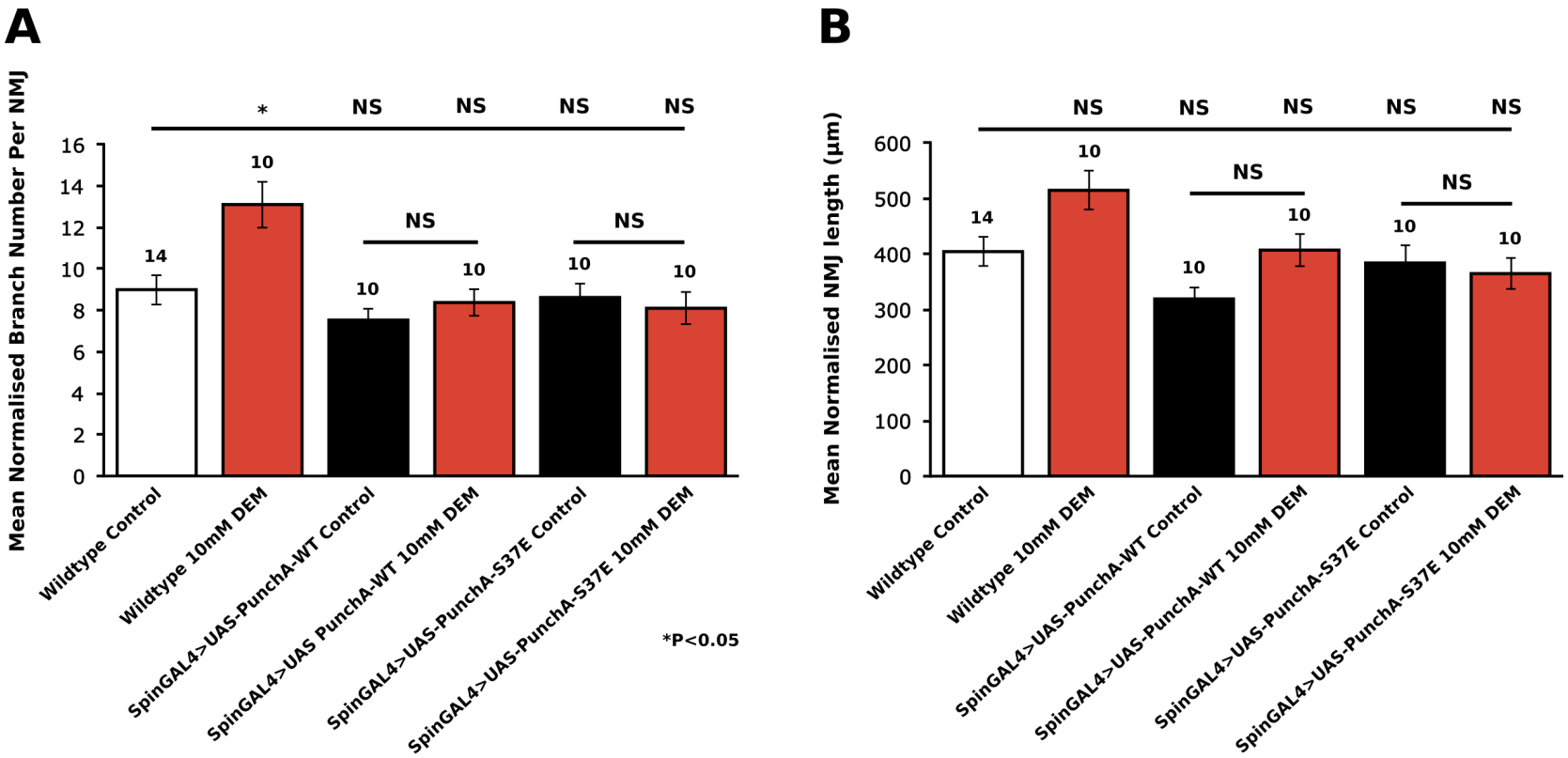

Figure 5.16 Punch overexpression rescues DEM-induced increases in branch number

A: Analysis of the NMJ at muscle 6/7 segment A3 of WT 3rd instar larvae treated with a yeast paste containing 10mM DEM during development show significantly increased mean normalised synaptic branch number per NMJ (13±1.1, n=10) compared to WT controls (9±0.7, n=14) (WT + 10% ethanol in yeast paste) (*p<0.05; ANOVA with post hoc Bonferroni correction). SpinGAL4 driven expression of UAS-PunchA-WT and UAS-PunchA-S37E (high enzymatic activity) in control conditions (7.5±0.6, n=10 and 8.6±40.6, n=10, respectively) and when treated with 10mM DEM (8.4±0.6, n=10 and 8.1±0.8, n=10, respectively) show no significant difference in mean normalised branch number compared to WT controls and each other (NS p>0.05; ANOVA with post hoc Bonferroni correction). Error bars display ±SEM. **B**: Treating WT with 10mM DEM showed no significant difference in mean normalised NMJ length (µm) (515±35, n=10) compared to WT controls (404±26, n=14) (NS p>0.05; ANOVA with post hoc Bonferroni correction). Treating SpinGAL4 driven UAS-PunchA-WT or UAS-PunchA-S37E (high enzymatic activity) with 10mM DEM (407±29, n=10 and 365±28.3, n=10, respectively) does not significantly alter mean normalised NMJ length (µm) compared to their relative control (319±21.7, n=10 and 384±32.1, n=10, respectively) (NS p>0.05; ANOVA with post hoc Bonferroni correction). Error bars display ±SEM.

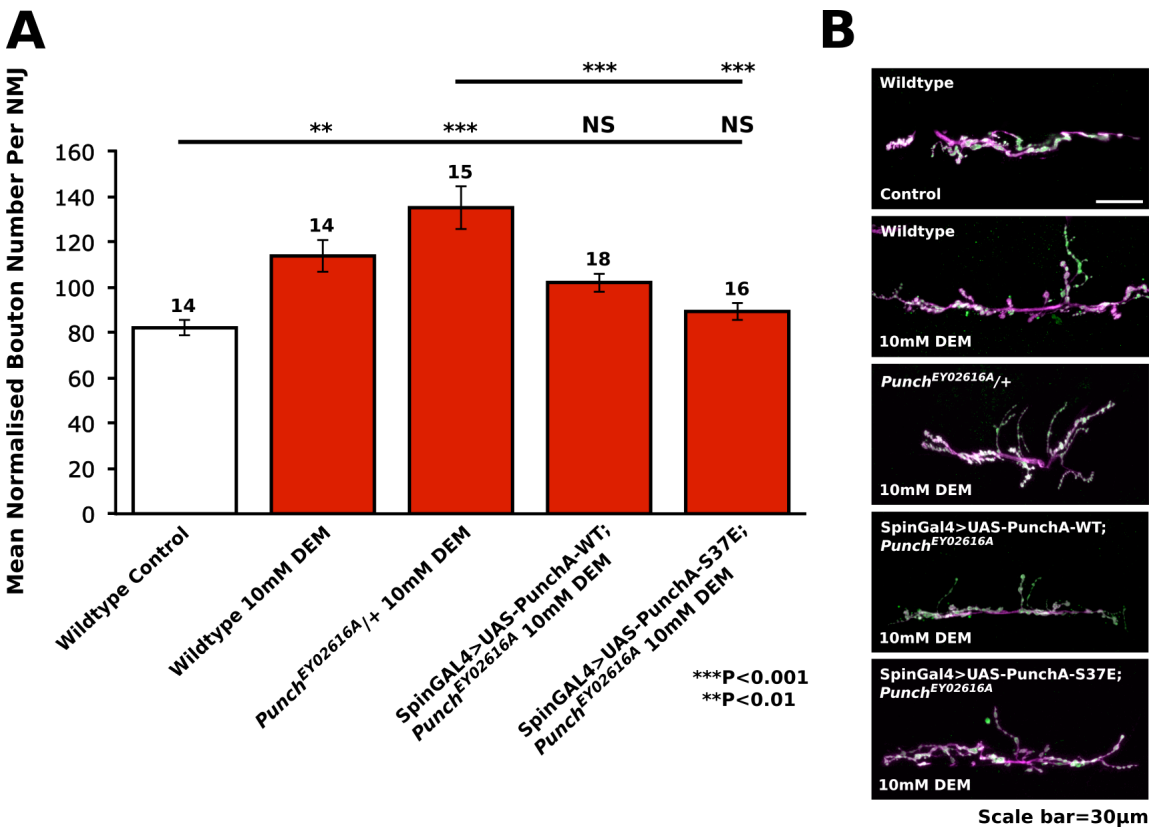

Figure 5.17 Punch overexpression rescues the synaptic overgrowth observed in heterozygous *Punch* mutants when treated with DEM

A: Analysis of the NMJ at muscle 6/7 segment A3 of WT and *Punch*^{EY02616A}/+ 3rd instar larvae when treating with 10mM DEM during development revealed significantly increased mean normalised synaptic bouton number per NMJ (114±7, n=14 and 135±9.4, n=15, respectively) compared to WT controls (82±3.3, n=14)(**p<0.01 and ***p<0.001 respectively; ANOVA with post hoc Bonferroni correction). SpinGAL4 driven expression of UAS-PunchA-WT and UAS-PunchA-S37E (high enzymatic activity) (102±4.1, n=18 and 90±3.9, n=16, respectively) in a heterozygous *Punch*^{EY02616A} mutant background and treated with 10mM DEM show no significant difference in mean normalised bouton number per NMJ compared to WT controls (NS p>0.05; ANOVA with post hoc Bonferroni correction). However, significant reduction in mean normalised bouton number per NMJ is observed when compared to *Punch*^{EY02616A}/+ treated with 10mM DEM (***p<0.001; ANOVA with post hoc Bonferroni correction). Error bars display ±SEM. **B**: Representative image of the NMJ at muscle 6/7 segment A3 imaged from each condition of the experiment. Scale bar 30µm.

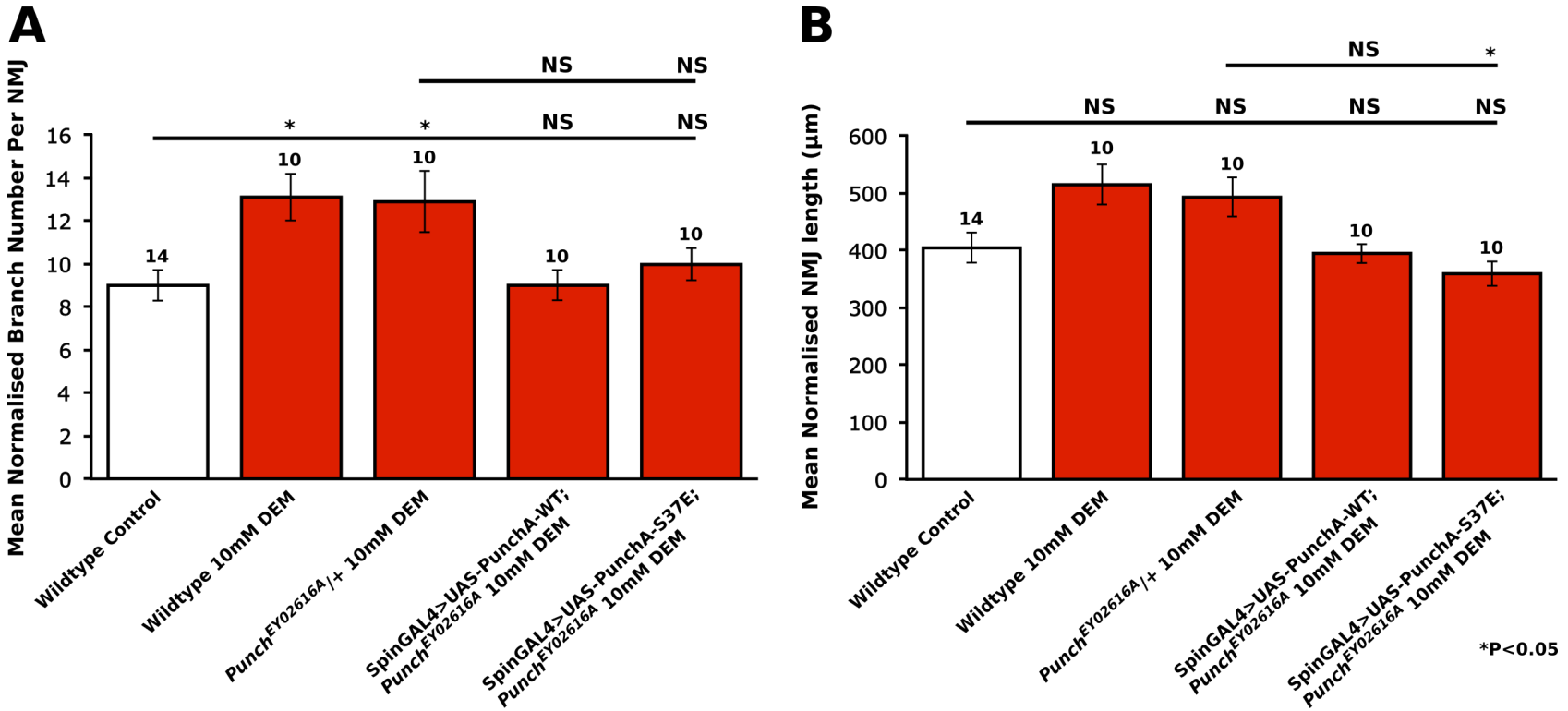

Figure 5.18 Overexpression of Punch restricts *Punch*- and DEM-induced increases in branch number and NMJ length

A: Analysis of the NMJ at muscle 6/7 segment A3 of $Punch^{EY02616A}$/+ larvae treated with DEM (12.9±1.4, n=10) and WT treated with DEM (13.1±1.1, n=10) revealed significantly increased mean normalised synaptic branch number per NMJ compared to WT controls (9±0.7, n=14)(*p<0.05; ANOVA with post hoc Bonferroni correction). SpinGAL4 driven expression of UAS-PunchA-WT and UAS-PunchA-S37E (9±0.7, n=10 and 10±0.75, n=10, respectively) in a heterozygous $Punch^{EY02616A}$ mutant background treated with DEM show no significant difference in mean normalised branch number per NMJ compared to WT controls (NS p>0.05; ANOVA with post hoc Bonferroni correction). No significant reduction in mean normalised branch number per NMJ is observed when compared to $Punch^{EY02616A}$/+ treated with DEM (NS p>0.05; ANOVA with post hoc Bonferroni correction, respectively). Error bars display ±SEM. **B:** None of the following lines treated with DEM (WT (515±35, n=10), $Punch^{EY02616A}$/+ (493±35, n=10) or SpinGAL4 expressed PunchA-WT (395±17, n=10) /PunchA-S37E (359±21, n=10) in a $Punch^{EY02616A}$ mutant background) show any significant difference in mean normalised NMJ length compared to WT controls (404±26, n=14) (NS p>0.05; ANOVA with post hoc Bonferroni correction). Only larvae expressing UAS-PunchA-S37E in a $Punch^{EY02616A}$ mutant background treated with DEM show significant differences in NMJ length compared to $Punch^{EY02616A}$/+ larvae treated with DEM (*p<0.05; ANOVA with post hoc Bonferroni correction). Error bars display ±SEM.

5.2.6 Punch overexpression rescues *highwire*-induced NMJ overgrowth

The *highwire* (*hiw*) mutation causes NMJ overgrowth via a failure to degrade the JNK kinase kinase, Wallenda (Wnd), increasing JNK activity. As shown previously, relieving the inhibition on JNK by mutating the negative regulator, *puckered*, also causes NMJ overgrowth (see section 3.2.4). Taken together it is clear that over activation of JNK signalling causes NMJ overgrowth. We aimed to determine whether overexpressing Punch could rescue the *highwire*-induced NMJ overgrowth. First we showed that expressing the newly created UAS-Punch, a fly line developed during this project, via nSybGAL4 caused no significant difference in synaptic bouton number compared to WT controls (Figure 5.19; $p>0.05$, ANOVA). Driving UAS-Punch in larvae treated with DEM or in a *Punch* mutant background also showed no significant differences to WT controls ($p>0.05$, ANOVA), suggesting our UAS-Punch also rescues the *Punch* mutant phenotype and bolsters the resistance to DEM. Knowing that nSybGAL4 driven Punch offers neuroprotection, we proceeded to test whether it could rescue the *highwire* mutant overgrowth.

We used the mutant allele of *highwire*, hiw^{ND9} that express a nonsense mutation in the N-terminal region of the *highwire* gene (Wan et al., 2000). The *highwire* gene is located on the X chromosome of *Drosophila*, so in order to analyse full *hiw* mutants we dissect the males. Analysis of *hiw* mutants revealed significantly increased synaptic bouton number compared to WT controls (Figure 5.20; $p<0.001$, ANOVA). Expressing UAS-Punch via nSybGAL4 in a *hiw* null background significantly reduced synaptic bouton number compared to *hiw* mutants alone ($p<0.001$, ANOVA) and no significant difference was found when comparing to WT controls ($p>0.05$, ANOVA). Branch number and NMJ length were also increased in *hiw* mutants compared to WT (Figure 5.21; $p<0.01$, ANOVA). Expression of UAS-Punch in the *hiw* background significantly reduced branch number (Figure 5.21A; $p<0.001$, ANOVA) and NMJ length (Figure 5.21B; $p<0.01$, ANOVA) compared to *hiw* mutants alone. Neither branch number nor NMJ length were significantly different to WT ($p>0.05$, ANOVA).

This may highlight a role for Punch in restraining JNK activity. Highwire acts to regulate Wallenda, and in its absence, JNK signalling becomes over activated

generating synaptic overgrowth in the absence of oxidative stress. Overexpressing Punch reduces the JNK-induced synaptic overgrowth, suggesting Punch may regulate JNK/AP-1 signalling. As we identify Punch as being associated with Fos and Jun, we postulate that Punch may act to regulate the activity of Fos and Jun, or AP-1 during non-stressed conditions.

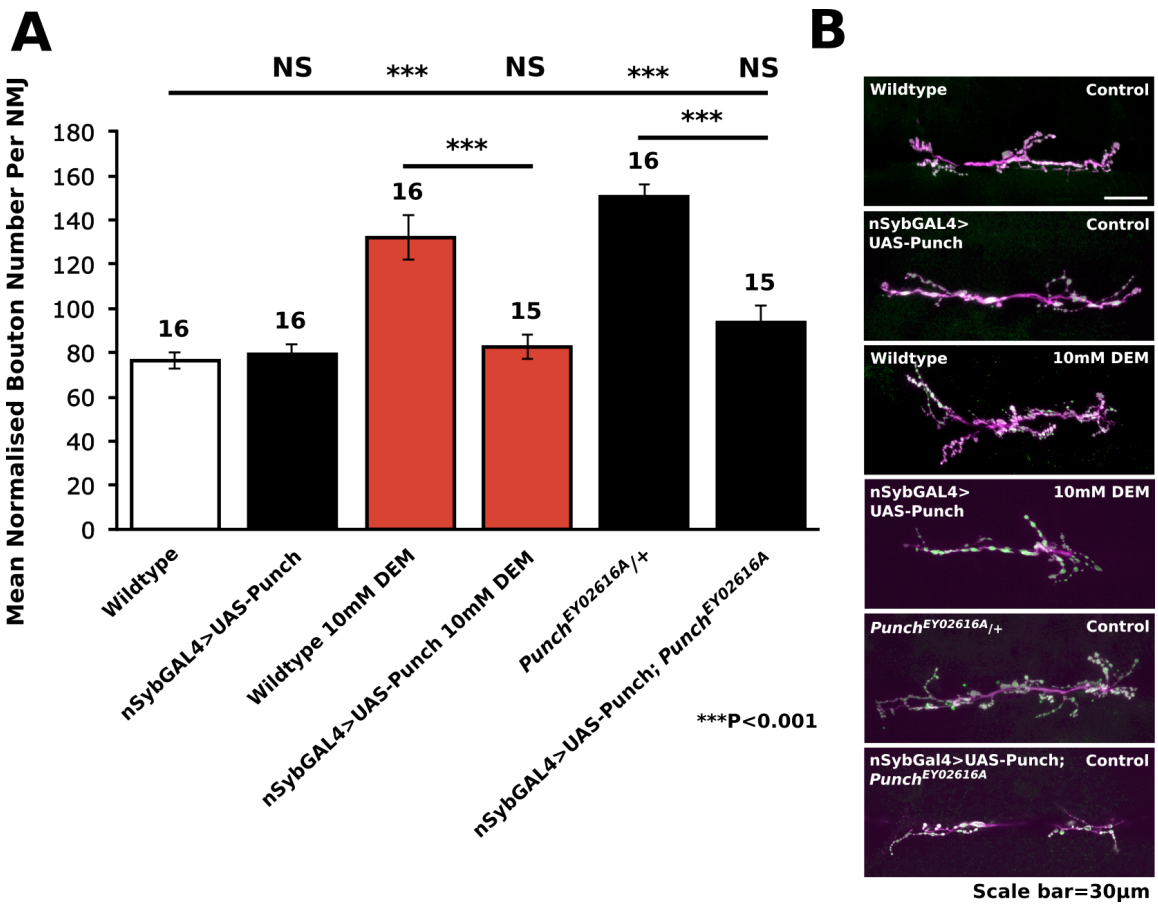

Figure 5.19 Pan-neuronal overexpression of Punch rescues the DEM- and *Punch* mutant-induced synaptic overgrowth

A: Analysis of the NMJ at muscle 6/7 segment A3 of 3rd instar larvae expressing UAS-Punch via nSybGAL4 revealed no significant difference in mean normalised synaptic bouton number per NMJ (79±4.5, n=16) compared to WT controls (76±3.7, n=16)(NS p>0.05; ANOVA with post hoc Bonferroni correction). Both WT treated with DEM (132±9.9, n=16) and $Punch^{EY02616A}$/+ (151±5.7, n=16) larvae show significant increases in mean normalised bouton number per NMJ (***p<0.001; ANOVA with post hoc Bonferroni correction). Expressing UAS-Punch via nSybGAL4 in larvae treated with DEM (83±5.4, n=15) or in a $Punch^{EY02616A}$ mutant background (94±7.4, n=15) showed no significant difference compared to WT controls. (NS p>0.05; ANOVA with post hoc Bonferroni correction). Expressing UAS-Punch via nSybGAL4 in both larvae treated with DEM and in a $Punch^{EY02616A}$ mutant background significantly reduced synaptic bouton numbers compared to their respective control (***p<0.001; ANOVA with post hoc Bonferroni correction). Error bars display ±SEM. **B**: Representative image of the NMJ at muscle 6/7 segment A3 imaged from each condition of the experiment. Scale bar 30µm.

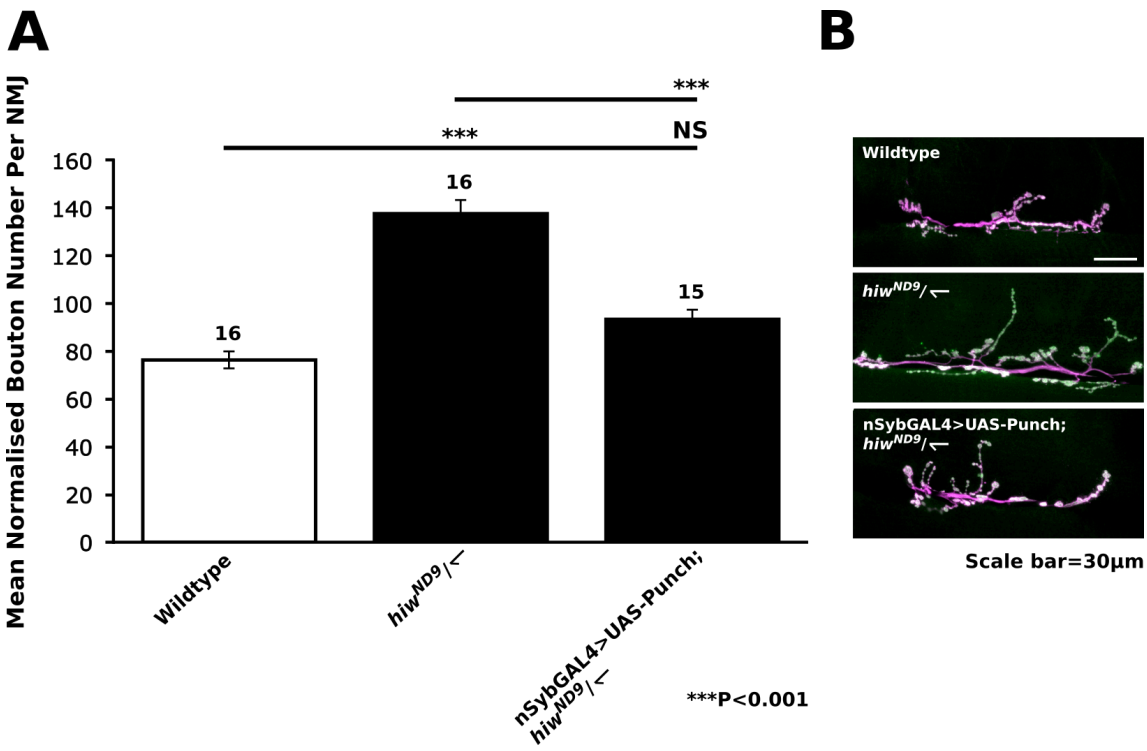

Figure 5.20 Pan-neuronal overexpression of Punch rescues the synaptic overgrowth observed in *highwire* mutants

A: Analysis of the NMJ at muscle 6/7 segment A3 of *hiw*^{ND9}/Y 3rd instar larvae revealed significantly increased mean normalised synaptic bouton number per NMJ (138±5.9, n=16) compared to WT controls (76±3.7, n=16)(***p<0.001; ANOVA with post hoc Bonferroni correction). nSybGAL4 driven expression of UAS-Punch in the *highwire* mutant background (93±3.7, n=15) show no significant difference in mean normalised bouton number per NMJ compared to WT controls (NS p>0.05; ANOVA with post hoc Bonferroni correction). However, significant reduction in mean normalised bouton number per NMJ is found when comparing to *hiw*^{ND9}/Y alone (***p<0.001; ANOVA with post hoc Bonferroni correction). Error bars display ±SEM. **B**: Representative image of the NMJ at muscle 6/7 segment A3 imaged from each condition of the experiment. Scale bar 30µm.

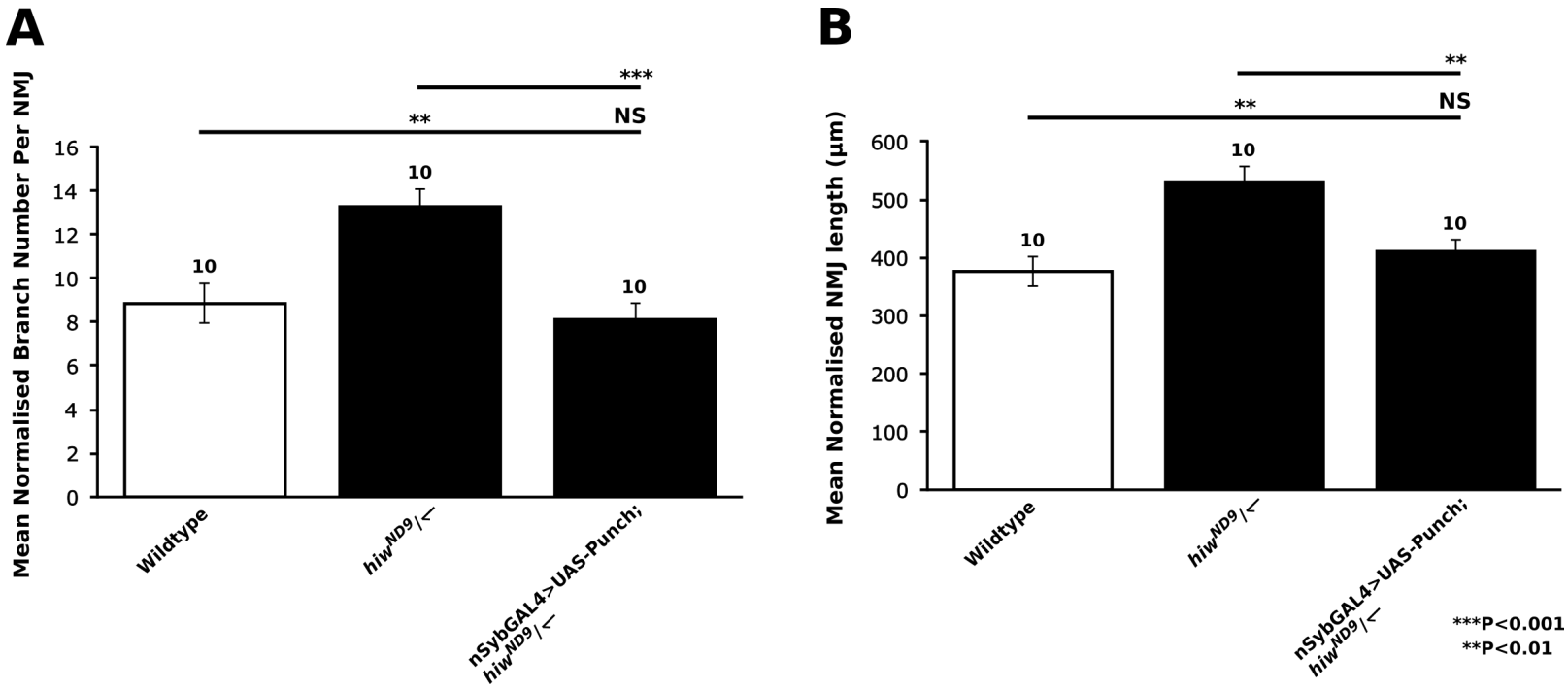

Figure 5.21 Pan-neuronal overexpression of Punch significantly reduces branch number and length in *highwire* mutants

A: Analysis of the NMJ at muscle 6/7 segment A3 of *hiw*^{ND9}/Y 3rd instar larvae revealed significantly increased mean normalised synaptic branch number per NMJ (13.3±0.8, n=10) compared to WT controls (9±0.9, n=10)(**p<0.01; ANOVA with post hoc Bonferroni correction). nSybGAL4 driven expression of UAS-Punch in a *highwire* mutant background (8±0.7, n=10) show no significant difference in mean normalised branch number per NMJ compared to WT controls (NS p>0.05; ANOVA with post hoc Bonferroni correction). Significant reduction in mean normalised branch number per NMJ is observed when compared to *hiw*^{ND9}/Y alone (***p<0.01; ANOVA with post hoc Bonferroni correction). Error bars display ±SEM. **B:** Significant increases in mean normalised NMJ length (µm) are observed when comparing *hiw*^{ND9}/Y (529±29, n=10) to WT controls (376±26, n=10) (**p<0.01; ANOVA with post hoc Bonferroni correction). nSybGAl4 driven expression of UAS-Punch in a heterozygous *highwire* background shows significantly reduced mean normalised NMJ length (µm) compared to *hiw*^{ND9}/Y alone (**p<0.01; ANOVA with post hoc Bonferroni correction). Error bars display ±SEM.

5.3 Discussion

Punch is responsible for the production of BH_4, an essential cofactor in a variety of mechanisms that act to protect the cell. Here we describe *Punch* as a haploinsufficient mutant that causes severe NMJ overgrowth when a single copy of the gene is mutated. We have shown that reducing Punch activity causes NMJ overgrowth that can be rescued by either relieving oxidative stress or the DA deficit. Similar to DEM treatment, *Punch*-induced NMJ overgrowth is mediated by Fos and Jun. This suggests the overgrowth is acting through JNK/AP-1 signalling. Overexpression of Punch offers neuroprotection against DEM treatment, reducing the associated overgrowth. The JNK mediated NMJ overgrowth observed in *hiw* mutants, is also rescued by Punch overexpression, raising the idea that Punch may normally act to inhibit AP-1 during non-stressed conditions. This is supported by our identification of Punch bound to Fos and Jun only in non-stressed conditions and lost when treated with DEM (see section 4.2.2). Finally, DA levels may inadvertently regulate JNK signalling through a Punch-mediated feedback response.

5.3.1 Reducing Punch activity causes NMJ overgrowth via oxidative stress

We show that reducing Punch activity causes NMJ overgrowth. This observation is very exciting; we see severe neuronal dysfunction, which closely aligns to heterozygous mutations in *GTPCH1* documented in humans. Both DOPA-responsive dystonia and *GTPCH1* deficiency are severe diseases in humans that result from a loss of BH_4 (Furukawa, 1993). Both result in reduced levels of DA, causing problems with movement and often lead to the onset of PD later in life (Mencacci et al., 2014). *GTPCH1* deficiency, which results from a loss of both copies is more severe, and the patient exhibits very high levels of phenylalanine, leading to mental retardation as well as the symptoms associated with DOPA-responsive dystonia (Thony and Blau, 2006). Our observations of NMJ overgrowth may result from an oxidative stress burden in *Punch* mutants. BH_4 acts as a potent ROS scavenger, and inhibiting the production of BH_4 leads to increases in superoxide anions (Nakamura et al., 2001, Antoniades et al., 2008). Low levels of BH_4 also lead to increased ROS production via the nitric oxide synthase (NOS) pathway due to the uncoupling of electron flow

during nitric oxide production (Bevers et al., 2006). Not only may our *Punch* mutants have reduced ROS scavenging ability, they may also be generating more superoxide anions via the NOS pathway. We tested whether our *Punch* mutants were exhibiting an oxidative stress burden by treating them with antioxidant, Trolox. Trolox is a vitamin E analogue that acts to scavenge ROS and has been shown to rescue the effects of DEM, which we also recapitulate in this chapter, where Trolox treatment can rescue DEM-induced NMJ overgrowth (Hamad et al., 2010, Vergauwen et al., 2015). Trolox reduces *Punch*-induced NMJ overgrowth, suggesting that the overgrowth at some level involves an increase in ROS.

5.3.2 Punch offers neuroprotection against ROS

Overexpression of Punch rescues the effects of DEM-treatment. This reinforces the idea that Punch/BH_4 can offer neuroprotection against oxidative stress. BH_4 is able to directly scavenge superoxide anions and hydrogen peroxide, which may explain how increased Punch expression, relieves oxidative stress (Kojima et al., 1995, Nakamura et al., 2001). Upon an increase in hydrogen peroxide, BH_4 is synthesised via an increase in JAK2 activation, suggesting this protective mechanism directly responds to oxidative stress (Shimizu et al., 2003). Interestingly, we identify the protein Hopscotch (*Hop*) bound to Jun in DEM-treated conditions. Hopscotch is the *Drosophila* homolog of JAK (Binari and Perrimon, 1994). This may indicate that upon an increase in oxidative stress, Jun interacts with and activates Hopscotch, triggering events that lead to BH_4 biosynthesis. Combined with the *Punch* mutant data, this suggests Punch/BH_4 is critical in the defence against oxidative stress, and that AP-1 may modulate this.

5.3.3 *Punch*-induced NMJ overgrowth is mediated by JNK/AP-1 signalling

We have previously shown that NMJ overgrowth caused by DEM treatment is mediated by JNK signalling. JNK and ASK1 are both activated by ROS, leading to the phosphorylation and activation of AP-1 (Adler et al., 1999b). When mitochondrial oxidative stress occurs, Fos and Jun dimerise causing NMJ overgrowth (Milton et al., 2011). We tested whether *Punch*-induced NMJ overgrowth was mediated by Fos or

Jun. Our findings indicate that reducing either Fos or Jun activity in a *Punch* mutant background completely rescues the observed overgrowth. This suggests that *Punch*-induced overgrowth requires the action of JNK/AP-1 signalling.

5.3.4 Punch restrains the activity of Fos and Jun

We identified Fos and Jun bound to Punch during non-stressed conditions and absent following oxidative stress. From this we theorise that Punch may restrain Fos and Jun when bound. This may highlight a novel link between the ROS activated stress response pathway, JNK/AP-1 and a constitutive defence pathway that acts to reduce ROS via standing levels of BH_4 scavenging. We tested this by overexpressing Punch in a *hiw* mutant background. The mutant *hiw* fails to degrade the JNKKK wallenda, leading to over-activation of the JNK pathway (Collins et al., 2006). We find that Punch can rescue this *hiw* mutant overgrowth, suggesting Punch can restrain the JNK signalling pathway, and this is likely to be occurring at Fos and Jun. We showed that expressing Punch restricts synaptic overgrowth, which may occur via either an increase in BH_4 and subsequent reduction in oxidative stress, or through inhibition of AP-1; and may be a combination of both.

We believe that during non-oxidatively stressed conditions, Punch is inhibited by high BH_4 levels and this inhibitory complex restrains AP-1 to prevent excessive JNK signalling. This final level of AP-1 regulation may act to reduce the frequency of synapse growth induction, avoiding responses to basal levels of cellular ROS. Punch, in complex with BH_4 may also act to protect AP-1 from oxidation as oxidative stress occurs. The DNA binding efficiency of AP-1 is reduced when oxidised, defeating the object of a redox response pathway (Abate et al., 1990). Our proposed model (Figure 5.22) aims to explain the relationship between Punch and AP-1. BH_4 may scavenge, or preferentially bind ROS in the vicinity of the AP-1/Punch-BH_4 complex. This releases AP-1 from Punch as BH_4 is oxidised and allows AP-1 to transcribe genes involved in synapse growth and cellular protection. Released Punch then induces the synthesis of BH_4, which scavenges ROS, reducing the level of oxidative stress. When the redox balance is restored, we believe BH_4 then reinhibits Punch into the inhibitory complex that is then able to continue restraining AP-1. This mechanism serves to elegantly regulate JNK signalling, a process that is critical to

synaptic plasticity and function. It is already apparent that the cell acts to rapidly regulate JNK signalling, as a transcriptional target of AP-1 is puckered, the negative feedback regulator of JNK which inhibits JNK signalling upon expression (Martín-Blanco et al., 1998).

In *Punch* mutants, we believe that not only are these larvae experiencing oxidative stress, they also fail to restrain AP-1. This explains the severe NMJ overgrowth compared to oxidative stress alone in DEM treated larvae.

This could be a critical finding in developing our understanding of oxidative stress, ageing and neurodegenerative diseases. Reductions in Punch activity as we age could lead to an oxidative stress burden and increases in JNK/AP-1 signalling, both of which have been implicated in AD and PD (Peng and Andersen, 2003, Borsello and Forloni, 2007, Yarza et al., 2015). Increased JNK signalling could occur from increases in oxidative stress with age, or potentially mutations in *Punch* if our theory is correct. Recently, SNP's have been identified in Punch that contributes to PD (Nalls et al., 2014, Lewthwaite et al., 2015). Whilst the contribution of Punch mutations to PD is most commonly associated with the decrease in DA, there may also be a role for increased JNK signalling.

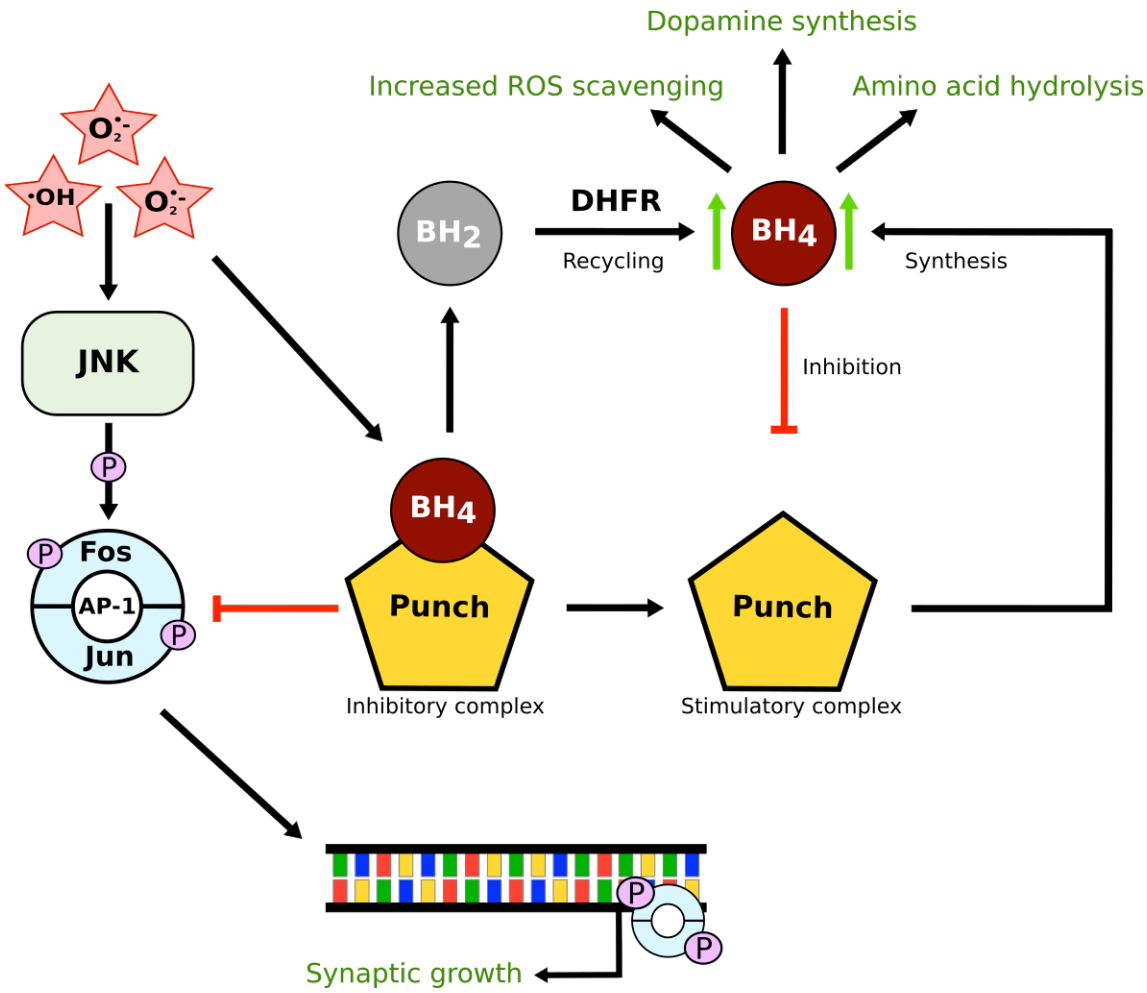

Figure 5.22 Proposed mechanism for the interaction between JNK/AP-1 and Punch/BH_4

Increases in neuronal ROS activate JNK signalling and AP-1. Inhibitory Punch restrains AP-1 until BH_4 is oxidised and released. Simultaneous release of Punch from AP-1 allows transcriptional activation by AP-1 and the synthesis of BH_4 by stimulatory Punch. Increased BH_4 scavenges the elevated ROS, reducing JNK activation and allowing the inhibitory Punch/BH_4 complex to reform and reinhibit AP-1, thus restoring the regulatory mechanism.

5.3.5 Synaptic plasticity may involve dopamine

During this chapter, it was shown that *DOPA decarboxylase* (*Ddc*) mutants exhibit NMJ overgrowth, and treating both these mutants and *Punch* mutants with L-DOPA significantly rescues this. Punch and Ddc are involved in cuticle pigmentation in *Drosophila* and are both required for proper synthesis of DA and Serotonin (Yamamoto, 2014). This suggests the DA may have a role in synaptic plasticity.

Reductions in the level of DA are often associated with the onset/progression of PD. The E3 ubiquitin ligase Parkin, encoded by the *parkin* gene, is frequently mutated in familial PD patients. Mutations in *parkin* lead to decreased levels of TH, disrupting the conversion of tyrosine to L-DOPA and consequently reducing the levels of DA. It has also been shown that mutations in *parkin* lead to an upregulation of JNK signalling, which we know is heavily involved in synaptic plasticity, is required for oxidative stress-induced synaptic overgrowth and directly causes synaptic growth when uninhibited (Cha et al., 2005). Whether the mutations in *parkin*, or the reducing DA activates JNK, is unknown, however, it does suggest that a reduction in DA in the *Ddc* mutant increases JNK signalling, which could cause NMJ overgrowth. Treatment using L-DOPA may exert its effect by inhibiting JNK signalling. Following our previously mentioned model, low levels of DA may stimulate Punch activation, releasing it from its inhibitory complex that acts to restrain JNK. This allows the biosynthesis of BH_4 to attempt to fulfil its role in the generation of DA. The side effect of this is the loss of AP-1 restraint, increasing JNK signalling and causing synaptic overgrowth. An alternative to this theory is that the *Ddc* mutants may be experiencing an oxidative stress burden, and a critical future experiment would be to treat the mutants with Trolox. It is also important to note that we should repeat this experiment using a different DA-deficient fly line to ensure synaptic overgrowth occurs when DA is low. To summarise, these data may represent a novel role for DA in the regulation of JNK signalling, which occurs via a Punch-mediated feedback mechanism that responds to low DA, releasing the restraint upon AP-1.

5.3.6 Conclusions

We have identified *Punch* as a haploinsufficient mutant, of which exhibit severe synaptic overgrowth due to reduced Punch/BH_4. This overgrowth can be rescued by treatment with Trolox, L-DOPA, reducing oxidative stress and DA deficit. Increasing Punch/BH_4 elicits a ROS-protective effect in the NMJ, rescuing the effects of DEM treatment. Punch-induced synaptic overgrowth is mediated by JNK/AP-1 signalling and reducing the activity of Fos and Jun completely rescues the mutant phenotype. Finally, increased Punch can rescue the *highwire* mutant overgrowth, which occurs due to increased JNK/AP-1 signalling, not oxidative stress. This implies that Punch may act to restrain Fos and Jun.

6. Discussion and Future Research

6.1 Introduction

The aims of this investigation were as follows:

1. Determine the role of AP-1/JNK signalling in a *Drosophila* model of oxidative stress in neurons.

2. Identify neuronal binding partners of Fos and Jun and determine how they might change during conditions of oxidative stress to generate response specificity.

3. Elucidate the relationship between our novel interacting protein Punch and AP-1 in the oxidative stress response in neurons.

During this chapter I will discuss how our work has contributed to these aims and outline the critical future experiments that would expand upon our data.

6.2 DEM treatment generates an oxidative stress burden

As a means to induce oxidative stress, DEM has proved to be efficient at eliciting an oxidative stress burden in *Drosophila* larvae. Most ROS are proposed to be produced by the mitochondria. Approximately 0.15% of cellular oxygen is converted into superoxide anions, and ROS then resides at a concentration of around 10^{-10}M in the mitochondrial matrix (Cadenas and Davies, 2000, St-Pierre et al., 2002). Superoxide anions are converted into hydrogen peroxide by the enzyme superoxide dismutase. Glutathione acts as a cofactor for the neutralisation of hydrogen peroxide via glutathione peroxidase and peroxiredoxin, as well as exhibiting its own ROS scavenging activity (Marí et al., 2009, Bhabak and Mugesh, 2010). Glutathione therefore is a key survival antioxidant in the mitochondria, and DEM acts to deplete its functional form. This is made apparent by the significant synaptic overgrowth that is observed when treating with at least 10mM DEM, and the reversal of this effect by the co-treating with an antioxidant, Trolox. The evident effects of DEM at

the larval synapse are only observed above a threshold of 10mM DEM in the food, at which concentration we believe is the point where glutathione is reduced significantly, causing a deficit in the antioxidant defence of the mitochondria and synaptic overgrowth. DEM does not act to increase ROS generation; it merely depletes the cells capacity to remove the ROS it generates naturally. This initial study shows that oxidative stress causes synaptic overgrowth in the larval NMJ. Oxidative stress-induced synaptic overgrowth has been shown previously in *spinster* loss of function mutants and larvae raised on the mitochondrial poison, paraquat (Milton et al., 2011). Furthermore, mutations in *parkin,* which induce mitochondrial dysfunction and resultant oxidative stress, have been shown to cause synaptic overgrowth (Vincent et al., 2012). This highlights the importance of the cellular antioxidant system and also shows that redox balance is essential for maintaining a healthy cellular environment. The use of DEM to induce oxidative stress and synaptic growth in larvae provides an experimental platform for the questions we wish to ask in this thesis.

Further experimentation would be to determine whether the effects of DEM result in a build up of hydrogen peroxide, or a general accumulation of ROS. It was shown in this investigation that Trolox treatment can rescue the effects of DEM, and this is likely to be occurring through increased hydrogen peroxide scavenging by this vitamin E analogue and antioxidant (Hamad et al., 2010). Expressing UAS-Catalase via SpinGAL4 in DEM-treated larvae and analysing bouton number may support this finding, and highlight a role for glutathione as a cofactor for hydrogen peroxide neutralisation which we would suggest is a major role for this antioxidant co-factor. Catalase is the main antioxidant involved in removing hydrogen peroxide in the cell. If DEM is truly causing a build up of hydrogen peroxide and this is causing oxidative stress, overexpression of Catalase would rescue the effects of DEM.

6.3 DEM-induced synaptic overgrowth is mediated by JNK/AP-1 signalling

Previous work published from the Sweeney lab demonstrated that oxidative stress-induced synaptic overgrowth is mediated by JNK/AP-1 signalling (Milton et al., 2011). They described a context dependent activation of AP-1, where putative cytosolic oxidative stress activates a Fos:Fos homodimer of AP-1 and Jun is not required. However, in the synaptic overgrowth caused by treatment with paraquat, Jun inhibition was able to rescue this overgrowth. We show during this investigation that mitochondrial oxidative stress via DEM treatment causes synaptic overgrowth that requires Fos and Jun, as well as ASK1. By reducing the activity of Fos, Jun and ASK1 we can ameliorate the synaptic overgrowth following DEM treatment. This suggests that Jun plays a role in responding to mitochondrial oxidative stress, but has a lesser role in cytosolic oxidative stress; an exciting development in uncovering the role of Fos and Jun. This falls in line with previous work from the Sweeney lab showing mutations in *parkin*, where mitochondrial dysfunction and oxidative stress ensues requires the action of Jun (Vincent, 2013). Mitochondrial generation of ROS occurs naturally and frequently, whereas cytosolic oxidative stress often results from dysfunction of the mitochondria or proteasome system, which are associated with age-related neurodegenerative diseases (Turner and Schapira, 2001, Trifunovic and Larsson, 2008). The idea that AP-1 shifts from a Fos:Jun heterodimer, to a Fos:Fos homodimer following shifts in cellular stress and redox status suggests that they serve different functions and would likely have different transcriptional outputs following activation. It is already well established that various signalling pathways can activate JNK signalling, specifically Fos which can be phosphorylated at distinct sites by overlapping JNK or ERK signalling in a context dependent manner (Ciapponi et al., 2001). This produces different signalling outcomes where ERK activation of Fos enables its role in wing vein formation and eye development, the latter of which is also regulated in part by JNK in distinct retinal cells. The differential phosphorylation of Fos that directs its function further strengthens the possibility of a context dependent dimer formation of AP-1 that is able to specifically respond to different sources of cellular stress and is likely to be occurring via phosphorylation at distinct sites upon Fos and/or Jun.

The phosphorylation code of Fos and Jun may hold critical information into their function, and identifying this is imperative if we are to fully characterise the neuronal role of Fos and Jun in the oxidative stress response. We would wish to bolster this finding in future by the use of ROS sensitive fluorescent proteins to image and localise more precisely the source of ROS in neurons undergoing oxidative stress.

As previously mentioned, we identified a role for ASK1 in the mitochondrial oxidative stress response. ASK1 has been shown to be localised in the mitochondria where it is inhibited by thioredoxin-2 (Trx2) and released following oxidative stress that cause cysteine-mediated conformational changes in Trx2 (Zhang et al., 2004). Other such upstream JNK kinases that have been shown to mediate overgrowth include wallenda (Wnd) and TGF-β-activated kinase 1 (TAK1). Previous research in the Sweeney lab has identified a role for the JNKKK TAK1 in mediating the synaptic overgrowth observed in *Rab8* mutants, which are thought to occur due to accumulations of plenty-of-SH3s (POSH) which induce ectopic activation of TAK1 and elevated JNK signalling (West et al., 2015). Furthermore they show overexpression of TAK1 also produces a synaptic overgrowth and that inhibiting Fos can reduce the *Rab8*-induced synaptic overgrowth. Similar observations for elevated JNK signalling in synaptic overgrowth are observed in *highwire* (*hiw*) mutants. The MAPKKK, Wnd is known to activate JNK signalling and is degraded by the actions of hiw. Synaptic overgrowth occurs in *hiw* mutants that fail to degrade Wnd, leading to over activation of upstream JNK kinases, which can be rescued through inhibition of Fos but not Jun (Collins et al., 2006). These investigations describe a clear role for upstream JNK kinases in synaptic overgrowth and our work with ASK1 is in keeping with this, appearing to regulate downstream JNK signalling when activated by mitochondrial oxidative stress. Also shown in these investigations are clear context dependencies for Fos, which appears to regulate synaptic growth downstream of both TAK1 and Wnd without the action of Jun. It would be interesting to determine whether neuronal overexpression of ASK1 causes synaptic overgrowth and whether neuronal Jun is required for such overgrowth, as this could help give context dependency to Jun as a possible mediator of mitochondrial oxidative stress in the neuron.

In summary, Jun appears to mediate response to mitochondrial oxidative stress as described by our work with DEM, and previous publications where paraquat is used or when the mitochondria are disrupted (Milton et al., 2011, Vincent, 2013). However, Jun does not have a role when synaptic overgrowth occurs due to putative cytosolic oxidative stress as seen in *spinster* mutants, or when various upstream JNK activators are misregulated (Collins et al., 2006, Milton et al., 2011, West et al., 2015).

6.4 Identifying the binding partners of Fos and Jun during mitochondrial oxidative stress

Our investigation into the context-dependent forms of AP-1 activated under conditions of oxidative stress started with identifying binding partners of Fos and Jun; and how these might change when we induce an oxidative stress burden. It was shown that NTAP-tagging Fos and Jun did not alter function, as the transgenes successfully rescue lethality in null-mutations of *Fos* (*kayak*) or *Jun* (*Jra*) when expressed. We also identified Jun in the tagged-Fos sample, and Fos in the tagged-Jun sample, suggesting the tag does not alter the ability for either to dimerise. This is also evidence that our protocol worked properly, pulling down targets we would expect. Whilst analysing the purified proteins bound to Fos and Jun, we identified several with roles in memory formation and synaptic plasticity. There appears to be a role for Fos and Jun in mediating mammalian memory formation (Abraham et al., 1993, Renier et al., 2016) though it is still not clear what the upstream signals are activating Fos and Jun during the processes of learning and memory. Given the energetic requirement for learning and memory formation via energy producing mitochondrial function, the proteins we identified may highlight how neuronal Fos and Jun mediate learning and memory responses. We suggest that the identified proteins are likely to, at least in part, facilitate the formation of memories in both mammals and *Drosophila*.

It would be very interesting to repeat this experiment but generate cytosolic oxidative stress and determine how the binding partners change and whether this helps explain the context dependant forms of AP-1. The protocol may have to change, in order to reduce the level of contamination. We believe much of the

contaminants come from the fly heads themselves due to them being raised in non-sterile conditions. Such contaminants included keratin, actin and casein, which are frequently found in mass spectrometry. To overcome this we could dissect the brain from the larvae or fly before homogenising. This would be an extremely time consuming task however, so the number of required brains would likely be reduced, and the subsequent purification steps scaled down in order to retain high protein concentration.

As mentioned previously in this chapter, it is possible that the phosphorylation code of Fos and Jun may be different in response to different cellular stresses. It would be extremely useful to identify how Fos and Jun are phosphorylated in both conditions and this can be done via similar methodology, however, this requires a much larger sample, as phosphorylated segments of digested proteins are identified far less frequently following LC-MS. This may help uncover how context and code is conferred on Fos/Fos homodimers and Fos/Jun heterodimers.

6.5 Reducing Punch activity causes synaptic overgrowth

We have shown that haploinsufficient *Punch* mutants exhibit severe synaptic overgrowth and that reducing the activity of Punch in the muscle or synapse produces the same results. This is an exciting discovery as heterozygous mutations in the *GTPCH1* gene, the human orthologue of *Punch*, causes DOPA-responsive dystonia, a severe movement disorder which can predispose the patient to PD later in life (Mencacci et al., 2014). Single nucleotide polymorphisms have also been identified in *Punch*, which contributes to the onset of PD (Nalls et al., 2014). Punch is responsible for the production of BH_4, an essential cofactor in a variety of processes including dopamine synthesis and ROS scavenging (Nakamura et al., 2001). Punch/GTPCH1 is the rate limiting step in BH_4 production and it is believed that BH_4 also acts as an electron donor in the NOS pathway, and in its absence this pathway generates ROS (Scott-Burden, 1995). Naturally, our investigation into how mutations in *Punch* cause synaptic overgrowth began with determining the role of Punch/BH_4 in regulating ROS. We determined that *Punch* mutants were subject to oxidative stress-induced synaptic overgrowth, as following Trolox treatment; we were able to rescue the overgrowth. We also demonstrated that overexpression of

Punch can protect against DEM-induced synaptic overgrowth. This indicates that BH_4 may be a critical regulator of ROS within the neuron, offering neuroprotection to oxidative stress, though a direct determination of BH_4 concentrations in these experiments would solidify this finding. However, it has been found that high levels of BH_4 may in fact be toxic to dopaminergic neurons, which may be mediated by DA. It is believed that BH_4 during the hydrolysis of phenylalanine, forms several intermediates that may generate hydrogen peroxide and the auto-oxidation of BH_4 may generate ROS and cause lipid peroxidation in dopaminergic neurons (Fisher and Kaufman, 1973, Davis et al., 1988). Also, BH_4 facilitates DA oxidation that may aid the formation of reactive protein-bound quinones that induce dopaminergic cell death (Choi et al., 2003). Furthermore, the catabolism of DA may increase hydrogen peroxide production, thereby linking the role of BH_4 in DA synthesis to increased ROS following the DA production and catabolism (Maker et al., 1981). Whilst we have shown BH_4 to protect against oxidative stress in the motor neurons, it may be possible that in dopaminergic neurons, elevated levels of BH_4 are toxic. This suggests that overexpression of Punch in dopaminergic neurons would also cause toxicity or lethality due to the increased synthesis of BH_4, which may be a critical future experiment in determining the context dependency of Punch. We treated *Punch* mutants with L-DOPA, which alleviated the observed synaptic overgrowth. Intriguingly, increasing DA has been shown to increase ROS generation and in *Punch* mutants that are already experiencing oxidative stress, we reduce the overgrowth. This further indicates that DA and BH_4 toxicity may be context dependent.

Treating *SOD1* mutants with L-DOPA did not rescue synaptic overgrowth, suggesting that to some degree, a lack of DA is contributing to the severe overgrowth observed in *Punch* mutants. We tested this further using the DA deficient DOPA decarboxylase (*Ddc*) mutants. A reduction in *Ddc* causes synaptic overgrowth, though not as severe as *Punch* mutants. Whilst this is interesting, we have not ruled out the possibility that *Ddc* mutants are experiencing oxidative stress, and it will be critical to assess this, simply by treating these mutants with Trolox and observing subsequent changes in synaptic growth. It has previously been shown that mutations in *parkin* and subsequent disruption of DA production

causes increases in JNK/AP-1 signalling which may contribute to the synaptic overgrowth we observe (Cha et al., 2005). A later study also revealed that parkin overexpression might suppress the transcription of bsk, the *Drosophila* JNK and the activity of the JNKK, Hemipterous (Hwang et al., 2010). It has also been shown that reductions in *parkin* cause synaptic overgrowth through mitochondrial dysfunction and generating oxidative stress, which may increase JNK signalling further in addition to relieving the suppression of JNK (Vincent et al., 2012). Further testing requires a DA deficient fly line to be investigated that does not result in mitochondrial dysfunction and oxidative stress. Several fly lines would fit these criteria, and they involve the manipulation of Tyrosine Hydroxylase (TH), which is one of the primary enzymes involved in DA synthesis that requires BH_4 as a cofactor. By using either a UAS-TH-RNAi line or the TH mutant, *ple4*, we could disrupt DA synthesis without directly affecting the mitochondria in a mechanism that would reflect a decrease in BH_4 without affecting the ROS scavenging capabilities of the cell. Measuring the synaptic bouton numbers in these flies would help us determine whether there truly is a role for dopamine in synaptic plasticity, and aid in confirming that *Punch* mutants, and potentially patients carrying *GTPCH1* mutations, are indeed subject to the combinatorial effects of oxidative stress and reductions in DA levels. However, a potential confounding factor may arise in these experiments. If DA reduces or restrains neuronal activity within networks of the CNS, then the increased metabolism of the CNS in the absence of DA due to hyperactivity may generate more mitochondrial ROS following increased activity and energy requirements and make these experiments difficult to determine.

Several experiments could help characterise the mutations in *Punch* further. It may be useful to overexpress Punch in a variety of other genetic backgrounds known to cause synaptic overgrowth. Specifically, it would be useful to express Punch in a *Dad* mutant background. We demonstrated that reducing the activity of Dad, an inhibitor of TGF-β signalling, generates synaptic overgrowth. The outcome of expressing Punch in the *Dad* mutant background would help us determine whether TGF-β signalling has a role in oxidative stress induced overgrowth, which could be supported by inhibiting TGF-β signalling in *Punch* mutants. Not only could this help us characterise the *Punch* mutant further, it could highlight the level of input TGF-β

signalling has in synaptic overgrowth that we believe in induced by over activation of JNK/AP-1 signalling.

Another important experiment would be to overexpress Punch in the *SOD1* mutant background. Whilst we demonstrated that Punch could rescue the effects of DEM, this was in a system where the antioxidant defence was fully functional. It would be useful to show that increased Punch/BH_4 could bolster the defence of flies with a debilitated antioxidant system. This would indicate whether Punch could compensate for this loss of antioxidants as well as increase resistance to ROS. Limitations in our studies showing the overexpression of Punch can reduce oxidative stress-induced synaptic overgrowth are that we are yet to show whether this rescue is a result of reducing ROS via increased BH_4 production or increasing the restraint upon AP-1. It is therefore important that we monitor the oxidative stress levels when using expressed Punch to rescue the effects of DEM-treatment or *SOD1* mutant expression. This would help us confirm that Punch/BH_4 restrains AP-1, and determine its role in the oxidative stress response.

To further characterise the *Punch* mutations, it would be ideal to determine whether the synapses are experiencing physiological defects. Because BH_4 is vital in the production of DA and serotonin, it is plausible that in *Punch* mutants there may be issues with neuronal signalling. Increased neuronal signalling is thought to promote synaptic growth, and dopamine has been shown to reduce neuronal firing (Cooper and Neckameyer, 1999, Berke et al., 2013). A reduction in *Punch* may reduce levels of DA and its dampening effects on neuronal networks in the fly, leading to increased neuronal activity and growth promotion leading to larger numbers of synaptic boutons. In this context, synaptic growth may also be mediated by increased ROS generated by the energetic demand made on neuronal mitochondria with increased neuronal activity. It may be useful to measure the excitation junction potentials of *Punch* mutant NMJ's as measures of neuronal activity; this may help explain the severity of the phenotype.

Our studies have mainly focused on the role of Punch/BH_4 in maintaining cellular redox balance and the synthesis of neurotransmitters; however, we have not currently looked at how it relates to NOS signalling. It is known that nitric oxide

(NO) has a role in synaptic plasticity, neuronal transmission and the immune response (Murphy, 2000, Esplugues, 2002). BH_4 is an important cofactor for NOS. With the roles of NO in mind it would be essential to investigate how JNK/AP-1 signalling is affected by NOS signalling. Important data could be obtained by inhibiting NOS signalling in the *Drosophila* larvae, and then analysing the NMJ for AP-1 dependent growth. This could be achieved by treating larvae with L-NAME, a potent NOS inhibitor. This may help us determine whether disruption in NO production is contributing to the synaptic overgrowth observed in *Punch* mutants. It is proposed that a reduction of BH_4 leads to the uncoupling of NOS during its redox reaction converting oxygen to NO, increasing ROS production, and that increasing BH_4 has more impact of the redox status of the cell by recoupling NOS than it does via its ROS scavenging ability (Pierce and LaRocca, 2008).

6.6 *Punch*-induced synaptic overgrowth is mediated by JNK/AP-1 signalling

We identified Punch in our purification of proteins bound to both Fos and Jun in control conditions, but not when inducing oxidative stress by treating with DEM. This suggests that Punch may have a role in regulating neuronal AP-1 activity in response to oxidative stress. We first determined that the *Punch*-mediated overgrowth requires Fos and Jun, which adds weight to our previous findings, that *Punch* mutants are subject to oxidative stress and that their severe synaptic overgrowth is a result of highly over activated JNK/AP-1 signalling. It is proposed that Punch/BH_4 are acting to restrain AP-1 in a redox-regulated manner. Previous studies have shown that both JNK and ASK1 are regulated by redox sensitive mechanisms. JNK is restrained by the binding of GSTp during non-oxidising conditions, and is displaced following oxidative stress allowing JNK to become phosphorylated and activated (Adler et al., 1999a). ASK1 is also restrained during non-oxidising conditions by the actions of reduced Trx1 in the cytosol or Trx2 in the mitochondria, which inhibits its kinase activity. Following oxidative stress from the mitochondria, redox sensitive cysteines of reduced Trx are oxidised, displacing ASK1 allowing for its activation (Saitoh et al., 1998, Zhang et al., 2004). What our data may represent is the uncovering of additional redox-sensitive regulatory

mechanisms that serve to finely tune the activity of JNK signalling in response to oxidative stress, specifically by the restraining action of Punch/BH_4 upon AP-1 during non-oxidising conditions.

It is critical that future work defines whether Punch binds directly to Fos or Jun and that this interaction is fully characterised. An initial proposed experiment is to repeat the pull down and purification of bound proteins, but this time to use Punch as the bait, in the hope we purify Fos and Jun. Also any other proteins identified here may help define how Punch, Fos and Jun regulate response to oxidative stress. This would help confirm that Punch and AP-1 are truly interacting. Also we aim to determine whether Punch binds Fos and Jun directly through immunoprecipitation experiments. So far using purified proteins samples of His-tagged Punch, which we incubate with GST-tagged Jun we have shown a dose-responsive increase in binding of Punch to Jun. However, Punch also seems to bind non-specifically to our GST control in a non-dose responsive manner. We are currently working to refine this experiment, though initial results prove promising.

6.7 Punch may restrain AP-1 signalling

We theorised that Punch, in an inhibitory complex with BH_4 may actually act to restrain Fos and Jun activity during non-stressed conditions. Upon an increase in ROS, BH_4 is oxidised, releasing Punch from the inhibitory complex that is restraining AP-1. Punch is then able to synthesise BH_4 to combat the increase in oxidative stress, and AP-1 is free to activate JNK signalling until the ROS levels are reduced and inhibitory Punch/BH_4 can restrain AP-1 again. We believe Punch is restraining AP-1 activity, because overexpression of Punch rescues synaptic overgrowth observed in *Highwire* mutants, which arises as a result of increased JNK/AP-1 signalling and not oxidative stress. Further work here is needed to measure the levels of Fos/Jun in the motor neuron of *hiw* mutants before and after Punch overexpression. However, our current work does suggests the role of Punch in synaptic plasticity extends beyond maintaining the cellular redox balance, and is likely to be restraining AP-1 activity. This may serve two functions, to rapidly inhibit excess AP-1, but also to preserve and stabilise free AP-1 in the cytosol. AP-1 is susceptible to becoming oxidised; therefore BH_4 may act to initially protect AP-1,

maintaining its DNA binding efficiency (Abate et al., 1990). Upon oxidisation, Punch releases the protected AP-1 to react to increases in ROS, and increases synthesis of neuroprotectant, BH_4.

This model may also incorporate responses to low levels of DA. Though further work is needed, we have shown that DA deficient *Ddc* mutants display overgrown synapses. It is possible that a feedback mechanism exists that increases JNK signalling and AP-1 activation, when DA levels are low. In the *Ddc* mutants, chronic low DA may cause over activation of JNK/AP-1 and subsequent synaptic overgrowth. Activated AP-1 is released from Punch, which may then proceed to induce the synthesis of BH_4, the essential cofactor required by TH for DA synthesis. Whilst this is purely hypothetical it could indicate that the restraint between AP-1 and Punch/BH_4 is mutual.

It has been shown that increased JNK activity contributes to cell death in PD via activation of proapoptotic pathways (Peng and Andersen, 2003). Therefore, a mechanism that appears neuroprotective in our model could rapidly shift to be detrimental if misregulation occurs. Reductions in Punch activity, increases in ROS and possibly decreases in DA synthesis may relieve the restraint between Punch/BH_4 and AP-1, acting to increase JNK signalling, which may cause apoptosis and cell death in dopaminergic neurons (Wang et al., 2004). Our *Punch* mutant data would support this, as we observe severe synaptic overgrowth, which is often associated with dysfunction and disease. Disrupting Fos and Jun activity rescues this dysfunction, which has also been shown by a study using the JNK inhibitor SP600125, which reduces Jun phosphorylation and activity and increases the protection against dopaminergic cell death (Wang et al., 2004). Our work may eventually contribute to the understanding and development of novel strategies for halting the progression of PD, and possibly other neurodegenerative diseases through manipulations of JNK/AP-1 activity.

Much work is required to fully elucidate this system. It is still unclear how AP-1 mediates synaptic plasticity in response to oxidative stress and where Punch/BH4 plays a role. However, we believe that our findings are of great importance, demonstrating what appears to be a critical redox-sensitive regulatory node

between Punch/BH_4, which rapidly act to reduce ROS and subsequently increase ROS scavenging, and JNK signalling, which is activated by ROS and confers cellular protection against ROS.

6.8 Summary

The key results of this investigation are outlined below:

1. Oxidative stress can cause synaptic overgrowth

2. Oxidative stress-induced synaptic overgrowth is mediated by JNK/AP-1 signalling

3. Punch binds to Fos and Jun under normal physiological conditions but dissociates under conditions of oxidative stress

4. Reducing Punch activity causes synaptic overgrowth via oxidative stress and a dopamine deficit

5. Increasing Punch activity elicits neuroprotection against oxidative stress

6. Punch-mediated synaptic overgrowth is facilitated by AP-1

7. Punch overexpression rescues non-oxidative stress-induced synaptic overgrowth and may act to restrain AP-1

Appendix 1: Bouton numbers and MSA

Genotype and conditions	Raw bouton Nº ± SEM	MSA±SEM (μm^2)	Normalised Bouton Nº	N
Figure 3.1. DEM increases bouton number without affecting muscle size				
WT 0mM DEM	78.389 ± 2.776	74892 ± 1956	NA	18
WT 1mM DEM	84.125 ± 4.309	81306 ± 3085	78.924 ± 4.831	16
WT 3mM DEM	90.533 ± 4.552	84375 ± 3014	80.360 ± 2.607	15
WT 10mM DEM	114.055 ± 3.812	70958 ± 2744	123.923 ± 6.898	18
WT 30mM DEM	119.188 ± 5.666	74900 ± 3597	122.724 ± 7.566	16
Figure 3.3. Trolox treatment rescues DEM-induced increases in bouton number				
WT Control	79.5 ± 2.387	79675 ± 2596	NA	17
WT 10mM Trolox	79.875 ± 3.927	86712 ± 2381	73.684 ± 3.551	16
WT 10mM DEM	128.063 ± 6.242	84310 ± 3997	125.779 ± 9.456	16
WT 10mM DEM + 10mM Trolox	91.188 ± 5.595	81954 ± 3798	89.315 ± 5.034	16
Figure 3.5. *SOD1* mutants exhibit synaptic overgrowth via an increase in oxidative stress				
WT Control	78.438 ± 3.679	76008 ± 3109	NA	16
WT 10mM DEM	117.769 ± 4.756	76005 ± 2316	118.741 ± 5.462	13
$SOD1^{n1}/SOD1^{n64}$ Control	123.313 ± 5.5	79215 ± 2052	120.225 ± 7.162	16
$SOD1^{n1}/SOD1^{n64}$ 10mM DEM	119.688 ± 4.25	73664 ± 1625	124.761 ± 6.027	16
Figure 3.6. Loss of *puckered* causes synaptic overgrowth by relieving JNK inhibition				
WT control	76.936 ± 2.254	85425 ± 1982	NA	16
WT 10mM DEM	114.933 ± 3.985	73719 ± 2316	120.945 ± 6.771	15
puc^{E69}/+ Control	119.625 ± 5.570	83700 ± 3788	126.559 ± 9.060	16
puc^{E69}/+ 10mM DEM	134.375 ± 7.253	82956 ± 2345	138.746 ± 6.854	16
Figure 3.7. Loss of *Dad* causes synaptic overgrowth by relieving TGF-β inhibition				
WT control	76.936 ± 2.254	85425 ± 1982	NA	16
WT 10mM DEM	114.933 ± 3.985	73719 ± 2316	120.945 ± 6.771	15
Dad^{lacz}/+ Control	151.625 ± 5.694	80936 ± 1574	160.506 ± 6.074	16
Dad^{lacz}/+ 10mM DEM	155.375 ± 8.249	87269 ± 2005	152.193 ± 7.828	16
Figure 3.8. Trolox treatment rescues synaptic overgrowth via a reduction in ROS, not by decreasing JNK activity				
WT control	79.75 ± 2.387	79675 ± 2596	NA	16
WT 10mM Trolox	79.875 ± 3.927	86712 ± 2381	73.684 ± 3.55	16
$SOD1^{n1}/SOD1^{n64}$ control	107.857 ± 6.181	78697 ± 5381	111.738 ± 4.945	14
$SOD1^{n1}/SOD1^{n64}$ 10mM Trolox	82.125 ± 2.908	79917 ± 2625	83.206 ± 4.003	16
puc^{E69}/+ control	119.625 ± 5.569	83700 ± 3787	118.041 ± 8.45	16
puc^{E69}/+ 10mM Trolox	116.813 ± 4.207	84234 ± 2013	111.808 ± 5.414	16

Figure 3.9. Permissive JNK signalling is required for oxidative stress-induced synaptic overgrowth

WT Control	66.848 ± 2.222	60432 ± 1739	NA	46
WT 10mM DEM	91.8 ± 3.110	54800 ± 1579	104.094 ± 4.682	35
SpinGAL4>UAS-*fos*^{DN} Control	77.481 ± 2.752	81059 ± 2439	59.719 ± 3.356	27
SpinGAL4>UAS-*fos*^{DN} 10mM DEM	73.8 ± 2.686	84807 ± 2078	53.553 ± 2.425	30
SpinGAL4>UAS-*jun*^{DN} Control	90.192 ± 3.710	89441 ± 2979	62.303 ± 3.003	26
SpinGAL4>UAS-*jun*^{DN} 10mM DEM	97.267 ± 3.946	85150 ± 2337	70.707 ± 3.829	30
SpinGAL4>UAS-*ask1*^{DN} Control	88.2 ± 5.238	79963 ± 2859	69.277 ± 5.249	25
SpinGAL4>UAS-*ask1*^{DN} 10mM DEM	91.714 ± 4.420	79967 ± 2236	70.731 ±3.818	28

Figure 5.1. Heterozygous *Punch* mutants exhibit synaptic overgrowth

WT	78.176 ± 2.606	82162 ± 3434	NA	34
Punch^{EY02616A}/*CS*	144.136 ± 6.812	77676 ± 2415	152.790 ± 6.516	22
Punch^{EY02616A}/*w*^{1118}	136.182 ± 6.319	77692 ± 2098	144.853 ± 6.744	22
Punch^{r1}/*CS*	139.684 ± 5.554	81548 ± 1669	141.867 ± 6.343	19
Punch^{r1}/*w*^{1118}	123 ± 4.975	70168 ± 1852	144.501 ± 5.331	14
Punch^{EY02616A}/*Punch*^{r1}	137.053 ± 6.803	78726 ± 2233	145.151 ± 7.834	19

Figure 5.3. Neuronal and muscle expression of Punch-RNAi causes synaptic overgrowth

WT	78.176 ± 2.606	82162 ± 3434	NA	34
SpinGAL4>UAS-Punch-RNAI	135.938 ± 6.3	82332 ± 2158	137.283 ± 7.922	16
elavGAL4>UAS-Punch-RNAI	131.75 ± 6.281	75077 ± 3423	146.683 ± 8.570	12
MHCGAL4>UAS-Punch-RNAI	106 ± 5.834	68126 ± 2681	129.974 ± 8.042	15

Figure 5.4. Flies deficient in the genomic region encoding the *Punch* gene display synaptic overgrowth

WT	83.125 ± 3.784	88647 ± 3263	NA	16
Punch^{EY02616A}/+	140.813 ± 6.280	80153 ± 3158	158.173 ± 8.277	16
Punch^{r1}/+	121.875 ± 6.150	76677 ± 2561	142.211 ± 7.730	16
Df(2R)Exel6072/+	129.25 ± 4.850	81024 ± 2562	143.163 ± 6.240	16
Df(2R)ED3791/+	116.8 ± 5.269	70878 ± 1428	145.570 ± 4.620	15

Figure 5.5. *Punch*-deficient flies combined with *Punch* mutants also display synaptic overgrowth but no further severity is observed

WT	83.125 ± 3.784	88647 ± 3263	NA	16
Df(2R)Exel6072/Punch^{EY02616A}	101.714 ± 5.885	74172 ± 3676	123.094 ± 7.008	14
Df(2R)Exel6072/Punch^{r1}	131 ± 4.6	84275 ± 2386	138.954 ± 5.707	14
Df(2R)ED3791/Punch^{EY02616A}	114.286 ± 4.511	67920 ± 1757	149.806 ± 6.263	14
Df(2R)ED3791/Punch^{r1}	130.462 ± 3.944	79469 ± 2500	148.830 ± 9.273	13

Figure 5.6. Synaptic overgrowth caused by reduced Punch activity is not exacerbated by DEM treatment

WT Control	78.176 ± 2.606	82162 ± 3434	NA	34
WT 10mM DEM	119.539 ± 4.245	85479 ± 1623	116.170 ± 4.781	26
Punch^{EY02616A}/+ Control	144.136 ± 6.812	77676 ± 2415	152.790 ± 6.516	22
Punch^{EY02616A}/+ 10mM DEM	177.926 ± 5.071	91595 ± 2505	162.198 ± 6.108	27
Punch^{r1}/+ Control	139.684 ± 5.554	81548 ± 1669	141.867 ± 6.343	19
Punch^{r1}/+ 10mM DEM	133.067 ± 7.397	72574 ± 2499	152.053 ± 8.616	15
SpinGAL4>UAS-Punch-RNAi	135.938 ± 6.3	82332 ± 2158	137.283 ± 7.922	16
SpinGAL4>UAS-Punch-RNAi 10mM DEM	136.15 ± 4.725	82316 ± 2428	137.744 ± 5.801	20
elavGAL4>UAS-Punch-RNAi	131.75 ± 6.281	75077 ± 3423	146.683 ± 8.570	12
elavGAL4>UAS-Punch-RNAi 10mM DEM	141.875 ± 6.381	78649 ± 1981	147.866 ± 6.030	16
MHCGAL4>UAS-Punch-RNAi	106 ± 5.834	68126 ± 2681	129.974 ± 8.042	15
MHCGAL4>UAS-Punch-RNAi 10mM DEM	125.375 ± 4.915	82934 ± 2425	125.386 ± 5.324	16

Figure 5.7. Trolox treatment rescues the increased bouton number observed in heterozygous *Punch* mutants

WT Control	79.5 ± 2.387	79675 ± 2596	NA	17
WT 10mM Trolox	79.875 ± 3.927	86712 ± 2381	73.684 ± 3.551	16
Punch^{EY02616A}/+ Control	135.938 ± 5.568	76008 ± 2424	143.438 ± 5.379	16
Punch^{EY02616A}/+ 10mM Trolox	99.563 ± 5.675	85354 ± 2020	93.335 ± 5.301	16
Punch^{r1}/+ Control	121.875 ± 6.149	76677 ± 2561	127.819 ± 6.948	16
Punch^{r1}/+ 10mM Trolox	103.467 ± 5.389	86201 ± 2769	96.303 ± 5.371	15

Figure 5.9. L-DOPA treatment rescues the synaptic overgrowth observed in heterozygous *Punch* mutants

WT Control	79.5 ± 2.387	79675 ± 2596	NA	17
WT L-DOPA	99.25 ± 4.823	92434 ± 2845	85.684 ± 3.614	16
Punch^{EY02616A}/+ Control	135.938 ± 5.568	76008 ± 2424	143.438 ± 5.379	16
Punch^{EY02616A}/+ L-DOPA	103.75 ± 7.183	80486 ± 2260	103.174 ± 7.273	16
Punch^{r1}/+ Control	121.875 ± 6.149	76677 ± 2561	127.819 ± 6.948	16
Punch^{r1}/+ L-DOPA	99.938 ± 5.75	85415 ± 2867	95.520 ± 6.823	16

Figure 5.10. L-DOPA treatment rescues the synaptic overgrowth observed in heterozygous *dopa decarboxylase* mutants

WT Control	79.5 ± 2.387	79675 ± 2596	NA	17
WT L-DOPA	99.25 ± 4.823	92434 ± 2845	85.684 ± 3.614	16
Ddc^{DE1}/+ Control	122.4 ± 6.037	85837 ± 3604	117.457 ± 8.588	15
Ddc^{DE1}/+ L-DOPA	95.25 ± 4.915	93066 ± 2374	81.524 ± 3.485	16
SOD1^{n1}/*SOD1*^{n64} Control	107.857 ± 6.181	78697 ± 5381	111.738 ± 4.945	14
SOD1^{n1}/*SOD1*^{n64} L-DOPA	104.5 ± 4.218	71721 ± 1780	117.699 ± 6.559	16

Figure 5.11. Reducing Jun activity rescues the synaptic overgrowth observed in heterozygous *Punch* mutants

WT	78.389 ± 2.776	74892 ± 1956	NA	19
$Punch^{EY02616A}$/+	144.136 ± 6.812	77676 ± 2415	152.790 ± 6.516	22
jra^{lA109}/+	81 ± 4.05	74095 ± 1970	83.115 ± 5.585	16
$Punch^{EY02616A}/jra^{lA109}$	84.778 ± 1.909	80369 ± 3430	82.124 ± 4.188	18
$Punch^{EY02616A}$/+;SpinGAL 4>UAS-jun^{DN}	88.125 ± 2.636	85085 ± 2826	78.485 ± 3.239	16

Figure 5.12. Reducing Fos activity rescues the synaptic overgrowth observed in heterozygous *Punch* mutants

WT	78.389 ± 2.776	74892 ± 1956	NA	19
$Punch^{EY02616A}$/+	144.136 ± 6.812	77676 ± 2415	152.790 ± 6.516	22
kay^{1}/+	89.938 ± 3.219	91915 ± 1847	73.726 ± 3.352	16
$Punch^{EY02616A}/kay^{1}$	88.625 ± 4.0793	70634 ± 2762	96.753 ± 5.069	16
$Punch^{EY02616A}$/+; SpinGAL4>UAS-fos^{DN}	72.688 ± 2.761	73970 ± 1735	74.891 ± 3.973	16

Figure 5.13. Punch overexpression rescues the synaptic overgrowth observed in heterozygous *Punch* mutants

WT	82.143 ± 3.28	76363 ± 3251	NA	14
$Punch^{EY02616A}$/+ SpinGAL4>UAS-PunchA-WT;	136.6 ± 3.433	77163 ± 1584	136.22 ± 4.771	15
$Punch^{EY02616A}$ SpinGAL4>UAS-PunchA-S37E;	76.733 ± 3.947	73460 ± 2766	80.7 ± 4.616	15
$Punch^{EY02616A}$	83 ± 3.559	86030 ± 3040	74.589 ± 3.569	16

Figure 5.15. Punch overexpression rescues DEM-induced synaptic overgrowth

WT	82.143 ± 3.28	76363 ± 3251	NA	14
WT 10mM DEM	117.429 ± 4.704	80280 ± 2873	113.887 ± 6.966	14
SpinGAL4>UAS-PunchA-WT Control	68.786 ± 4.897	76497 ± 2781	69.225 ± 4.973	14
SpinGAL4>UAS-PunchA-WT 10mM DEM	84.067 ± 3.445	79483 ± 2265	80.857 ± 2.632	15
SpinGAL4>UAS-PunchA-S37E Control	78.4 ± 3.810	80751 ± 4035	76.495 ± 4.886	16
SpinGAL4>UAS-PunchA-S37E 10mM DEM	67.933 ± 3.874	75885 ± 3118	68.600 ± 3.287	15

Figure 5.17. Punch overexpression rescues the synaptic overgrowth observed in heterozygous *Punch* mutants when treated with DEM

WT	82.143 ± 3.28	76363 ± 3251	NA	14
WT 10mM DEM	117.429 ± 4.704	80280 ± 2873	113.887 ± 6.966	14
$Punch^{EY02616A}$/+ 10mM DEM	134.133 ± 5.754	78262 ± 3324	135.217 ± 9.417	15
SpinGAL4>UAS-PunchA-WT; $Punch^{EY02616A}$ 10mM DEM	100.944 ± 4.123	75477 ± 3453	102.181 ± 4.100	18
SpinGAL4>UAS-PunchA-S37E;	93.813 ± 4.267	80372 ± 1691	89.378 ± 3.922	16

Punch^{EY02616A} 10mM DEM				

Figure 5.19. Pan-neuronal overexpression of Punch rescues the DEM- and *Punch* mutant-induced synaptic overgrowth

WT	76.375 ± 3.696	83660 ± 2394	NA	16
nSybGAL4>UAS-Punch	77.187 ± 3.312	83489 ± 3462	79.252 ± 4.540	16
WT 10mM DEM	128.063±6.242	84310±3997	132.07±9.929	16
nSybGAL4>UAS-Punch 10mM DEM	78.4 ± 4.769	80648 ± 3475	82.559 ± 5.429	15
Punch^{EY02616A}/+	135.938±5.568	76008±2424	150.612±5.648	16
nSybGAL4>UAS-Punch; *Punch*^{EY02616A}	91 ± 6.272	81820 ± 1914	93.657 ± 7.359	15

Figure 5.20. Pan-neuronal overexpression of Punch rescues the synaptic overgrowth observed in *highwire* mutants

WT	76.375 ± 3.696	83660 ± 2394	NA	16
hiw^{ND9}/Y	138.25 ± 5.379	85062 ± 3107	137.712 ± 5.862	16
nSybGAL4>UAS-Punch; *hiw*^{ND9}/Y	99.467 ± 4.232	89174 ± 2063	93.426 ± 3.713	15

Appendix 2:Branch numbers and MSA

Genotype and conditions	Raw Branch Nº ± SEM	MSA±SEM (μm²)	Normalised Branch Nº	N
Figure 3.2. DEM increases NMJ branch number and length, causing synaptic overgrowth				
WT 0mM DEM	9.25 ± 1.082	74892 ± 1956	NA	8
WT 1mM DEM	12 ± 0.866	81306 ± 3085	10.99 ± 0.776	9
WT 3mM DEM	12.1 ± 1.197	84375 ± 3014	11.369 ± 1.148	10
WT 10mM DEM	15 ± 1.011	70958 ± 2744	17.13 ± 1.320	10
WT 30mM DEM	16.7 ± 1.667	74900 ± 3597	16.864 ± 1.375	10
Figure 3.4 Trolox treatment rescues DEM-induced increases in branch number and NMJ length				
WT Control	8.7 ± 0.512	79675 ± 2596	NA	10
WT 10mM Trolox	9.3 ± 0.857	86712 ± 2381	8.311 ± 0.691	10
WT 10mM DEM	12 ± 0.897	84310 ± 3997	11.910 ± 1.026	9
WT 10mM DEM + 10mM Trolox	7.2 ± 0.463	81954 ± 3798	7.177 ± 0.559	9
Figure 5.2. Heterozygous *Punch* mutants exhibit increased NMJ length and branching				
WT	9 ± 0.942	82162 ± 3434	NA	10
$Punch^{EY02616A}/CS$	16.455 ± 1.575	77676 ± 2415	18.285 ± 1.848	11
$Punch^{EY02616A}/w^{1118}$	15.4 ± 1.147	77692 ± 2098	16.867 ± 1.310	10
$Punch^{r1}/CS$	19.2 ± 1.162	81548 ± 1669	19.216 ± 1.017	10
$Punch^{r1}/w^{1118}$	14.444 ± 1.237	70168 ± 1852	17.013 ± 1.248	9
Figure 5.8. Trolox treatment rescues increased branch number observed in heterozygous *Punch* mutants				
WT Control	8.7 ± 0.512	79675 ± 2596	NA	10
WT 10mM Trolox	9.3 ± 0.857	86712 ± 2381	8.311 ± 0.691	10
$Punch^{EY02616A}$/+ Control	12.8 ± 1.052	76008 ± 2424	13.315 ± 0.878	10
$Punch^{EY02616A}$/+ 10mM Trolox	9 ± 1.047	85354 ± 2020	8.441 ± 0.831	10
$Punch^{r1}$/+ Control	12.4 ± 1.035	76677 ± 2561	13.195 ± 1.156	10
$Punch^{r1}$/+ 10mM Trolox	9.1 ± 0.852	86201 ± 2769	8.833 ± 1.0451	10
Figure 5.14. Overexpression of PunchA-S37E significantly reduces branch number and length in heterozygous *Punch* mutants				
WT	9 ± 0.719	76363 ± 3251	NA	14
$Punch^{EY02616A}$/+	14 ± 0.730	77163 ± 1584	14.210 ± 0.795	10
SpinGAL4>UAS-PunchA-WT; $Punch^{EY02616A}$	9.1 ± 0.526	73460 ± 2766	9.638 ± 0.624	10
SpinGAL4>UAS-PunchA-S37E; $Punch^{EY02616A}$	9.1 ± 0.547	86030 ± 3040	8.395 ± 0.576	10

Figure 5.16. Punch overexpression rescues DEM-induced increases in branch number

WT	9 ± 0.719	76363 ± 3251	NA	14
WT 10mM DEM	13.7 ± 0.955	80280 ± 2873	13.111 ± 1.116	10
SpinGAL4>UAS-PunchA-WT Control	7.5 ± 0.671	76497 ± 2781	7.532 ± 0.571	10
SpinGAL4>UAS-PunchA-WT 10mM DEM	8.6 ± 0.777	79483 ± 2265	8.379 ± 0.649	10
SpinGAL4>UAS-PunchA-S37E Control	9 ± 0.696	80751 ± 4035	8.623 ± 0.638	10
SpinGAL4>UAS-PunchA-S37E 10mM DEM	7.8 ± 0.867	75885 ± 3118	8.103 ± 0.775	10

Figure 5.18. Overexpression of Punch restricts *Punch*- and DEM-induced increases in branch number and NMJ length

WT	9 ± 0.719	76363 ± 3251	NA	14
WT 10mM DEM	13.7 ± 0.955	80280 ± 2873	13.111 ± 1.116	10
$Punch^{EY02616A}$/+ 10mM DEM	12.9 ± 1.233	78262 ± 3324	12.897 ± 1.436	10
SpinGAL4>UAS-PunchA-WT; $Punch^{EY02616A}$ 10mM DEM	9.3 ± 0.873	75477 ± 3453	9.003 ± 0.693	10
SpinGAL4>UAS-PunchA-S37E; $Punch^{EY02616A}$ 10mM DEM	10.5 ± 0.833	80372 ± 1691	9.746 ± 0.751	10

Figure 5.21. Pan-neuronal overexpression of Punch significantly reduces branch number and length in *highwire* mutants

WT	8.8 ± 0.784	83660 ± 2394	8.849 ± 0.899	10
hiw^{ND9}/Y	13.9 ± 0.924	85062 ± 3107	13.283 ± 0.803	10
nSybGAL4>UAS-Punch; hiw^{ND9}/Y	8.6 ± 0.718	89174 ± 2063	8.121 ± 0.718	10

Appendix 3: NMJ length and MSA

Genotype and conditions	Raw NMJ length (µm) ± SEM	MSA ± SEM (µm²)	Normalised NMJ Length (µm)	N
Figure 3.2. DEM increases NMJ branch number and length, causing synaptic overgrowth				
WT 0mM DEM	373 ± 37.829	74892 ± 1956	NA	8
WT 1mM DEM	442 ± 25.018	81306 ± 3085	402.63 ± 21.205	9
WT 3mM DEM	431 ± 25.399	84375 ± 3014	402.60 ± 21.536	10
WT 10mM DEM	432.7 ± 17.305	70958 ± 2744	496.07 ± 33.068	10
WT 30mM DEM	505.7 ± 37.199	74900 ± 3597	511.32 ± 25.513	10
Figure 3.4 Trolox treatment rescues DEM-induced increases in branch number and NMJ length				
WT Control	399.9 ± 25.531	79675 ± 2596	NA	10
WT 10mM Trolox	454.4 ± 32.243	86712 ± 2381	406.142 ± 24.812	10
WT 10mM DEM	527.111 ± 42.941	84310 ± 3997	515.416 ± 32.634	9
WT 10mM DEM + 10mM Trolox	383.888 ± 36.798	81954 ± 3798	372.527 ±26.226	9
Figure 5.2. Heterozygous *Punch* mutants exhibit increased NMJ length and branching				
WT	378.92 ± 28.768	82162 ± 3434	NA	10
$Punch^{EY02616A}/CS$	542.636 ± 26.457	77676 ± 2415	598.294 ± 33.944	11
$Punch^{EY02616A}/w^{1118}$	465.2 ± 26.937	77692 ± 2098	505.374 ± 20.262	10
$Punch^{r1}/CS$	617.8 ± 35.058	81548 ± 1669	615.729 ± 24.836	10
$Punch^{r1}/w^{1118}$	401.222 ± 24.520	70168 ± 1852	471.556 ± 19.613	9
Figure 5.8. Trolox treatment rescues increased branch number observed in heterozygous *Punch* mutants				
WT Control	399.9 ± 25.531	79675 ± 2596	NA	10
WT 10mM Trolox	454.4 ± 32.243	86712 ± 2381	406.142 ± 24.812	10
$Punch^{EY02616A}$/+ Control	494.9 ± 32.897	76008 ± 2424	516.193 ± 26.493	10
$Punch^{EY02616A}$/+ 10mM Trolox	449.7 ± 38.664	85354 ± 2020	424.765 ± 36.029	10
$Punch^{r1}$/+ Control	460.8 ± 24.848	76677 ± 2561	491.651 ± 30.263	10
$Punch^{r1}$/+ 10mM Trolox	506 ± 30.242	86201 ± 2769	487.454 ± 31.920	10
Figure 5.14. Overexpression of PunchA-S37E significantly reduces branch number and length in heterozygous *Punch* mutants				
WT	404.429 ± 25.817	76363 ± 3251	NA	14
$Punch^{EY02616A}$/+	516 ± 16.508	77163 ± 1584	524.760 ± 23.068	10
SpinGAL4>UAS-PunchA-WT; $Punch^{EY02616A}$	407.5 ± 31.442	73460 ± 2766	424.793 ± 23.150	10
SpinGAL4>UAS-PunchA-S37E; $Punch^{EY02616A}$	402.6 ± 17.898	86030 ± 3040	370.84 ± 19.1	10
Figure 5.16. Punch overexpression rescues DEM-induced increases in branch number				
WT	404.429 ± 25.817	76363 ± 3251	NA	14

WT 10mM DEM	537.9 ± 17.944	80280 ± 2873	514.870 ± 34.625	10
SpinGAL4>UAS-PunchA-WT Control	317.5 ± 23.615	76497 ± 2781	319.224 ± 21.701	10
SpinGAL4>UAS-PunchA-WT 10mM DEM	416.7 ± 30.880	79483 ± 2265	407.197 ± 29.012	10
SpinGAL4>UAS-PunchA-S37E Control	401.2 ± 30.152	80751 ± 4035	383.989 ± 32.088	10
SpinGAL4>UAS-PunchA-S37E 10mM DEM	347.5 ± 20.769	75885 ± 3118	364.840 ± 28.268	10

Figure 5.18. Overexpression of Punch restricts *Punch*- and DEM-induced increases in branch number and NMJ length

WT	404.429 ± 25.817	76363 ± 3251	NA	14
WT 10mM DEM	537.9 ± 17.944	80280 ± 2873	514.870 ± 34.625	10
$Punch^{EY02616A}$/+ 10mM DEM	498.4 ± 30.278	78262 ± 3324	492.980 ± 34.885	10
SpinGAL4>UAS-PunchA-WT; $Punch^{EY02616A}$ 10mM DEM	405.9 ± 28.534	75477 ± 3453	394.841 ± 17.039	10
SpinGAL4>UAS-PunchA-S37E; $Punch^{EY02616A}$ 10mM DEM	377.8 ± 22.125	80372 ± 1691	359.278 ± 21.234	10

Figure 5.21. Pan-neuronal overexpression of Punch significantly reduces branch number and length in *highwire* mutants

WT	375.8 ± 20.024	83660 ± 2394	376.350 ± 26.426	10
hiw^{ND9}/Y	558.4 ± 39.417	85062 ± 3107	528.959 ± 28.665	10
nSybGAL4>UAS-Punch; hiw^{ND9}/Y	436.8 ± 22.087	89174 ± 2063	410.702 ± 19.505	10

Appendix 4: LC-MS/MS pilot run data

LC-MS/MS Pilot Run: Proteins bound to NTAP-empty vector in Control conditions

Accession	Score	Mass	Nº of sig. matches	Nº of sig. sequences	emPAI	Molar%	Description
A4V3J5	74	39014	4	3	0.28	26.42	Heterogeneous nuclear ribonucleoprotein at 98DE, isoform C OS=*Drosophila* melanogaster GN=Hrb98DE PE=4 SV=1
Q7KRU0	40	42913	3	1	0.08	7.55	CG2246, isoform C OS=*Drosophila* melanogaster GN=CG2246 PE=4 SV=1
A4V3Q6	40	51030	1	1	0.06	5.66	Elongation factor 1-alpha OS=*Drosophila* melanogaster GN=Ef1alpha100E PE=3 SV=1
E1JHA4	31	44970	1	1	0.07	6.60	Heterogeneous nuclear ribonucleoprotein at 27C, isoform D OS=*Drosophila* melanogaster GN=Hrb27C PE=4 SV=1
Q7JW61	28	110916	1	1	0.03	2.83	Ubiquitin carboxyl-terminal hydrolase OS=*Drosophila* melanogaster GN=CG8494 PE=2 SV=1
Q24185	27	77187	1	1	0.04	3.77	Protein hook OS=*Drosophila* melanogaster GN=hk PE=1 SV=2
E1JGX3	24	236244	1	1	0.01	0.94	Nipped-B, isoform G OS=*Drosophila* melanogaster GN=Nipped-B PE=4 SV=1
Q1W9P9	23	194724	1	1	0.02	1.89	Echinus splice form 3 OS=*Drosophila* melanogaster GN=ec PE=2 SV=1
H9XVM5	18	152135	1	1	0.02	1.89	CG31998, isoform B OS=*Drosophila* melanogaster GN=CG31998 PE=4 SV=1
Q9W3D2	18	185652	2	1	0.02	1.89	Calmodulin-binding protein related to a Rab3 GDP/GTP exchange protein, isoform B OS=*Drosophila* melanogaster GN=Crag PE=2 SV=3
Q7KMG7	17	28736	2	1	0.12	11.32	Ercc1 OS=*Drosophila* melanogaster GN=Ercc1 PE=4 SV=1
A8DYZ4	17	62630	1	1	0.05	4.72	CG34162 OS=*Drosophila* melanogaster GN=CG34162 PE=4 SV=2
P92177	15	29951	1	1	0.11	10.38	14-3-3 protein epsilon OS=*Drosophila* melanogaster GN=14-3-3epsilon PE=1 SV=2

Q9W3W8	14	21922	1	1	0.15	14.15	60S ribosomal protein L17 OS=*Drosophila* melanogaster GN=RpL17 PE=1 SV=1

LC-MS/MS Pilot Run: Proteins bound to NTAP-empty vector in DEM-treated conditions

Accession	Score	Mass	Nº of sig. matches	Nº of sig. sequences	emPAI	Molar%	Description
A4V3J5	89	39014	5	3	0.28	21.54	Heterogeneous nuclear ribonucleoprotein at 98DE, isoform C OS=*Drosophila* melanogaster GN=Hrb98DE PE=4 SV=1
E1JHA4	54	44970	1	1	0.07	5.38	Heterogeneous nuclear ribonucleoprotein at 27C, isoform D OS=*Drosophila* melanogaster GN=Hrb27C PE=4 SV=1
P35381	53	59612	2	2	0.11	8.46	ATP synthase subunit alpha, mitochondrial OS=*Drosophila* melanogaster GN=blw PE=1 SV=2
Q24439	51	22465	1	1	0.15	11.54	ATP synthase subunit O, mitochondrial OS=*Drosophila* melanogaster GN=Oscp PE=2 SV=2
Q0KHZ6	43	27258	1	1	0.12	9.23	CG7834, isoform A OS=*Drosophila* melanogaster GN=CG7834 PE=4 SV=1
Q7KRU0	33	42913	2	1	0.08	6.15	CG2246, isoform C OS=*Drosophila* melanogaster GN=CG2246 PE=4 SV=1
Q1W9P9	28	194724	3	1	0.02	1.54	Echinus splice form 3 OS=*Drosophila* melanogaster GN=ec PE=2 SV=1
Q7KMG7	25	28736	1	1	0.12	9.23	Ercc1 OS=*Drosophila* melanogaster GN=Ercc1 PE=4 SV=1
M9ND86	23	104102	1	1	0.03	2.31	Spellchecker1, isoform D OS=*Drosophila* melanogaster GN=spel1 PE=3 SV=1
A8JNP1	20	40126	1	1	0.08	6.15	Arginine kinase, isoform G OS=*Drosophila* melanogaster GN=Argk PE=3 SV=2
Q9VUC2	17	196543	1	1	0.02	1.54	Bluestreak OS=*Drosophila* melanogaster GN=blue PE=4 SV=1
Q7YU67	17	124911	1	1	0.03	2.31	RE68041p OS=*Drosophila* melanogaster GN=Sema-5c PE=2 SV=1
Q8IRY5	14	40740	1	1	0.08	6.15	CG32815 OS=*Drosophila* melanogaster GN=CG32815 PE=4 SV=2

A1ZBB1	14	37132	1	1	0.09	6.92	Galectin OS=*Drosophila* melanogaster GN=CG5335-RA PE=2 SV=1
Q9VVG0	14	201330	1	1	0.02	1.54	Cadherin 74A, isoform A OS=*Drosophila* melanogaster GN=Cad74A PE=4 SV=1

LC-MS/MS Pilot Run: Proteins bound to NTAP-Fos in Control conditions

Accession	Score	Mass	Nº of sig. matches	Nº of sig. sequences	emPAI	Molar %	Description
E1JGP0	74	40574	3	3	0.26	15.20	Actin 57B, isoform C OS=*Drosophila* melanogaster GN=Act57B PE=2 SV=1
E1JIK0	43	39533	3	3	0.27	15.79	Heterogeneous nuclear ribonucleoprotein at 87F, isoform C OS=*Drosophila* melanogaster GN=Hrb87F PE=2 SV=1
Q9VBX0	31	92441	1	1	0.04	2.34	Band4.1 inhibitor LRP interactor, isoform B OS=*Drosophila* melanogaster GN=Bili PE=2 SV=4
Q9V3P0	30	21952	1	1	0.15	8.77	Peroxiredoxin 1 OS=*Drosophila* melanogaster GN=Jafrac1 PE=1 SV=1
A1ZA58	24	64366	1	1	0.05	2.92	CG33464 OS=*Drosophila* melanogaster GN=sli PE=4 SV=2
Q9W0D3	23	221067	1	1	0.01	0.58	CG13917, isoform A OS=*Drosophila* melanogaster GN=CG13917 PE=2 SV=1
E2QD61	21	195649	1	1	0.02	1.17	CG34384, isoform B OS=*Drosophila* melanogaster GN=CG14462 PE=4 SV=1
Q8I8V0-2	20	48856	1	1	0.07	4.09	Isoform A of Transcriptional adapter 2B OS=*Drosophila* melanogaster GN=Ada2b
Q9VFE0	20	24433	2	1	0.14	8.19	AT11516p OS=*Drosophila* melanogaster GN=RpL10Aa PE=2 SV=1
M9MRK1	19	126045	1	1	0.03	1.75	Phosphodiesterase 11, isoform E OS=*Drosophila* melanogaster GN=Pde11 PE=4 SV=1
Q7K540	19	29422	1	1	0.11	6.43	GH14032p OS=*Drosophila* melanogaster GN=yuri PE=2 SV=1
Q9W309	18	17778	1	1	0.19	11.11	CG9686 OS=*Drosophila* melanogaster GN=CG9686 PE=2 SV=1
P19107	17	45342	1	1	0.07	4.09	Phosrestin-1 OS=*Drosophila* melanogaster GN=Arr2 PE=1 SV=2

Q7KUW4	17	45872	2	1	0.07	4.09	CG7206, isoform B OS=*Drosophila* melanogaster GN=CG7206-RB PE=2 SV=1
Q8MLW8	16	55163	1	1	0.06	3.51	Cht12 OS=*Drosophila* melanogaster GN=Cht12 PE=3 SV=1
Q9VXQ7	16	21383	1	1	0.16	9.36	CG8206 OS=*Drosophila* melanogaster GN=CG8206 PE=2 SV=1
Q7KU92	15	449937	1	1	0.01	0.58	Ankyrin 2, isoform L OS=*Drosophila* melanogaster GN=Ank2 PE=4 SV=2

LC-MS/MS Pilot Run: Proteins bound to NTAP-Fos in DEM-treated conditions

Accession	Score	Mass	Nº of sig. matches	Nº of sig. sequences	emPAI	Molar %	Description
P19107	49	45342	3	3	0.24	20.51	Phosrestin-1 OS=*Drosophila* melanogaster GN=Arr2 PE=1 SV=2
P35381	48	59612	2	2	0.11	9.40	ATP synthase subunit alpha, mitochondrial OS=*Drosophila* melanogaster GN=blw PE=1 SV=2
B7YZP9	42	55345	2	2	0.12	10.26	Muscle LIM protein at 60A, isoform B OS=*Drosophila* melanogaster GN=Mlp60A PE=4 SV=1
B7Z098	39	70654	1	1	0.05	4.27	CG7414, isoform D OS=*Drosophila* melanogaster GN=CG7414 PE=4 SV=2
O62619	34	57917	1	1	0.06	5.13	Pyruvate kinase OS=*Drosophila* melanogaster GN=PyK PE=2 SV=2
Q9VJB0	25	25461	2	1	0.13	11.11	Elfless, isoform B OS=*Drosophila* melanogaster GN=elfless PE=2 SV=2
E1JJN9	24	258571	1	1	0.01	0.85	Set2, isoform B OS=*Drosophila* melanogaster GN=Set2 PE=4 SV=1
Q9VGR0	20	34863	1	1	0.1	8.55	CG17187 OS=*Drosophila* melanogaster GN=CG17187 PE=2 SV=2
Q8T3Z0	17	49975	1	1	0.07	5.98	AT25102p OS=*Drosophila* melanogaster GN=Tektin-C PE=2 SV=1
M9NES0	15	41315	1	1	0.08	6.84	Arrestin 1, isoform B OS=*Drosophila* melanogaster GN=Arr1 PE=4 SV=1
M9PDV2	15	32810	1	1	0.1	8.55	Tetraspanin 5D, isoform C OS=*Drosophila* melanogaster GN=Tsp5D PE=4 SV=1

M9MRK1	15	126045	1	1	0.03	2.56	Phosphodiesterase 11, isoform E OS=*Drosophila* melanogaster GN=Pde11 PE=4 SV=1
Q8IMA2	14	52240	1	1	0.06	5.13	CG32006 OS=*Drosophila* melanogaster GN=CG32006-RA PE=2 SV=1
Q7KV69	14	475126	1	1	0.01	0.85	Karst, isoform B OS=*Drosophila* melanogaster GN=kst PE=4 SV=1

LC-MS/MS Pilot Run: Proteins bound to NTAP-Jun in Control conditions

Accession	Score	Mass	Nº of sig. matches	Nº of sig. sequences	emPAI	Molar %	Description
E1JIK0	143	39533	8	5	0.49	17.31	Heterogeneous nuclear ribonucleoprotein at 87F, isoform C OS=*Drosophila* melanogaster GN=Hrb87F PE=2 SV=1
L0MQ04	71	54649	4	3	0.19	6.71	ATP synthase subunit beta OS=*Drosophila* melanogaster GN=ATPsyn-beta PE=3 SV=1
Q9VT23	63	28337	3	2	0.25	8.83	CG8329 OS=*Drosophila* melanogaster GN=CG8329 PE=3 SV=1
Q9W3M7	52	100698	1	1	0.03	1.06	CG10777 OS=*Drosophila* melanogaster GN=CG10777 PE=2 SV=1
P19107	41	45342	1	1	0.07	2.47	Phosrestin-1 OS=*Drosophila* melanogaster GN=Arr2 PE=1 SV=2
E1JIR4	39	112058	2	2	0.06	2.12	Na pump alpha subunit, isoform I OS=*Drosophila* melanogaster GN=ATPalpha PE=3 SV=1
Q9VRL0	36	33857	1	1	0.1	3.53	CG4769, isoform A OS=*Drosophila* melanogaster GN=CG4769 PE=2 SV=1
P11147	35	71372	2	2	0.09	3.18	Heat shock 70 kDa protein cognate 4 OS=*Drosophila* melanogaster GN=Hsc70-4 PE=1 SV=3
Q9Y091	33	59517	4	1	0.06	2.12	Pre-mRNA-splicing regulator female-lethal(2)D OS=*Drosophila* melanogaster GN=fl(2)d PE=1 SV=2
E1JGP0	32	40574	2	2	0.17	6.01	Actin 57B, isoform C OS=*Drosophila* melanogaster GN=Act57B PE=2 SV=1

B7Z061	26	28327	1	1	0.12	4.24	Photoreceptor dehydrogenase, isoform D OS=*Drosophila* melanogaster GN=Pdh PE=3 SV=1
P29845	24	74248	1	1	0.04	1.41	Heat shock 70 kDa protein cognate 5 OS=*Drosophila* melanogaster GN=Hsc70-5 PE=1 SV=2
O62619	24	57917	1	1	0.06	2.12	Pyruvate kinase OS=*Drosophila* melanogaster GN=PyK PE=2 SV=2
Q9VVL7	22	53565	1	1	0.06	2.12	Dihydrolipoyl dehydrogenase OS=*Drosophila* melanogaster GN=CG7430 PE=2 SV=1
Q9VXP3	22	65238	1	1	0.05	1.77	GH05406p OS=*Drosophila* melanogaster GN=mRpS30 PE=2 SV=1
Q1RL12	22	37343	1	1	0.09	3.18	IP16413p OS=*Drosophila* melanogaster GN=nrv2 PE=2 SV=1
Q9VHJ8	21	55172	1	1	0.06	2.12	SkpA associated protein, isoform A OS=*Drosophila* melanogaster GN=skap PE=3 SV=2
P48596	20	35804	1	1	0.09	3.18	GTP cyclohydrolase 1 OS=*Drosophila* melanogaster GN=Pu PE=2 SV=3
Q9VJ21	18	148749	1	1	0.02	0.71	CG31792, isoform B OS=*Drosophila* melanogaster GN=CG31792 PE=3 SV=4
E1JJM7	18	138872	1	1	0.02	0.71	LIM-kinase1, isoform E OS=*Drosophila* melanogaster GN=LIMK1 PE=4 SV=1
A1Z9R4	18	137056	1	1	0.02	0.71	Zinc finger protein 423 homolog OS=*Drosophila* melanogaster GN=Oaz PE=2 SV=2
M9MRK1	17	126045	1	1	0.03	1.06	Phosphodiesterase 11, isoform E OS=*Drosophila* melanogaster GN=Pde11 PE=4 SV=1
E2QD61	17	195649	1	1	0.02	0.71	CG34384, isoform B OS=*Drosophila* melanogaster GN=CG14462 PE=4 SV=1
P40797	16	60448	1	1	0.05	1.77	Protein peanut OS=*Drosophila* melanogaster GN=pnut PE=1 SV=2
Q9V4E6	16	82046	1	1	0.04	1.41	Maverick OS=*Drosophila* melanogaster GN=mav PE=2 SV=1
Q9VDN3	16	68681	1	1	0.05	1.77	Ionotropic receptor 92a OS=*Drosophila* melanogaster GN=Ir92a PE=4 SV=3

Q9VHT2	15	36839	1	1	0.09	3.18	FI07663p OS=*Drosophila* melanogaster GN=tex PE=2 SV=1
B5RIM9	14	39931	1	1	0.08	2.83	FI03663p OS=*Drosophila* melanogaster GN=Gpdh PE=2 SV=1
Q8INE6	14	13510	1	1	0.25	8.83	AT25705p OS=*Drosophila* melanogaster GN=Oscp PE=2 SV=1
L0MPS3	14	374386	1	1	0.01	0.35	Retinoid-and fatty acid-binding glycoprotein, isoform B OS=*Drosophila* melanogaster GN=Rfabg PE=4 SV=1
Q9VNF5	14	46920	1	1	0.07	2.47	3-oxoacyl-[acyl-carrier-protein] synthase OS=*Drosophila* melanogaster GN=CG12170 PE=3 SV=1

LC-MS/MS Pilot Run: Proteins bound to NTAP-Jun in DEM-treated conditions

Accession	Score	Mass	Nº of sig. matches	Nº of sig. sequences	emPAI	Molar %	Description
Q9VT23	84	28337	3	3	0.4	21.16	CG8329 OS=*Drosophila* melanogaster GN=CG8329 PE=3 SV=1
Q8INE6	67	13510	1	1	0.25	13.23	AT25705p OS=*Drosophila* melanogaster GN=Oscp PE=2 SV=1
P19107	40	45342	1	1	0.07	3.70	Phosrestin-1 OS=*Drosophila* melanogaster GN=Arr2 PE=1 SV=2
B7Z061	33	28327	1	1	0.12	6.35	Photoreceptor dehydrogenase, isoform D OS=*Drosophila* melanogaster GN=Pdh PE=3 SV=1
Q9Y091	30	59517	5	1	0.06	3.17	Pre-mRNA-splicing regulator female-lethal(2)D OS=*Drosophila* melanogaster GN=fl(2)d PE=1 SV=2
Q9V429	28	12859	1	1	0.27	14.29	Thioredoxin-2 OS=*Drosophila* melanogaster GN=Trx-2 PE=1 SV=2
Q9VB18	28	155635	1	1	0.02	1.06	Tusp OS=*Drosophila* melanogaster GN=Tusp PE=4 SV=3
E1JJM7	27	138872	1	1	0.02	1.06	LIM-kinase1, isoform E OS=*Drosophila* melanogaster GN=LIMK1 PE=4 SV=1
Q9W309	26	17778	1	1	0.19	10.05	CG9686 OS=*Drosophila* melanogaster GN=CG9686 PE=2 SV=1

Q8IMI5	20	64115	1	1	0.05	2.65	FI04474p OS=*Drosophila* melanogaster GN=spdo PE=2 SV=1
M9PF59	18	95157	1	1	0.03	1.59	CG43759, isoform B OS=*Drosophila* melanogaster GN=CG42506 PE=4 SV=1
E1JIV0	18	28503	1	1	0.12	6.35	CG5902, isoform C OS=*Drosophila* melanogaster GN=CG5902 PE=4 SV=1
Q9W444	18	231343	1	1	0.01	0.53	CG5937, isoform C OS=*Drosophila* melanogaster GN=CG5937 PE=4 SV=3
A1Z9R4	17	137056	1	1	0.02	1.06	Zinc finger protein 423 homolog OS=*Drosophila* melanogaster GN=Oaz PE=2 SV=2
E2QD61	17	195649	1	1	0.02	1.06	CG34384, isoform B OS=*Drosophila* melanogaster GN=CG14462 PE=4 SV=1
Q9VA18	16	24397	1	1	0.14	7.41	Lethal (3) 03670 OS=*Drosophila* melanogaster GN=l(3)03670 PE=2 SV=1
M9PDT5	15	103120	1	1	0.03	1.59	Bric a brac 1, isoform D OS=*Drosophila* melanogaster GN=bab1 PE=4 SV=1
Q7KUW4	14	45872	1	1	0.07	3.70	CG7206, isoform B OS=*Drosophila* melanogaster GN=CG7206-RB PE=2 SV=1

Appendix 5: LC-MS/MS main run data

LC-MS Main Run: Proteins bound to NTAP-empty vector in Control conditions

Accession	Score	Mass	Nº of sig. matches	Nº of sig. sequences	emPAI	Molar %	Description
Q0E9E2	225	133332	16	16	0.44	9.64	CG1516, isoform I OS=*Drosophila* melanogaster GN=PCB PE=4 SV=1
P06603	131	50561	9	8	0.61	13.37	Tubulin alpha-1 chain OS=*Drosophila* melanogaster GN=alphaTub84B PE=2 SV=1
C6TP87	63	50561	3	3	0.19	4.16	Elongation factor 1-alpha OS=*Drosophila* melanogaster GN=Ef1alpha48D-RA PE=2 SV=1
C7LA75	55	71372	4	3	0.14	3.07	Heat shock protein cognate 4, isoform G OS=*Drosophila* melanogaster GN=Hsc70-4-RA PE=2 SV=1
A0A0B4LGH1	86	51316	3	2	0.12	2.63	Beta-Tubulin at 60D, isoform B OS=*Drosophila* melanogaster GN=betaTub60D PE=4 SV=1
Q9VWH4	60	41160	2	2	0.16	3.51	Probable isocitrate dehydrogenase [NAD] subunit alpha, mitochondrial OS=*Drosophila* melanogaster GN=l(1)G0156 PE=2 SV=1
F3YDH0	53	72330	2	2	0.09	1.97	Heat shock 70-kDa protein cognate 3, isoform E OS=*Drosophila* melanogaster GN=Hsc70-3 PE=2 SV=1
Q9VD58	38	40698	2	2	0.16	3.51	CG6439, isoform A OS=*Drosophila* melanogaster GN=CG6439 PE=2 SV=1
Q7KN94	34	34274	2	2	0.19	4.16	Walrus, isoform A OS=*Drosophila* melanogaster GN=wal PE=2 SV=1
A0A0B4LH50	32	42174	2	2	0.15	3.29	Actin 87E, isoform C OS=*Drosophila* melanogaster GN=Act87E PE=4 SV=1
L0MQ04	59	54649	1	1	0.06	1.31	ATP synthase subunit beta OS=*Drosophila* melanogaster GN=ATPsynbeta PE=3 SV=1
Q7KY08	58	107348	4	1	0.001	0.02	Argonaute protein OS=*Drosophila* melanogaster GN=AGO1 PE=2 SV=1
A8DYH1	55	197410	3	1	0.02	0.44	Muscle wasted, isoform C OS=*Drosophila* melanogaster GN=mute PE=4 SV=1
Q9VRP8	52	37594	2	1	0.08	1.75	Cellular retinaldehyde binding protein OS=*Drosophila* melanogaster

							GN=Cralbp PE=4 SV=1
M9NDP0	45	212195	3	1	0.001	0.02	CG9932, isoform C OS=*Drosophila* melanogaster GN=CG9932 PE=4 SV=1
A8JRB8	39	43402	1	1	0.07	1.53	CG5028, isoform C OS=*Drosophila* melanogaster GN=CG5028-RC PE=2 SV=1
Q7KMG7	36	28736	5	1	0.11	2.41	Ercc1 OS=*Drosophila* melanogaster GN=Ercc1 PE=4 SV=1
Q9VTP0	36	411349	11	1	0.01	0.22	CG42255 OS=*Drosophila* melanogaster GN=CG32092 PE=4 SV=4
A0A0B4KHZ3	29	159101	2	1	0.02	0.44	Tusp, isoform G OS=*Drosophila* melanogaster GN=Tusp PE=4 SV=1
X2JAP0	28	36952	2	1	0.08	1.75	CG4623, isoform C OS=*Drosophila* melanogaster GN=Gdap1 PE=4 SV=1
P35381	27	59612	1	1	0.05	1.10	ATP synthase subunit alpha, mitochondrial OS=*Drosophila* melanogaster GN=blw PE=1 SV=2
X2JF59	27	21952	1	1	0.14	3.07	Thioredoxin peroxidase 1, isoform C OS=*Drosophila* melanogaster GN=Jafrac1 PE=4 SV=1
Q9VA48	24	72871	5	1	0.04	0.88	Serpin 100A OS=*Drosophila* melanogaster GN=Spn100A PE=3 SV=1
Q8MZG9	24	36730	4	1	0.08	1.75	CG2070, isoform A OS=*Drosophila* melanogaster GN=CG2070 PE=2 SV=1
Q8IQH4	23	89778	1	1	0.03	0.66	CG10948, isoform D OS=*Drosophila* melanogaster GN=CG10948 PE=4 SV=2
M9PJN8	23	35518	1	1	0.09	1.97	Glyceraldehyde-3-phosphate dehydrogenase OS=*Drosophila* melanogaster GN=Gapdh2 PE=3 SV=1
A0A0B4LG2396	23	44912	1	1	0.07	1.53	Peptidyl-alpha-hydroxyglycine-alpha-amidating lyase 2, isoform E OS=*Drosophila* melanogaster GN=Pal2 PE=4 SV=1
A0A0B4KES0	22	246680	1	1	0.01	0.22	Slit, isoform F OS=*Drosophila* melanogaster GN=sli PE=4 SV=1
A1Z992	22	79345	1	1	0.04	0.88	1,4-Alpha-Glucan branching enzyme OS=*Drosophila* melanogaster GN=AGBE PE=4 SV=1
Q9VAJ9	22	34825	1	1	0.09	1.97	CG1907 OS=*Drosophila* melanogaster GN=CG1907 PE=2 SV=1
Q9VPG1	21	257318	1	1	0.01	0.22	Zye OS=*Drosophila* melanogaster GN=zye PE=4 SV=1

Q7KT60	20	273958	1	1	0.01	0.22	CG31817 OS=*Drosophila* melanogaster GN=CG31817 PE=4 SV=2
Q7KTK9	20	44318	1	1	0.07	1.53	Acetyltransferase component of pyruvate dehydrogenase complex OS=*Drosophila* melanogaster GN=CG5261 PE=3 SV=1
Q95U34	20	54777	1	1	0.06	1.31	GH11113p OS=*Drosophila* melanogaster GN=Galk PE=2 SV=1
Q7KNQ9	20	172254	2	1	0.02	0.44	Connector enhancer of KSR protein CNK OS=*Drosophila* melanogaster GN=cnk PE=1 SV=1
E1JJM7	19	138872	1	1	0.02	0.44	LIM-kinase1, isoform E OS=*Drosophila* melanogaster GN=LIMK1 PE=4 SV=1
X2J969	19	35368	1	1	0.09	1.97	Mediator complex subunit 19, isoform B OS=*Drosophila* melanogaster GN=MED19 PE=4 SV=1
P18167	19	61415	1	1	0.05	1.10	Esterase P OS=*Drosophila* melanogaster GN=Est-P PE=2 SV=2
Q9VEV2	19	52111	1	1	0.06	1.31	CG14882, isoform A OS=*Drosophila* melanogaster GN=CG14882 PE=4 SV=1
M9PCF1	19	179058	1	1	0.02	0.44	Dual oxidase, isoform C OS=*Drosophila* melanogaster GN=Duox PE=4 SV=1
A0A0B4LG6	18	168030	1	1	0.02	0.44	Lost PHDs of trr, isoform B OS=*Drosophila* melanogaster GN=Lpt PE=4 SV=1
A0A0B4KEY9	18	163351	1	1	0.02	0.44	Activated Cdc42 kinase-like, isoform C OS=*Drosophila* melanogaster GN=Ack-like PE=4 SV=1
A0A0B4K7L8	17	123367	1	1	0.02	0.44	Slamdance, isoform C OS=*Drosophila* melanogaster GN=sda PE=4 SV=1
Q9VW15	17	248850	1	1	0.01	0.22	Histone-lysine N-methyltransferase ash1 OS=*Drosophila* melanogaster GN=ash1 PE=1 SV=3
P55830	17	30549	1	1	0.1	2.19	40S ribosomal protein S3a OS=*Drosophila* melanogaster GN=RpS3A PE=1 SV=4
Q9VZ81	16	141219	1	1	0.02	0.44	CG13708, isoform A OS=*Drosophila* melanogaster GN=CG13708 PE=4 SV=1
Q8IRG3	16	53581	1	1	0.06	1.31	Succinyl-CoA:3-ketoacid-coenzyme A transferase OS=*Drosophila* melanogaster GN=SCOT PE=3 SV=1
X2JAH0	16	30710	1	1	0.1	2.19	Adh-related, isoform C OS=*Drosophila* melanogaster GN=Adhr PE=3 SV=1

Q9VB05	16	92938	1	1	0.03	0.66	ALG-2 interacting protein X OS=*Drosophila* melanogaster GN=ALiX PE=1 SV=1
Q9VVH0	16	66606	1	1	0.05	1.10	AT14039p OS=*Drosophila* melanogaster GN=CG12229 PE=2 SV=1
Q9I7V0	15	137381	1	1	0.02	0.44	Mid1 ortholog, isoform A OS=*Drosophila* melanogaster GN=Mid1 PE=2 SV=3
Q9W2U2	15	41763	1	1	0.07	1.53	CG32687, isoform A OS=*Drosophila* melanogaster GN=CG32687 PE=2 SV=2
Q9Y162	15	49736	1	1	0.06	1.31	BcDNA.GH02678 OS=*Drosophila* melanogaster GN=Vps4 PE=2 SV=1
A0A0B4JD23	15	43075	1	1	0.07	1.53	CG2246, isoform J OS=*Drosophila* melanogaster GN=CG2246 PE=4 SV=1
Q9W3W6	15	375647	1	1	0.01	0.22	CG14438, isoform A OS=*Drosophila* melanogaster GN=CG14438 PE=4 SV=2
Q9VXQ7	14	21383	1	1	0.15	3.29	CG8206, isoform A OS=*Drosophila* melanogaster GN=CG8206 PE=2 SV=1
Q7KU24	14	213066	1	1	0.001	0.02	Chromodomain-helicase-DNA-binding protein 1 OS=*Drosophila* melanogaster GN=Chd1 PE=1 SV=1

LC-MS/MS Main Run: Proteins bound to NTAP-empty vector in DEM-treated conditions

Accession	Score	Mass	Nº of sig. matches	Nº of sig. sequences	emPAI	Molar %	Description
Q0E9E2	158	133332	9	7	0.15	2.87	CG1516, isoform I OS=*Drosophila* melanogaster GN=PCB PE=4 SV=1
X2JCP8	103	42194	7	7	0.64	12.26	Actin 5C, isoform E OS=*Drosophila* melanogaster GN=Act5C PE=3 SV=1
A1Z992	83	79345	6	6	0.26	4.98	1,4-Alpha-Glucan branching enzyme OS=*Drosophila* melanogaster GN=AGBE PE=4 SV=1
A1ZBL0	122	51720	9	5	0.34	6.51	Beta-Tubulin at 56D, isoform A OS=*Drosophila* melanogaster GN=betaTub56D PE=2 SV=1
P06603	103	50561	5	4	0.27	5.17	Tubulin alpha-1 chain OS=*Drosophila* melanogaster GN=alphaTub84B PE=2 SV=1
X2J8Y6	45	102032	4	4	0.13	2.49	Accessory gland protein 36DE, isoform B OS=*Drosophila* melanogaster GN=Acp36DE PE=4 SV=1

C6TP87	69	50561	3	3	0.19	3.64	Elongation factor 1-alpha OS=*Drosophila* melanogaster GN=Ef1alpha48D-RA PE=2 SV=1
P35381	61	59612	3	3	0.16	3.06	ATP synthase subunit alpha, mitochondrial OS=*Drosophila* melanogaster GN=blw PE=1 SV=2
A0A0B4KHJ5	39	79811	3	3	0.12	2.30	Glycogen synthase, isoform D OS=*Drosophila* melanogaster GN=GlyS PE=4 SV=1
Q9VNW6	67	84610	2	2	0.04	0.77	CG7470, isoform A OS=*Drosophila* melanogaster GN=CG7470 PE=2 SV=1
C7LA75	58	71372	2	2	0.09	1.72	Heat shock protein cognate 4, isoform G OS=*Drosophila* melanogaster GN=Hsc70-4-RA PE=2 SV=1
Q9VAC1	34	52278	2	2	0.12	2.30	CG7920, isoform A OS=*Drosophila* melanogaster GN=CG7920 PE=2 SV=1
A0A0B4JCW4	27	49181	2	2	0.13	2.49	SkpA associated protein, isoform G OS=*Drosophila* melanogaster GN=skap PE=4 SV=1
L0MQ04	17	54649	2	2	0.12	2.30	ATP synthase subunit beta OS=*Drosophila* melanogaster GN=ATPsynbeta PE=3 SV=1
Q7KY08	85	107348	6	1	0.03	0.57	Argonaute protein OS=*Drosophila* melanogaster GN=AGO1 PE=2 SV=1
M9NDP0	66	212195	4	1	0.001	0.02	CG9932, isoform C OS=*Drosophila* melanogaster GN=CG9932 PE=4 SV=1
Q9VRP8	60	37594	3	1	0.08	1.53	Cellular retinaldehyde binding protein OS=*Drosophila* melanogaster GN=Cralbp PE=4 SV=1
Q7KMG7	55	28736	14	1	0.11	2.11	Ercc1 OS=*Drosophila* melanogaster GN=Ercc1 PE=4 SV=1
A8DYH1	50	197410	3	1	0.02	0.38	Muscle wasted, isoform C OS=*Drosophila* melanogaster GN=mute PE=4 SV=1
Q9VLZ7	39	58570	3	1	0.05	0.96	Probable cytochrome P450 4d21 OS=*Drosophila* melanogaster GN=Cyp4d21 PE=3 SV=1
X2JCX8	35	16312	1	1	0.2	3.83	Ribosomal protein S14b, isoform B OS=*Drosophila* melanogaster GN=RpS14b PE=3 SV=1
A0A0B4KH25	34	14972	1	1	0.21	4.02	Histone H2A variant, isoform B OS=*Drosophila*

							melanogaster GN=His2Av PE=4 SV=1
Q9VTP0	30	411349	7	1	0.01	0.19	CG42255 OS=*Drosophila* melanogaster GN=CG32092 PE=4 SV=4
X2JAP0	29	36952	3	1	0.08	1.53	CG4623, isoform C OS=*Drosophila* melanogaster GN=Gdap1 PE=4 SV=1
M9NEA7	28	135539	1	1	0.02	0.38	Defective chorion 1, isoform E OS=*Drosophila* melanogaster GN=dec-1 PE=4 SV=1
E1JJM7	27	138872	1	1	0.02	0.38	LIM-kinase1, isoform E OS=*Drosophila* melanogaster GN=LIMK1 PE=4 SV=1
Q9VWH4	27	41160	1	1	0.08	1.53	Probable isocitrate dehydrogenase [NAD] subunit alpha, mitochondrial OS=*Drosophila* melanogaster GN=l(1)G0156 PE=2 SV=1
Q9V3Y7	26	36733	1	1	0.08	1.53	CG15293, isoform A OS=*Drosophila* melanogaster GN=CG15293 PE=4 SV=1
A0A0B4KES0	26	246680	1	1	0.01	0.19	Slit, isoform F OS=*Drosophila* melanogaster GN=sli PE=4 SV=1
X2J7M7	26	54884	1	1	0.06	1.15	CG4658, isoform E OS=*Drosophila* melanogaster GN=CG4658 PE=4 SV=1
Q9VD58	25	40698	1	1	0.08	1.53	CG6439, isoform A OS=*Drosophila* melanogaster GN=CG6439 PE=2 SV=1
M9ND19	24	39071	1	1	0.08	1.53	UDP-galactose 4'-epimerase, isoform B OS=*Drosophila* melanogaster GN=Gale PE=3 SV=1
A0A0B4KHZ3	24	159101	2	1	0.02	0.38	Tusp, isoform G OS=*Drosophila* melanogaster GN=Tusp PE=4 SV=1
P06002	23	42208	1	1	0.07	1.34	Opsin Rh1 OS=*Drosophila* melanogaster GN=ninaE PE=1 SV=1
A0A0B4JD23	22	43075	5	1	0.07	1.34	CG2246, isoform J OS=*Drosophila* melanogaster GN=CG2246 PE=4 SV=1
Q8SYU5	22	52762	1	1	0.06	1.15	CG10086 OS=*Drosophila* melanogaster GN=CG10086 PE=2 SV=1
Q9V4I0	22	59268	1	1	0.05	0.96	Cytochrome P450 9b1 OS=*Drosophila* melanogaster GN=Cyp9b1 PE=2 SV=1
Q9VAJ9	22	34825	1	1	0.09	1.72	CG1907 OS=*Drosophila* melanogaster GN=CG1907 PE=2 SV=1

A0A023GPV6	22	125997	1	1	0.02	0.38	CG3632, isoform J OS=*Drosophila* melanogaster GN=CG3632 PE=4 SV=1
A0A0B4KF23	21	225555	1	1	0.01	0.19	Nipped-B, isoform J OS=*Drosophila* melanogaster GN=Nipped-B PE=4 SV=1
A0A0B4KEY9	21	163351	3	1	0.02	0.38	Activated Cdc42 kinase-like, isoform C OS=*Drosophila* melanogaster GN=Ack-like PE=4 SV=1
A1ZBM3	20	155575	1	1	0.02	0.38	Outer segment 6 OS=*Drosophila* melanogaster GN=Oseg6 PE=4 SV=1
Q7KT60	20	273958	4	1	0.01	0.19	CG31817 OS=*Drosophila* melanogaster GN=CG31817 PE=4 SV=2
Q9VRM6	20	215630	1	1	0.01	0.19	Lethal (3) persistent salivary gland 2 OS=*Drosophila* melanogaster GN=l(3)psg2 PE=4 SV=2
Q9W3D2	20	185652	2	1	0.02	0.38	Calmodulin-binding protein related to a Rab3 GDP/GTP exchange protein, isoform B OS=*Drosophila* melanogaster GN=Crag PE=2 SV=3
A8JQX3	20	72804	1	1	0.04	0.77	Curled, isoform D OS=*Drosophila* melanogaster GN=cu PE=4 SV=1
Q9VA48	20	72871	4	1	0.04	0.77	Serpin 100A OS=*Drosophila* melanogaster GN=Spn100A PE=3 SV=1
X2JF59	20	21952	1	1	0.14	2.68	Thioredoxin peroxidase 1, isoform C OS=*Drosophila* melanogaster GN=Jafrac1 PE=4 SV=1
Q0E8E2	19	128674	1	1	0.02	0.38	CG4998, isoform B OS=*Drosophila* melanogaster GN=CG4998 PE=3 SV=1
Q9W2U2	19	41763	1	1	0.07	1.34	CG32687, isoform A OS=*Drosophila* melanogaster GN=CG32687 PE=2 SV=2
A0A0B4JDD0	18	144355	1	1	0.02	0.38	PFTAIRE-interacting factor 1A, isoform H OS=*Drosophila* melanogaster GN=Pif1A PE=4 SV=1
Q8IQH9	18	127564	1	1	0.02	0.38	Sin3A-associated protein 130, isoform B OS=*Drosophila* melanogaster GN=Sap130 PE=4 SV=1
A0A0B4KG03	17	91996	1	1	0.03	0.57	Flyers-cup, isoform F OS=*Drosophila* melanogaster GN=f-cup PE=4 SV=1
E2QCY9	17	109721	1	1	0.03	0.57	Synapsin, isoform D OS=*Drosophila* melanogaster

							GN=Syn PE=4 SV=1
Q9VU52	17	84541	1	1	0.04	0.77	Sneaky OS=*Drosophila* melanogaster GN=snky PE=4 SV=3
A0A0B4LGB7	16	110137	1	1	0.03	0.57	Calcium ATPase at 60A, isoform I OS=*Drosophila* melanogaster GN=Ca-P60A PE=4 SV=1
A0A0B4K6B9	16	98526	1	1	0.03	0.57	CG2698, isoform D OS=*Drosophila* melanogaster GN=CG2698 PE=4 SV=1
Q86P48	16	43142	1	1	0.07	1.34	AT-rich binding protein OS=*Drosophila* melanogaster GN=ATbp PE=2 SV=2
M9PD43	16	28020	1	1	0.11	2.11	CG16865, isoform B OS=*Drosophila* melanogaster GN=CG16865 PE=4 SV=1
X2JCU8	16	105252	1	1	0.03	0.57	Dipeptidase OS=*Drosophila* melanogaster GN=CG14129 PE=3 SV=1
A0A0B4KEK1	15	217320	2	1	0.001	0.02	Enhancer of polycomb, isoform C OS=*Drosophila* melanogaster GN=E(Pc) PE=4 SV=1
Q9VLU4	15	59483	1	1	0.05	0.96	LP15633p OS=*Drosophila* melanogaster GN=Spn28Dc PE=2 SV=2

LC-MS/MS Main Run: Proteins bound to NTAP-Fos in Control conditions

Accession	Score	Mass	Nº of sig. matches	Nº of sig. sequences	emPAI	Molar %	Description
A0A0B4LHU8	144	68949	5	4	0.19	9.88	Kayak, isoform G OS=*Drosophila* melanogaster GN=kay PE=4 SV=1
A0A0B4KEI6	41	40070	2	2	0.16	8.32	Jun-related antigen, isoform C OS=*Drosophila* melanogaster GN=Jra PE=4 SV=1
P48596	40	35804	2	2	0.18	9.36	GTP cyclohydrolase 1 OS=*Drosophila* melanogaster GN=Pu PE=2 SV=3
E1JHA4	29	44970	2	2	0.14	7.28	Heterogeneous nuclear ribonucleoprotein at 27C, isoform D OS=*Drosophila* melanogaster GN=Hrb27C PE=4 SV=1
Q7K5K3	49	39611	1	1	0.08	4.16	CG11876, isoform A OS=*Drosophila* melanogaster GN=CG11876 PE=2 SV=1
Q9VIX7	46	58112	2	1	0.05	2.60	CG15825-PB, isoform B OS=*Drosophila* melanogaster GN=fon PE=2 SV=1

O01666	36	33078	1	1	0.09	4.68	ATP synthase subunit gamma, mitochondrial OS=*Drosophila* melanogaster GN=ATPsyn-gamma PE=2 SV=2
A0A0B4KEH0	35	28324	1	1	0.11	5.72	14-3-3zeta, isoform K OS=*Drosophila* melanogaster GN=14-3-3zeta PE=4 SV=1
M9MS20	30	27645	2	1	0.11	5.72	Jonah 74E, isoform B OS=*Drosophila* melanogaster GN=Jon74E PE=3 SV=1
A0A0B4KGK0	29	22020	1	1	0.14	7.28	Protein-L-isoaspartate (D-aspartate) O-methyltransferase, isoform C OS=*Drosophila* melanogaster GN=Pcmt PE=4 SV=1
Q9Y119	26	92046	1	1	0.03	1.56	BcDNA.GH08860 OS=*Drosophila* melanogaster GN=Tps1 PE=2 SV=1
X2JFT2	26	100239	1	1	0.001	0.05	CG9634, isoform B OS=*Drosophila* melanogaster GN=goe PE=4 SV=1
Q9VMQ3	25	26904	1	1	0.12	6.24	CG14016-PA OS=*Drosophila* melanogaster GN=tomb PE=2 SV=1
Q9VGD8	21	82275	1	1	0.04	2.08	GH27720p OS=*Drosophila* melanogaster GN=ssp5 PE=2 SV=1
A0A0B4LG45	19	68668	1	1	0.04	2.08	CG11180, isoform B OS=*Drosophila* melanogaster GN=CG11180 PE=4 SV=1
X2JIQ5	18	21922	3	1	0.14	7.28	Ribosomal protein L17, isoform E OS=*Drosophila* melanogaster GN=RpL17 PE=3 SV=1
Q9V3H9	17	113870	1	1	0.03	1.56	BcDNA.LD27873 OS=*Drosophila* melanogaster GN=Nab2 PE=2 SV=1
Q9VC40	16	38348	1	1	0.001	0.05	CG5805, isoform A OS=*Drosophila* melanogaster GN=CG5805 PE=2 SV=1
Q9V477	16	154976	1	1	0.02	1.04	Cell surface receptor TOLLO OS=*Drosophila* melanogaster GN=Tollo PE=2 SV=1
D2CFV7	16	32763	1	1	0.001	0.05	CG42619 (Fragment) OS=*Drosophila* melanogaster GN=PRY PE=4 SV=1
A1ZAY9	16	67827	1	1	0.05	2.60	Ionotropic receptor 54a OS=*Drosophila* melanogaster GN=Ir54a PE=4 SV=2
Q8IRS2	14	88069	1	1	0.001	0.05	CG2861, isoform C OS=*Drosophila* melanogaster GN=CG2861-RA PE=2 SV=2
A1ZAH8	14	16968	1	1	0.19	9.88	Ribosomal protein S15,

							isoform B OS=*Drosophila* melanogaster GN=RpS15 PE=2 SV=1
Q9VUB5	14	337664	1	1	0.01	0.52	UpSET, isoform A OS=*Drosophila* melanogaster GN=upSET PE=4 SV=3

LC-MS/MS Main Run: Proteins bound to NTAP-Fos in DEM-treated conditions

Accession	Score	Mass	Nº of sig. matches	Nº of sig. sequences	emPAI	Molar %	Description
A0A0B4LHU8	104	68949	3	3	0.14	6.16	Kayak, isoform G OS=*Drosophila* melanogaster GN=kay PE=4 SV=1
P02283	41	13688	1	1	0.24	10.56	Histone H2B OS=*Drosophila* melanogaster GN=His2B PE=1 SV=2
A0A0B4K661	30	29248	1	1	0.11	4.84	Tropomyosin 1, isoform Q OS=*Drosophila* melanogaster GN=Tm1 PE=4 SV=1
Q9VMQ3	29	26904	1	1	0.12	5.28	CG14016-PA OS=*Drosophila* melanogaster GN=tomb PE=2 SV=1
M9MS20	27	27645	2	1	0.11	4.84	Jonah 74E, isoform B OS=*Drosophila* melanogaster GN=Jon74E PE=3 SV=1
Q7KW14	26	134607	1	1	0.02	0.88	Coiled-coil domain-containing protein CG32809 OS=*Drosophila* melanogaster GN=CG32809 PE=2 SV=1
Q8SZ30	25	31474	1	1	0.1	4.40	RE19845p OS=*Drosophila* melanogaster GN=spn-D PE=2 SV=1
A0A0B4KFD1	24	550276	1	1	0.01	0.44	LDL receptor protein 1, isoform F OS=*Drosophila* melanogaster GN=LRP1 PE=4 SV=1
A0A0B4KGK0	22	22020	1	1	0.14	6.16	Protein-L-isoaspartate (D-aspartate) O-methyltransferase, isoform C OS=*Drosophila* melanogaster GN=Pcmt PE=4 SV=1
B7Z0E5	22	190251	1	1	0.02	0.88	Misfire, isoform F OS=*Drosophila* melanogaster GN=mfr PE=4 SV=1
Q9VYU0	22	225775	1	1	0.01	0.44	Rudhira, isoform C OS=*Drosophila*

							melanogaster GN=rudhira PE=4 SV=3
Q9VFQ9	21	56069	1	1	0.06	2.64	Dipeptidase B, isoform A OS=*Drosophila* melanogaster GN=Dip-B PE=2 SV=2
A0A0B4KGH0	21	361856	1	1	0.01	0.44	Dystrophin, isoform K OS=*Drosophila* melanogaster GN=Dys PE=4 SV=1
Q9W1M7	20	108504	2	1	0.03	1.32	GH13170p OS=*Drosophila* melanogaster GN=Pi3K59F PE=1 SV=2
Q9VC40	19	38348	1	1	0.001	0.04	CG5805, isoform A OS=*Drosophila* melanogaster GN=CG5805 PE=2 SV=1
A0A0B4K709	19	85185	1	1	0.04	1.76	CG34355, isoform E OS=*Drosophila* melanogaster GN=CG34355 PE=4 SV=1
Q9VGW4	19	318080	1	1	0.01	0.44	CG14692 OS=*Drosophila* melanogaster GN=CG14692 PE=4 SV=4
F3YD80	18	26351	1	1	0.12	5.28	CG42814 OS=*Drosophila* melanogaster GN=CG42814-RA PE=2 SV=1
Q7JYK1	18	15005	1	1	0.21	9.24	RE10554p OS=*Drosophila* melanogaster GN=RpL40 PE=2 SV=1
Q8IPB7	18	123343	1	1	0.02	0.88	Alpha-mannosidase OS=*Drosophila* melanogaster GN=LManII PE=3 SV=1
M9NCV1	18	85699	1	1	0.04	1.76	Four way stop, isoform D OS=*Drosophila* melanogaster GN=fws PE=4 SV=1
A8DYS8	18	100829	1	1	0.03	1.32	CG4341, isoform C OS=*Drosophila* melanogaster GN=CG4341 PE=4 SV=2
X2JIQ5	17	21922	3	1	0.14	6.16	Ribosomal protein L17, isoform E OS=*Drosophila* melanogaster GN=RpL17 PE=3 SV=1
X2J6P6	17	162711	2	1	0.02	0.88	Phosphodiesterase 11, isoform F OS=*Drosophila* melanogaster GN=Pde11 PE=4 SV=1
Q9VH26	17	34128	1	1	0.09	3.96	CG3940, isoform A OS=*Drosophila* melanogaster GN=CG3940

							PE=4 SV=2
Q7KVQ7	17	48206	1	1	0.06	2.64	Transport and golgi organization 5, isoform B OS=*Drosophila* melanogaster GN=Tango5 PE=4 SV=1
Q8MRN4	16	115660	2	1	0.03	1.32	GH12664p OS=*Drosophila* melanogaster GN=Ppi1 PE=2 SV=1
Q9VIH0	16	43940	1	1	0.07	3.08	CG9272 OS=*Drosophila* melanogaster GN=CG9272 PE=4 SV=2
Q9VCW3	16	136088	1	1	0.02	0.88	LP09464p OS=*Drosophila* melanogaster GN=Nup133 PE=2 SV=2
Q9VXK9	15	140258	1	1	0.02	0.88	CG9170, isoform A OS=*Drosophila* melanogaster GN=CG9170 PE=2 SV=1
Q9W599	15	60692	1	1	0.05	2.20	CG32813, isoform H OS=*Drosophila* melanogaster GN=CG32813 PE=4 SV=3
Q9VB20	15	151595	1	1	0.02	0.88	Distracted, isoform B OS=*Drosophila* melanogaster GN=dsd PE=4 SV=2
Q9VB02	15	71794	1	1	0.04	1.76	CG12428, isoform A OS=*Drosophila* melanogaster GN=CG12428 PE=2 SV=1
X2J9A4	14	43981	1	1	0.07	3.08	Translocation protein 1, isoform D OS=*Drosophila* melanogaster GN=Trp1 PE=4 SV=1
Q4V671	14	19494	1	1	0.001	0.04	CG16739 OS=*Drosophila* melanogaster GN=CG16739 PE=2 SV=1
A1ZAQ4	14	58576	1	1	0.05	2.20	CG15611, isoform A OS=*Drosophila* melanogaster GN=CG15611 PE=4 SV=1

LC-MS/MS Main Run: Proteins bound to NTAP-Jun in Control conditions

Accession	Score	Mass	Nº of sig. matches	Nº of sig. sequences	emPAI	Molar %	Description
A0A0B4KEI6	143	40070	5	3	0.25	11.78	Jun-related antigen, isoform C OS=*Drosophila* melanogaster GN=Jra PE=4 SV=1
Q9VVU1	43	45565	4	3	0.22	10.37	CG3902-PA OS=*Drosophila* melanogaster GN=CG3902-RA PE=2 SV=1
A0A0B4LH	109	68949	2	2	0.09	4.24	Kayak, isoform G

U8							OS=*Drosophila* melanogaster GN=kay PE=4 SV=1
P48596	50	35804	2	2	0.18	8.48	GTP cyclohydrolase 1 OS=*Drosophila* melanogaster GN=Pu PE=2 SV=3
Q9VGD8	28	82275	2	1	0.04	1.89	GH27720p OS=*Drosophila* melanogaster GN=ssp5 PE=2 SV=1
Q9VGW4	28	318080	2	1	0.01	0.47	CG14692 OS=*Drosophila* melanogaster GN=CG14692 PE=4 SV=4
Q9VN14	17	159110	2	1	0.001	0.05	Contactin OS=*Drosophila* melanogaster GN=Cont PE=1 SV=2
P00334	68	27858	1	1	0.11	5.18	Alcohol dehydrogenase OS=*Drosophila* melanogaster GN=Adh PE=1 SV=2
Q7K5K3	56	39611	1	1	0.08	3.77	CG11876, isoform A OS=*Drosophila* melanogaster GN=CG11876 PE=2 SV=1
O01666	50	33078	1	1	0.09	4.24	ATP synthase subunit gamma, mitochondrial OS=*Drosophila* melanogaster GN=ATPsyn-gamma PE=2 SV=2
A0A0B4KGK0	44	22020	1	1	0.14	6.60	Protein-L-isoaspartate (D-aspartate) O-methyltransferase, isoform C OS=*Drosophila* melanogaster GN=Pcmt PE=4 SV=1
P48588	44	13193	1	1	0.24	11.31	40S ribosomal protein S25 OS=*Drosophila* melanogaster GN=RpS25 PE=1 SV=3
Q9VSA3	36	46185	1	1	0.07	3.30	Probable medium-chain specific acyl-CoA dehydrogenase, mitochondrial OS=*Drosophila* melanogaster GN=CG12262 PE=1 SV=1
Q9VCD1	36	234865	1	1	0.01	0.47	Rootletin, isoform D OS=*Drosophila* melanogaster GN=Rootletin PE=4 SV=3
M9MS20	35	27645	1	1	0.11	5.18	Jonah 74E, isoform B OS=*Drosophila* melanogaster GN=Jon74E PE=3 SV=1

Q9Y119	31	92046	1	1	0.03	1.41	BcDNA.GH08860 OS=*Drosophila* melanogaster GN=Tps1 PE=2 SV=1
Q9VIX7	27	58112	1	1	0.05	2.36	CG15825-PB, isoform B OS=*Drosophila* melanogaster GN=fon PE=2 SV=1
B7Z0E0	26	54065	1	1	0.06	2.83	Isocitrate dehydrogenase [NADP] OS=*Drosophila* melanogaster GN=Idh PE=3 SV=2
Q9W1M7	22	108504	1	1	0.03	1.41	GH13170p OS=*Drosophila* melanogaster GN=Pi3K59F PE=1 SV=2
E1JGU6	21	106867	1	1	0.03	1.41	Phosphodiesterase 8, isoform N OS=*Drosophila* melanogaster GN=Pde8 PE=4 SV=1
A1ZAY9	20	67827	1	1	0.05	2.36	Ionotropic receptor 54a OS=*Drosophila* melanogaster GN=Ir54a PE=4 SV=2
M9PB21	17	268083	1	1	0.01	0.47	V(2)k05816, isoform B OS=*Drosophila* melanogaster GN=v(2)k05816 PE=4 SV=1
Q9VIU5	16	105611	1	1	0.03	1.41	CG10137 OS=*Drosophila* melanogaster GN=CG10137 PE=2 SV=2
P20007	15	71882	1	1	0.04	1.89	Phosphoenolpyruvate carboxykinase [GTP] OS=*Drosophila* melanogaster GN=Pepck PE=2 SV=2
Q0KIB3	15	48144	1	1	0.06	2.83	CG2051, isoform A OS=*Drosophila* melanogaster GN=CG2051 PE=4 SV=1
Q9VGB4	15	56815	1	1	0.05	2.36	Probable cytochrome P450 313a2 OS=*Drosophila* melanogaster GN=Cyp313a2 PE=3 SV=3
A0A0B4K6I1	15	278200	1	1	0.01	0.47	Scribbled, isoform N OS=*Drosophila* melanogaster GN=scrib PE=4 SV=1
Q9VB46	14	63547	1	1	0.001	0.05	FI18644p1 OS=*Drosophila* melanogaster GN=Hmu PE=2 SV=1
Q9VTK2	14	102155	1	1	0.03	1.41	Protein O-mannosyltransferase1 OS=*Drosophila*melanogaster GN=rt PE=2 SV=2

LC-MS/MS Main Run: Proteins bound to NTAP-Jun in DEM-treated conditions

Accession	Score	Mass	Nº of sig. matches	Nº of sig. sequences	emPAI	Molar %	Description
A0A0B4KEI6	219	40070	7	5	0.45	34.59	Jun-related antigen, isoform C OS=*Drosophila* melanogaster GN=Jra PE=4 SV=1
X2JIQ5	18	21922	3	1	0.14	10.76	Ribosomal protein L17, isoform E OS=*Drosophila* melanogaster GN=RpL17 PE=3 SV=1
A0A0B4LHU8	36	68949	2	2	0.09	6.92	Kayak, isoform G OS=*Drosophila* melanogaster GN=kay PE=4 SV=1
Q9VCD1	47	234865	1	1	0.01	0.77	Rootletin, isoform D OS=*Drosophila* melanogaster GN=Rootletin PE=4 SV=3
M9PI58	33	108864	1	1	0.03	2.31	Stonewall, isoform B OS=*Drosophila* melanogaster GN=stwl PE=4 SV=1
Q7K5K3	30	39611	1	1	0.08	6.15	CG11876, isoform A OS=*Drosophila* melanogaster GN=CG11876 PE=2 SV=1
Q24592	26	136230	1	1	0.02	1.54	Tyrosine-protein kinase hopscotch OS=*Drosophila* melanogaster GN=hop PE=1 SV=2
Q8SZ30	22	31474	1	1	0.1	7.69	RE19845p OS=*Drosophila* melanogaster GN=spn-D PE=2 SV=1
A1ZAQ4	21	58576	1	1	0.05	3.84	CG15611, isoform A OS=*Drosophila* melanogaster GN=CG15611 PE=4 SV=1
Q9W1S3	21	103179	1	1	0.03	2.31	CG9861 OS=*Drosophila* melanogaster GN=CG9861-RA PE=2 SV=1
Q9NF31	19	143750	1	1	0.02	1.54	EG:BACN25G24.3 protein (Fbgn0004860;ph-d protein) OS=*Drosophila* melanogaster GN=ph-d PE=4 SV=1
Q9VCM6	17	145636	1	1	0.02	1.54	CG4393, isoform B OS=*Drosophila* melanogaster GN=CG4393 PE=2 SV=4
P20007	16	71882	1	1	0.04	3.07	Phosphoenolpyruvate carboxykinase [GTP] OS=*Drosophila* melanogaster GN=Pepck

							PE=2 SV=2
Q7K1L4	15	74744	1	1	0.001	0.08	CG8468, isoform A OS=*Drosophila* melanogaster GN=CG8468 PE=2 SV=1
Q9VJ80	15	157700	1	1	0.02	1.54	CG10211, isoform A OS=*Drosophila* melanogaster GN=CG10211 PE=2 SV=3
Q9VLS8	15	64849	1	1	0.05	3.84	CG8668, isoform A OS=*Drosophila* melanogaster GN=CG8668 PE=2 SV=2
A8DYS8	15	100829	1	1	0.03	2.31	CG4341, isoform C OS=*Drosophila* melanogaster GN=CG4341 PE=4 SV=2
Q9VV75	14	45559	1	1	0.07	5.38	AT02348p OS=*Drosophila* melanogaster GN=UQCR-C2 PE=2 SV=1
Q9VNU3	14	64678	1	1	0.05	3.84	CG11449 OS=*Drosophila* melanogaster GN=CG11449 PE=4 SV=1

Abbreviations

•OH	Hydroxyl radical
AD	Alzheimer's Disease
Adh	Alcohol dehydrogenase
ALS	Amyotrophic lateral sclerosis
AMP	Ampicillin
AP-1	Activator protein-1
APE-1	Apurinic/apyramidic endonuclease
ARE	Antioxidant response element
ASK1	Apoptosis signal regulating kinase 1
ATG	Autophagy
ATP	adenosine triphosphate
Aβ	β-amyloid peptide
BCA	Bicinchoninic acid assay
BH_4	tetrahydrobiopterin
BMP	Bone morphogenetic proteins
BRP	Bruchpilot
BSA	Bovine serum albumin
Bsk	Basket
C_{18}	octadecylsilyl
Cat	Catalse
cDNA	Complementary DNA
CNC	Cap'n'Collar
CO	Carbon monoxide
CoQ	Coenzyme Q
CS	*Canton-S*
CyO	Curly of Oyster (2nd Chromosome marker)
DA	Dopamine
Dad	Daughters against dpp
Ddc	DOPA decarboxylase
DEM	Diethyl Maleate
DGC	Dystrophin Glycoprotein Complex
DHFR	Dihydrofolate reductase
Dlg	Disks large
DLK	Dual leucine-zipper-bearing Kinase
DNA	Deoxyribonucleic acid
DRD	DOPA-responsive dystonia
dsRNA	Double stranded RNA
Dys	Dystrophin
ECL	Enhanced chemiluminescence
elav	Embryonic Lethal Abnormal Vision
emPAI	exponentially modified Protein Abundance Index
eNOS	Endothelial nitric oxide synthase
ERK	Extracellular signal-regulated kinase

ERO1	endoplasmic reticulum oxidoreductin 1
ESI	Electrospary ionisation
ETC	Electron Transport Chain
FAD	oxidised flavin adenine dinucleotide
$FADH_2$	reduced flavin adenine dinucleotide
Fe^{2+}	Ferrous ion
Fe^{3+}	Ferric
Gbb	Glass bottom boat
GDF	Growth and differentiation factors
GFP	Green Fluorescent Protein
GFRP	GTPCH1 feedback regulatory protein
GluR	Glutamate receptor
GPx	Glutathione peroxidase
GR	Glutathione reductase
GSH	Glutathione
GST	Glutathione S-transferase
GSTp	Glutathione S-transferase pi
GTP	Guanosine-5'-triphosphate
GTPCH1	GTP cyclohydrolase 1
H^+	Hydrogen
H_2O_2	Hydrogen Peroxide
hep	Hemipterous
Hiw	Highwire
Hop	Hopscotch
HPA	Hyperphenylalaninemia
HRP	Horseradish peroxidase
HSPG	Heparin sulphate proteoglycan
Idh	Isocitrate dehydrogenase
if	irregular facets (second chromosome marker)
IgG	Immunoglobulin G
ISN	Intersegmental nerve
JAK	Janus Kinase
JNK	Jun N-terminal kinase
JNKK	JNK kinase
JNKKK	JNK kinase kniase
Jra	Jun-related antigen
kay	Kayak
Keap1	Kelch-like erythroid cell-derived protein with CNC homology [ECH]-associated protein 1
L-DOPA	Levodopa
LB	Luria broth
LC-MS/MS	Liquid chromatography–mass spectrometry/mass spectrometry
LPO	Lipid peroxidation products
LRRK2	Leucine-rich repeat kinase 2
LTD	Long-term depression
LTP	Long-term potentiation

LZK	Leucine-zipper-bearing kinase
Mad	Mothers against dpp
MAPK	Mitogen-activated protein kinase
MBF1	Multiprotein bridging factor-1
mCD8	Mmus\Cd8a
MCS	Multiple cloning site
Med	Medea
MHC	Myosin heavy chain
MKRS	M(3)76A1, kar+, ry2, Sb1 (Partial Third chromosome marker)
MSA	Muscle surface area
msn	Misshapen
NADH	nicotinamide adenine nucleotide
NADPH	reduced nicotinamide adenine dinucleotide phosphate
NF-kB	Nuclear-factor kB
NMJ	Neuromuscular junction
NO	nitric oxide
NOS	Nitric oxide synthase
Nrf2	Nuclear factor erythroid 2 [NF-E2]-related factor 2
nSyb	neuronal Synaptobrevin
NTAP	Nterminal Tandem affinty purification (tag)
Nwk	Nervous wreck
O_2	Oxygen
$O_2^{\bullet -}$	Superoxide anion
OH^-	Hydroxyl anion
ORF	Open reading frame
PBS	Phosphate buffered saline
PBS-T	Phosphate buffered saline-Triton
PCR	Polymerase chain reaction
PD	Parkinson's Disease
PDI	Protein disulphide isomerase
PEPCK	Phosphoenolpyruvate carboxykinase
Pi	Phosphate
PIC	Protease inhibitor cocktail
PINK1	Phosphatase and tensin homolog-induced putative kinase 1
PKU	Phenylketonuria
POSH	Plenty-of-SH3s
Pu	Punch
Puc	Puckered
PUFA	Polyunsaturated fatty acids
PVDF	Polyvinylidene fluoride
Ref-1	Redox factor 1
RH2	Organic Substrates
RIPA	Radioimmunoprecipitation assay
RNA	Ribonucleic acid
RNAi	Interfering RNA
RNS	reactive nitrogen species

ROS	Reactive Oxygen Species
RSNO	S-nitrosothiols
SAPK	Stress-activated protein kinase
Sax	Saxophone
Sco	Scutella (2nd chromosome marker)
Scrib	Scribbled
SDS	Sodium Dodecyl Sulfate
SDS-PAGE	Sodium Dodecyl Sulphate PolyAcrylamide Gel Electrophoresis
SEM	Standard error of the mean
Slpr	Slipper
SN	Segmental nerve
SOD	Superoxide Dismutase
Spin	Spinster
SR	Sepiapterin reducatse
SSR	Subsynaptic reticulum
TAK1	TGF-β activated kinase 1
Tango5	Transport and golgi organisation 5
TAP	Tandem affinity purification
TBS-T	Tris buffered saline-Tween
TEV	Tobacco Etch Virus
TFA	Trifluoroacetic acid
TGF-β	Transforming growth factor beta
TH	Tyrosine hydroxylase
tkv	Thickveins
Tm1	Tropomyosin 1
TM3	Third multiple 3 (3rd Chromosome marker)
TM6b	Third multiple 6b (3rd chromosome marker)
TOF	Time-of-flight
TPA	12-O-tetradecanoylphorbol-13-acetate
TRE	TPA DNA responsive element
Trx	Thioredoxin reductase
UAS	Upstream activating sequence
UPLC	Ultra Performance Liquid Chromatography
VMP1	Vacuole membrane protein 1
VNC	Ventral nerve cord
WebGestalt	WEB-based GEne SeT AnaLysis Toolkit
Wg	Wingless
Wit	Wishful thinking
Wnd	Wallenda
WT	Wild-type
XO	Xanthine oxidase

References

ABATE, C., PATEL, L., RAUSCHER, F. J., 3RD & CURRAN, T. 1990. Redox regulation of fos and jun DNA-binding activity in vitro. *Science,* 249**,** 1157-61.

ABERLE, H., HAGHIGHI, A. P., FETTER, R. D., MCCABE, B. D., MAGALHAES, T. R. & GOODMAN, C. S. 2002. wishful thinking encodes a BMP type II receptor that regulates synaptic growth in Drosophila. *Neuron,* 33**,** 545-58.

ABRAHAM, W. C., MASON, S. E., DEMMER, J., WILLIAMS, J. M., RICHARDSON, C. L., TATE, W. P., LAWLOR, P. A. & DRAGUNOW, M. 1993. Correlations between immediate early gene induction and the persistence of long-term potentiation. *Neuroscience,* 56**,** 717-27.

ADAMS, M. D., CELNIKER, S. E., HOLT, R. A., EVANS, C. A., GOCAYNE, J. D., AMANATIDES, P. G., SCHERER, S. E., LI, P. W., HOSKINS, R. A., GALLE, R. F., GEORGE, R. A., LEWIS, S. E., RICHARDS, S., ASHBURNER, M., HENDERSON, S. N., SUTTON, G. G., WORTMAN, J. R., YANDELL, M. D., ZHANG, Q., CHEN, L. X., BRANDON, R. C., ROGERS, Y. H., BLAZEJ, R. G., CHAMPE, M., PFEIFFER, B. D., WAN, K. H., DOYLE, C., BAXTER, E. G., HELT, G., NELSON, C. R., GABOR, G. L., ABRIL, J. F., AGBAYANI, A., AN, H. J., ANDREWS-PFANNKOCH, C., BALDWIN, D., BALLEW, R. M., BASU, A., BAXENDALE, J., BAYRAKTAROGLU, L., BEASLEY, E. M., BEESON, K. Y., BENOS, P. V., BERMAN, B. P., BHANDARI, D., BOLSHAKOV, S., BORKOVA, D., BOTCHAN, M. R., BOUCK, J., BROKSTEIN, P., BROTTIER, P., BURTIS, K. C., BUSAM, D. A., BUTLER, H., CADIEU, E., CENTER, A., CHANDRA, I., CHERRY, J. M., CAWLEY, S., DAHLKE, C., DAVENPORT, L. B., DAVIES, P., DE PABLOS, B., DELCHER, A., DENG, Z., MAYS, A. D., DEW, I., DIETZ, S. M., DODSON, K., DOUP, L. E., DOWNES, M., DUGAN-ROCHA, S., DUNKOV, B. C., DUNN, P., DURBIN, K. J., EVANGELISTA, C. C., FERRAZ, C., FERRIERA, S., FLEISCHMANN, W., FOSLER, C., GABRIELIAN, A. E., GARG, N. S., GELBART, W. M., GLASSER, K., GLODEK, A., GONG, F., GORRELL, J. H., GU, Z., GUAN, P., HARRIS, M., HARRIS, N. L., HARVEY, D., HEIMAN, T. J., HERNANDEZ, J. R., HOUCK, J., HOSTIN, D., HOUSTON, K. A., HOWLAND, T. J., WEI, M. H., IBEGWAM, C., et al. 2000. The genome sequence of Drosophila melanogaster. *Science,* 287**,** 2185-95.

ADLER, V., YIN, Z., FUCHS, S. Y., BENEZRA, M., ROSARIO, L., TEW, K. D., PINCUS, M. R., SARDANA, M., HENDERSON, C. J., WOLF, C. R., DAVIS, R. J. & RONAI, Z. 1999a. Regulation of JNK signaling by GSTp. *Embo j,* 18**,** 1321-34.

ADLER, V., YIN, Z., TEW, K. D. & RONAI, Z. 1999b. Role of redox potential and reactive oxygen species in stress signaling. *Oncogene,* 18**,** 6104-11.

ALFONSO-PRIETO, M., BIARNES, X., VIDOSSICH, P. & ROVIRA, C. 2009. The molecular mechanism of the catalase reaction. *J Am Chem Soc,* 131**,** 11751-61.

AMATO, S. & MAN, H. Y. 2012. AMPK signaling in neuronal polarization: Putting the brakes on axonal traffic of PI3-Kinase. *Commun Integr Biol,* 5**,** 152-5.

ANDERSEN, P. M. 2006. Amyotrophic lateral sclerosis associated with mutations in the CuZn superoxide dismutase gene. *Curr Neurol Neurosci Rep,* 6**,** 37-46.

ANDO, K., HIRAO, S., KABE, Y., OGURA, Y., SATO, I., YAMAGUCHI, Y., WADA, T. & HANDA, H. 2008. A new APE1/Ref-1-dependent pathway leading to reduction of NF-kappaB and AP-1, and activation of their DNA-binding activity. *Nucleic Acids Res,* 36**,** 4327-36.

ANTONIADES, C., SHIRODARIA, C., VAN ASSCHE, T., CUNNINGTON, C., TEGEDER, I., LOTSCH, J., GUZIK, T. J., LEESON, P., DIESCH, J., TOUSOULIS, D., STEFANADIS, C., COSTIGAN, M., WOOLF, C. J., ALP, N. J. & CHANNON, K. M. 2008. GCH1 haplotype determines vascular and plasma biopterin availability in coronary artery disease effects on vascular superoxide production and endothelial function. *J Am Coll Cardiol,* 52**,** 158-65.

APEL, K. & HIRT, H. 2004. Reactive oxygen species: metabolism, oxidative stress, and signal transduction. *Annu Rev Plant Biol,* 55**,** 373-99.

ARDAN, T., KOVACEVA, J. & CEJKOVA, J. 2004. Comparative histochemical and immunohistochemical study on xanthine oxidoreductase/xanthine oxidase in mammalian corneal epithelium. *Acta Histochem,* 106**,** 69-75.

ARKING, R., BUCK, S., BERRIOS, A., DWYER, S. & BAKER, G. T., 3RD 1991. Elevated paraquat resistance can be used as a bioassay for longevity in a genetically based long-lived strain of Drosophila. *Dev Genet,* 12**,** 362-70.

ASAOKA, Y. & NISHINA, H. 2010. Diverse physiological functions of MKK4 and MKK7 during early embryogenesis. *J Biochem,* 148**,** 393-401.

ATAMAN, B., BUDNIK, V. & THOMAS, U. 2006. Scaffolding proteins at the Drosophila neuromuscular junction. *Int Rev Neurobiol,* 75**,** 181-216.

BAINTON, D. F. 1981. The discovery of lysosomes. *J Cell Biol,* 91**,** 66-76.

BARAIBAR, M. A., LIU, L., AHMED, E. K. & FRIGUET, B. 2012. Protein oxidative damage at the crossroads of cellular senescence, aging, and age-related diseases. *Oxid Med Cell Longev,* 2012**,** 919832.

BARJA, G. 1999. Mitochondrial oxygen radical generation and leak: sites of production in states 4 and 3, organ specificity, and relation to aging and longevity. *J Bioenerg Biomembr,* 31**,** 347-66.

BARJA, G. & HERRERO, A. 1998. Localization at complex I and mechanism of the higher free radical production of brain nonsynaptic mitochondria in the short-lived rat than in the longevous pigeon. *J Bioenerg Biomembr,* 30**,** 235-43.

BECKMAN, J. S. & KOPPENOL, W. H. 1996. Nitric oxide, superoxide, and peroxynitrite: the good, the bad, and ugly. *Am J Physiol,* 271**,** C1424-37.

BELL, K. F., AL-MUBARAK, B., MARTEL, M. A., MCKAY, S., WHEELAN, N., HASEL, P., MARKUS, N. M., BAXTER, P., DEIGHTON, R. F., SERIO, A., BILICAN, B., CHOWDHRY, S., MEAKIN, P. J., ASHFORD, M. L., WYLLIE, D. J., SCANNEVIN, R. H., CHANDRAN, S., HAYES, J. D. & HARDINGHAM, G. E. 2015. Neuronal development is promoted by weakened intrinsic antioxidant defences due to epigenetic repression of Nrf2. *Nat Commun,* 6**,** 7066.

BELLEN, H. J., LEVIS, R. W., LIAO, G., HE, Y., CARLSON, J. W., TSANG, G., EVANS-HOLM, M., HIESINGER, P. R., SCHULZE, K. L., RUBIN, G. M., HOSKINS, R. A. & SPRADLING, A. C. 2004. The BDGP gene disruption project: single transposon insertions associated with 40% of Drosophila genes. *Genetics,* 167**,** 761-81.

BENN, S. C. & WOOLF, C. J. 2004. Adult neuron survival strategies--slamming on the brakes. *Nat Rev Neurosci,* 5**,** 686-700.

BERKE, B., WITTNAM, J., MCNEILL, E., VAN VACTOR, D. L. & KESHISHIAN, H. 2013. Retrograde BMP signaling at the synapse: a permissive signal for synapse maturation and activity-dependent plasticity. *J Neurosci,* 33**,** 17937-50.

BERLETT, B. S. & STADTMAN, E. R. 1997. Protein oxidation in aging, disease, and oxidative stress. *J Biol Chem,* 272**,** 20313-6.

BERNARD, K. E., PARKES, T. L. & MERRITT, T. J. S. 2011. A Model of Oxidative Stress Management: Moderation of Carbohydrate Metabolizing Enzymes in SOD1-Null Drosophila melanogaster. *PLoS One,* 6.

BERNDT, N. & HOLZHUTTER, H. G. 2013. The high energy demand of neuronal cells caused by passive leak currents is not a waste of energy. *Cell Biochem Biophys,* 67**,** 527-35.

BEVERS, L. M., BRAAM, B., POST, J. A., VAN ZONNEVELD, A. J., RABELINK, T. J., KOOMANS, H. A., VERHAAR, M. C. & JOLES, J. A. 2006. Tetrahydrobiopterin, but not L-arginine, decreases NO synthase uncoupling in cells expressing high levels of endothelial NO synthase. *Hypertension,* 47**,** 87-94.

BHABAK, K. P. & MUGESH, G. 2010. Functional mimics of glutathione peroxidase: bioinspired synthetic antioxidants. *Acc Chem Res,* 43**,** 1408-19.

BHANDARY, B., MARAHATTA, A., KIM, H. R. & CHAE, H. J. 2013. An Involvement of Oxidative Stress in Endoplasmic Reticulum Stress and Its Associated Diseases. *Int J Mol Sci,* 14**,** 434-56.

BIER, E. 2005. Drosophila, the golden bug, emerges as a tool for human genetics. *Nat Rev Genet,* 6**,** 9-23.

BINARI, R. & PERRIMON, N. 1994. Stripe-specific regulation of pair-rule genes by hopscotch, a putative Jak family tyrosine kinase in Drosophila. *Genes Dev,* 8**,** 300-12.

BIRBEN, E., SAHINER, U. M., SACKESEN, C., ERZURUM, S. & KALAYCI, O. 2012. Oxidative stress and antioxidant defense. *World Allergy Organ J,* 5**,** 9-19.

BISHOP, C. P. & WRIGHT, T. R. 1987. DdcDE1, a mutant differentially affecting both stage and tissue specific expression of dopa decarboxylase in Drosophila. *Genetics,* 115**,** 477-91.

BONDY, S. C. & NADERI, S. 1994. The formation of reactive oxygen species in a fraction of rat brain by metabolism of nitric oxide. *Neurosci Lett,* 168**,** 34-6.

BORSELLO, T. & FORLONI, G. 2007. JNK signalling: a possible target to prevent neurodegeneration. *Curr Pharm Des,* 13**,** 1875-86.

BOVERIS, A. & CHANCE, B. 1973. The mitochondrial generation of hydrogen peroxide. General properties and effect of hyperbaric oxygen. *Biochem J,* 134**,** 707-16.

BOVERIS, A., OSHINO, N. & CHANCE, B. 1972. The cellular production of hydrogen peroxide. *Biochem J,* 128**,** 617-30.

BRACE, E. J., WU, C., VALAKH, V. & DIANTONIO, A. 2014. SkpA Restrains Synaptic Terminal Growth during Development and Promotes Axonal Degeneration following Injury. *J Neurosci,* 34**,** 8398-410.

BRAND, A. H. & PERRIMON, N. 1993. Targeted gene expression as a means of altering cell fates and generating dominant phenotypes. *Development,* 118**,** 401-15.

BROADIE, K. & BATE, M. 1993. Innervation directs receptor synthesis and localization in Drosophila embryo synaptogenesis. *Nature,* 361**,** 350-3.

BURKHARD, P., DOMINICI, P., BORRI-VOLTATTORNI, C., JANSONIUS, J. N. & MALASHKEVICH, V. N. 2001. Structural insight into Parkinson's disease treatment from drug-inhibited DOPA decarboxylase. *Nat Struct Biol,* 8**,** 963-7.

CADENAS, E. 1989. Biochemistry of oxygen toxicity. *Annu Rev Biochem,* 58**,** 79-110.

CADENAS, E. & DAVIES, K. J. 2000. Mitochondrial free radical generation, oxidative stress, and aging. *Free Radic Biol Med,* 29**,** 222-30.

CADET, J., DELATOUR, T., DOUKI, T., GASPARUTTO, D., POUGET, J. P., RAVANAT, J. L. & SAUVAIGO, S. 1999. Hydroxyl radicals and DNA base damage. *Mutat Res,* 424**,** 9-21.

CHA, G. H., KIM, S., PARK, J., LEE, E., KIM, M., LEE, S. B., KIM, J. M., CHUNG, J. & CHO, K. S. 2005. Parkin negatively regulates JNK pathway in the dopaminergic neurons of Drosophila. *Proc Natl Acad Sci U S A,* 102**,** 10345-50.

CHASSEAUD, L. F. 1979. The role of glutathione and glutathione S-transferases in the metabolism of chemical carcinogens and other electrophilic agents. *Adv Cancer Res,* 29**,** 175-274.

CHEN, K. & FEATHERSTONE, D. E. 2005. Discs-large (DLG) is clustered by presynaptic innervation and regulates postsynaptic glutamate receptor subunit composition in Drosophila. *BMC Biol,* 3**,** 1.

CHERRA, S. J., 3RD, STEER, E., GUSDON, A. M., KISELYOV, K. & CHU, C. T. 2013. Mutant LRRK2 elicits calcium imbalance and depletion of dendritic mitochondria in neurons. *Am J Pathol,* 182**,** 474-84.

CHI, L., KE, Y., LUO, C., GOZAL, D. & LIU, R. 2007. Depletion of reduced glutathione enhances motor neuron degeneration in vitro and in vivo. *Neuroscience,* 144**,** 991-1003.

CHOI, H. J., KIM, S. W., LEE, S. Y. & HWANG, O. 2003. Dopamine-dependent cytotoxicity of tetrahydrobiopterin: a possible mechanism for selective neurodegeneration in Parkinson's disease. *J Neurochem,* 86**,** 143-52.

CHRISTOPHERSON, K. S., ULLIAN, E. M., STOKES, C. C., MULLOWNEY, C. E., HELL, J. W., AGAH, A., LAWLER, J., MOSHER, D. F., BORNSTEIN, P. & BARRES, B. A. 2005. Thrombospondins are astrocyte-secreted proteins that promote CNS synaptogenesis. *Cell,* 120**,** 421-33.

CIAPPONI, L., JACKSON, D. B., MLODZIK, M. & BOHMANN, D. 2001. Drosophila Fos mediates ERK and JNK signals via distinct phosphorylation sites. *Genes Dev,* 15**,** 1540-53.

COLLINS, C. A., WAIRKAR, Y. P., JOHNSON, S. L. & DIANTONIO, A. 2006. Highwire restrains synaptic growth by attenuating a MAP kinase signal. *Neuron,* 51**,** 57-69.

COOKE, M. S., EVANS, M. D., DIZDAROGLU, M. & LUNEC, J. 2003. Oxidative DNA damage: mechanisms, mutation, and disease. *Faseb j,* 17**,** 1195-214.

COOPER, R. L. & NECKAMEYER, W. S. 1999. Dopaminergic modulation of motor neuron activity and neuromuscular function in Drosophila melanogaster. *Comp Biochem Physiol B Biochem Mol Biol,* 122**,** 199-210.

COPF, T., GOGUEL, V., LAMPIN-SAINT-AMAUX, A., SCAPLEHORN, N. & PREAT, T. 2011. Cytokine signaling through the JAK/STAT pathway is required for long-term memory in Drosophila. *Proc Natl Acad Sci U S A,* 108**,** 8059-64.

CRABTREE, M. J. & CHANNON, K. M. 2011. Synthesis and recycling of tetrahydrobiopterin in endothelial function and vascular disease. *Nitric Oxide,* 25**,** 81-8.

CRAWFORD, D. R. & DAVIES, K. J. 1994. Adaptive response and oxidative stress. *Environ Health Perspect,* 102**,** 25-8.

DAUBNER, S. C., LE, T. & WANG, S. 2011. Tyrosine Hydroxylase and Regulation of Dopamine Synthesis. *Arch Biochem Biophys,* 508**,** 1-12.

DAUER, W. & PRZEDBORSKI, S. 2003. Parkinson's disease: mechanisms and models. *Neuron,* 39**,** 889-909.

DAVIS, M. D., KAUFMAN, S. & MILSTIEN, S. 1988. The auto-oxidation of tetrahydrobiopterin. *Eur J Biochem,* 173**,** 345-51.
DE VRIES, D. D., VAN ENGELEN, B. G., GABREELS, F. J., RUITENBEEK, W. & VAN OOST, B. A. 1993. A second missense mutation in the mitochondrial ATPase 6 gene in Leigh's syndrome. *Ann Neurol,* 34**,** 410-2.
DEAS, E., WOOD, N. W. & PLUN-FAVREAU, H. 2011. Mitophagy and Parkinson's disease: The PINK1–parkin link(). *Biochim Biophys Acta,* 1813**,** 623-33.
DERYNCK, R. & ZHANG, Y. E. 2003. Smad-dependent and Smad-independent pathways in TGF-beta family signalling. *Nature,* 425**,** 577-84.
DU, J., XU, H., WEI, N., WAKIM, B., HALLIGAN, B., PRITCHARD, K. A. & SHI, Y. 2009. Identification of Proteins Interacting with GTP Cyclohydrolase I. *Biochem Biophys Res Commun,* 385**,** 143-7.
DUFFY, J. B. 2002. GAL4 system in Drosophila: a fly geneticist's Swiss army knife. *Genesis,* 34**,** 1-15.
DUTTAROY, A., PARKES, T., EMTAGE, P., KIRBY, K., BOULIANNE, G. L., WANG, X., HILLIKER, A. J. & PHILLIPS, J. P. 1997. The manganese superoxide dismutase gene of Drosophila: structure, expression, and evidence for regulation by MAP kinase. *DNA Cell Biol,* 16**,** 391-9.
ERESH, S., RIESE, J., JACKSON, D. B., BOHMANN, D. & BIENZ, M. 1997. A CREB-binding site as a target for decapentaplegic signalling during Drosophila endoderm induction. *Embo j,* 16**,** 2014-22.
ESPLUGUES, J. V. 2002. NO as a signalling molecule in the nervous system. *Br J Pharmacol,* 135**,** 1079-95.
ETTER, P. D., NARAYANAN, R., NAVRATILOVA, Z., PATEL, C., BOHMANN, D., JASPER, H. & RAMASWAMI, M. 2005. Synaptic and genomic responses to JNK and AP-1 signaling in Drosophila neurons. *BMC Neurosci,* 6**,** 39.
FATTMAN, C. L., CHANG, L. Y., TERMIN, T. A., PETERSEN, L., ENGHILD, J. J. & OURY, T. D. 2003. Enhanced bleomycin-induced pulmonary damage in mice lacking extracellular superoxide dismutase. *Free Radic Biol Med,* 35**,** 763-71.
FIELD, L. S., FURUKAWA, Y., O'HALLORAN, T. V. & CULOTTA, V. C. 2003. Factors controlling the uptake of yeast copper/zinc superoxide dismutase into mitochondria. *J Biol Chem,* 278**,** 28052-9.
FIRE, A., XU, S., MONTGOMERY, M. K., KOSTAS, S. A., DRIVER, S. E. & MELLO, C. C. 1998. Potent and specific genetic interference by double-stranded RNA in Caenorhabditis elegans. *Nature,* 391**,** 806-11.
FISHER, D. B. & KAUFMAN, S. 1973. Tetrahydropterin oxidation without hydroxylation catalyzed by rat liver phenylalanine hydroxylase. *J Biol Chem,* 248**,** 4300-4.
FORWOOD, J. K., LAM, M. H. & JANS, D. A. 2001. Nuclear import of Creb and AP-1 transcription factors requires importin-beta 1 and Ran but is independent of importin-alpha. *Biochemistry,* 40**,** 5208-17.
FRANK, S., MADLENER, M., PFEILSCHIFTER, J. & WERNER, S. 1998. Induction of inducible nitric oxide synthase and its corresponding tetrahydrobiopterin-cofactor-synthesizing enzyme GTP-cyclohydrolase I during cutaneous wound repair. *J Invest Dermatol,* 111**,** 1058-64.
FRIDOVICH, I. 1989. Superoxide dismutases. An adaptation to a paramagnetic gas. *J Biol Chem,* 264**,** 7761-4.
FUNDERBURK, C. D., BOWLING, K. M., XU, D., HUANG, Z. & O'DONNELL, J. M. 2006. A typical N-terminal extensions confer novel regulatory properties on GTP

cyclohydrolase isoforms in Drosophila melanogaster. *J Biol Chem,* 281**,** 33302-12.

FURUKAWA, Y. 1993. GTP Cyclohydrolase 1-Deficient Dopa-Responsive Dystonia. *In:* PAGON, R. A., ADAM, M. P., ARDINGER, H. H., WALLACE, S. E., AMEMIYA, A., BEAN, L. J. H., BIRD, T. D., FONG, C. T., MEFFORD, H. C., SMITH, R. J. H. & STEPHENS, K. (eds.) *GeneReviews(R).* Seattle (WA): University of Washington, Seattle. University of Washington, Seattle. All rights reserved.

GABAI, V. L., MERIIN, A. B., MOSSER, D. D., CARON, A. W., RITS, S., SHIFRIN, V. I. & SHERMAN, M. Y. 1997. Hsp70 prevents activation of stress kinases. A novel pathway of cellular thermotolerance. *J Biol Chem,* 272**,** 18033-7.

GABAI, V. L., MERIIN, A. B., YAGLOM, J. A., VOLLOCH, V. Z. & SHERMAN, M. Y. 1998. Role of Hsp70 in regulation of stress-kinase JNK: implications in apoptosis and aging. *FEBS Lett,* 438**,** 1-4.

GEROMEL, V., KADHOM, N., CEBALOS-PICOT, I., OUARI, O., POLIDORI, A., MUNNICH, A., ROTIG, A. & RUSTIN, P. 2001. Superoxide-induced massive apoptosis in cultured skin fibroblasts harboring the neurogenic ataxia retinitis pigmentosa (NARP) mutation in the ATPase-6 gene of the mitochondrial DNA. *Hum Mol Genet,* 10**,** 1221-8.

GROSS, E., SEVIER, C. S., HELDMAN, N., VITU, E., BENTZUR, M., KAISER, C. A., THORPE, C. & FASS, D. 2006. Generating disulfides enzymatically: reaction products and electron acceptors of the endoplasmic reticulum thiol oxidase Ero1p. *Proc Natl Acad Sci U S A,* 103**,** 299-304.

GUADAGNO, J., XU, X., KARAJGIKAR, M., BROWN, A. & CREGAN, S. P. 2013. Microglia-derived TNFalpha induces apoptosis in neural precursor cells via transcriptional activation of the Bcl-2 family member Puma. *Cell Death Dis,* 4**,** e538.

HALAZONETIS, T. D., GEORGOPOULOS, K., GREENBERG, M. E. & LEDER, P. 1988. c-Jun dimerizes with itself and with c-Fos, forming complexes of different DNA binding affinities. *Cell,* 55**,** 917-24.

HALLIWELL, B. 1996. Oxidative stress, nutrition and health. Experimental strategies for optimization of nutritional antioxidant intake in humans. *Free Radic Res,* 25**,** 57-74.

HALLIWELL B, G. J. 1989. *Free Radicals in Biology and Medicine. 2nd Edition. Clarendon Press. Oxford. UK,* 2nd Edition.

HAMAD, I., ARDA, N., PEKMEZ, M., KARAER, S. & TEMIZKAN, G. 2010. Intracellular scavenging activity of Trolox (6-hydroxy-2,5,7,8-tetramethylchromane-2-carboxylic acid) in the fission yeast, Schizosaccharomyces pombe. *J Nat Sci Biol Med,* 1**,** 16-21.

HARLAN, J. M., LEVINE, J. D., CALLAHAN, K. S., SCHWARTZ, B. R. & HARKER, L. A. 1984. Glutathione redox cycle protects cultured endothelial cells against lysis by extracellularly generated hydrogen peroxide. *J Clin Invest,* 73**,** 706-13.

HARMAN, D. 1992. Free radical theory of aging. *Mutat Res,* 275**,** 257-66.

HATAKEYAMA, K., INOUE, Y., HARADA, T. & KAGAMIYAMA, H. 1991. Cloning and sequencing of cDNA encoding rat GTP cyclohydrolase I. The first enzyme of the tetrahydrobiopterin biosynthetic pathway. *J Biol Chem,* 266**,** 765-9.

HAYASHI, Y., HOMMA, K. & ICHIJO, H. 2015. SOD1 in neurotoxicity and its controversial roles in SOD1 mutation-negative ALS. *Adv Biol Regul*.

HESS, J., ANGEL, P. & SCHORPP-KISTNER, M. 2004. AP-1 subunits: quarrel and harmony among siblings. *J Cell Sci,* 117**,** 5965-73.

HETTIARACHCHI, N., DALLAS, M., AL-OWAIS, M., GRIFFITHS, H., HOOPER, N., SCRAGG, J., BOYLE, J. & PEERS, C. 2014. Heme oxygenase-1 protects against Alzheimer's amyloid-beta(1-42)-induced toxicity via carbon monoxide production. *Cell Death Dis,* 5**,** e1569.

HEYMANN, D. 2006. Autophagy: A protective mechanism in response to stress and inflammation. *Curr Opin Investig Drugs,* 7**,** 443-50.

HIBI, M., LIN, A., SMEAL, T., MINDEN, A. & KARIN, M. 1993. Identification of an oncoprotein- and UV-responsive protein kinase that binds and potentiates the c-Jun activation domain. *Genes Dev,* 7**,** 2135-48.

HIDAKA, T., FURUNO, H., INOKUCHI, T. & OGURA, R. 1990. Effects of diethyl maleate (DEM), a glutathione depletor, on prostaglandin synthesis in the isolated perfused spleen of rabbits. *Arch Toxicol,* 64**,** 103-8.

HIRTH, F. 2010. Drosophila melanogaster in the Study of Human Neurodegeneration. *CNS Neurol Disord Drug Targets,* 9**,** 504-23.

HO, C., LAM, C., CHAN, M., CHEUNG, R., LAW, L., LIT, L., NG, K., SUEN, M. & TAI, H. 2003. Electrospray Ionisation Mass Spectrometry: Principles and Clinical Applications. *Clin Biochem Rev,* 24**,** 3-12.

HOLMGREN, A. & LU, J. 2010. Thioredoxin and thioredoxin reductase: current research with special reference to human disease. *Biochem Biophys Res Commun,* 396**,** 120-4.

HOU, X. S., GOLDSTEIN, E. S. & PERRIMON, N. 1997. Drosophila Jun relays the Jun amino-terminal kinase signal transduction pathway to the Decapentaplegic signal transduction pathway in regulating epithelial cell sheet movement. *Genes Dev,* 11**,** 1728-37.

HOULE, F., ROUSSEAU, S., MORRICE, N., LUC, M., MONGRAIN, S., TURNER, C. E., TANAKA, S., MOREAU, P. & HUOT, J. 2003. Extracellular signal-regulated kinase mediates phosphorylation of tropomyosin-1 to promote cytoskeleton remodeling in response to oxidative stress: impact on membrane blebbing. *Mol Biol Cell,* 14**,** 1418-32.

HULBERT, A. J., PAMPLONA, R., BUFFENSTEIN, R. & BUTTEMER, W. A. 2007. Life and death: metabolic rate, membrane composition, and life span of animals. *Physiol Rev,* 87**,** 1175-213.

HWANG, S., KIM, D., CHOI, G., AN, S. W., HONG, Y. K., SUH, Y. S., LEE, M. J. & CHO, K. S. 2010. Parkin suppresses c-Jun N-terminal kinase-induced cell death via transcriptional regulation in Drosophila. *Mol Cells,* 29**,** 575-80.

ICHIJO, H., NISHIDA, E., IRIE, K., TEN DIJKE, P., SAITOH, M., MORIGUCHI, T., TAKAGI, M., MATSUMOTO, K., MIYAZONO, K. & GOTOH, Y. 1997. Induction of apoptosis by ASK1, a mammalian MAPKKK that activates SAPK/JNK and p38 signaling pathways. *Science,* 275**,** 90-4.

ICHINOSE, H., OHYE, T., TAKAHASHI, E., SEKI, N., HORI, T., SEGAWA, M., NOMURA, Y., ENDO, K., TANAKA, H., TSUJI, S. & ET AL. 1994. Hereditary progressive dystonia with marked diurnal fluctuation caused by mutations in the GTP cyclohydrolase I gene. *Nat Genet,* 8**,** 236-42.

IP, Y. T. & DAVIS, R. J. 1998. Signal transduction by the c-Jun N-terminal kinase (JNK)--from inflammation to development. *Curr Opin Cell Biol,* 10**,** 205-19.

ISHIHAMA, Y., ODA, Y., TABATA, T., SATO, T., NAGASU, T., RAPPSILBER, J. & MANN, M. 2005. Exponentially modified protein abundance index (emPAI) for estimation of absolute protein amount in proteomics by the number of sequenced peptides per protein. *Mol Cell Proteomics,* 4**,** 1265-72.

ISHII, T., ITOH, K., TAKAHASHI, S., SATO, H., YANAGAWA, T., KATOH, Y., BANNAI, S. & YAMAMOTO, M. 2000. Transcription factor Nrf2 coordinately regulates a group of oxidative stress-inducible genes in macrophages. *J Biol Chem,* 275**,** 16023-9.

ITO, K., AWANO, W., SUZUKI, K., HIROMI, Y. & YAMAMOTO, D. 1997. The Drosophila mushroom body is a quadruple structure of clonal units each of which contains a virtually identical set of neurones and glial cells. *Development,* 124**,** 761-71.

ITOH, K., CHIBA, T., TAKAHASHI, S., ISHII, T., IGARASHI, K., KATOH, Y., OYAKE, T., HAYASHI, N., SATOH, K., HATAYAMA, I., YAMAMOTO, M. & NABESHIMA, Y. 1997. An Nrf2/small Maf heterodimer mediates the induction of phase II detoxifying enzyme genes through antioxidant response elements. *Biochem Biophys Res Commun,* 236**,** 313-22.

ITOH, K., WAKABAYASHI, N., KATOH, Y., ISHII, T., IGARASHI, K., ENGEL, J. D. & YAMAMOTO, M. 1999. Keap1 represses nuclear activation of antioxidant responsive elements by Nrf2 through binding to the amino-terminal Neh2 domain. *Genes Dev,* 13**,** 76-86.

JINDRA, M., GAZIOVA, I., UHLIROVA, M., OKABE, M., HIROMI, Y. & HIROSE, S. 2004. Coactivator MBF1 preserves the redox-dependent AP-1 activity during oxidative stress in Drosophila. *Embo j,* 23**,** 3538-47.

JOHANSEN, J., HALPERN, M. E., JOHANSEN, K. M. & KESHISHIAN, H. 1989a. Stereotypic morphology of glutamatergic synapses on identified muscle cells of Drosophila larvae. *J Neurosci,* 9**,** 710-25.

JOHANSEN, J., HALPERN, M. E. & KESHISHIAN, H. 1989b. Axonal guidance and the development of muscle fiber-specific innervation in Drosophila embryos. *J Neurosci,* 9**,** 4318-32.

JOHRI, A. & BEAL, M. F. 2012. Mitochondrial dysfunction in neurodegenerative diseases. *J Pharmacol Exp Ther,* 342**,** 619-30.

JOLLY, R. D., DOUGLAS, B. V., DAVEY, P. M. & ROIRI, J. E. 1995. Lipofuscin in bovine muscle and brain: a model for studying age pigment. *Gerontology,* 41 Suppl 2**,** 283-95.

KAMIMURA, K., UENO, K., NAKAGAWA, J., HAMADA, R., SAITOE, M. & MAEDA, N. 2013. Perlecan regulates bidirectional Wnt signaling at the Drosophila neuromuscular junction. *J Cell Biol,* 200**,** 219-33.

KARIN, M. 1995. The regulation of AP-1 activity by mitogen-activated protein kinases. *J Biol Chem,* 270**,** 16483-6.

KATZ, M. L. & ROBISON, W. G., JR. 2002. What is lipofuscin? Defining characteristics and differentiation from other autofluorescent lysosomal storage bodies. *Arch Gerontol Geriatr,* 34**,** 169-84.

KAUFMAN, S. 1999. A model of human phenylalanine metabolism in normal subjects and in phenylketonuric patients. *Proc Natl Acad Sci U S A,* 96**,** 3160-4.

KESHISHIAN, H., BROADIE, K., CHIBA, A. & BATE, M. 1996. The drosophila neuromuscular junction: a model system for studying synaptic development and function. *Annu Rev Neurosci,* 19**,** 545-75.

KIM, H., KIM, K. & YIM, J. 2013. Biosynthesis of drosopterins, the red eye pigments of Drosophila melanogaster. *IUBMB Life,* 65**,** 334-40.

KIM, I., RODRIGUEZ-ENRIQUEZ, S. & LEMASTERS, J. J. 2007a. Selective degradation of mitochondria by mitophagy. *Arch Biochem Biophys,* 462**,** 245-53.

KIM, L. K., CHOI, U. Y., CHO, H. S., LEE, J. S., LEE, W. B., KIM, J., JEONG, K., SHIM, J., KIM-HA, J. & KIM, Y. J. 2007b. Down-regulation of NF-kappaB target genes by the AP-1 and STAT complex during the innate immune response in Drosophila. *PLoS Biol,* 5**,** e238.

KITTEL, R. J., WICHMANN, C., RASSE, T. M., FOUQUET, W., SCHMIDT, M., SCHMID, A., WAGH, D. A., PAWLU, C., KELLNER, R. R., WILLIG, K. I., HELL, S. W., BUCHNER, E., HECKMANN, M. & SIGRIST, S. J. 2006. Bruchpilot promotes active zone assembly, Ca2+ channel clustering, and vesicle release. *Science,* 312**,** 1051-4.

KOH, Y. H., REHFELD, K. & GANETZKY, B. 2004. A Drosophila model of early onset torsion dystonia suggests impairment in TGF-beta signaling. *Hum Mol Genet,* 13**,** 2019-30.

KOH, Y. H., RUIZ-CANADA, C., GORCZYCA, M. & BUDNIK, V. 2002. The Ras1-mitogen-activated protein kinase signal transduction pathway regulates synaptic plasticity through fasciclin II-mediated cell adhesion. *J Neurosci,* 22**,** 2496-504.

KOJIMA, S., ONA, S., IIZUKA, I., ARAI, T., MORI, H. & KUBOTA, K. 1995. Antioxidative activity of 5,6,7,8-tetrahydrobiopterin and its inhibitory effect on paraquat-induced cell toxicity in cultured rat hepatocytes. *Free Radic Res,* 23**,** 419-30.

KONG, J. & XU, Z. 1998. Massive mitochondrial degeneration in motor neurons triggers the onset of amyotrophic lateral sclerosis in mice expressing a mutant SOD1. *J Neurosci,* 18**,** 3241-50.

KÖNIG, H. G., KÖGEL, D., RAMI, A. & PREHN, J. H. M. 2005. TGF-β1 activates two distinct type I receptors in neurons: implications for neuronal NF-κB signaling. *J Cell Biol,* 168**,** 1077-86.

KOSHIMURA, K., MURAKAMI, Y., TANAKA, J. & KATO, Y. 1998. Self-protection of PC12 cells by 6R-tetrahydrobiopterin from nitric oxide toxicity. *Journal of Neuroscience Research,* 54**,** 664-672.

KOSHLAND, D. E., JR. 1992. The molecule of the year. *Science,* 258**,** 1861.

KUKREJA, R. C., KONTOS, H. A., HESS, M. L. & ELLIS, E. F. 1986. PGH synthase and lipoxygenase generate superoxide in the presence of NADH or NADPH. *Circ Res,* 59**,** 612-9.

KURANAGA, E., KANUKA, H., IGAKI, T., SAWAMOTO, K., ICHIJO, H., OKANO, H. & MIURA, M. 2002. Reaper-mediated inhibition of DIAP1-induced DTRAF1 degradation results in activation of JNK in Drosophila. *Nat Cell Biol,* 4**,** 705-10.

KURZ, T., TERMAN, A., GUSTAFSSON, B. & BRUNK, U. T. 2008. Lysosomes in iron metabolism, ageing and apoptosis. *Histochem Cell Biol,* 129**,** 389-406.

KYRIAKIS, J. M. 1999. Activation of the AP-1 transcription factor by inflammatory cytokines of the TNF family. *Gene Expr,* 7**,** 217-31.

LANDGRAF, M., SANCHEZ-SORIANO, N., TECHNAU, G. M., URBAN, J. & PROKOP, A. 2003. Charting the Drosophila neuropile: a strategy for the standardised characterisation of genetically amenable neurites. *Dev Biol,* 260**,** 207-25.

LAUGHON, A. & GESTELAND, R. F. 1984. Primary structure of the Saccharomyces cerevisiae GAL4 gene. *Mol Cell Biol,* 4**,** 260-7.

LEE, T. & LUO, L. 1999. Mosaic analysis with a repressible cell marker for studies of gene function in neuronal morphogenesis. *Neuron,* 22**,** 451-61.

LEVINE, B. & KLIONSKY, D. J. 2004. Development by self-digestion: molecular mechanisms and biological functions of autophagy. *Dev Cell,* 6**,** 463-77.

LEVINE, B. & KROEMER, G. 2008. Autophagy in the pathogenesis of disease. *Cell,* 132**,** 27-42.
LEWTHWAITE, A. J., LAMBERT, T. D., ROLFE, E. B., OLGIATI, S., QUADRI, M., SIMONS, E. J., MORRISON, K. E., BONIFATI, V. & NICHOLL, D. J. 2015. Novel GCH1 variant in Dopa-responsive dystonia and Parkinson's disease. *Parkinsonism Relat Disord,* 21**,** 394-7.
LI, D. D., WANG, L. L., DENG, R., TANG, J., SHEN, Y., GUO, J. F., WANG, Y., XIA, L. P., FENG, G. K., LIU, Q. Q., HUANG, W. L., ZENG, Y. X. & ZHU, X. F. 2009a. The pivotal role of c-Jun NH2-terminal kinase-mediated Beclin 1 expression during anticancer agents-induced autophagy in cancer cells. *Oncogene,* 28**,** 886-98.
LI, S., HONG, S., SHEPARDSON, N. E., WALSH, D. M., SHANKAR, G. M. & SELKOE, D. 2009b. Soluble oligomers of amyloid Beta protein facilitate hippocampal long-term depression by disrupting neuronal glutamate uptake. *Neuron,* 62**,** 788-801.
LIBERATI, N. T., DATTO, M. B., FREDERICK, J. P., SHEN, X., WONG, C., ROUGIER-CHAPMAN, E. M. & WANG, X. F. 1999. Smads bind directly to the Jun family of AP-1 transcription factors. *Proc Natl Acad Sci U S A,* 96**,** 4844-9.
LIEBL, F. L. 2006. Highwire balances synaptic growth. *J Neurosci,* 26**,** 2143-4.
LIN, A., MINDEN, A., MARTINETTO, H., CLARET, F. X., LANGE-CARTER, C., MERCURIO, F., JOHNSON, G. L. & KARIN, M. 1995. Identification of a dual specificity kinase that activates the Jun kinases and p38-Mpk2. *Science,* 268**,** 286-90.
LIPINSKI, B. 2011. Hydroxyl radical and its scavengers in health and disease. *Oxid Med Cell Longev,* 2011**,** 809696.
LLOYD, D. R., PHILLIPS, D. H. & CARMICHAEL, P. L. 1997. Generation of putative intrastrand cross-links and strand breaks in DNA by transition metal ion-mediated oxygen radical attack. *Chem Res Toxicol,* 10**,** 393-400.
LOWELL, B. B. & SHULMAN, G. I. 2005. Mitochondrial dysfunction and type 2 diabetes. *Science,* 307**,** 384-7.
LUO, H., ASHA, H., KOCKEL, L., PARKE, T., MLODZIK, M. & DEAROLF, C. R. 1999. The Drosophila Jak kinase hopscotch is required for multiple developmental processes in the eye. *Dev Biol,* 213**,** 432-41.
MA, X., XU, W., ZHANG, D., YANG, Y., LI, W. & XUE, L. 2015. Wallenda regulates JNK-mediated cell death in Drosophila. *Cell Death Dis,* 6**,** e1737-.
MACKAY, W. J., REYNOLDS, E. R. & O'DONNELL, J. M. 1985. Tissue-specific and complex complementation patterns in the Punch locus of Drosophila melanogaster. *Genetics,* 111**,** 885-904.
MAGRANE, J., SAHAWNEH, M. A., PRZEDBORSKI, S., ESTEVEZ, A. G. & MANFREDI, G. 2012. Mitochondrial dynamics and bioenergetic dysfunction is associated with synaptic alterations in mutant SOD1 motor neurons. *J Neurosci,* 32**,** 229-42.
MAKER, H. S., WEISS, C., SILIDES, D. J. & COHEN, G. 1981. Coupling of dopamine oxidation (monoamine oxidase activity) to glutathione oxidation via the generation of hydrogen peroxide in rat brain homogenates. *J Neurochem,* 36**,** 589-93.
MALLICK, P. & KUSTER, B. 2010. Proteomics: a pragmatic perspective. *Nat Biotechnol,* 28**,** 695-709.

MARÍ, M., MORALES, A., COLELL, A., GARCÍA-RUIZ, C. & FERNÁNDEZ-CHECA JÉ, C. 2009. Mitochondrial Glutathione, a Key Survival Antioxidant. *Antioxid Redox Signal,* 11**,** 2685-700.

MARNETT, L. J. & PLASTARAS, J. P. 2001. Endogenous DNA damage and mutation. *Trends Genet,* 17**,** 214-21.

MARQUES, G., BAO, H., HAERRY, T. E., SHIMELL, M. J., DUCHEK, P., ZHANG, B. & O'CONNOR, M. B. 2002. The Drosophila BMP type II receptor Wishful Thinking regulates neuromuscular synapse morphology and function. *Neuron,* 33**,** 529-43.

MARTÍN-BLANCO, E., GAMPEL, A., RING, J., VIRDEE, K., KIROV, N., TOLKOVSKY, A. M. & MARTINEZ-ARIAS, A. 1998. puckered encodes a phosphatase that mediates a feedback loop regulating JNK activity during dorsal closure in Drosophila. *Genes Dev,* 12**,** 557-70.

MARTINDALE, J. L. & HOLBROOK, N. J. 2002. Cellular response to oxidative stress: signaling for suicide and survival. *J Cell Physiol,* 192**,** 1-15.

MARTINS, R. N., HARPER, C. G., STOKES, G. B. & MASTERS, C. L. 1986. Increased cerebral glucose-6-phosphate dehydrogenase activity in Alzheimer's disease may reflect oxidative stress. *J Neurochem,* 46**,** 1042-5.

MASSARO, C. M., PIELAGE, J. & DAVIS, G. W. 2009. Molecular mechanisms that enhance synapse stability despite persistent disruption of the spectrin/ankyrin/microtubule cytoskeleton. *J Cell Biol,* 187**,** 101-17.

MATTSON, M. P. & LIU, D. 2002. Energetics and oxidative stress in synaptic plasticity and neurodegenerative disorders. *Neuromolecular Med,* 2**,** 215-31.

MAY, D. W. 1901. CATALASE, A NEW ENZYM OF GENERAL OCCURRENCE. *Science,* 14**,** 815-6.

MAZZITELLI, S., XU, P., FERRER, I., DAVIS, R. J. & TOURNIER, C. 2011. The loss of c-Jun N-terminal protein kinase activity prevents the amyloidogenic cleavage of amyloid precursor protein and the formation of amyloid plaques in vivo. *J Neurosci,* 31**,** 16969-76.

MCCABE, B. D., HOM, S., ABERLE, H., FETTER, R. D., MARQUES, G., HAERRY, T. E., WAN, H., O'CONNOR, M. B., GOODMAN, C. S. & HAGHIGHI, A. P. 2004. Highwire regulates presynaptic BMP signaling essential for synaptic growth. *Neuron,* 41**,** 891-905.

MCCABE, B. D., MARQUES, G., HAGHIGHI, A. P., FETTER, R. D., CROTTY, M. L., HAERRY, T. E., GOODMAN, C. S. & O'CONNOR, M. B. 2003. The BMP homolog Gbb provides a retrograde signal that regulates synaptic growth at the Drosophila neuromuscular junction. *Neuron,* 39**,** 241-54.

MCCORD, J. M. & FRIDOVICH, I. 1969a. Superoxide dismutase. An enzymic function for erythrocuprein (hemocuprein). *J Biol Chem,* 244**,** 6049-55.

MCCORD, J. M. & FRIDOVICH, I. 1969b. The utility of superoxide dismutase in studying free radical reactions. I. Radicals generated by the interaction of sulfite, dimethyl sulfoxide, and oxygen. *J Biol Chem,* 244**,** 6056-63.

MCNALLY, J. S., DAVIS, M. E., GIDDENS, D. P., SAHA, A., HWANG, J., DIKALOV, S., JO, H. & HARRISON, D. G. 2003. Role of xanthine oxidoreductase and NAD(P)H oxidase in endothelial superoxide production in response to oscillatory shear stress. *Am J Physiol Heart Circ Physiol,* 285**,** H2290-7.

MENCACCI, N. E., ISAIAS, I. U., REICH, M. M., GANOS, C., PLAGNOL, V., POLKE, J. M., BRAS, J., HERSHESON, J., STAMELOU, M., PITTMAN, A. M., NOYCE, A. J., MOK, K. Y., OPLADEN, T., KUNSTMANN, E., HODECKER, S., MUNCHAU, A.,

VOLKMANN, J., SAMNICK, S., SIDLE, K., NANJI, T., SWEENEY, M. G., HOULDEN, H., BATLA, A., ZECCHINELLI, A. L., PEZZOLI, G., MAROTTA, G., LEES, A., ALEGRIA, P., KRACK, P., CORMIER-DEQUAIRE, F., LESAGE, S., BRICE, A., HEUTINK, P., GASSER, T., LUBBE, S. J., MORRIS, H. R., TABA, P., KOKS, S., MAJOUNIE, E., RAPHAEL GIBBS, J., SINGLETON, A., HARDY, J., KLEBE, S., BHATIA, K. P. & WOOD, N. W. 2014. Parkinson's disease in GTP cyclohydrolase 1 mutation carriers. *Brain,* 137**,** 2480-92.

MENON, K. P., CARRILLO, R. A. & ZINN, K. 2013. Development and plasticity of the Drosophila larval neuromuscular junction. *Wiley Interdiscip Rev Dev Biol,* 2**,** 647-70.

MICHIELS, C. 2004. Physiological and pathological responses to hypoxia. *Am J Pathol,* 164**,** 1875-82.

MILTON, V. J., JARRETT, H. E., GOWERS, K., CHALAK, S., BRIGGS, L., ROBINSON, I. M. & SWEENEY, S. T. 2011. Oxidative stress induces overgrowth of the Drosophila neuromuscular junction. *Proc Natl Acad Sci U S A,* 108**,** 17521-6.

MISSIRLIS, F., HU, J., KIRBY, K., HILLIKER, A. J., ROUAULT, T. A. & PHILLIPS, J. P. 2003. Compartment-specific protection of iron-sulfur proteins by superoxide dismutase. *J Biol Chem,* 278**,** 47365-9.

MOLEJON, M. I., ROPOLO, A., RE, A. L., BOGGIO, V. & VACCARO, M. I. 2013. The VMP1-Beclin 1 interaction regulates autophagy induction. *Sci Rep,* 3**,** 1055.

MONASTIRIOTI, M., GORCZYCA, M., RAPUS, J., ECKERT, M., WHITE, K. & BUDNIK, V. 1995. Octopamine immunoreactivity in the fruit fly Drosophila melanogaster. *J Comp Neurol,* 356**,** 275-87.

MORIGUCHI, T., TOYOSHIMA, F., MASUYAMA, N., HANAFUSA, H., GOTOH, Y. & NISHIDA, E. 1997. A novel SAPK/JNK kinase, MKK7, stimulated by TNFalpha and cellular stresses. *Embo j,* 16**,** 7045-53.

MORTIBOYS, H., JOHANSEN, K. K., AASLY, J. O. & BANDMANN, O. 2010. Mitochondrial impairment in patients with Parkinson disease with the G2019S mutation in LRRK2. *Neurology,* 75**,** 2017-20.

MULLER, H. J. 1918. Genetic Variability, Twin Hybrids and Constant Hybrids, in a Case of Balanced Lethal Factors. *Genetics,* 3**,** 422-99.

MURPHY, S. 2000. Production of nitric oxide by glial cells: regulation and potential roles in the CNS. *Glia,* 29**,** 1-13.

NAGATSU, T. & ICHINOSE, H. 1999. Regulation of pteridine-requiring enzymes by the cofactor tetrahydrobiopterin. *Mol Neurobiol,* 19**,** 79-96.

NAKAMURA, K., BINDOKAS, V. P., KOWLESSUR, D., ELAS, M., MILSTIEN, S., MARKS, J. D., HALPERN, H. J. & KANG, U. J. 2001. Tetrahydrobiopterin scavenges superoxide in dopaminergic neurons. *J Biol Chem,* 276**,** 34402-7.

NAKANO, Y., FUJITANI, K., KURIHARA, J., RAGAN, J., USUI-AOKI, K., SHIMODA, L., LUKACSOVICH, T., SUZUKI, K., SEZAKI, M., SANO, Y., UEDA, R., AWANO, W., KANEDA, M., UMEDA, M. & YAMAMOTO, D. 2001. Mutations in the Novel Membrane Protein Spinster Interfere with Programmed Cell Death and Cause Neural Degeneration in Drosophila melanogaster. *Mol Cell Biol,* 21**,** 3775-88.

NALLS, M. A., PANKRATZ, N., LILL, C. M., DO, C. B., HERNANDEZ, D. G., SAAD, M., DESTEFANO, A. L., KARA, E., BRAS, J., SHARMA, M., SCHULTE, C., KELLER, M. F., AREPALLI, S., LETSON, C., EDSALL, C., STEFANSSON, H., LIU, X., PLINER, H., LEE, J. H., CHENG, R., IKRAM, M. A., IOANNIDIS, J. P., HADJIGEORGIOU, G. M., BIS, J. C., MARTINEZ, M., PERLMUTTER, J. S., GOATE, A., MARDER, K., FISKE,

B., SUTHERLAND, M., XIROMERISIOU, G., MYERS, R. H., CLARK, L. N., STEFANSSON, K., HARDY, J. A., HEUTINK, P., CHEN, H., WOOD, N. W., HOULDEN, H., PAYAMI, H., BRICE, A., SCOTT, W. K., GASSER, T., BERTRAM, L., ERIKSSON, N., FOROUD, T. & SINGLETON, A. B. 2014. Large-scale meta-analysis of genome-wide association data identifies six new risk loci for Parkinson's disease. *Nat Genet,* 46**,** 989-93.

NAR, H., HUBER, R., MEINING, W., SCHMID, C., WEINKAUF, S. & BACHER, A. 1995. Atomic structure of GTP cyclohydrolase I. *Structure,* 3**,** 459-66.

NICOLAS CÉ , S., PEINEAU, S., AMICI, M., CSABA, Z., FAFOURI, A., JAVALET, C., COLLETT V , J., HILDEBRANDT, L., SEATON, G., CHOI, S. L., SIM, S. E., BRADLEY, C., LEE, K., ZHUO, M., KAANG, B. K., GRESSENS, P., DOURNAUD, P., FITZJOHN S , M., BORTOLOTTO Z , A., CHO, K. & COLLINGRIDGE G , L. 2012. The JAK/STAT Pathway Is Involved in Synaptic Plasticity. *Neuron,* 73**,** 374-90.

NOORI 2012. An overview of oxidative stress and antioxidant defensive system. 1:413. DOI: 10.4172/scientificreports.413.

NÜSSLEIN-VOLHARD, C., WIESCHAUS, E. & KLUDING, H. 1984. Mutations affecting the pattern of the larval cuticle inDrosophila melanogaster. *Wilhelm Roux's archives of developmental biology,* 193**,** 267-282.

O'CONNOR-GILES, K. M., HO, L. L. & GANETZKY, B. 2008. Nervous wreck interacts with thickveins and the endocytic machinery to attenuate retrograde BMP signaling during synaptic growth. *Neuron,* 58**,** 507-18.

O'DONNELL, V. B. & AZZI, A. 1996. High rates of extracellular superoxide generation by cultured human fibroblasts: involvement of a lipid-metabolizing enzyme. *Biochem J,* 318 (Pt 3)**,** 805-12.

OPPENHEIM, R. W. 1991. Cell death during development of the nervous system. *Annu Rev Neurosci,* 14**,** 453-501.

PACKARD, M., KOO, E. S., GORCZYCA, M., SHARPE, J., CUMBERLEDGE, S. & BUDNIK, V. 2002. The Drosophila Wnt, wingless, provides an essential signal for pre- and postsynaptic differentiation. *Cell,* 111**,** 319-30.

PALADE, G. E. 1953. An electron microscope study of the mitochondrial structure. *J Histochem Cytochem,* 1**,** 188-211.

PARKES, T. L., ELIA, A. J., DICKINSON, D., HILLIKER, A. J., PHILLIPS, J. P. & BOULIANNE, G. L. 1998. Extension of Drosophila lifespan by overexpression of human SOD1 in motorneurons. *Nat Genet,* 19**,** 171-4.

PATHAK, R., CHEEMA, A. K., BOCA, S. M., KRAGER, K. J., HAUER-JENSEN, M. & AYKIN-BURNS, N. 2015. Modulation of Radiation Response by the Tetrahydrobiopterin Pathway. *Antioxidants (Basel),* 4**,** 68-81.

PENG, J. & ANDERSEN, J. K. 2003. The role of c-Jun N-terminal kinase (JNK) in Parkinson's disease. *IUBMB Life,* 55**,** 267-71.

PEPPER, A., BHOGAL, B. & JONGENS, T. 2012. Tandem Affinity Purification in Drosophila Heads and Ovaries. *Bio Protoc,* 2.

PERKINS, K. K., ADMON, A., PATEL, N. & TJIAN, R. 1990. The Drosophila Fos-related AP-1 protein is a developmentally regulated transcription factor. *Genes Dev,* 4**,** 822-34.

PERRIMON, N., NI, J. Q. & PERKINS, L. 2010. In vivo RNAi: Today and Tomorrow. *Cold Spring Harb Perspect Biol,* 2.

PIERCE, G. L. & LAROCCA, T. J. 2008. Reduced vascular tetrahydrobiopterin (BH(4)) and endothelial function with ageing: is it time for a chronic BH(4)

supplementation trial in middle-aged and older adults? *J Physiol,* 586**,** 2673-4.

PILGRAM, G. S., POTIKANOND, S., BAINES, R. A., FRADKIN, L. G. & NOORDERMEER, J. N. 2010. The roles of the dystrophin-associated glycoprotein complex at the synapse. *Mol Neurobiol,* 41**,** 1-21.

RADISKY, D. C. & KAPLAN, J. 1998. Iron in cytosolic ferritin can be recycled through lysosomal degradation in human fibroblasts. *Biochem J,* 336 (Pt 1)**,** 201-5.

RAHMANI, M., NADORI, F., DURAND-SCHNEIDER, A. M., LARDEUX, B. & BERNUAU, D. 1999. Hepatocyte growth factor activates the AP-1 complex: a comparison between normal and transformed rat hepatocytes. *J Hepatol,* 30**,** 916-25.

RANDERATH, K., RANDERATH, E., SMITH, C. V. & CHANG, J. 1996. Structural origins of bulky oxidative DNA adducts (type II I-compounds) as deduced by oxidation of oligonucleotides of known sequence. *Chem Res Toxicol,* 9**,** 247-54.

RAWSON, J. M., LEE, M., KENNEDY, E. L. & SELLECK, S. B. 2003. Drosophila neuromuscular synapse assembly and function require the TGF-beta type I receptor saxophone and the transcription factor Mad. *J Neurobiol,* 55**,** 134-50.

REITER, L. T., POTOCKI, L., CHIEN, S., GRIBSKOV, M. & BIER, E. 2001. A systematic analysis of human disease-associated gene sequences in Drosophila melanogaster. *Genome Res,* 11**,** 1114-25.

RENIER, N., ADAMS, E. L., KIRST, C., WU, Z., AZEVEDO, R., KOHL, J., AUTRY, A. E., KADIRI, L., UMADEVI VENKATARAJU, K., ZHOU, Y., WANG, V. X., TANG, C. Y., OLSEN, O., DULAC, C., OSTEN, P. & TESSIER-LAVIGNE, M. 2016. Mapping of Brain Activity by Automated Volume Analysis of Immediate Early Genes. *Cell,* 165**,** 1789-802.

RHEE, S. G., KANG, S. W., CHANG, T. S., JEONG, W. & KIM, K. 2001. Peroxiredoxin, a novel family of peroxidases. *IUBMB Life,* 52**,** 35-41.

RHEUBEN, M. B., YOSHIHARA, M. & KIDOKORO, Y. 1999. Ultrastructural correlates of neuromuscular junction development. *Int Rev Neurobiol,* 43**,** 69-92.

RICHARDSON, J., THOMAS, K. A., RUBIN, B. H. & RICHARDSON, D. C. 1975. Crystal structure of bovine Cu,Zn superoxide dismutase at 3 A resolution: chain tracing and metal ligands. *Proc Natl Acad Sci U S A,* 72**,** 1349-53.

RING, J. M. & MARTINEZ ARIAS, A. 1993. puckered, a gene involved in position-specific cell differentiation in the dorsal epidermis of the Drosophila larva. *Dev Suppl***,** 251-9.

ROCHE, J. P., PACKARD, M. C., MOECKEL-COLE, S. & BUDNIK, V. 2002. Regulation of synaptic plasticity and synaptic vesicle dynamics by the PDZ protein Scribble. *J Neurosci,* 22**,** 6471-9.

RONNBACK, A., PAVLOV, P. F., MANSORY, M., GONZE, P., MARLIERE, N., WINBLAD, B., GRAFF, C. & BEHBAHANI, H. 2015. Mitochondrial dysfunction in a transgenic mouse model expressing human amyloid precursor protein (APP) with the Arctic mutation. *J Neurochem*.

ROOTE, J. & PROKOP, A. 2013. How to design a genetic mating scheme: a basic training package for Drosophila genetics. *G3 (Bethesda),* 3**,** 353-8.

ROSE, M. R. (1991). Evolutionary Biology of Aging. New York: Oxford University Press.

ROY, P., ROY, S. K., MITRA, A. & KULKARNI, A. P. 1994. Superoxide generation by lipoxygenase in the presence of NADH and NADPH. *Biochim Biophys Acta,* 1214**,** 171-9.

RUBIN, G. M. & LEWIS, E. B. 2000. A brief history of Drosophila's contributions to genome research. *Science,* 287**,** 2216-8.

SAITOH, M., NISHITOH, H., FUJII, M., TAKEDA, K., TOBIUME, K., SAWADA, Y., KAWABATA, M., MIYAZONO, K. & ICHIJO, H. 1998. Mammalian thioredoxin is a direct inhibitor of apoptosis signal-regulating kinase (ASK) 1. *Embo j,* 17**,** 2596-606.

SANYAL, S., NARAYANAN, R., CONSOULAS, C. & RAMASWAMI, M. 2003. Evidence for cell autonomous AP1 function in regulation of Drosophila motor-neuron plasticity. *BMC Neurosci,* 4**,** 20.

SANYAL, S., SANDSTROM, D. J., HOEFFER, C. A. & RAMASWAMI, M. 2002. AP-1 functions upstream of CREB to control synaptic plasticity in Drosophila. *Nature,* 416**,** 870-4.

SATHYANARAYANA, P., BARTHWAL, M. K., LANE, M. E., ACEVEDO, S. F., SKOULAKIS, E. M., BERGMANN, A. & RANA, A. 2003. Drosophila mixed lineage kinase/slipper, a missing biochemical link in Drosophila JNK signaling. *Biochim Biophys Acta,* 1640**,** 77-84.

SCHUSTER, C. M., DAVIS, G. W., FETTER, R. D. & GOODMAN, C. S. 1996. Genetic dissection of structural and functional components of synaptic plasticity. I. Fasciclin II controls synaptic stabilization and growth. *Neuron,* 17**,** 641-54.

SCOTT, R. C., JUHASZ, G. & NEUFELD, T. P. 2007. Direct induction of autophagy by Atg1 inhibits cell growth and induces apoptotic cell death. *Curr Biol,* 17**,** 1-11.

SCOTT-BURDEN, T. 1995. Regulation of nitric oxide production by tetrahydrobiopterin. *Circulation,* 91**,** 248-50.

SHEN, K. & COWAN, C. W. 2010. Guidance molecules in synapse formation and plasticity. *Cold Spring Harb Perspect Biol,* 2**,** a001842.

SHEN, W. & GANETZKY, B. 2009. Autophagy promotes synapse development in Drosophila. *J Cell Biol,* 187**,** 71-9.

SHIMIZU, S., SHIOTA, K., YAMAMOTO, S., MIYASAKA, Y., ISHII, M., WATABE, T., NISHIDA, M., MORI, Y., YAMAMOTO, T. & KIUCHI, Y. 2003. Hydrogen peroxide stimulates tetrahydrobiopterin synthesis through the induction of GTP-cyclohydrolase I and increases nitric oxide synthase activity in vascular endothelial cells. *Free Radic Biol Med,* 34**,** 1343-52.

SIES, H. 1997. Oxidative stress: oxidants and antioxidants. *Exp Physiol,* 82**,** 291-5.

SIMONSEN, A., CUMMING, R. C., BRECH, A., ISAKSON, P., SCHUBERT, D. R. & FINLEY, K. D. 2008. Promoting basal levels of autophagy in the nervous system enhances longevity and oxidant resistance in adult Drosophila. *Autophagy,* 4**,** 176-84.

SONNTAG, C. V. 1987. The Chemical Basis of Radiation Biology. *Taylor and Francis New York.*

SORBI, S., BIRD, E. D. & BLASS, J. P. 1983. Decreased pyruvate dehydrogenase complex activity in Huntington and Alzheimer brain. *Ann Neurol,* 13**,** 72-8.

SPINA, M. B. & COHEN, G. 1989. Dopamine turnover and glutathione oxidation: implications for Parkinson disease. *Proc Natl Acad Sci U S A,* 86**,** 1398-400.

SPOKONY, R. & WHITE, K. 2013. *RE: Spokony insertions.*

ST-PIERRE, J., BUCKINGHAM, J. A., ROEBUCK, S. J. & BRAND, M. D. 2002. Topology of superoxide production from different sites in the mitochondrial electron transport chain. *J Biol Chem,* 277**,** 44784-90.

SU, Y. C., TREISMAN, J. E. & SKOLNIK, E. Y. 1998. The Drosophila Ste20-related kinase misshapen is required for embryonic dorsal closure and acts through a JNK MAPK module on an evolutionarily conserved signaling pathway. *Genes Dev,* 12**,** 2371-80.

SÜDHOF, T. C. 2012. The Presynaptic Active Zone. *Neuron,* 75**,** 11-25.

SWEENEY, S. T. & DAVIS, G. W. 2002. Unrestricted synaptic growth in spinster-a late endosomal protein implicated in TGF-beta-mediated synaptic growth regulation. *Neuron,* 36**,** 403-16.

SWERDLOW, R. H. 2007. Mitochondria in cybrids containing mtDNA from persons with mitochondriopathies. *J Neurosci Res,* 85**,** 3416-28.

SWERDLOW, R. H., BURNS, J. M. & KHAN, S. M. 2010. The Alzheimer's disease mitochondrial cascade hypothesis. *J Alzheimers Dis,* 20 Suppl 2**,** S265-79.

SZKLARCZYK, D., FRANCESCHINI, A., WYDER, S., FORSLUND, K., HELLER, D., HUERTA-CEPAS, J., SIMONOVIC, M., ROTH, A., SANTOS, A., TSAFOU, K. P., KUHN, M., BORK, P., JENSEN, L. J. & VON MERING, C. 2015. STRING v10: protein-protein interaction networks, integrated over the tree of life. *Nucleic Acids Res,* 43**,** D447-52.

TAGUCHI, K., MOTOHASHI, H. & YAMAMOTO, M. 2011. Molecular mechanisms of the Keap1-Nrf2 pathway in stress response and cancer evolution. *Genes Cells,* 16**,** 123-40.

TAYLOR, R. W. & TURNBULL, D. M. 2005. MITOCHONDRIAL DNA MUTATIONS IN HUMAN DISEASE. *Nat Rev Genet,* 6**,** 389-402.

TEGEDER, I., COSTIGAN, M., GRIFFIN, R. S., ABELE, A., BELFER, I., SCHMIDT, H., EHNERT, C., NEJIM, J., MARIAN, C., SCHOLZ, J., WU, T., ALLCHORNE, A., DIATCHENKO, L., BINSHTOK, A. M., GOLDMAN, D., ADOLPH, J., SAMA, S., ATLAS, S. J., CARLEZON, W. A., PARSEGIAN, A., LOTSCH, J., FILLINGIM, R. B., MAIXNER, W., GEISSLINGER, G., MAX, M. B. & WOOLF, C. J. 2006. GTP cyclohydrolase and tetrahydrobiopterin regulate pain sensitivity and persistence. *Nat Med,* 12**,** 1269-77.

TESSEUR, I., ZOU, K., ESPOSITO, L., BARD, F., BERBER, E., CAN, J. V., LIN, A. H., CREWS, L., TREMBLAY, P., MATHEWS, P., MUCKE, L., MASLIAH, E. & WYSS-CORAY, T. 2006. Deficiency in neuronal TGF-beta signaling promotes neurodegeneration and Alzheimer's pathology. *J Clin Invest,* 116**,** 3060-9.

THOMPSON, V. 1977. Recombination and response to selection in Drosophila melanogaster. *Genetics,* 85**,** 125-40.

THONY, B., AUERBACH, G. & BLAU, N. 2000. Tetrahydrobiopterin biosynthesis, regeneration and functions. *Biochem J,* 347 Pt 1**,** 1-16.

THONY, B. & BLAU, N. 2006. Mutations in the BH4-metabolizing genes GTP cyclohydrolase I, 6-pyruvoyl-tetrahydropterin synthase, sepiapterin reductase, carbinolamine-4a-dehydratase, and dihydropteridine reductase. *Hum Mutat,* 27**,** 870-8.

TIAN, X., LI, J., VALAKH, V., DIANTONIO, A. & WU, C. 2011. Drosophila Rae1 controls the abundance of the ubiquitin ligase Highwire in post-mitotic neurons. *Nat Neurosci,* 14**,** 1267-1275.

TRIFUNOVIC, A. & LARSSON, N. G. 2008. Mitochondrial dysfunction as a cause of ageing. *J Intern Med,* 263**,** 167-78.

TRUJILLO, M., ALVAREZ, M. N., PELUFFO, G., FREEMAN, B. A. & RADI, R. 1998. Xanthine oxidase-mediated decomposition of S-nitrosothiols. *J Biol Chem,* 273**,** 7828-34.

TSUNEIZUMI, K., NAKAYAMA, T., KAMOSHIDA, Y., KORNBERG, T. B., CHRISTIAN, J. L. & TABATA, T. 1997. Daughters against dpp modulates dpp organizing activity in Drosophila wing development. *Nature,* 389**,** 627-31.

TURNER, C. & SCHAPIRA, A. H. 2001. Mitochondrial dysfunction in neurodegenerative disorders and ageing. *Adv Exp Med Biol,* 487**,** 229-51.

TURRENS, J. F. 2003. Mitochondrial formation of reactive oxygen species. *J Physiol,* 552**,** 335-44.

TURRENS, J. F. & BOVERIS, A. 1980. Generation of superoxide anion by the NADH dehydrogenase of bovine heart mitochondria. *Biochem J,* 191**,** 421-7.

TURRENS, J. F., FREEMAN, B. A., LEVITT, J. G. & CRAPO, J. D. 1982. The effect of hyperoxia on superoxide production by lung submitochondrial particles. *Arch Biochem Biophys,* 217**,** 401-10.

UNIPROTCONSORTIUM 2015. UniProt: a hub for protein information. *Nucleic Acids Res,* 43**,** D204-12.

VAN DER BLIEK, A. M., SHEN, Q. & KAWAJIRI, S. 2013. Mechanisms of mitochondrial fission and fusion. *Cold Spring Harb Perspect Biol,* 5.

VAN DER PLAS, M. C., PILGRAM, G. S., PLOMP, J. J., DE JONG, A., FRADKIN, L. G. & NOORDERMEER, J. N. 2006. Dystrophin is required for appropriate retrograde control of neurotransmitter release at the Drosophila neuromuscular junction. *J Neurosci,* 26**,** 333-44.

VASQUEZ-VIVAR, J., MARTASEK, P., WHITSETT, J., JOSEPH, J. & KALYANARAMAN, B. 2002. The ratio between tetrahydrobiopterin and oxidized tetrahydrobiopterin analogues controls superoxide release from endothelial nitric oxide synthase: an EPR spin trapping study. *Biochem J,* 362**,** 733-9.

VERAKSA, A., BAUER, A. & ARTAVANIS-TSAKONAS, S. 2005. Analyzing protein complexes in Drosophila with tandem affinity purification-mass spectrometry. *Dev Dyn,* 232**,** 827-34.

VERGAUWEN, H., TAMBUYZER, B., JENNES, K., DEGROOTE, J., WANG, W., DE SMET, S., MICHIELS, J. & VAN GINNEKEN, C. 2015. Trolox and ascorbic acid reduce direct and indirect oxidative stress in the IPEC-J2 cells, an in vitro model for the porcine gastrointestinal tract. *PLoS One,* 10**,** e0120485.

VINCENT, A. 2013. *A D. melanogaster parkin mutant larval model of Parkinson's Disease.* PhD, University of York.

VINCENT, A., BRIGGS, L., CHATWIN, G. F., EMERY, E., TOMLINS, R., OSWALD, M., MIDDLETON, C. A., EVANS, G. J., SWEENEY, S. T. & ELLIOTT, C. J. 2012. parkin-induced defects in neurophysiology and locomotion are generated by metabolic dysfunction and not oxidative stress. *Hum Mol Genet,* 21**,** 1760-9.

WALLACE, D. C. 1992. Mitochondrial genetics: a paradigm for aging and degenerative diseases? *Science,* 256**,** 628-32.

WAN, H. I., DIANTONIO, A., FETTER, R. D., BERGSTROM, K., STRAUSS, R. & GOODMAN, C. S. 2000. Highwire regulates synaptic growth in Drosophila. *Neuron,* 26**,** 313-29.

WANG, M. C., BOHMANN, D. & JASPER, H. 2003. JNK signaling confers tolerance to oxidative stress and extends lifespan in Drosophila. *Dev Cell,* 5**,** 811-6.

WANG, W., SHI, L., XIE, Y., MA, C., LI, W., SU, X., HUANG, S., CHEN, R., ZHU, Z., MAO, Z., HAN, Y. & LI, M. 2004. SP600125, a new JNK inhibitor, protects dopaminergic

neurons in the MPTP model of Parkinson's disease. *Neurosci Res,* 48**,** 195-202.
WANG, X. & MICHAELIS, E. K. 2010. Selective Neuronal Vulnerability to Oxidative Stress in the Brain. *Front Aging Neurosci,* 2.
WEBER, C. A., DUNCAN, C. A., LYONS, M. J. & JENKINSON, S. G. 1990. Depletion of tissue glutathione with diethyl maleate enhances hyperbaric oxygen toxicity. *Am J Physiol,* 258**,** L308-12.
WEITZMAN, S. A., TURK, P. W., MILKOWSKI, D. H. & KOZLOWSKI, K. 1994. Free radical adducts induce alterations in DNA. *Proc Natl Acad Sci U S A,* 91**,** 1261-4.
WEST, R. J. H., LU, Y., MARIE, B., GAO, F. B. & SWEENEY, S. T. 2015. Rab8, POSH, and TAK1 regulate synaptic growth in a Drosophila model of frontotemporal dementia. *J Cell Biol,* 208**,** 931-47.
WEVER, R. M., VAN DAM, T., VAN RIJN, H. J., DE GROOT, F. & RABELINK, T. J. 1997. Tetrahydrobiopterin regulates superoxide and nitric oxide generation by recombinant endothelial nitric oxide synthase. *Biochem Biophys Res Commun,* 237**,** 340-4.
WICHMANN, C. & SIGRIST, S. J. 2010. The active zone T-bar--a plasticity module? *J Neurogenet,* 24**,** 133-45.
WU, C., DANIELS, R. W. & DIANTONIO, A. 2007. DFsn collaborates with Highwire to down-regulate the Wallenda/DLK kinase and restrain synaptic terminal growth. *Neural Develop,* 2**,** 16.
WU, H., WANG, M. C. & BOHMANN, D. 2009. JNK protects Drosophila from oxidative stress by trancriptionally activating autophagy. *Mech Dev,* 126**,** 624-37.
WU, H., XIONG, W. C. & MEI, L. 2010. To build a synapse: signaling pathways in neuromuscular junction assembly. *Development,* 137**,** 1017-33.
XIONG, X., WANG, X., EWANEK, R., BHAT, P., DIANTONIO, A. & COLLINS, C. A. 2010. Protein turnover of the Wallenda/DLK kinase regulates a retrograde response to axonal injury. *J Cell Biol,* 191**,** 211-23.
YAMAGATA, N., ICHINOSE, T., ASO, Y., PLAÇAIS, P. Y., FRIEDRICH, A. B., SIMA, R. J., PREAT, T., RUBIN, G. M. & TANIMOTO, H. 2015. Distinct dopamine neurons mediate reward signals for short- and long-term memories. *Proc Natl Acad Sci U S A,* 112**,** 578-83.
YAMAMOTO, S. 2014. Dopamine Dynamics and Signaling in Drosophila. 63**,** 107-19.
YANG, D., TOURNIER, C., WYSK, M., LU, H. T., XU, J., DAVIS, R. J. & FLAVELL, R. A. 1997. Targeted disruption of the MKK4 gene causes embryonic death, inhibition of c-Jun NH2-terminal kinase activation, and defects in AP-1 transcriptional activity. *Proc Natl Acad Sci U S A,* 94**,** 3004-9.
YARZA, R., VELA, S., SOLAS, M. & RAMIREZ, M. J. 2015. c-Jun N-terminal Kinase (JNK) Signaling as a Therapeutic Target for Alzheimer's Disease. *Front Pharmacol,* 6**,** 321.
YONEYAMA, T. & HATAKEYAMA, K. 2001. Ligand binding to the inhibitory and stimulatory GTP cyclohydrolase I/GTP cyclohydrolase I feedback regulatory protein complexes. *Protein Sci,* 10**,** 871-8.
ZHAI, R. G. & BELLEN, H. J. 2004. The architecture of the active zone in the presynaptic nerve terminal. *Physiology (Bethesda),* 19**,** 262-70.
ZHANG, B., KIROV, S. & SNODDY, J. 2005. WebGestalt: an integrated system for exploring gene sets in various biological contexts. *Nucleic Acids Res,* 33**,** W741-8.

ZHANG, R., AL-LAMKI, R., BAI, L., STREB, J. W., MIANO, J. M., BRADLEY, J. & MIN, W. 2004. Thioredoxin-2 inhibits mitochondria-located ASK1-mediated apoptosis in a JNK-independent manner. *Circ Res,* 94**,** 1483-91.

ZHANG, Y., ZHAO, H., LIU, T., WAN, C., LIU, X., GAO, Z., HOU, X., JIANG, L. & LIU, F. 2015. Activation of transcription factor AP-1 in response to thermal injury in rat small intestine and IEC-6 cells. *BMC Gastroenterol,* 15.

ZHOU, H., GAO, J., LU, Z. Y., LU, L., DAI, W. & XU, M. 2007. Role of c-Fos/JunD in protecting stress-induced cell death. *Cell Prolif,* 40**,** 431-44.